A SEARCH FOR FRACTIONALLY CHARGED PARTICLES IN COSMIC RAYS AND A THEORETICAL INTERPRETATION OF THE RESULTS

Thesis by

Charles Douglas Orth

In Partial Fulfillment of the Requirements

For the Degree of

Doctor of Philosophy

California Institute of Technology

Pasadena, California

1970

(Submitted December 2, 1969)

ACKNOWLEDGEMENTS

I would like to take this opportunity to thank both of my advisors, Dr. George Zweig and Dr. Ricardo Gomez, for it was through their efforts that I was allowed to participate in the quark-experiment program. Their advice and guidance were quite helpful.

Dr. Hans Kobrak and Mr. Alan Moline are to be thanked for setting up the test version of the quark experiment. I am grateful to Dr. Joe H. Mullins and Dr. James Van Putten for some interesting conversations on the efficiency of spark chambers.

I would like to thank Mr. Richard Lipes for many informative discussions on the multi-Regge-exchange hypothesis and related topics.

My wife, Shirley, is to be thanked for the encouragement she gave in times of difficulty and for the typing of this thesis.

I would also like to express my gratitude to the California Institute of Technology for financial assistance while conducting this research.

ABSTRACT

An array of two spark chambers and six trays of plastic scintillation counters was used to search for unaccompanied fractionally charged particles in cosmic rays near sea level. No acceptable events were found with energy losses by ionization between 0.04 and 0.7 that of unit-charged minimum-ionizing particles. New 90%-confidence upper limits were thereby established for the fluxes of fractionally charged particles in cosmic rays, namely, $(1.04 \pm 0.07)\mathrm{x}10^{-10}$ and $(2.03 \pm 0.16)\mathrm{x}10^{-10}$ $\mathrm{cm}^{-2}\mathrm{sr}^{-1}\mathrm{sec}^{-1}$ for minimum-ionizing particles with charges 1/3 and 2/3, respectively.

In order to be certain that the spark chambers could have functioned for the low levels of ionization expected from particles with small fractional charges, tests were conducted to estimate the efficiency of the chambers as they had been used in this experiment. These tests showed that the spark-chamber system with the track-selection criteria used might have been over 99% efficient for the entire range of energy losses considered.

Lower limits were then obtained for the mass of a quark by considering the above flux limits and a particular model for the production of quarks in cosmic rays. In this model, which is one involving the multi-peripheral Regge hypothesis, the production cross section and a corresponding mass limit are critically dependent on the Regge trajectory assigned to a quark. If quarks are

"elementary" with a flat trajectory, the mass of a quark can be expected to be at least 6 ± 2 BeV/c^2. If quarks have a trajectory with unit slope, just as the existing hadrons do, the mass of a quark might be as small as 1.3 ± 0.2 BeV/c^2. For a trajectory with unit slope and a mass larger than a couple of BeV/c^2, the production cross section may be so low that quarks might never be observed in nature.

To Shirley

TABLE OF CONTENTS

PART	TITLE	PAGE
I.	INTRODUCTION	1
II.	EXPERIMENTAL APPARATUS	9
	A. The Array	9
	B. Data-Recording Equipment	14
	C. The Electronics	16
III.	ACQUISITION OF DATA	20
	A. Regular Calibration Runs	20
	B. Special Calibration Runs	24
IV.	ANALYSIS OF THE DATA	25
	A. General Procedure	25
	B. Scanning the Spark-Chamber Film	28
	C. Pulse-Height Calibrations	29
	D. Chi-Square Analysis	30
	E. G-Counter Agreement	44
	F. Measurement of Track Misalignments	45
	G. Oscilloscope Check and A Summary	52
	H. Estimating a Particle's Charge From a MPPH	53
V.	THE EXPERIMENTAL EFFICIENCIES	60
	A. Detection Efficiency of the Counters	60
	B. Detection Efficiency of the Spark Chambers	62
	C. The Overall Efficiency	106

TABLE OF CONTENTS (Continued)

PART	TITLE	PAGE
VI.	THE EXPERIMENTAL RESULTS	107
	A. A Summary	107
	B. Upper Limits For the Flux of Quarks in Cosmic Rays	111
	C. Significance of the Results	113
VII.	LOWER LIMITS FOR THE MASS OF A QUARK	122
	A. Introduction	122
	B. Production Cross Section Near Threshold	126
	C. Production Cross Section As A Function of s	153
	D. Quark Production and Loss in the Atmosphere	157
	E. Lower Limits for the Mass of a Quark	163
	F. Dependence of the Results on the Parameter Values and the Assumptions	176
	G. Discussion of the Results	181
APPENDICES		183
REFERENCES		260

APPENDICES

APPENDIX	TITLE	PAGE
A.	ELECTRONIC DETAILS	183
	1. The Trigger Inhibitor	183
	2. B-Logic	184
	3. G-Logic	190
	4. Triggering the System with Q-TR	193
B.	THE TECHNIQUES USED TO COMPUTE MPPH AND X^2	195
	1. MPPH Techniques	195
	2. X^2 Techniques	203
C.	THEORETICAL MODELS FOR THE SPARK-CHAMBER EFFICIENCY FITS	205
	1. Introduction	205
	2. Poisson Theory	207
	3. Poisson Theory + Delta Rays	213
	4. Poisson Theory + Metastables	225
	5. Poisson Theory + Constant Probability	228
D.	THE MECHANISM OF SPARK BREAKDOWN IN PLANE-PARALLEL GAPS	229
E.	CROSS SECTION FORMULAS, PARAMETER VALUES, AND $(-t)_{min}$	233
	1. Cross Section Formulas	233
	2. Parameter Values	246
	3. Minimum Four-Momentum Transfer For A 2-Body Process	249
F.	THE DIFFUSION EQUATION FOR QUARKS AND ITS SOLUTION	252

LIST OF FIGURES

NUMBER	CAPTION	PAGE
1	The Array	10
2	A Block Diagram of the Electronics	17
3	A Typical G-Counter Pulse-Height Distribution Obtained from a L-CR-A Run	34
4	The Differential Distribution of X^2's for Cosmic-Ray Events	38
5	The Integral Distribution of X^2's for Cosmic-Ray Events	39
6	The Integral Distributions of X^2's for Charges 1/3, 2/3, and 1	41
7	Measurement of Spark-Chamber Track Misalignments	46
8	Front-View Lateral Misalignments for Cosmic-Ray Events	48
9	Front-View Angular Misalignments for Cosmic-Ray Events	49
10	Side-View Lateral Misalignments for Cosmic-Ray Events	50
11	Side-View Angular Misalignments for Cosmic-Ray Events	51
12	Monte Carlo MPPH Distributions for Minimum-Ionizing Particles with Charges 1/3, 2/3, or 1	57
13	Various Pulse-Height Distributions for Cosmic-Ray Events (B Counters Ignored)	58
14	The Efficiency of the Counter System as a Function of the Square of the Charge of Any Minimum-Ionizing Particle Detected	63
15	Character of the Efficiency Data for Helium	69
16	Character of the Efficiency Data for the AHE Mixture	70
17	Character of the Efficiency Data for Argon	71

LIST OF FIGURES (Continued)

NUMBER	CAPTION	PAGE
18	Efficiency vs t_{delay} and Fits for N=1: Helium Gap #1	77
19	Efficiency vs t_{delay} and Fits for N=1: Helium Gap #4	78
20	Efficiency vs t_{delay} and Various Fits: AHE Gap #1: Parameters Held Constant During Fitting are Indicated	79
21	Efficiency vs t_{delay} and Various Fits: AHE Gap #4: Parameters Held Constant During Fitting are Indicated	80
22	Efficiency vs t_{delay} and Poisson Theory + Metastables Fit for N=1: Argon Gap #1	81
23	Efficiency vs t_{delay} and Poisson Theory + Metastables Fit for N=1: Argon Gap #4	82
24	Chi-Square of Fit vs N: Gap #1	84
25	Chi-Square of Fit vs N: Gap #4	85
26	Primary Ion Density "m" vs N: Gap #1	86
27	Primary Ion Density "m" vs N: Gap #4	87
28	Electron Drift Velocity vs N: Gap #1	88
29	Electron Drift Velocity vs N: Gap #4	89
30	Mean Lifetime of Metastable States vs N: Gaps #1 and #4	90
31	Total Number of Electrons Produced by the De-excitation of Metastable States: Gaps #1 and #4	91
32	The Effects of Changes in the Parameters Held Constant in Fitting the Poisson Theory to the Efficiency Data	94
33	Decomposition of Mesons and Baryons	128
34	The Empirical Total Cross Section for Anti-Proton Production in Proton-Proton Interactions	130

LIST OF FIGURES (Continued)

NUMBER	CAPTION	PAGE
35	Diagrams for Quark Production	133
36	Lowest-Order Diagrams for Quark Production	135
37	Total Cross Sections $\sigma(m_q, s_o, s)$ For $\alpha_q(t) = -m_q^2 + t$ and $s_o = 1$ BeV^2, Normalized to Unity at $s^{\#} = 500$ BeV^2	145
38	Total Cross Sections $\sigma(m_q, s_o, s)$ For $\alpha_q(t) = 0$ and Any s_o, Normalized to Unity at $s^{\#} = 1200 + 800(m_q - 3)$ BeV^2	149
39	Dependence of the Production Cross Section on the Energy Above Threshold in the CM Frame	155
40	Production Off A Nucleus	158
41	$(m_q)_{min}$ vs Λ_q For $\eta=1.0$ and $s_o=1.0$: $\alpha_q(t) = -m_q^2 + t$	164
42	$(m_q)_{min}$ vs Λ_q For $\eta=1.0$ and $s_o=5.0$: $\alpha_q(t) = -m_q^2 + t$	165
43	$(m_q)_{min}$ vs η For $\Lambda_q=120$ and $s_o=1.0$: $\alpha_q(t) = -m_q^2 + t$	166
44	$(m_q)_{min}$ vs η For $\Lambda_q=120$ and $s_o=5.0$: $\alpha_q(t) = -m_q^2 + t$	167
45	$(m_q)_{min}$ vs s_o For $\Lambda_q=120$ and $\eta=1.0$: $\alpha_q(t) = -m_q^2 + t$	168
46	$(m_q)_{min}$ vs Λ_q For $\eta=1.0$ and $s_o=1.0$: $\alpha_q(t) = 0$	169
47	$(m_q)_{min}$ vs Λ_q For $\eta=1.0$ and $s_o=5.0$: $\alpha_q(t) = 0$	170

LIST OF FIGURES (Continued)

NUMBER	CAPTION	PAGE
48	$(m_q)_{min}$ vs η For Λ_q=120 and s_o=1.0: $\alpha_q(t) = 0$	171
49	$(m_q)_{min}$ vs η For Λ_q=120 and s_o=5.0: $\alpha_q(t) = 0$	172
50	$(m_q)_{min}$ vs s_o For Λ_q=120 and η=1.0: $\alpha_q(t) = 0$	173
51	B-Logic	185
52	G-Logic	191
53	Distribution of Q-TR	194
54	Coordinate System Considered for the Motion of an Electron Column	210
55	Diagram for 3-Body Production Showing Relevant Scalers	234
56	Diagram for 2-Body Production Showing Relevant Scalers	250
57	Depth x at which Quark Flux is Maximum	258

LIST OF TABLES

NUMBER	HEADING	PAGE
1	Properties of Quarks	2
2	B and G Counter Characteristics	13
3	The Different Types of Runs	21
4	The Analysis Requirements and Their Effects	54
5	Summary of the Values Obtained for the Parameters When Considering N=1 and the Poisson Theory + Metastable Fits	92
6	Relative Cosmic-Ray Abundances for Some Strongly Interacting Particles	127
7	Values of $\sigma_{threshold}(m_q, s_o)$ in Millibarns For the Case $\alpha_q(t) = -m_q^2 + t$	147
8	Values of $\sigma_{threshold}(m_q, s_o)$ in Millibarns For the Case $\alpha_q(t) = 0$	151
9	Sensitivity of $\sigma_{threshold}(m_q, s_o)$ to Changes in a_i and Trajectory Parameters	179
10	Electronic-Circuit Nomenclature	186
11	The Convergence of μ's Toward a MPPH	202
12	Notation for Poisson Theory + Delta Rays	215

I. INTRODUCTION

In 1964, Gell-Mann and Zweig independently proposed that a set of three objects called quarks would be convenient in expressing certain symmetries of the strong interactions.[1,2] These objects were assigned properties just like those of the proton, neutron, and lambda except that they had baryon number 1/3 and charges +2/3, -1/3, and -1/3 (see table 1).* All strongly interacting particles were regarded in a mathematical sense as being composed of these objects.[3] Mesons were constructed from quark-antiquark pairs (e.g. a negative pion was composed of one anti-P_o and one N_o). Baryons were constructed from combinations of three quarks (e.g. a proton was composed of two P_o's and one N_o).

After this "quark model" of the strong interactions was introduced, it was natural to assume that there might be objects in nature, as yet undiscovered, which had charges that were not integral multiples of the charge of the proton or electron. In particular, it was thought that quarks might correspond to actual physical particles even though they appeared in the theory only as algebraic entities. As a result, many experimental searches were conducted for particles in nature having fractional charges.†

---

*A particle's charge will always be given in units of the proton's charge.

†It is possible that the stable objects with non-integral charge could have charges larger than 2/3 (e.g., 4/3, or 5/3,... see reference 4). Nevertheless, we shall be concerned here only with objects having charges smaller than one.

TABLE 1: PROPERTIES OF QUARKS

Quark Symbol	Charge Q	Isospin		Strangeness	Baryon Number	Spin
		I	I_z			
P_o	+2/3	1/2	+1/2	0	1/3	1/2
N_o	-1/3	1/2	-1/2	0	1/3	1/2
Λ_o	-1/3	0	0	-1	1/3	1/2

In the first experiments, accelerators were used in attempts to produce fractionally charged particles through pair production (e.g. proton + nucleus $\longrightarrow$ proton + nucleus + quark + antiquark).[5-10] Nuclei were bombarded with protons of momenta up to 31 BeV/c, and the reaction products were searched for particles having charges between 0.2 and 0.7. Because the energy loss by ionization of a particle with charge Q in passing through matter is proportional to Q^2,[11]* fractional-charge detection could be accomplished by searching for particles with energy losses smaller than the minimum energy loss which is probable for a particle with unit charge. Quarks, for instance, could be distinguished from all known particles because the energy loss of a quark is expected to be approximately one-ninth or four-ninths that of a particle with unit charge.

No particles with fractional charges were detected in the accelerator experiments. The conclusions were that, if quarks do exist as real particles, then either: 1) the mass of a quark is more than 2.5 to 4.5 BeV/c^2 so that the pair-production reactions were below threshold, or 2) the production cross section for quarks was for some reason smaller than about 10^{-34} cm^2 even though the production was expected to proceed through a strong interaction.‡

---

*We assume that particles with fractional charges lose energy in the same manner as particles with integral charges. In particular, we assume that quarks have no magnetic charge (see reference 12).

‡It is possible, for example, that a quark inside a meson or a baryon sits in a potential well which is quite shallow relative to the zero-energy level but which has huge barriers that must be surmounted (or tunnelled through) before the quark can be freed. A quark need therefore not be very massive, but merely be bound within huge barriers. Nevertheless, where more energy is required to produce them we shall speak as though they were more massive.

To study pair production for quarks of larger mass,* investigators turned to cosmic rays to obtain higher incident proton energies. Scintillation-counter arrays were set up at various altitudes to search for particles with energy losses significantly below that for a particle with unit charge.[13-22]

The results of the early cosmic-ray experiments were limited by background. One reason for the background was the poor energy-loss resolution of the scintillation counters used in these experiments. This allowed the experimental energy-loss spectrum for cosmic-ray muons to partially overlap the spectrum expected for quarks of charge 2/3. Some cosmic-ray muon events could thus appear quark-like because they had energy losses which were also appropriate for the quarks.

Another reason for the background was probably the sole use of scintillation counters as particle detectors. Experiments of this kind are apparently susceptible to a background caused by photon showers. A photon can produce a low-energy Compton electron which stops in a counter and thereby provides the low energy loss expected for a fractionally charged particle traversing the counter. A background event results when this happens in all of the counters within the coincidence time interval determined by the electronics. The number of these events generally increases as the energies of the Compton electrons decrease.[23] The early cosmic-ray experiments thus had an inherent difficulty in searching for quarks of charge

---

*See footnote † on the previous page.

1/3 because this and possibly other unknown background overlapped and swamped the energy-loss spectrum expected for the quarks.

Several techniques can be used to reduce the background from Compton electrons. One way is simply to add more scintillation counters in coincidence because this requires more coincident Compton conversions. The addition of proportional counters can also help because their small thickness (in grams per square centimeter) reduces the probability that a photon will produce a Compton electron while traversing such a counter.[21]

The addition of spark chambers to the counter array can provide an even greater reduction in the background. A "fake" track will be produced in a spark chamber only if the Compton conversions in the gaps are co-linear, but a pulse will result in a counter if a Compton electron is produced anywhere inside the counter. The relative backgrounds due to Compton electrons produced by photon showers in a spark-chamber gap and a counter of the same thickness (in g/cm^2) might therefore be expected to be approximately in the ratio of the cross-sectional area of the spark channel to the area of the counter, respectively.

A difficulty with the use of spark chambers, however, was that no test had ever been made to see if spark chambers could operate for ionizations as low as those expected from particles with fractional charges.*

---

*A. Buhler-Broglin, et. al., (reference 22), mentioned the problem, but they went no further.

Although the energy-loss techniques of the accelerator and cosmic-ray experiments were the most common, other techniques to find fractionally charged particles were also being developed. For instance, a search for quarks in iron meteorites, air, and sea water had been conducted by vaporizing the materials near a hot filament then collecting and examining certain ions, but no quarks were found.[24] There had also been attempts to find quarks in magnetic-levitation modifications of Millikan's oil-drop experiment.[25-28] There had even been suggestions that there might be evidence for the existence of quarks using astronomical and radio-astronomical techniques.[29-33]

By the middle of 1966, the only cosmic-ray experiments which had been completed were those whose results were limited by background. An array of two spark chambers and six trays of plastic scintillation counters with good resolution was then set up at the California Institute of Technology. The intention was to search for relativistic fractionally charged particles in cosmic rays near sea level by searching for a particle having an energy loss anywhere between 0.04 and 0.7 that of a minimum-ionizing cosmic-ray muon.* The scintillation counters were to be used for triggering purposes

---

*A charged particle which is "minimum-ionizing" is one whose speed is such that its most probable energy loss per gram/cm^2 is the minimum possible for a particle with that charge. For particles much heavier than the electron, the ratio of such a particle's speed to the speed of light is about 0.95 to 0.97. The source of minimum-ionizing particles for this experiment was the cosmic-ray flux, which at sea level consists mostly of muons which are essentially minimum-ionizing.

and to determine the energy loss for the event. The spark chambers were to be used to minimize the background from Compton electrons.

Criteria were established for the acceptance of an event as a "fractionally-charged-particle event" which were based on the response of the system to cosmic-ray muons. Any event with the following properties would be regarded as an event produced by a fractionally charged particle:

1) an energy loss smaller than the minimum energy loss which is probable for a particle with unit charge,

2) counter pulse heights which are consistent with the hypothesis that a single particle has traversed the array, and

3) spark-chamber tracks which are representative of those produced by a particle, according to the cosmic-ray criteria.

By using spark chambers, good-resolution counters, and these acceptance criteria, it was believed that the backgrounds could be reduced enough so that a single event would, in principle, be sufficient to establish the existence of fractionally charged particles.

The experiment was run for 4,664 hours, and no particles with fractional charges were found. New upper limits on the flux of quarks in cosmic rays near sea level were then set which were more than a factor of ten under the previously existing limits.[18]

To discover whether a null experimental result would merely reflect the inability of spark chambers to function for particle ionizations as small as those expected from fractionally charged particles, methods had been devised to estimate the efficiency of the spark chambers as they were used in this experiment. The tests conducted using these methods are described in Chapter V. These tests showed that the spark-chamber system might have been over 99% efficient for the entire range of energy losses considered.

In Chapter VII, we re-express the experimental results in the form of lower limits for the mass of a quark. By considering particular models for the production of quarks in cosmic rays and for the interactions of quarks with nuclei they encounter on their way down to sea level, we estimate what the rate of quarks traversing our array might be expected to be. The production model considered for this purpose is one involving the multi-peripheral Regge hypothesis. Because the theoretical estimate for the rate is dependent on the mass of a quark, a comparison of this estimate with the rate observed experimentally allows one to determine a lower limit for the quark mass. We find that such a lower limit is critically dependent on the Regge trajectory assigned to a quark. If quarks are "elementary" with a flat trajectory, the mass of a quark can be expected to be at least 6 ± 2 BeV/c^2. On the other hand, if quarks have a trajectory with unit slope, just as the existing hadrons do, the mass of a quark might be as small as 1.3 ± 0.2 BeV/c^2. For a trajectory with unit slope and a mass larger than a couple of BeV/c^2, the production cross section may be so low that quarks might never be observed in nature.

II. EXPERIMENTAL APPARATUS

The experimental apparatus consisted of an array of spark chambers and scintillation counters, some recording equipment, and a system of electronics. The array is described in section A. A description of the recording equipment is given in section B. The electronics is described in section C and in appendix A.

A. The Array

The array was a vertical stack of two narrow-gap spark chambers and twelve plastic scintillation counters, as illustrated in figure 1, with an acceptance of $0.15 \pm 0.01\ m^2$ sr.

Because the number of ion pairs produced in each gap of a spark chamber by the passage of a particle with a given speed is proportional to the square of the particle's charge, there had been some question whether spark chambers could function efficiently for the low levels of ionization expected from particles with small fractional charges. Consequently, an attempt was made to operate our chambers in a fashion which would tend to optimize their efficiency at these low levels of ionization.

When spark chambers are operated with pure helium under a pressure of one atmosphere, their efficiency for the detection of

FIGURE 1: THE ARRAY

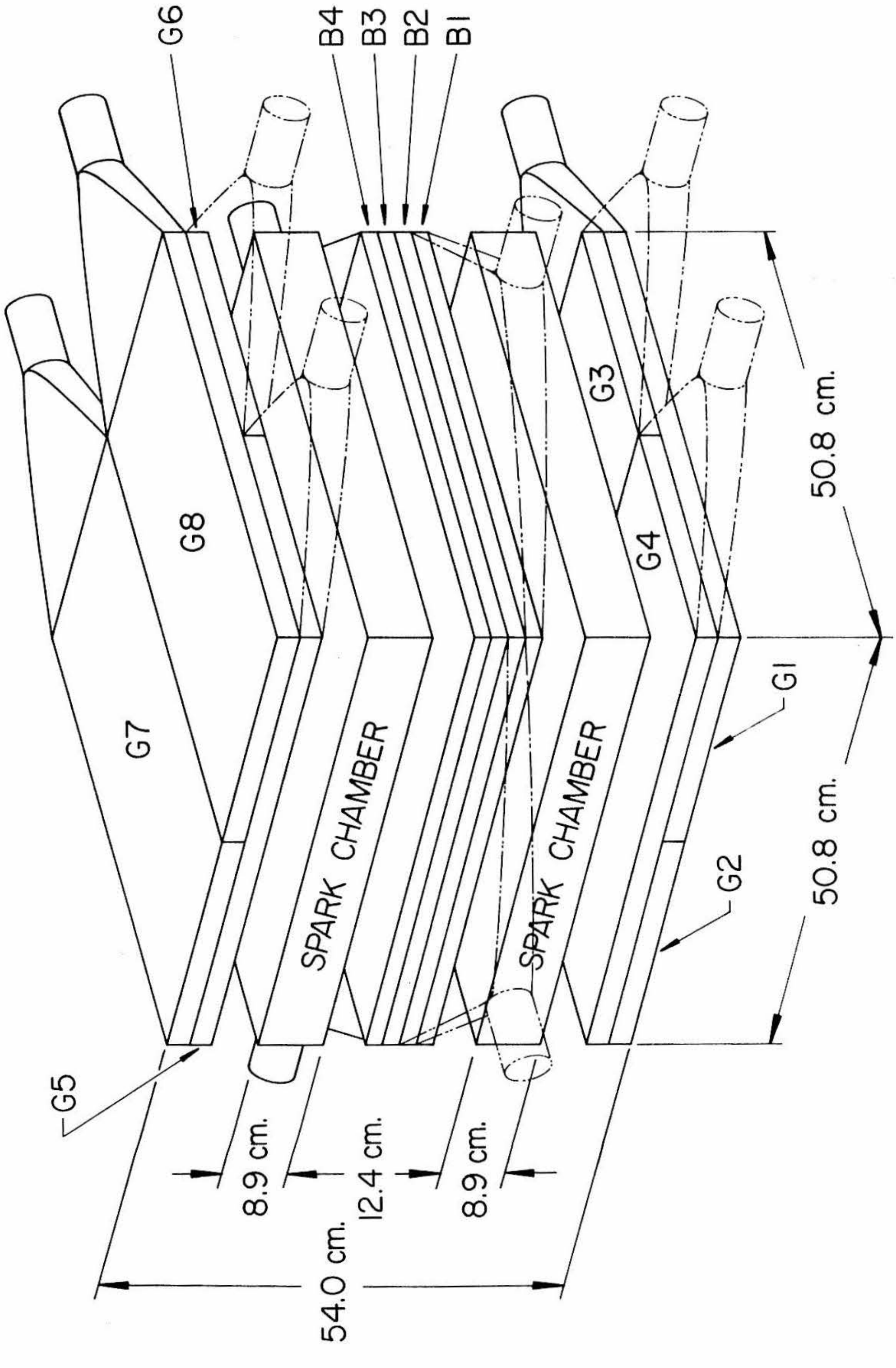

cosmic-ray muons is known to be nearly 100%.* Moreover, because a particle's energy loss by ionization is proportional to the number of electrons encountered, the number of ion pairs produced per centimeter (i.e. ion density) increases if a gas with a higher atomic number (Z) is used.(34) For this reason, the spark chambers in the array were operated with a large percentage of argon (Z=18). The ion density expected from particles with the small fractional charges to be considered would then be at least as large as the ion density obtained for unit-charged particles in helium.† The gas mixture used was in fact 76.0 ± 2.0 percent argon, 22.5 ± 2.0 percent helium, and 1.5 ± 0.5 percent ethanol all at room temperature and at atmospheric pressure (plus 1/8" head of oil).**

To further improve the chances for proper spark-chamber operation, a large pulsing field was used: the two chambers were pulsed by discharging a 0.008-microfarad capacitor charged to 29 ± 1 kilovolts. Each spark chamber had four 3/8-inch gaps and was operated with a clearing field of ten volts per centimeter.

---

*E.g. see section V.B, where a test is described in which the efficiency per gap of the spark chambers used in the array was measured for the detection of cosmic-ray muons in pure helium and found to be 96.6% ± 0.2%.

†We assumed that spark-chamber operation would not be significantly different for different gas mixtures if the ion densities were identical (see appendix D).

**The helium and ethanol were added to the argon in the proportions given because this mixture resulted in a sparking efficiency per gap for cosmic-ray muons of 99.6% with bright well-defined sparks. Moreover, the ethanol (a quenching agent) was expected to reduce spurious sparking. The total flow rate was 0.37 ± 0.03 liter per minute.

The array also contained twelve scintillation counters, whose properties are listed in table 2. Four of the counters, labelled B counters, were obtained from a previous experiment run at the California Institute of Technology synchrotron laboratory. To improve the effective resolution of these counters,* the outputs of their photomultiplier tubes were added in pairs (B1+B3, B2+B4) and the two resulting "counters" were denoted as S1 and S2 respectively. In making these sums, counters were chosen with their phototubes opposite each other to obtain more uniform responses over the surfaces of S1 and S2. The effective resolution of the B counters was thereby improved by 30%.

With the B counters paired electronically into two counters and the G counters paired physically in four layers, there were at most six counters which could be traversed by a particle in rectilinear motion: S1, S2, G1 or G2, G3 or G4, G5 or G6, and G7 or G8. The array was thus divided into six counter trays.

As one can see from figure 1, the counters in adjacent G trays were arranged in crisscrossed pairs. This was done for several reasons. One was to divide the top and the bottom of the array into quadrants, and thus to allow the array to be divided electronically into sixteen different sections. The pulse heights of one section could then serve as the basis for the generation of the trigger pulse even if another section had large pulse heights

*The resolution of a counter in the array is defined as the ratio of the full width at half maximum to the position of the maximum of the pulse-height distribution obtained from the passage of cosmic-ray muons through the array.

TABLE 2: B AND G COUNTER CHARACTERISTICS

Counter	B1-B4	G1	G2	G3	G4	G5	G6	G7	G8
Scintillator:									
Material	NE102	Pilot-Y	NE102	Pilot-Y	Pilot-Y	NE102	NE102	NE102	NE102
Length (in.)	19	$20\frac{1}{4}$	18	21	21	21	21	21	21
Width (in.)	19	8	$8\frac{1}{2}$	10	10	10	10	10	10
Thickness (in.)	3/4	1	1	1	1	1	1	1	1
Absorption Length (in.)	75*	630	40	$\sim\infty$	630	230	550	220	380
Lightpipe:									
Material	PVT				All UVT				
Design	Tri				All 3pc				
A_k/A_s	0.17				All 1.00				
Phototubes:									
Number	ONE				ONE				
Type	RCA#7850				RCA#8055				
Cosmic-Ray Response:									
Peak # of Photocathode electrons	40				600				
Resolution	0.6	.25	.32	.25	.28	.26	.27	.27	.27

All phototubes had magnetic shields, and all lightpipes and scintillators were wrapped with one sheet of aluminum foil and then with black photographic tape.

Symbols:
- A_k, A_s Cross-sectional areas at photocathode, and at scintillator
- PVT Polyvinyltoluene (unpolished)
- UVT Ultraviolet-transmitting lucite (polished)
- * B1-B4 average; see Eric Adelberger, C.I.T. Synchrotron CTSL INTERNAL REPORT No. 9, Pi counters, p.6.
- Tri Triangular, i.e. the intersection of a wedge and a cone
- 3pc 3-pieced, made by bending (e.g.) two 3" rectangular outside pieces and glueing them to a center 4" rectangular piece

because of the production of Compton electrons. The advantage was a decrease in the probability of rejecting events when the fractionally charged particle entered the system accompanied by a photon shower. The sectioning also provided a space resolution which was useful in the analysis of the data (section IV.D).

The crisscrossing of the counters made it impossible for one particle to traverse a lightpipe in every tray. Such an arrangement therefore reduced the background due to Cherenkov radiation from integrally charged particles traversing the lightpipes close to the phototubes.

Each photomultiplier tube was operated in its linear region, as measured by a calibrated light pulser, for the entire range of pulses considered. This was done to facilitate analysis of the data.

B. Data-Recording Equipment

Data were recorded on papertape by a pulse-height analyzer and on film by a system of cameras which photographed the spark chambers (in two stereo views), a system of lights, and the displays of two oscilloscopes.

For each event, the counter pulse heights for S1, S2, and G1 through G8, and a number identifying that event, were recorded by utilizing Ransom Research Inc.'s Sampling Digitizer Model 1138B with a Tally papertape punch.[35] This digitizer is a charge-sensitive multi-input 100-channel pulse-height analyzer which integrates input current for five microseconds.

To enable correlations between the pulse-height data and the spark-chamber data, it was imperative to know whether the tracks in the chambers for a given event has resulted from the passage of the same particle whose energy losses were measured by the pulse heights in the counters. A system of lights was therefore used to indicate whether an additional particle had traversed the array within the resolving time of the chambers, which was approximately seven microseconds (section V.B). One light indicated whether a particle losing more than 0.7 minimum* had traversed S1 and S2 at any time within ten microseconds before the event causing the trigger pulse to be generated. Another light indicated whether such a particle had traversed these counters at any time between approximately 120 nanoseconds after the event and the time that a current probe near the spark chambers indicated that the chambers had been pulsed. The light system was insensitive for about 120 nanoseconds after the event because this was the dead time of the electronics.

To detect the presence of cosmic-ray particles during the insensitive period of the light system, and also for general timing and pulse-height information, the outputs of all eight G counters were displayed on two type 517 Tektronics oscilloscopes. Each

---

*Throughout this thesis, the term "minimum" will refer to the most probable energy loss by ionization in a counter of a unit-charged cosmic-ray particle traversing the array vertically.

oscilloscope displayed the pulses from four G counters on a ten-centimeter grid with a scale of 100 nanoseconds per centimeter.

C. The Electronics

The main function of the electronics was to generate a trigger pulse if and only if energy losses between 0.03 and 0.7 minimum occurred in time coincidence in all six counter trays (i.e. in S1, in S2, and in at least one G counter in each G tray).* Because only one counter per G tray was required to have an appropriate pulse height, one G counter in each G tray could have any pulse height. As explained in section II.A, this was allowed to reduce the chance of rejecting events where the fractionally charged particle entered the system accompanied by a photon shower.

If generated, the trigger pulse was used to trigger the spark chambers and the recording equipment. It was also used to render the entire system insensitive to further events until the data were recorded for the event being processed.

A simplified block diagram of the electronics is presented in figure 2 (for more detail, see appendix A). For historical reasons, the discrimination-coincidence circuitry was divided into two blocks (labelled "B-Logic" and "G-Logic") corresponding to the two types of scintillation counters used. The counter symbols

---

*The upper biases for the discriminator circuits were set at 0.7 minimum or higher, and the lower biases were set at 0.03 minimum or lower.

FIGURE 2: A BLOCK DIAGRAM OF THE ELECTRONICS

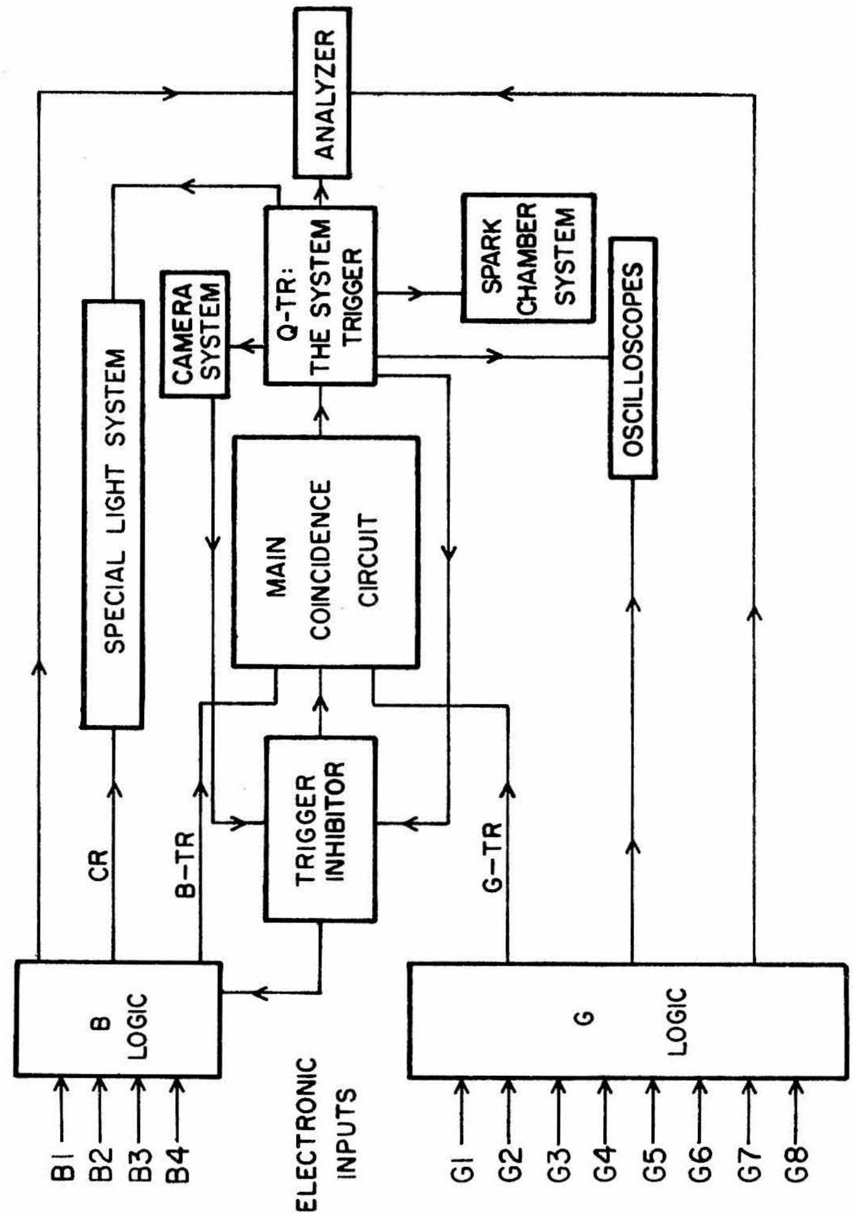

preceding these blocks represent pulses from the counters indicated, and will be termed the "electronic inputs" for the counters. Depending on the type of run being made, the signals entering the electronic inputs were either the phototube pulses, the phototube pulses attenuated by a factor of five, or artificial phototube pulses generated for calibration purposes.

The functions of the block B-Logic were the following: 1) to add the B counter pulses to produce S1 and S2, 2) to distribute S1 and S2 to the analyzer, 3) to generate the signal "B-TR" if the pulses in S1 and in S2 were in time coincidence and the pulse heights were between 0.03 and 0.7 minimum, and 4) to generate the "extra-particle" (i.e. cosmic-ray) signal "CR" for the light system if the coincident pulses in S1 and S2 were both above 0.7 minimum.

The functions of the block G-Logic were 1) to divide the G counters into counter trays (G1 or G2, G3 or G4, G5 or G6, G7 or G8), 2) to generate the signal "G-TR" if the pulses in the four G trays were in time coincidence and the pulse heights were between 0.03 and 0.7 minimum, and 3) to distribute G1 through G8 to the analyzer and to the oscilloscopes.

The trigger pulse, "Q-TR," was generated whenever there was a three-fold coincidence among B-TR, G-TR, and a signal from the "trigger inhibitor" indicating that the system was not busy recording data for a previous event. Q-TR was used to trigger the spark chambers, the pulse-height analyzer, the oscilloscopes, and the camera system. It was used in conjunction with the signal CR from

B-Logic to operate the light system. Q-TR also caused the trigger inhibitor to generate a veto signal to prevent the generation of subsequent Q-TR pulses until the camera system had indicated that the necessary pictures had been taken.

III. ACQUISITION OF DATA

For most of the running time, the experiment was setup to detect particles with fractional charges. These runs were called quark runs. At least twice a week, the quark runs were stopped for a few hours to allow the equipment to be checked and three calibration runs to be made. In addition, there were a few runs made once or twice during the experiment for special calibration purposes. A summary of the types of runs made is given in table 3 together with the symbol by which a run of each type will be designated throughout this thesis. The calibration runs are described in the following sections.

A. Regular Calibration Runs

After a quark run had been stopped, one 14-db (5X) passive attenuator was placed at the electronic input of each counter. This was done so the pulse heights resulting from the passage of cosmic-ray muons would fall within the 0.03-to-0.7-minimum range accepted by the electronics. Two calibration runs were then made by triggering on cosmic-ray particles. The spark-chamber pictures from the first run, a CR-P run, were examined to monitor the efficiency of the chambers for minimum-ionizing unit-charged particles. The oscilloscope pictures could be examined to determine the positions of cosmic-ray pulses on the displays, and thus to determine the

TABLE 3: THE DIFFERENT TYPES OF RUNS

RUN SYMBOL	FULL NAME	DATA ACQUIRED	NO. EVENTS	DATA USE
Quark	Quark run	Pulse-height date Spark-chamber pictures Oscilloscope pictures	~400/day	To search for particles with fractional charges
CR-P	Cosmic-Ray Picture run	Spark-chamber pictures Oscilloscope pictures	100	To determine the spark-chamber efficiency for minimum ionization, and to locate the time of particle passage on the oscilloscope displays
CR-A	Cosmic-Ray Analyzer run	Pulse-height date	~ 2,400	To normalize the quark-run pulse-height date
SKL	SKL run (using Spencer-Kennedy Labs pulse generators)	Pulse-height date and Oscilloscope pictures for enough SKL voltages to cover the entire range of the analyzer		To remove the nonlinearities in the pulse-height data, and to calibrate the oscilloscope gain

TABLE 3: (Continued)

RUN SYMBOL	FULL NAME	DATA ACQUIRED	NO. EVENTS	DATA USE
L-CR-A	Long Cosmic-Ray Analyzer run	Pulse-height data	20,000	To determine accurate properties of the counters' pulse-height distributions
L-V-CR	Long Vertical-Cosmic-Ray run	Pulse-height data	20,000	To determine accurate properties of the counters' pulse-height distributions for particle traversal perpendicular to the counter trays
S-CR-P	Special Cosmic-Ray Picture run	Spark-chamber pictures	3,350	To calibrate the chi-square measure (IV.D), and to determine the distributions of spark-chamber track-misalignments (IV.F)

positions corresponding to the time at which the particle had traversed the counters. Quark-run events with "extra" particles traversing the chambers within the insensitive period of the light system could then be identified because the oscilloscope pictures for those events would have pulses which did not occur at these positions.

The pulse-height data from the second calibration run, a CR-A run, were collected to form a pulse-height distribution for each counter. The moments of these distributions, and the distributions furnished by the L-V-CR and L-CR-A runs, were used in normalizing the pulse-height data acquired during neighboring quark runs.

For the third calibration run, an SKL run, two pulse generators were used with resistive dividers to supply the electronic inputs with pulses simulating the pulses from the photomultiplier tubes on the counters. These artificial phototube pulses were generated using model 503(a) Spencer-Kennedy Laboratories pulse generators. The shape of the output pulse of one of these SKL generators was made to match the shape of the phototube pulses from G counters. The other SKL generator was used to produce pulses matching those from B counters. SKL pulses covering the whole range of the analyzer were fed into the electronics. The channel-number-versus-SKL-voltage data which resulted were used to convert the pulse heights obtained during quark runs to a linear scale. Such conversion was necessary because the responses of the analyzer and the electronics were slightly nonlinear. The oscilloscope pictures taken during SKL runs were examined to calibrate the gain for the oscilloscope displays.

Besides the three calibration runs, certain checks and adjustments were always made to keep the equipment in proper working order. For example, if any lower or upper biases for the discriminator circuits had shifted, they were readjusted to the proper levels.

B. Special Calibration Runs

Twice during the experiment, a L-CR-A run and a L-V-CR run were made so that accurate pulse-height distributions could be obtained for the counters. The L-V-CR runs were made by adding more scintillation counters to the array to restrict the acceptance to only those particles traversing the array nearly perpendicular to the counter trays. In addition, a S-CR-P run was made to calibrate the chi-square measure used in the analysis of the data (section IV.D) and to determine the spark-chamber criteria for the acceptance of an event as one resulting from the passage of a particle through the array (section IV.F).

IV. ANALYSIS OF THE DATA

A. General Procedure

The steps used in the analysis of the data from the quark runs are given below. The basic task which had to be performed was to determine if any event had resulted from the passage of a particle through the array. The criteria established for this purpose were based on the response of the system to cosmic-ray particles. The pulse-height and spark-chamber data for acceptable events were required to resemble the corresponding data for cosmic-ray events.

As the first step, the spark-chamber film was scanned to select only those events with a single track in each spark chamber, where only rough alignment of the tracks in the two chambers was required at this stage. A track was defined to be a nearly co-linear arrangement of at least two sparks in one chamber or of at least three sparks in the other chamber.

Because the responses of the analyzer and the electronics were slightly nonlinear, the pulse-height data had been expressed on a nonlinear scale. The pulse-height data for the events satisfying the scanning criteria were therefore linearized to facilitate further analysis. They were then normalized to make the effective overall gains of all of the counters be the same.

A pulse-height restriction was imposed at this point to determine the limits on the range of acceptable pulse heights more accurately than they had been for triggering purposes. For an event to be considered for futher analysis, there had to be at least one counter in each tray with a normalized pulse height between 0.04 and 0.7 minimum.

The next step was to compute a most probable pulse height (MPPH) for each event satisfying the above requirements. For an event which had resulted from the passage of a particle through the array, the MPPH was a measure of the particle's most probable energy loss.

To avoid the difficulties involved in determining which four of the eight G counters had most likely been traversed by the particle for a given event, assuming there had been a particle, a MPPH was computed for all possible combinations of pulse heights between 0.04 and 0.7 minimum. Each combination corresponded to a set of six counters: S1, S2, and one G counter from each G tray. Because there were four G trays, each event could have at most $2^4 = 16$ combinations.

A quantity termed a modified chi square (X^2) was computed for each combination. The smallness of this quantity was an indication of the probability that the six pulse heights actually represented the energy losses of a particle traversing the corresponding six counters. An upper limit on acceptable values of X^2 was set which was well above most of the X^2's computed for single-particle cosmic-ray events. All combinations with X^2's above this limit were rejected. Each event considered for further analysis was required to have at least one combination whose X^2 was below this limit.

To define the fiducial volume for the spark chambers and to limit the X^2 analysis of each event to effectively only those counters most likely traversed by the particle for that event, each acceptable combination was required to have "G-counter agreement." In other words, the events kept for further consideration were only those having at least one combination whose set of G counters was consistent with the location of the tracks seen in the spark chambers.

The degree of misalignment of the tracks in the two spark chambers was measured for each event satisfying the above requirements and was required to be no worse than those measured for cosmic-ray particles. This was done to ensure that the spark-chamber tracks for each acceptable event were representative of those produced by a particle traversing both chambers.

Finally, the oscilloscope data were required to be consistent with the pulse-height data recorded by the analyzer and with the hypothesis that only one particle had traversed the array.

No event had the necessary properties to satisfy all of these requirements. If any event had been determined to have resulted from the passage of a particle through the array, the particle's charge would have been estimated using the techniques described in section H.

The above procedure is described in detail in the following sections.

B. Scanning the Spark-Chamber Film

The film with the 93,000 spark-chamber pictures acquired during quark runs was scanned in order to select all of the events having "single" tracks. An event was said to have "single" tracks if the following three conditions were satisfied:

1) there were at least two sparks in one chamber and at least three sparks in the other chamber, with the sparks in each chamber being colinear or nearly so (i.e., there was a "track" in each chamber),

2) there were no indications that more than one particle had traversed the chambers (i.e. there were not more than one track in each chamber and no "extra-particle" lights were lit), and

3) the tracks were sufficiently aligned to allow the centers of all of the sparks seen in both chambers in each view on a projection screen to fit inside two ruled lines whose separation was set so that nearly 100% of the tracks made by cosmic-ray particles would be accepted.

For an event having single tracks, the spark chambers thus appeared to have been traversed by a single particle with little or no scattering.

To increase the scanning efficiency, and to determine this efficiency, two-thirds of the film was rescanned. A total of 1,948 events were found which had single tracks.

Only rough alignment of the tracks in the two spark chambers was required at this stage in order to save time in scanning. More stringent criteria for track alignment were imposed at a later stage, when measurement of track misalignments was more practical (see section F).

C. Pulse-Height Calibrations

Because the responses of the analyzer and the electronics were slightly nonlinear, the pulse heights recorded by the analyzer were not expressed on a scale linearly proportional to output charge from the counters. The pulse-height data for each event having single tracks were therefore linearized to facilitate further analysis. The linearization was accomplished by converting each pulse height to its corresponding value on an arbitrary linear voltage scale using the channel-number-versus-SKL-voltage data from the SKL runs.*

The pulse-height data were then normalized to make the effective overall gains of all of the counters be the same (i.e. to make the most probable energy loss of a particle in terms of normalized pulse heights be the same in every counter). The normalization was accomplished by multiplying each pulse height by a factor which had been prepared for the counter and the quark run being considered by analyzing the pulse-height distributions obtained from the CR-A runs.*

---

*The SKL and CR-A runs which were appropriate for linearizing and normalizing the pulse-height data from a particular quark run were the runs of these types which either immediately preceded or immediately followed that quark run. The linearization coefficients and the normalization factors determined from these runs usually varied so little, however, that averages were taken over one to two month periods in order to reduce statistical fluctuations. The average quantities were then used as the appropriate coefficients and factors.

The normalization adopted placed the most probable pulse height for a unit-charged cosmic-ray particle traversing the array vertically at normalized channel 150.0. With this normalization, the most probable pulse height for the normalized distributions obtained from CR-A runs was approximately channel thirty-three. The most probable channel for CR-A runs was not 30.0, as for L-V-CR runs, because the average path length of a particle in a counter is longer if the restriction is not imposed to accept only those particles traversing the counter nearly perpendicularly.

D. Chi-Square Analysis

A pulse-height restriction was imposed at this stage to determine the limits on the range of acceptable pulse heights more accurately than they had been for triggering purposes (see section II.C). No event was considered for further analysis unless it had single tracks and there was at least one counter in each tray with normalized pulse heights between 0.04 and 0.7 minimum.

Each event satisfying these requirements was tentatively assumed to have resulted from the passage of a particle through the array. To determine the most probable energy loss of this particle, a most probable pulse height (MPPH) was to be computed. To determine whether the pulse heights for each event actually corresponded to the energy losses of a particle traversing the array, a quantity termed a modified chi square (X^2) was to be computed.

Instead of computing one MPPH and one X^2 for each event, MPPH's and X^2's were computed for all possible combinations of pulse heights which were within the range 0.04 to 0.7 minimum. This was done for the following reasons.

There were many events in which the pulse heights in both counters in one or more G trays were between 0.04 and 0.7 minimum. The four G counters which had supposedly been traversed for each of these events could not be determined by examining the pulse-height data alone. The G counters most likely traversed could be identified, however, by examining the spark-chamber picture for each event to determine the location of the tracks.

Nevertheless, making these examinations at this point for almost every event would not have been as practical as making them at a later stage for only a small fraction of the number of events (section E). Therefore, for each event, a MPPH and a X^2 were computed for every combination of six pulse heights, one pulse height per tray, which were all between 0.04 and 0.7 minimum. Each combination was labelled by the corresponding set of six counters: S1, S2, and one G counter from each G tray.

If the pulse heights in S1, S2, or both counters in any G tray were below 0.04 minimum or above 0.7 minimum for a particular event, that event was rejected. If the pulse heights in all ten counters were within the acceptable range, there would be sixteen combinations for that event. Although many "wrong" combinations were thereby considered, the combination corresponding to the set of counters traversed by the particle (if there had been one) was certain to be included.

The techniques used to compute the MPPH for a given combination were modifications of those used in a maximum-likelihood method.[36] To use the maximum-likelihood method directly, one first forms a likelihood function. In the case at hand, this would be the product of six theoretical expressions. Each expression would describe the pulse-height distribution which would result when particles with a given speed and a particular fractional charge are passed through one of the six counters for the combination being considered.

Because no equipment had been included in the array for the purpose of determining a particle's speed, an assumption would have to be made to determine the speed of the particle tentatively assumed to have traversed the array for the event considered. The six theoretical pulse-height distributions would then be a function only of the common MPPH, to be determined, and the properties of the corresponding counters (e.g. resolutions). To maximize the likelihood of obtaining a given set of six pulse heights, one would maximize the likelihood function relative to the MPPH.

A difficulty with this direct approach was that it would incur too much computer expense. There are two reasons for this. First, the theoretical pulse-height distributions do not have a simple algebraic form. This is true even if they are assumed to be essentially the same as suitably scaled versions of the distributions resulting from the passage of cosmic-ray muons through these counters, because the latter distributions are expressed only in numerical form.[37-39]

Second, even if the distributions could be expressed in numerical (e.g. tabular) form, tedious calculations would be involved in producing the final distributions applicable for each combination. The reason is that the width of each distribution is a function of the MPPH, which is as yet undertermined.

For example, to obtain a particular distribution having a certain MPPH, the corresponding cosmic-ray distribution would have to have its contribution from electron statistics removed, the resulting distribution would have to be scaled to the given MPPH, and the electron statistics appropriate for this MPPH would then have to be incorporated (see appendix B). Maximizing the likelihood function by varying the MPPH would involve repeated calculations of this type for each combination until the "best" value of the MPPH was obtained.

If the pulse-height distributions had been Gaussian, the direct procedure would reduce to minimizing a chi square. However, as illustrated by the experimentally observed pulse-height distribution shown in figure 3 for the passage of cosmic-ray muons through a typical G counter, the theoretical distributions would not be symmetrical. They would be skewed toward larger energy losses as described by Symon-Landau statistics.[37-39] The usual least-squares analysis could therefore not be used.

FIGURE 3: A TYPICAL G-COUNTER PULSE-HEIGHT DISTRIBUTION

OBTAINED FROM A L-CR-A RUN

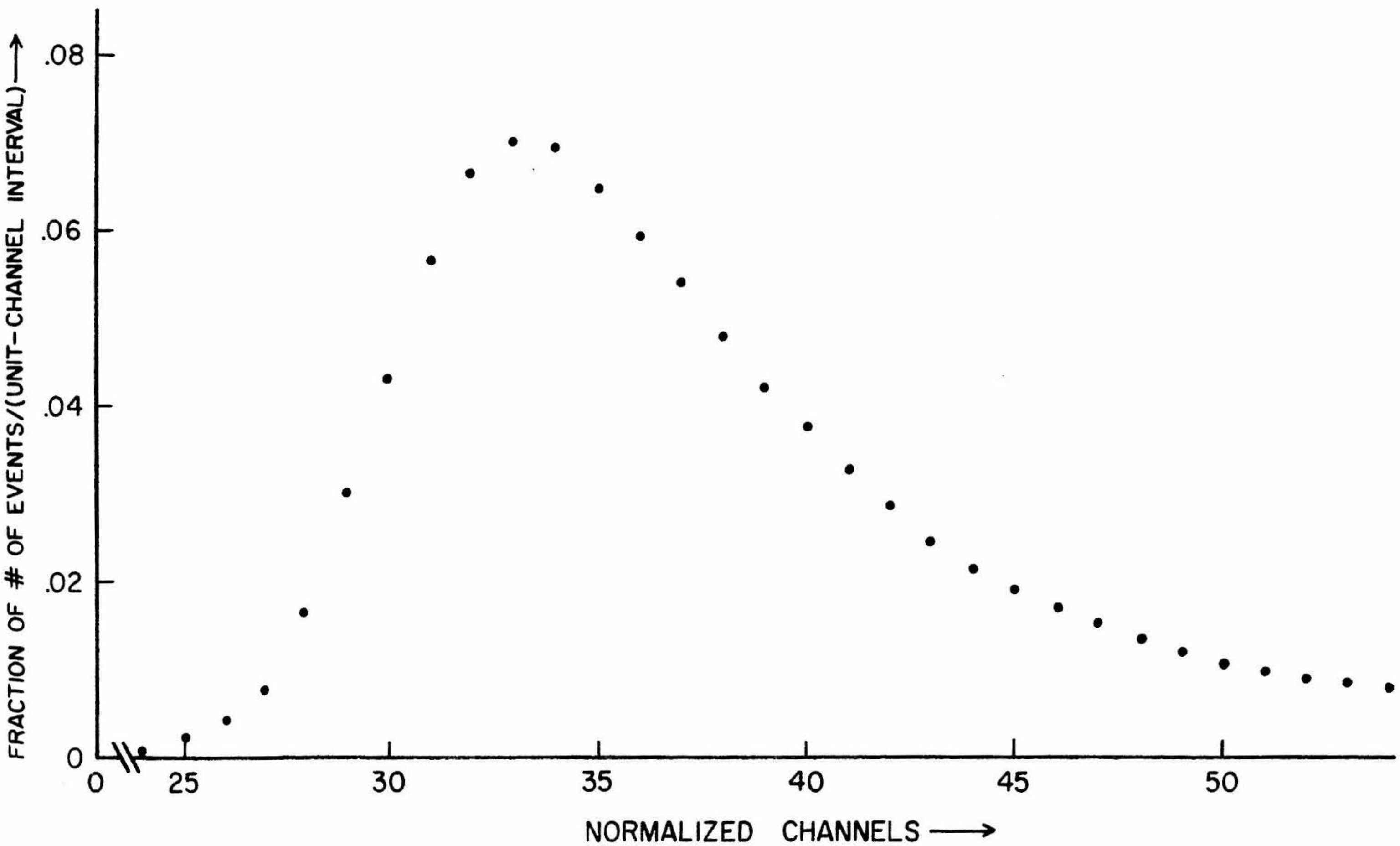

For these reasons, an analysis procedure was developed which was based on the observed distributions for cosmic-ray particles and which incorporated the use of relatively simple expressions to approximate the complex shape of these distributions. The criteria used to determine whether the six pulse heights for a particular combination actually corresponded to the energy losses of a particle traversing the array were then relaxed to such an extent that the procedure was effectively rather insensitive to the exact form assumed for the energy-loss distributions.

The methods utilized can be summarized as follows. A formula to be used in MPPH computations was derived using a maximum-likelihood method based on Gaussian distributions. An expression for a chi-square was obtained as a by-product of this derivation. The formulas developed, however, were not used in a straight-forward manner. Instead, they were used in an iterative computational procedure which allowed the asymmetry of the pulse-height distributions to be introduced.

The expression for a MPPH was obtained by maximizing a product of six Gaussian distributions relative to their common mean. The distributions were given different standard deviations to represent the different resolutions of the counters. The expression which resulted was the following weighted mean pulse height:

$$\text{MPPH} = \frac{\sum_{i=1}^{6} \left(x_i/\sigma_i^{\,2} \right)}{\sum_{i=1}^{6} \left(1/\sigma_i^{\,2} \right)}$$

Here, the x_i, $i=1,\ldots,6$, are the six pulse heights for a given combination, and the σ_i are the corresponding standard deviations.

Because Gaussian distributions were being considered, maximizing the likelihood function was equivalent to minimizing the associated chi square:

$$X^2 = \sum_{i=1}^{6} \left[\frac{(x_i - \text{MPPH})^2}{\sigma_i^{\,2}} \right]$$

Note that the X^2 is a measure of the deviation of the six pulse heights from the MPPH.

The assumption was then made that the part of a pulse-height distribution on each side of its peak could be approximated as being one-half of a Gaussian distribution.* The standard deviations corresponding to the "left" and "right" halves, σ_{L_i} and σ_{R_i}, were computed as functions of the MPPH for each of the six distributions involved for the combination considered. The skewness of the pulse-height distributions was introduced by the use of the above formulas in an

*This is an excellent approximation for the low-energy-loss side, but not a very good approximation for the high-energy-loss side because of the "tail" extending to very large energy losses (see figure 3). Nevertheless, the Gaussian approximations are close enough so that no significant error was introduced.

iterative computational procedure in which either σ_{L_i} or σ_{R_i} was used in place of σ_i depending on whether x_i was smaller or larger than the value of the MPPH computed in a previous step. The techniques employed are described in detail in appendix B.

Because the usual chi-square probability distribution can not be used when treating asymmetric distributions, the significance of having a particular value of X^2 was determined through calibration with cosmic-ray events. X^2's were computed for 1,404 cosmic-ray events having "single" spark-chamber tracks.* The differential distribution of the number of cosmic-ray events as a function of X^2 was formed, and is shown in figure 4. The corresponding integral distribution is shown in figure 5. From the integral distribution, one can see that 90% of all cosmic-ray events would be included in the X^2 analysis by placing an upper limit on acceptable X^2 values at sixteen, 96% would be included by placing the limit at thirty, et cetera.

To determine whether the same percentages would also apply for fractionally charged particle events, integral X^2 distributions were computed for minimum-ionizing particles of charge 1/3 and charge 2/3 using Monte Carlo techniques. Pulse-height distributions corresponding to the passage of these particles through the array were formed by suitably scaling the experimentally observed cosmic-ray distributions in accordance with electron

---

*For these events, the combinations with the smallest X^2's were also the combinations whose set of G counters was the same set which had been traversed by a particle according to the location of the tracks in the spark-chamber pictures.

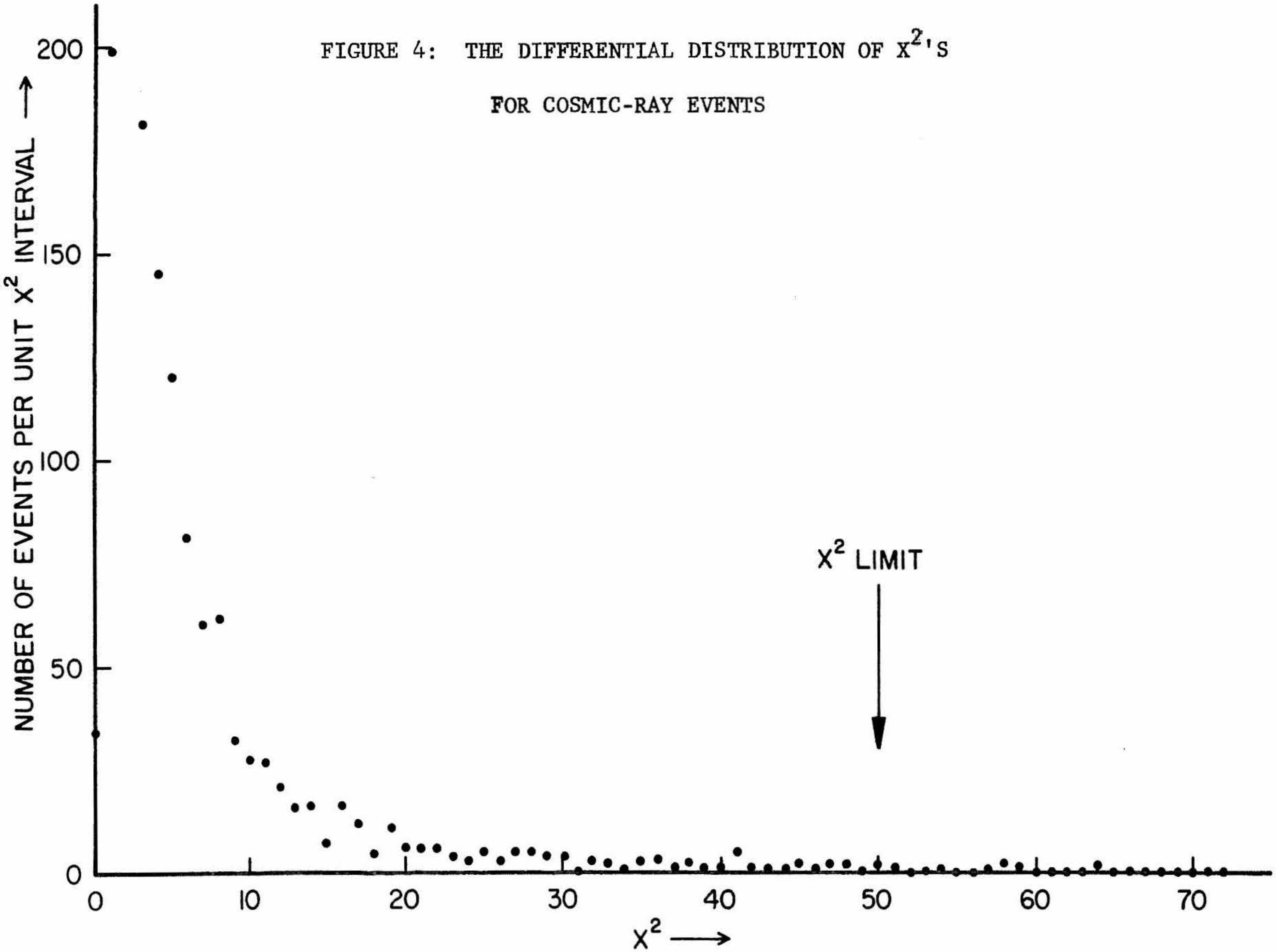

FIGURE 4: THE DIFFERENTIAL DISTRIBUTION OF X^2'S FOR COSMIC-RAY EVENTS

FIGURE 5: THE INTEGRAL DISTRIBUTION OF X^2'S

FOR COSMIC-RAY EVENTS

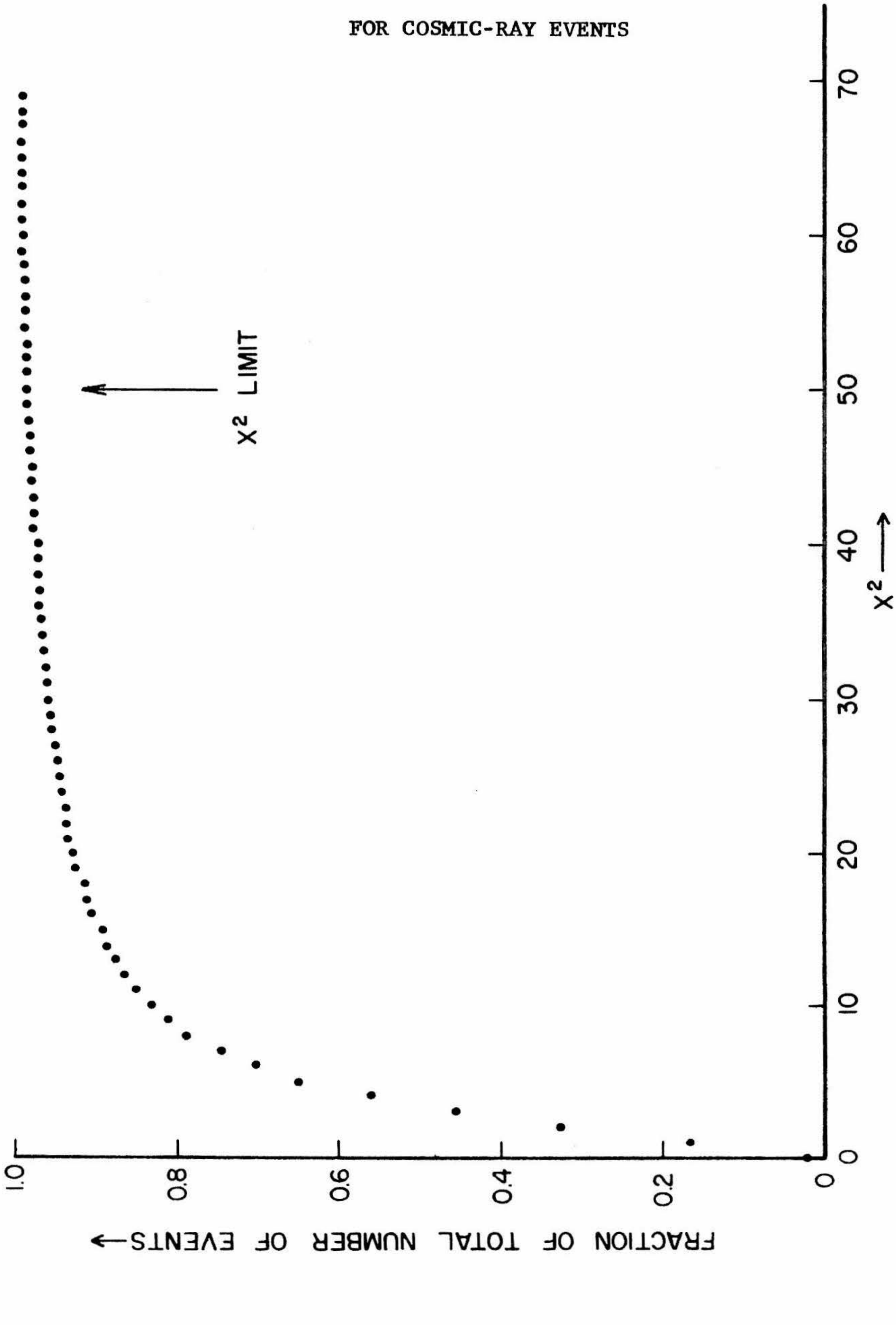

statistics in the photomultiplier tubes on the counters.* In forming these pulse-height distributions, S1 and S2 were assumed to have the same resolution, as were G1 through G8.

Events simulating the passage of particles with charge 1/3 or charge 2/3 were then generated by choosing pulse heights between 0.04 and 0.7 minimum at random in accordance with the distributions just formed. Two S-counter pulse heights and four G-counter pulse heights were chosen for each Monte Carlo event. X^2's were computed for these events in the same manner as for cosmic-ray events, and integral X^2 distributions were formed.

For purposes of comparison, an integral X^2 distribution was computed for minimum-ionizing particles of unit charge using similar techniques. In this case, however, the Monte Carlo events were generated by choosing two S-counter pulse heights and four G-counter pulse heights directly from the observed cosmic-ray distributions (after scaling them up by a factor of five, and ignoring the 0.04- and 0.7-minimum pulse-height limits).

The integral X^2 distribution which resulted for each charge is given in figure 6. For comparison, the curve shown in figure 5 for cosmic-ray events is reproduced and is labelled "CR." The difference between the distribution for unit charge and the

---

*This entailed removing the contribution from electron statistics from the cosmic-ray distributions, scaling the resulting distributions to 1/9 or 4/9 minimum, and then incorporating the electron statistics appropriate for the counters considered and for 1/9 or 4/9 minimum.

FIGURE 6: THE INTEGRAL DISTRIBUTIONS OF X^2'S FOR CHARGES 1/3, 2/3, AND 1

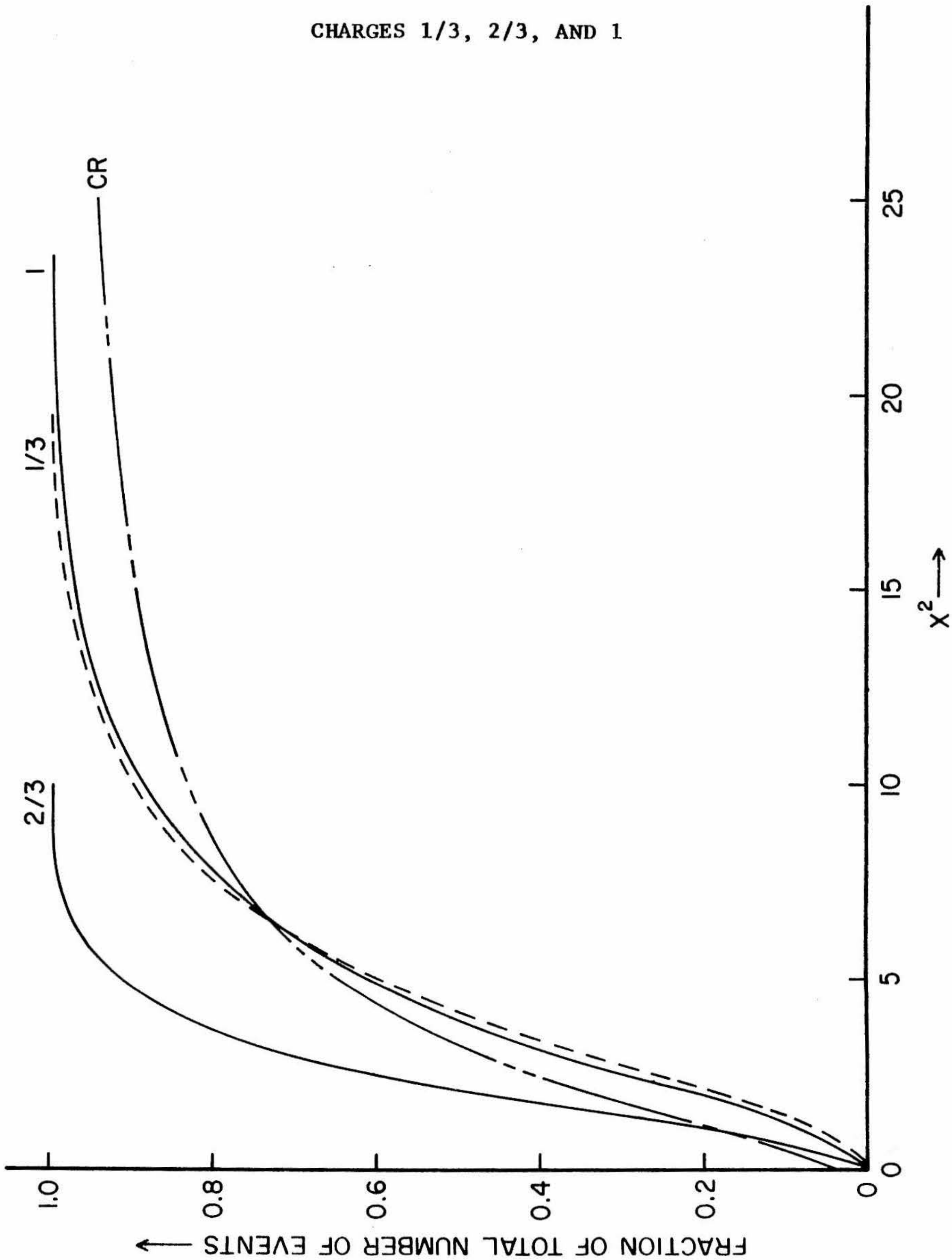

CR distribution was attributed to correlations between the pulse heights in adjacent counters.*

The integral distribution for charge 2/3 rises faster than the one for unit charge because a sizeable fraction of the pulse heights for charge 2/3 are above the 0.7-minimum pulse-height limit. The integral distribution for charge 1/3 is almost identical to the one for unit charge because very few pulse heights for charge 1/3 are below the 0.04-minimum pulse-height limit.

In other words, an inefficiency resulted from the use of counters with finite energy-loss resolution to detect particles with certain charges because limits were imposed on the range of acceptable pulse heights (see section V.A). This inefficiency is reflected here in an integral X^2 distribution which rises faster than the one for unit charge, for which no pulse-height restrictions were imposed. As a result, the integral X^2 distributions for fractionally charged particle events rise just as fast or faster than the one shown for cosmic-ray events.† **

---

*The correlations may have been caused by energetic delta rays which were produced in one counter but stopped in the counter below.

†The faster rise is expected to persist even if the 1/3 and 2/3 distributions are modified to include the effect which accounts for the difference between the unit-charge and CR distributions.

**The curves shown in figure 6 were computed for minimum-ionizing particles. The statement referred to above is true, however, even if the particles are not minimum-ionizing. The reason for this is that, for this discussion, a shift in speed is equivalent to a shift in effective charge.

The reasons for choosing a particular upper limit on acceptable X^2 values can now be enumerated. On the basis of the above discussion, the percentage of all fractionally charged particle events which would be included in the X^2 analysis by placing the upper limit at a particular value of X^2 is at least as high as the percentage indicated in figure 5 for that X^2 limit. For example, at least 96% of all events would be included by placing the limit at thirty.

Furthermore, events with no combinations with X^2's smaller than seventy almost always had spark-chamber tracks which were not "single." "Wrong" combinations (e.g. cosmic-ray combinations whose corresponding counters were not the ones traversed by the particle) generally had X^2's larger than 100.

For these reasons, the maximum acceptable X^2 value was arbitrarily chosen to be fifty. Only twelve out of the seventy-eight quark-run events with pulse-heights between 0.04 and 0.7 minimum in each tray had X^2 values below this limit. These twelve events had a total of nineteen acceptable combinations.

With the X^2 limit set this high, the efficiency of the X^2 analysis was quite insensitive to the exact details of the energy-loss distributions assumed for particles with fractional charges. The analysis procedure was thus less dependent than the procedures used in other counter experiments upon the assumption that these distributions were essentially the same as that for cosmic-ray muons.

E. G-Counter Agreement

To define the fiducial volume for the spark chambers and to limit the X^2 analysis of each event to effectively only those counters most likely traversed by the particle for that event, each acceptable combination was required to have "G-counter agreement." That is, its corresponding set of G counters was required to be the same set which should have been traversed by the particle for that event according to the location of the tracks seen in the spark-chamber picture. The G counters which should have been traversed were determined by placing a counter template over the projected image of the spark chambers, aligning the template relative to the spark-chamber fiducial lights, and seeing which G counters marked on the template were intersected by rectilinear extensions of the tracks.*

If one or more G counters chosen for a particular combination were not intersected by the track extensions, that combination was rejected. If the track extensions passed through an outside edge of a counter, indicating that the particle had not traversed the entire thickness of the counter, all combinations for that event were rejected. If a combination had G-counter agreement except in (e.g.) one tray, in which the G counter that should have been traversed could not be identified because the track extensions

---

*The positions of the G counters had been marked on the template for this purpose according to the positions of the edges of the counters as seen on the projection screen when viewing spark-chamber pictures taken when the array had been suitably lighted.

passed between the two counters in that tray, then the combination was not rejected. Only three events (combinations) had G-counter agreement.*

F. Measurement of Track Misalignments

In an effort to ensure that each acceptable event had resulted from the passage of a particle through the array, three requirements had been imposed. The first and second, discussed respectively in sections D and E, were having at least one combination with both a X^2 less than or equal to fifty and G-counter agreement. The third, discussed in this section, was having spark-chamber tracks whose degree of misalignment was no worse than those determined for cosmic-ray tracks.

For a particular event, the track misalignment was determined by making four measurements: one "angular misalignment" and one "lateral misalignment" of the tracks seen in both the front view and the side view on a projection screen with a scale of one to three (projected size to actual size in the array). As illustrated in figure 7, the angular misalignment was determined

---

*The MPPH's for these combinations were 19.6, 43.4, and 29.1. Their X^2's were respectively 24.4, 36.0 and 31.3.

FIGURE 7: MEASUREMENT OF SPARK-CHAMBER TRACK MISALIGNMENTS

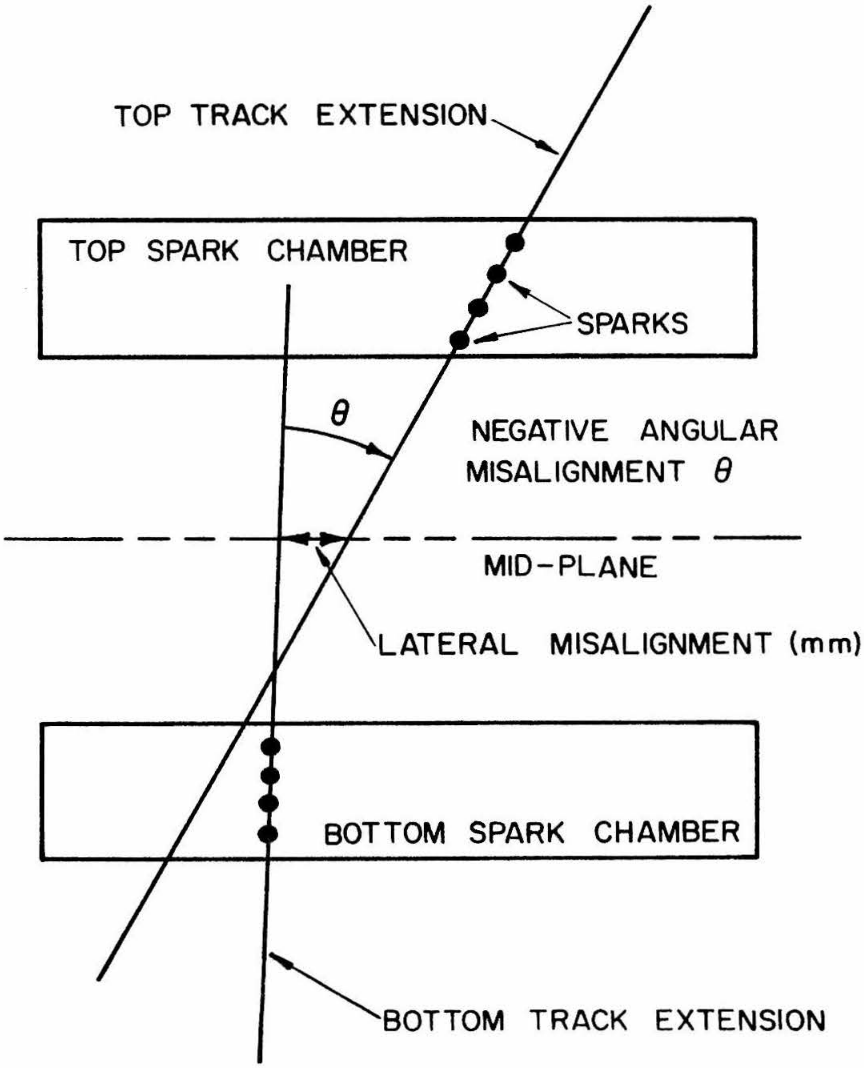

Angular misalignments were measured from the bottom track extension to the top track extension (positive counterclockwise).

by measuring the (signed) angle between the track extensions.*
The lateral misalignment was determined by measuring the (unsigned) distance in millimeters between the intercepts of the track extensions with a plane located midway between the two chambers.*

The four measurements for each of the three events having G-counter agreement were compared with the distributions of the corresponding quantities measured for 206 cosmic-ray events (each having "single" tracks and at least one combination with a $X^2 \leqslant 50$ and G-counter agreement). The differential and integral distributions for the number of cosmic-ray events as a function of each track misalignment are given in figures 8 through 11.†

For a quark-run event to be acceptable, each of the four misalignments measured for its tracks had to be smaller than the worst misalignments measured for the cosmic-ray events. As shown by the positions in figures 8 through 11 of the labels 1, 2, and 3, which refer to the track misalignments measured for the three quark-run events with G-counter agreement, no event was acceptable. To be sure, larger cosmic-ray misalignments might have been recorded if more than 206 events had been measured. For example, an event having a larger scattering but still having "single" tracks might then have been observed. Nevertheless, even

*The measurements were accurate to ± 0.5 mm and ± 0.5 degree.

†One may note that the most probable side-view angular misalignment was not zero degrees as for the front view; this shift could have resulted from a non-coplanar orientation of the two side-view mirrors.

FIGURE 8: FRONT-VIEW LATERAL MISALIGNMENTS

FOR COSMIC-RAY EVENTS

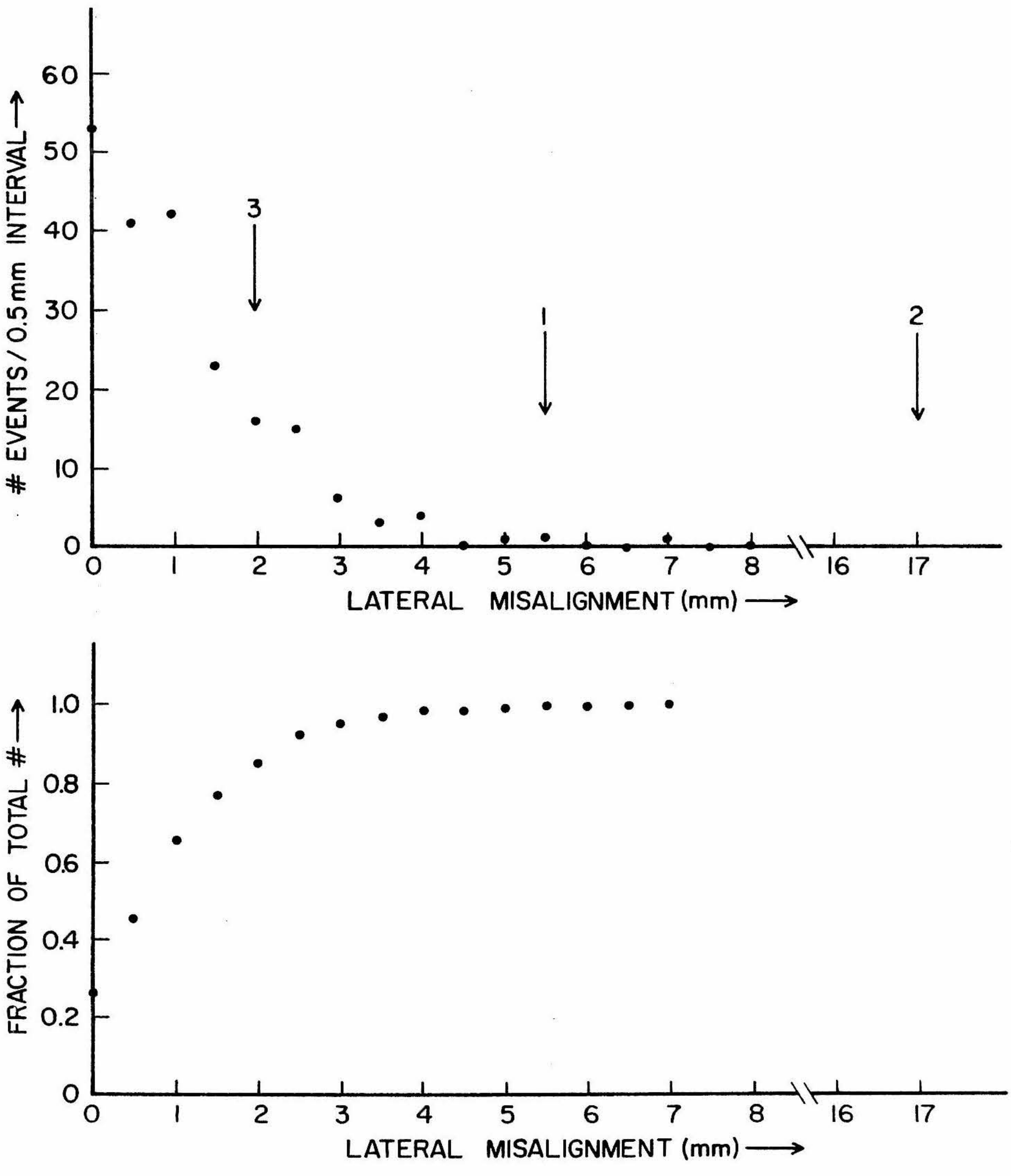

FIGURE 9: FRONT-VIEW ANGULAR MISALIGNMENTS

FOR COSMIC-RAY EVENTS

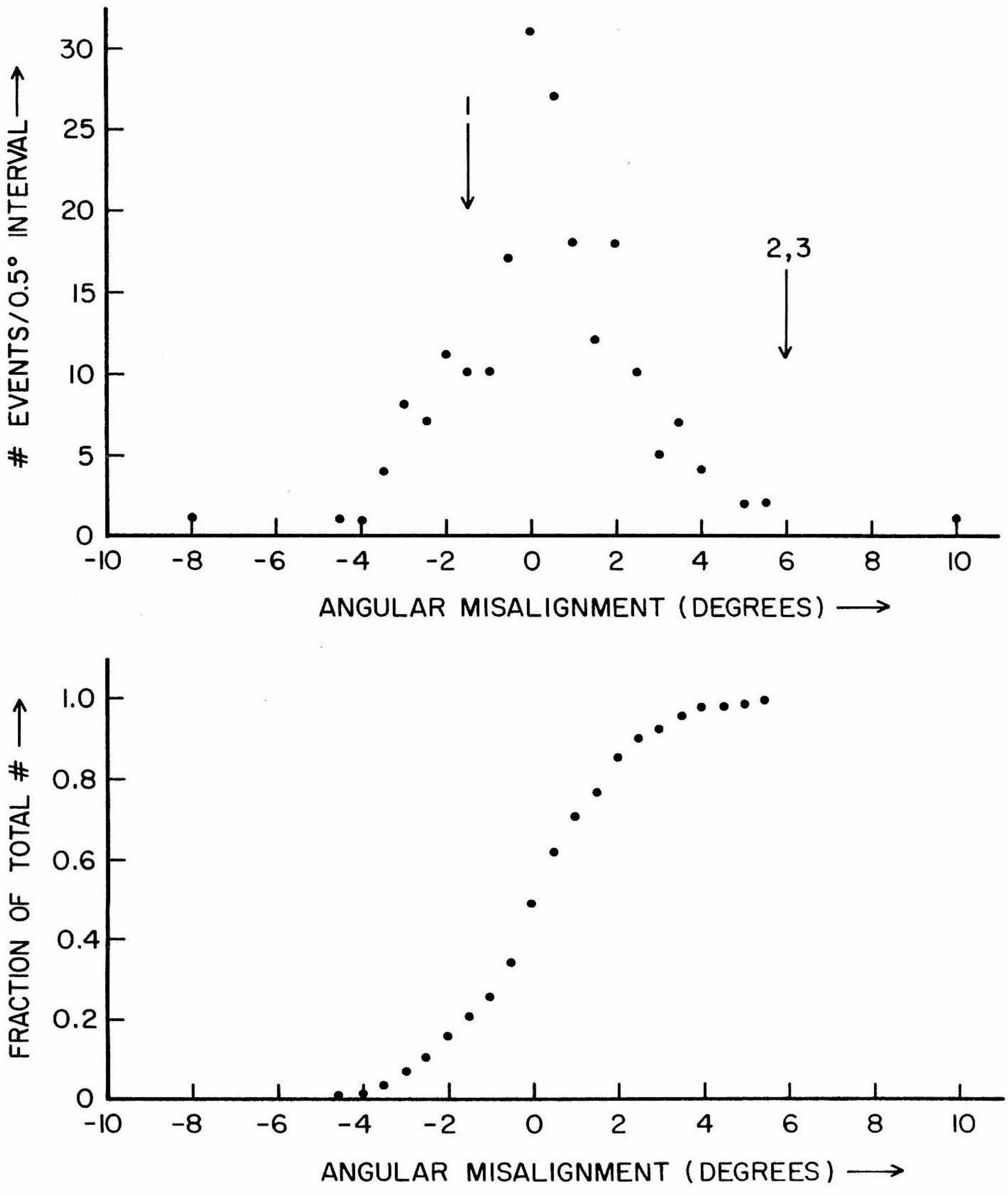

FIGURE 10: SIDE-VIEW LATERAL MISALIGNMENTS

FOR COSMIC-RAY EVENTS

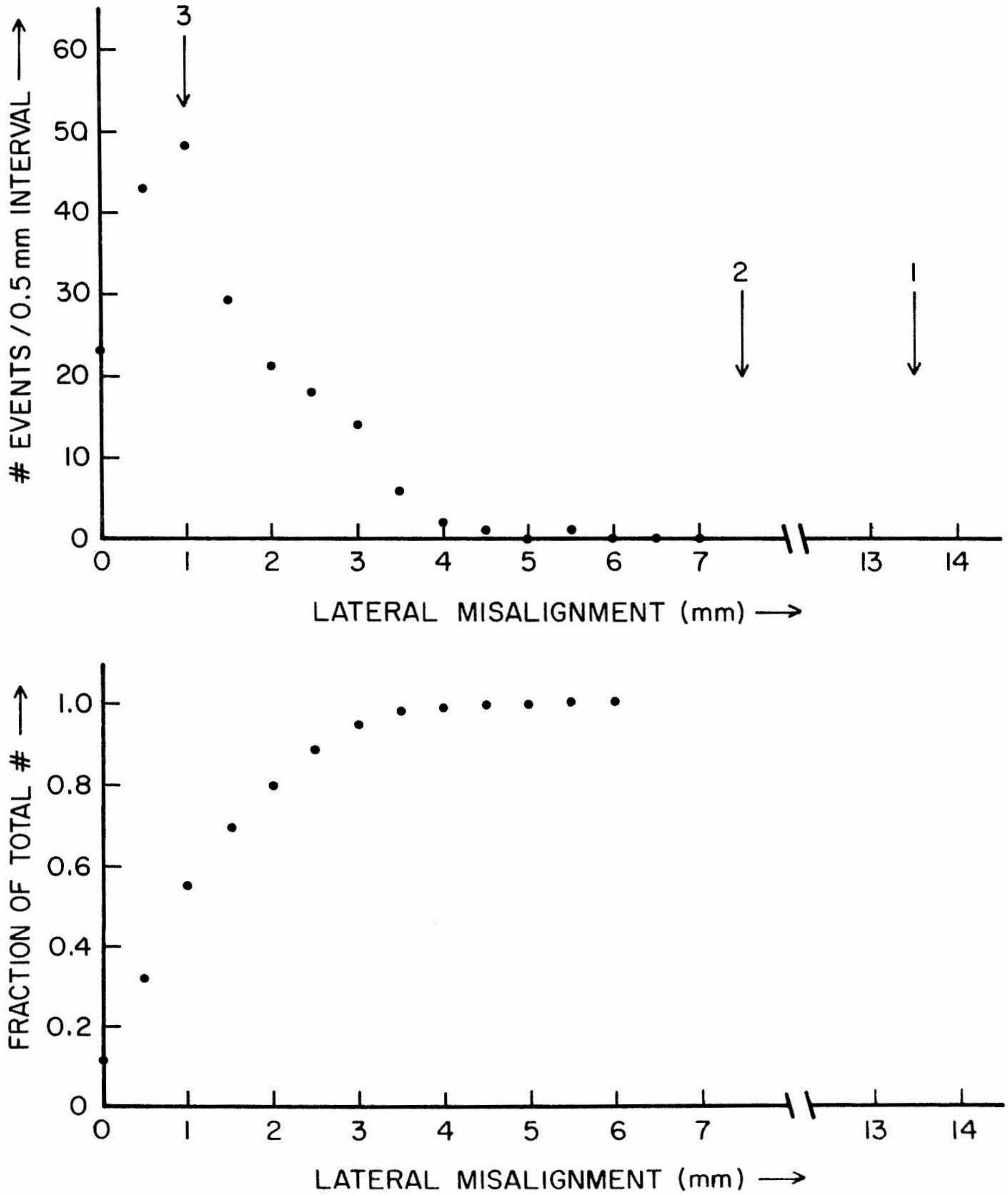

FIGURE 11: SIDE-VIEW ANGULAR MISALIGNMENTS

FOR COSMIC-RAY EVENTS

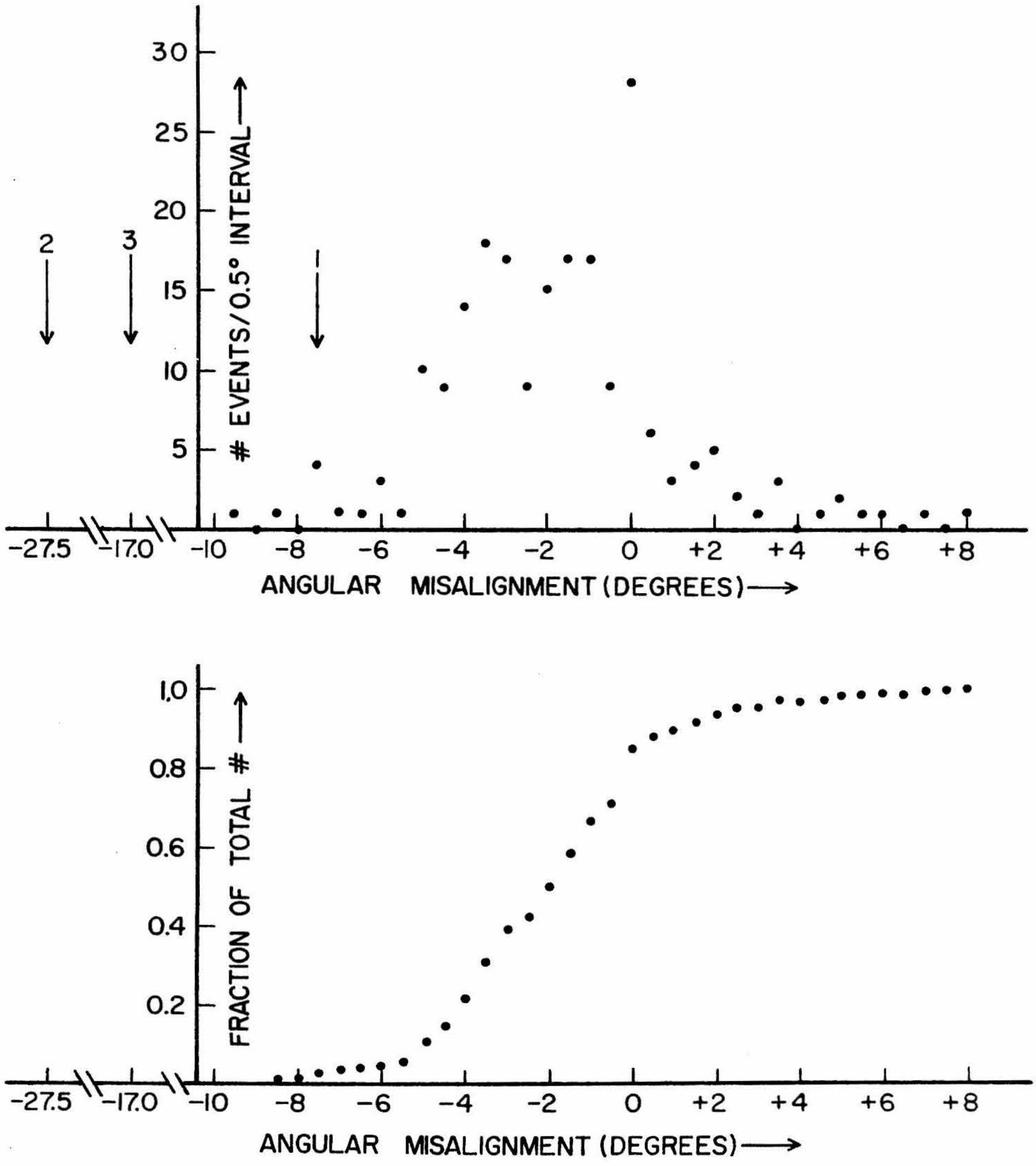

if one of the three quark-run events had then been able to satisfy the above requirements, the probability that its tracks had resulted from a particle traversing the array would still be expected to be much smaller than 1/206.*

G. Oscilloscope Check and A Summary

Had there been any events satisfying the track-misalignment criteria described in the previous section, their oscilloscope pictures would have been examined. Such an examination would have been made to see if there were any pulses which might indicate that the spark-chamber tracks had actually formed along the ionization path of a cosmic-ray particle which had traversed the chambers within a few tenths of a microsecond from the time of occurrence of the ionization that resulted in the generation of the trigger pulse.

Because there were no events reaching this stage in the analysis, the oscilloscope checks were made for the three events having G-Counter agreement. The oscilloscope data for each of these events were found to be in complete agreement with the pulse-height data recorded by the analyzer and with the hypothesis

---

*It is difficult to determine the probability that a particular set of tracks had resulted from a particle traversing the array because there are correlations among the four misalignment measurements. However, an upper limit for this probability is given by the smallest of the four probability figures which can be obtained on the basis of the four integral distributions shown in figures 8, 9, 10, and 11.

that only one particle had traversed the array.

A summary of the cumulative restrictions imposed during the analysis of the data is given in table 4 along with the effectiveness of each analysis requirement in reducing the number of background events.*

H. Estimating a Particle's Charge From a MPPH

If there had been events with the necessary properties to satisfy all of the requirements, they would have been assumed to have resulted from the passage of fractionally charged particles through the array. The charges of these particles could have been estimated in the manner described below.

Consider an event which resulted from the passage of a particle of charge Q and speed v through the array. Let $\emptyset$ be the angle from the normal to a tray made by the particle's tracks in the spark chambers. Let the particle's most probable energy loss in a counter in units of normalized channels be designated by MPPH($\emptyset$). This is the quantity which was experimentally predicated to be the MPPH for that event.

*Some of the 1,856 events which were eliminated by requiring normalized pulse heights between 0.04 and 0.7 minimum were cosmic-ray events which had been accepted by the electronics because the upper biases on the discriminators were set somewhat above 0.7 minimum. The overwhelming majority of the 1,856 events, however, were background events which had been included because the lower biases were set between one-fortieth and one-sixtieth minimum.

TABLE 4: THE ANALYSIS REQUIREMENTS AND THEIR EFFECTS

Cumulative Analysis Requirements	Remaining Events	Combinations
1. Quark-run trigger generated	93,000	
2. "Single" spark-chamber tracks according to original scan and/or rescan	1,948	
3. Pulse heights recorded by the analyzer on papertape	1,934	
4. At least one combination with all normalized pulse heights between channels 6. and 106. (i.e. between 0.04 and 0.7 minimum)	78	150
5. At least one combination with a X^2 less than or equal to 50	12	19
6. At least one combination with "G-counter agreement"	3	3
7. All four spark-chamber track misalignments smaller than the worst misalignments measured for cosmic-ray events	0	0
8. Oscilloscope data consistent with the analyzer's pulse-height data and the hypothesis that only one particle had traversed the array	0	0

Because the most probable energy loss of a particle traversing a counter is very nearly proportional to its path length in that counter,[37] the most probable energy loss which would have resulted if the particle had traversed the array vertically ($\emptyset=0$) is given by $\mathrm{MPPH}(0) = \mathrm{MPPH}(\emptyset)\cdot\mathrm{Cos}\emptyset$. The particle's most probable energy loss in units where 1.0 represents minimum is therefore given by MPPH(0)/150.0, because pulse heights were normalized so that minimum was channel 150.0.

To determine the particle's charge, we first note that a particle's most probable energy loss is proportional to the square of its charge, and is a function of its speed v.[11,37-39]

$$\mathrm{MPPH}(0) = Q^2\cdot f(v)$$

With the pulse-height normalization used in this experiment, $f(v) = 150.0$ if the particle considered is minimum-ionizing. In such a case, the particle's charge would be given by $Q^2 = \mathrm{MPPH}(\emptyset)\cdot\mathrm{Cos}\emptyset/150.0$.

In general, however, v is entirely unknown because no equipment was included in the array for the purpose of measuring the speed of a particle. Q, therefore, can not be determined unless an assumption is made which allows v to be specified.

Suppose we assume that the particle was minimum-ionizing. There are still complications, however, because the MPPH($\emptyset$) for a given event is known only to within experimental error. A MPPH had been computed with the intention of obtaining the MPPH($\emptyset$), but the MPPH and the MPPH($\emptyset$) are in general not the same.

The difference results because there is inherent uncertainty involved in predicting a parameter of a pulse-height distribution when given only six pulse heights as a sample. This uncertainty gives rise to a possible statistical error in the MPPH. In other words, the distribution of MPPH's which would result if many samples of six pulse heights were chosen in accordance with a given set of six pulse-height distributions would have a non-zero width. As examples of the fluctuations expected for MPPH's computed for particles with different charges, the distributions of MPPH's for events corresponding to the passage of minimum-ionizing particles of charge 1/3 or charge 2/3 through the array are shown in figure 12 normalized to unit area.* The dashed curve shown is a portion of the corresponding distribution for particles of charge 1.

The MPPH, to be sure, is a better estimator for the MPPH(Ø) than the average pulse height (AVPH) is for the mean energy loss. This is demonstrated by the relative widths of the corresponding distributions shown in figure 13 as they were computed for cosmic-ray events by ignoring the pulse heights from the B counters. For purposes of comparison, the G-counter pulse-height distribution is also shown. All of these distributions are normalized to unit area. The cosmic-ray events considered are the 1404 events used in the computations for figures 4 and 5 ("single" tracks, G-counter agreement). As one can see, the full width at half maximum for the

*These distributions were formed using Monte Carlo techniques similar to those used to obtain the integral χ^2 distributions shown in figure 6 in section D.

FIGURE 12: MONTE CARLO MPPH DISTRIBUTIONS FOR MINIMUM-IONIZING PARTICLES WITH CHARGES 1/3, 2/3, OR 1

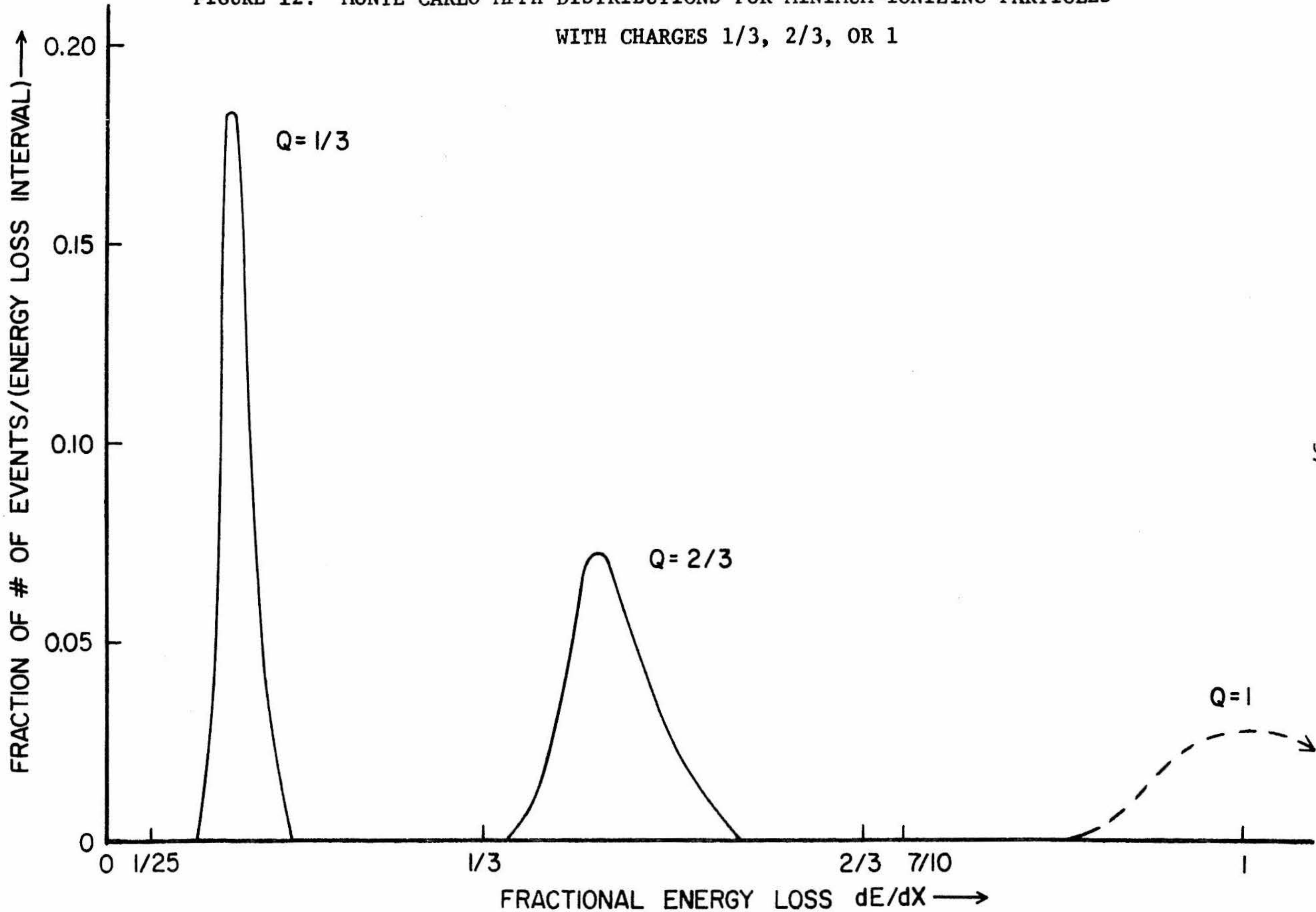

FIGURE 13: VARIOUS PULSE-HEIGHT DISTRIBUTIONS FOR COSMIC-RAY EVENTS

(B COUNTERS IGNORED)

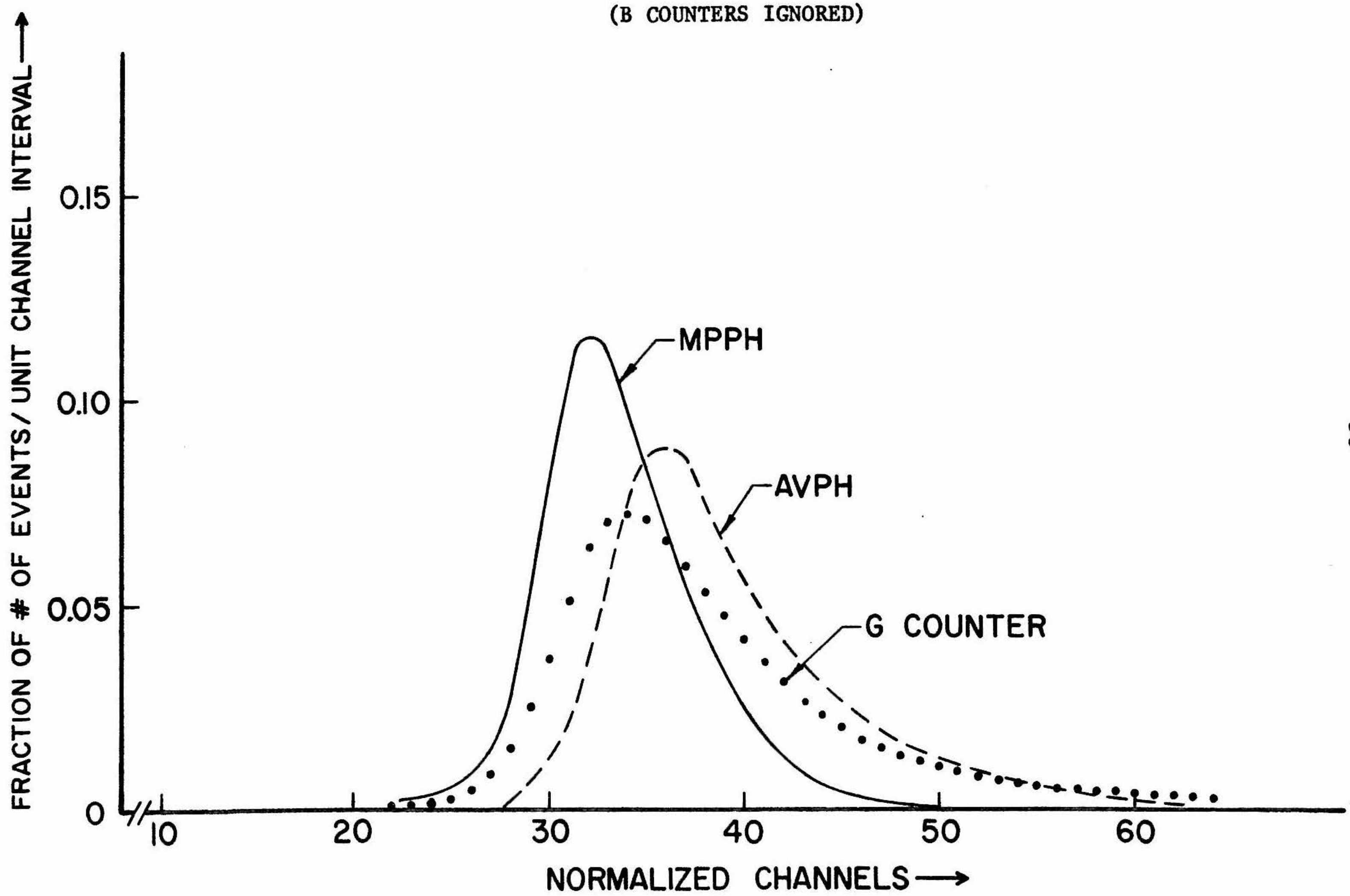

MPPH distribution is approximately 17% smaller than the corresponding width of the AVPH distribution.*

One can also note that the peak of the MPPH distribution does not coincide with the peak of the G-counter pulse-height distribution, and it should. The particular method used to compute MPPH's involved a slight systematic error which caused the most probable value for a MPPH to underestimate the value of the MPPH(Ø).

In summary, any charge determination would be dependent on the particular model assumed for the distribution of speeds for the particles detected. If the particle for a given event is assumed to have been minimum-ionizing, its charge can be determined, but only within the limits of experimental error. If one ignores the systematic error incurred, or computes MPPH's using a more accurate method, the most probable value for the charge of a particle for a given event can be estimated by using $Q^2 = \mathrm{MPPH} \cdot \mathrm{Cos}\phi / 150.0$.

---

*If Monte Carlo events for Q=1 are considered, the improvement is not 17%, but approximately 28%. The difference is attributed to pulse-height correlations which were present in the observed cosmic-ray data (c.f. figure 6).

V: THE EXPERIMENTAL EFFICIENCIES

Although there were no events which corresponded to the passage of fractionally charged particles through the array, the product of the running time, the acceptance of the array, and the experimental efficiency could be used to set upper limits for the fluxes of fractionally charged particles in cosmic rays near sea level. In order to do this, the overall efficiency of the system was determined.

Inefficiencies arose in detecting particles in the counters and in the spark chambers, in scanning the film in search of events with "single" tracks, in recording data by the pulse-height analyzer, and in accepting events using the X^2 and track-misalignment analyses. The determination of the efficiency of the counter system as a function of the square of the charge of the particle detected is described in section A. The difficulties encountered in estimating the efficiency of the spark chambers are discussed in section B. The other experimental efficiencies are given in section C, which considers the overall efficiency.

A. Detection Efficiency of the Counters

An inefficiency resulted from the use of scintillation counters with finite energy-loss resolutions to detect particles with certain charges because limits were imposed on the range of acceptable pulse heights. If a particle with a particular charge and a given speed had traversed one of the counters, any of a number of possible pulse heights could have resulted, as described by a pulse-height distribution (e.g., figure 3). In the analysis of the data, however, no pulse height was considered if it was not between 0.04 and 0.7 minimum. Consequently, the effective efficiency of the counter system decreased as the most probable energy loss of the particle detected increased toward 0.7 minimum because more of the pulse heights in the expected pulse-height distributions were above the 0.7-minimum pulse-height limit. In a similar manner, the effective efficiency decreased as the most probably energy loss decreased toward 0.04 minimum because of the 0.04-minimum pulse-height limit.

An explicit computation of this efficiency is dependent on the particular pulse-height distributions considered. The pulse-height distributions are a function of the speed of the particles detected, as well as their charge.[11,37] The effective efficiency is therefore dependent on the distribution of speeds assumed for these particles. To be specific, we assumed that the distribution of speeds was the same as that for cosmic-ray muons.

The distribution of normalized pulse heights resulting from the passage of a particle with a given charge through a particular counter in the array was then obtained from the corresponding cosmic-ray distribution in the same manner as that used for the Monte Carlo calculations in section IV.D. That is, the contribution from electron statistics was removed from the cosmic-ray distribution, the resulting distribution was suitably scaled, and the electron statistics appropriate for the new energy-loss level were incorporated.

The effective efficiency of the counter system for detecting particles with this charge was determined as follows. Using a computer program, many sets of six pulse heights were constructed; each set contained one pulse height chosen at random in accordance with the distribution formed for each of two S counters and four G counters. The desired efficiency was the ratio of the number of such sets for which none of the six pulse heights was either below 0.04 minimum or above 0.7 minimum to the total number of sets. The results of these computations as a function of the square of the charge of a minimum-ionizing particle detected are shown in figure 14.

The efficiency of the counter system was 100% for the detection of particles with charges near one-half and decreased for the detection of particles with charges smaller or larger than one-half. The efficiency decreased more slowly for the larger charges because the pulse-height distributions are skewed toward higher energy losses (figure 3).

B. Detection Efficiency of the Spark Chambers

As mentioned in Chapters I and II, there had been some question as to whether spark chambers could function for the low

FIGURE 14: THE EFFICIENCY OF THE COUNTER SYSTEM AS A FUNCTION OF THE SQUARE OF THE CHARGE OF ANY MINIMUM-IONIZING PARTICLE DETECTED

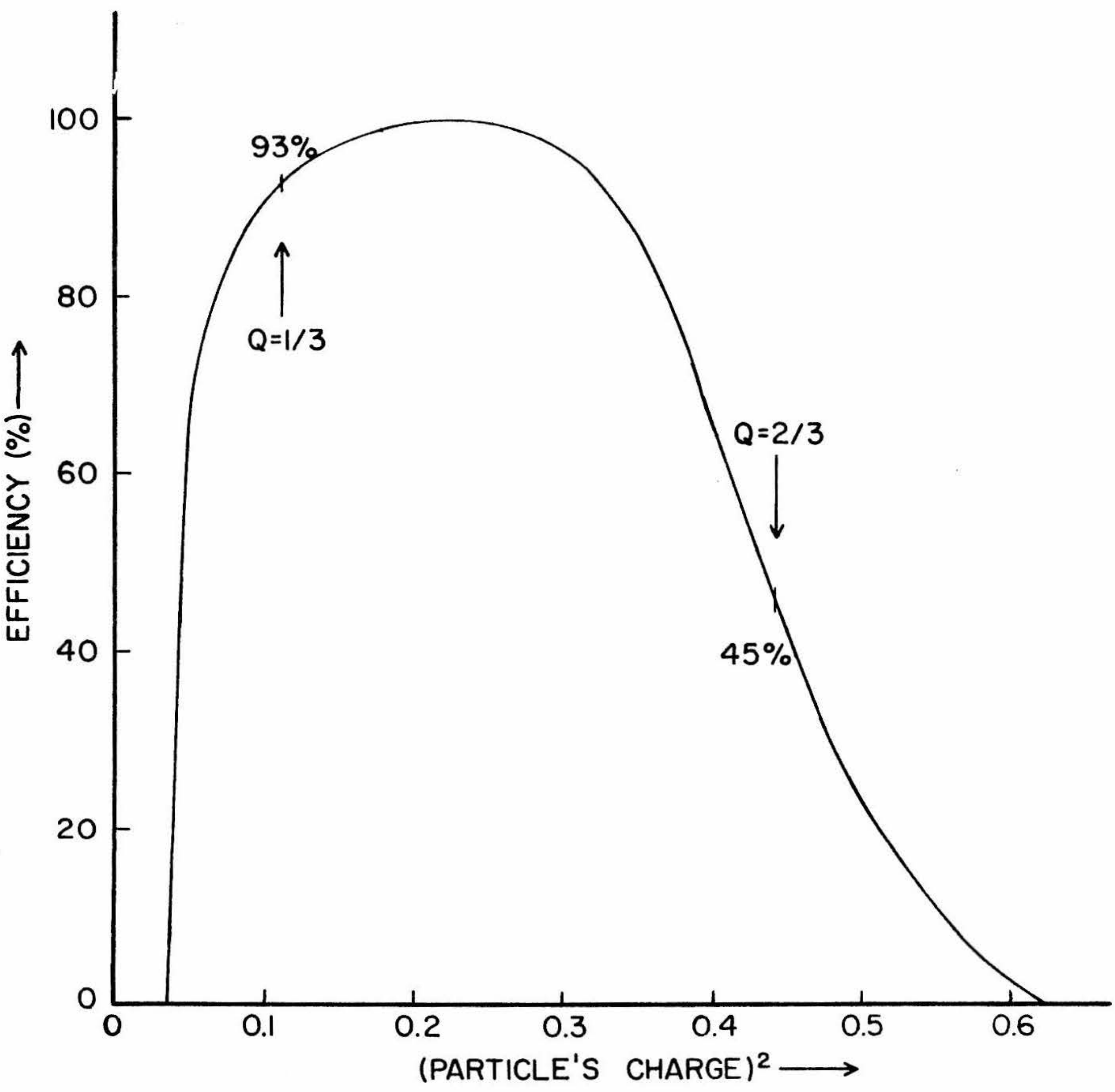

levels of ionization expected from fractionally charged particles. The ionization was expected to be weak because the number of electron-ion pairs produced in each gap by a particle passing through a spark chamber is proportional to the square of the particle's charge. To discover whether our spark chambers could function for the entire range of energy losses considered, some method had to be devised to measure the efficiency of the chambers when operated in search of particles with small fractional charges.

The usual procedure which one employs to measure the efficiency of a spark chamber is to use a convenient source of particles that will produce the desired ionization, repeatedly trigger the chamber on the passage of single particles of this type, and determine the ratio of the total number of gaps which contained sparks along the paths of the particles and the total number of gaps which should have had sparks. This procedure can not be used here, however, because the only particles which can produce ionization significantly below 0.7 minimum are particles with fractional charges, and these particles have not yet been discovered. A direct measurement of the efficiency was therefore not possible.

For this reason, various tests were conducted in an effort to obtain the efficiency by indirect means. These tests indicated that the spark chambers might have been nearly 100% efficient for the entire range of energy losses considered.

In one test, the chambers were operated with tank-pure helium rather than with the 76.0%-argon 22.5%-helium 1.5%-ethanol mixture (hereafter referred to as the AHE mixture). Because a particle produces fewer ion pairs per centimeter in helium than it does in the AHE mixture, the use of helium allows one to simulate a level of ionization with unit-charged particles which should correspond to the level obtained from the passage of a fractionally charged particle through the AHE mixture.

When triggering on unit-charged cosmic-ray particles, the efficiency per gap for spark formation in pure helium was determined to be 96.6% ± 0.2%. The chambers were then operated with 99.35% ± 0.05% helium and 0.65% ± 0.05% ethanol to determine the effect of a small concentration of ethanol, which is a "quenching" agent. In this case, the sparking efficiency per gap was determined to be 97.2% ± 0.2%.*

With the results of these tests in mind, one might expect the efficiency per gap to be at least 96% when the chambers are filled with the AHE mixture and operated in search of any fractionally charged particle which produces no fewer ion pairs per centimeter than that produced by a unit-charged particle in helium. As we will explain later on in this section, only about 5 electron-ion pairs are produced per centimeter for minimum ionization in pure helium while about 37 electron-ion pairs are produced per centimeter for

---

*The efficiency per gap for spark formation in the AHE mixture was determined in the same way to be 99.61% ± 0.04%.

minimum ionization in the AHE mixture.[37,40-42] One might therefore expect the chambers as operated in this experiment to have a sparking efficiency per gap of at least 96% for the detection of particles with fractional charges at least as small as $(5/37)^{1/2} \cong (0.37)$.

For an efficiency per gap of 96.0%, the probability that there will be at least two sparks in one chamber and at least three sparks in the other chamber is 99.1%, according to binomial statistics. Therefore, if one assumes that the efficiency per gap for the passage of a fractionally charged particle is the same as that measured for the passage of unit-charged cosmic-ray particles through a gas mixture which provides the same average number of electron-ion pairs per gap, the efficiency of the spark-chamber system with the track-selection criteria used in this experiment was at least 99%.

Theoretical considerations also indicate that the efficiency of the spark-chamber system might have been this high. Although the theory of spark formation is still not well developed, the present understanding of the phenomenon would lead one to believe that, neglecting statistical fluctuations, only one electron is needed to cause streamer formation in gaps which are operated with a sufficiently large pulsing field (see appendix D).[43-45] For the gap width and gas mixture used in this experiment, one would expect

the sparking threshold to be somewhere between 4 and 11 kilovolts.*
Because the pulsing field used in the experiment was nearly 30 kV/cm, each gap had a percentage overvoltage of at least 170%. Furthermore, 0.04 minimum should have corresponded to about 0.04 X 37 $\simeq$ 1.5 electrons per gap, on the average. Therefore, on the basis of the present understanding of spark formation, the efficiency per gap was expected to have been nearly 100% even for the particles with the smallest charges which could have been detected.

To ascertain whether these considerations were correct, a test was conducted to experimentally determine the minimum number N of electrons which were required in a gap in the spark chambers to cause spark formation upon application of the pulsing field. This test, which was only partially successful, was performed by

1) operating the chambers with a sweeping field (10 v/cm) so that the column of electrons produced by the passage of a particle would be slowly swept out of the gap,

2) introducing a variable time delay between the formation of the ionization in the chambers and the application of the pulsing field,

3) measuring the efficiency per gap for spark formation as a function of the time delay while triggering on unit-charged cosmic-ray particles, and

4) fitting a theoretical expression for the efficiency per gap as a function of time delay to the measured data in order to determine the best value for the parameter N.

---

*This is the range expected for mixtures of helium and argon, according to three different considerations: 1) the Townsend sparking criterion, 2) the single-to-multiple avalanche transition (the E/p at which the spark formative times equal the reciprocal of the electron drift velocity), and 3) the Meek streamer criterion. See appendix D. A tacit assumption here is that the ethanol in the AHE mixture had no significant effect on the sparking efficiency.

Because a fractionally charged particle was expected to provide at least one or two electrons per gap on the average, as noted above, the efficiency per gap would be expected to have been quite high if N = 1. On the other hand, if N were found to be much larger than two, the spark chambers could not have detected particles with small fractional charges.

In conducting the test, the system was operated in the same manner as for a CR-P run, except that

1) two additional spark chambers were added to the array (one directly under the array and one directly on top of the array), and were operated without the time delay so that their tracks would indicate where the cosmic-ray particle for each event had traversed the system,

2) additional scintillation counters were added to the array, as for L-V-CR runs, to restrict the acceptance to only those particles traversing the array nearly perpendicular to the counter trays,* and

3) at least 1,000 spark-chamber pictures were taken for each of many time-delay settings.

The efficiency for a particular gap as a function of time delay was measured by examining the spark-chamber pictures taken for each time-delay setting and determining the fraction of the number of events (with "single" tracks) in which a spark did appear in that gap along the path defined by the tracks in the two additional chambers. The results are shown in figures 15 through 17 for the three gases considered: tank-pure helium, the AHE mixture,

---

*An event was not considered if any spark-chamber track was inclined from the vertical by more than 15 degrees in either view.

FIGURE 15: CHARACTER OF THE EFFICIENCY DATA FOR HELIUM

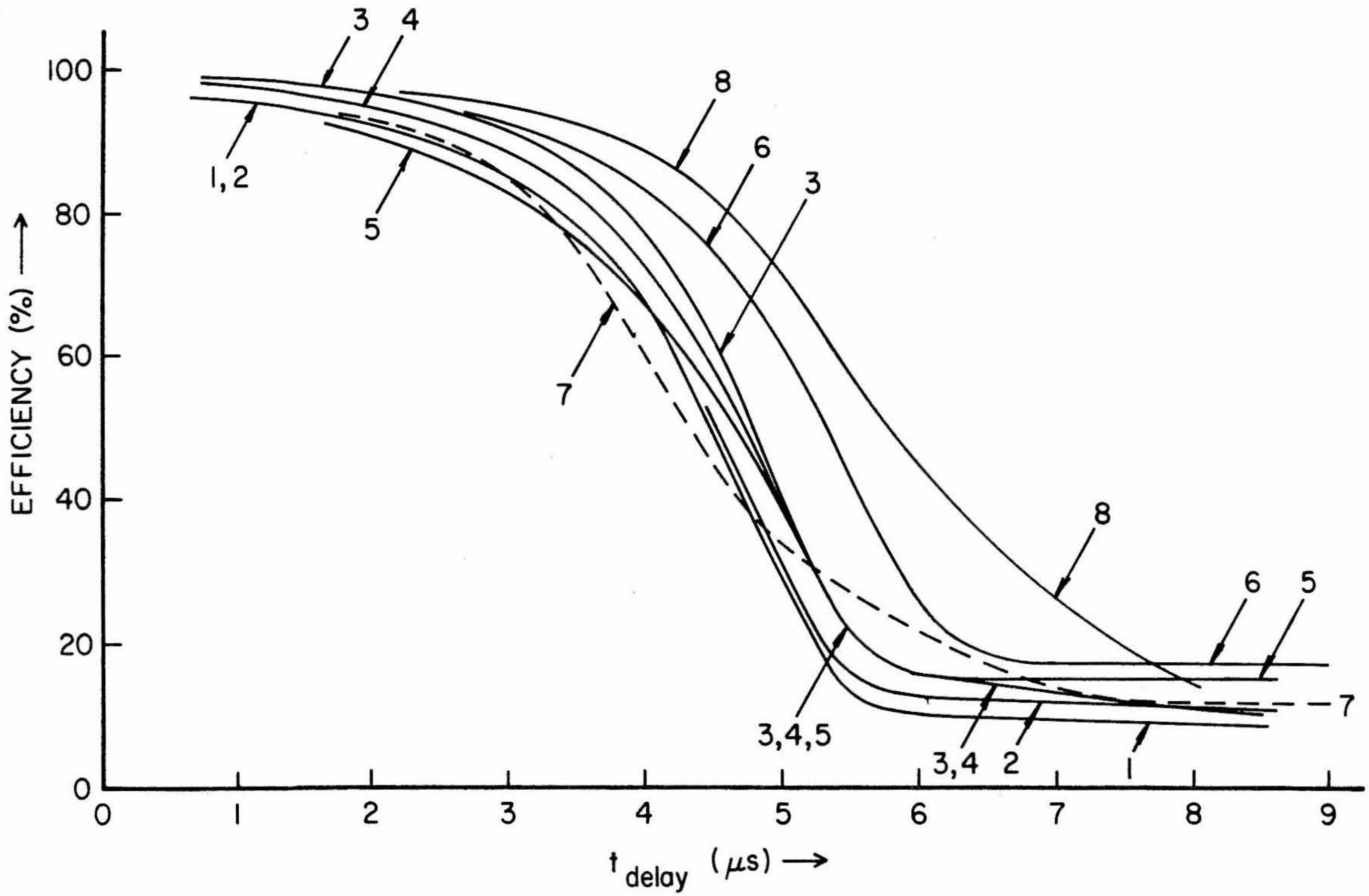

FIGURE 16: CHARACTER OF THE EFFICIENCY DATA FOR THE AHE MIXTURE

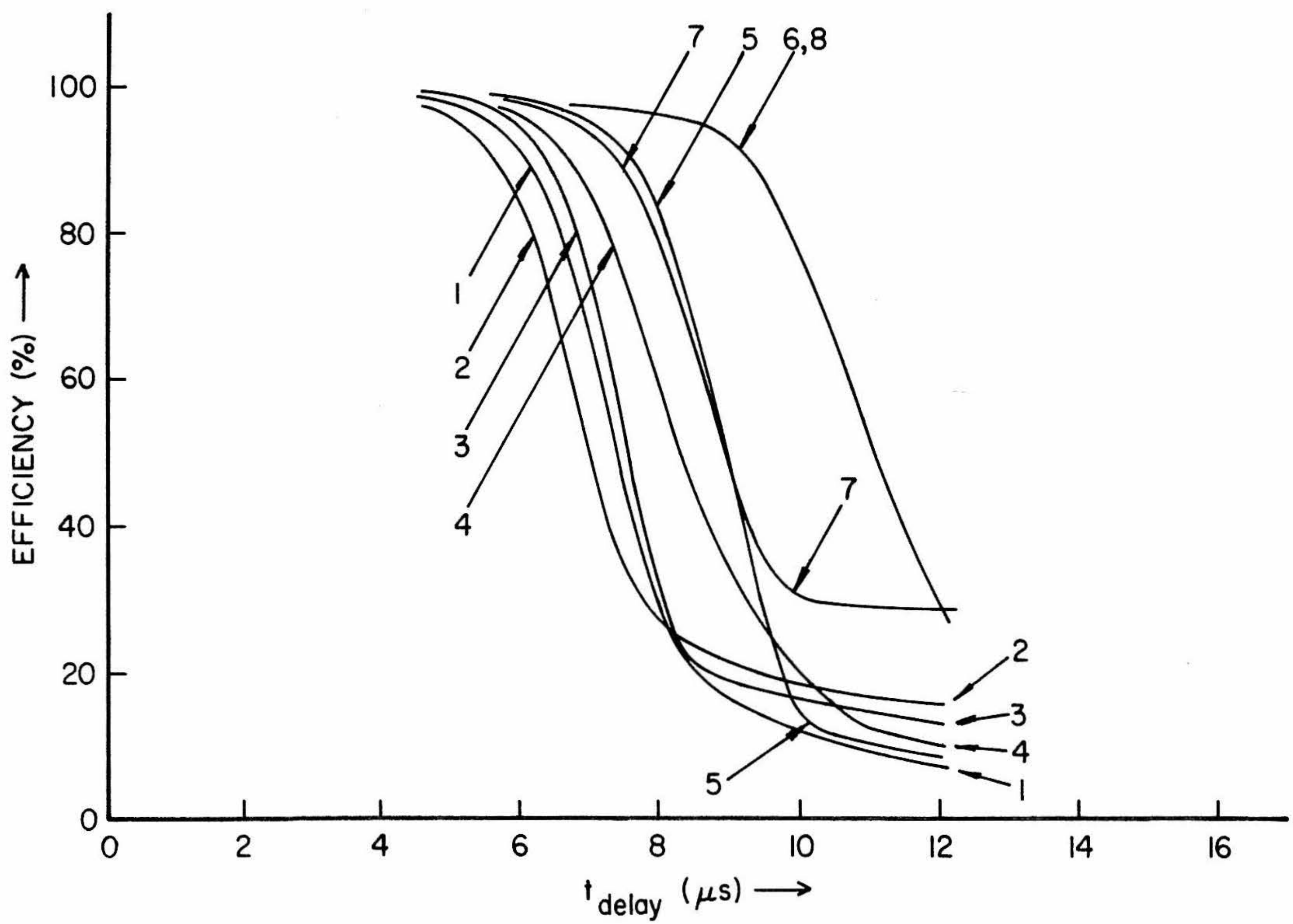

FIGURE 17: CHARACTER OF THE EFFICIENCY DATA FOR ARGON

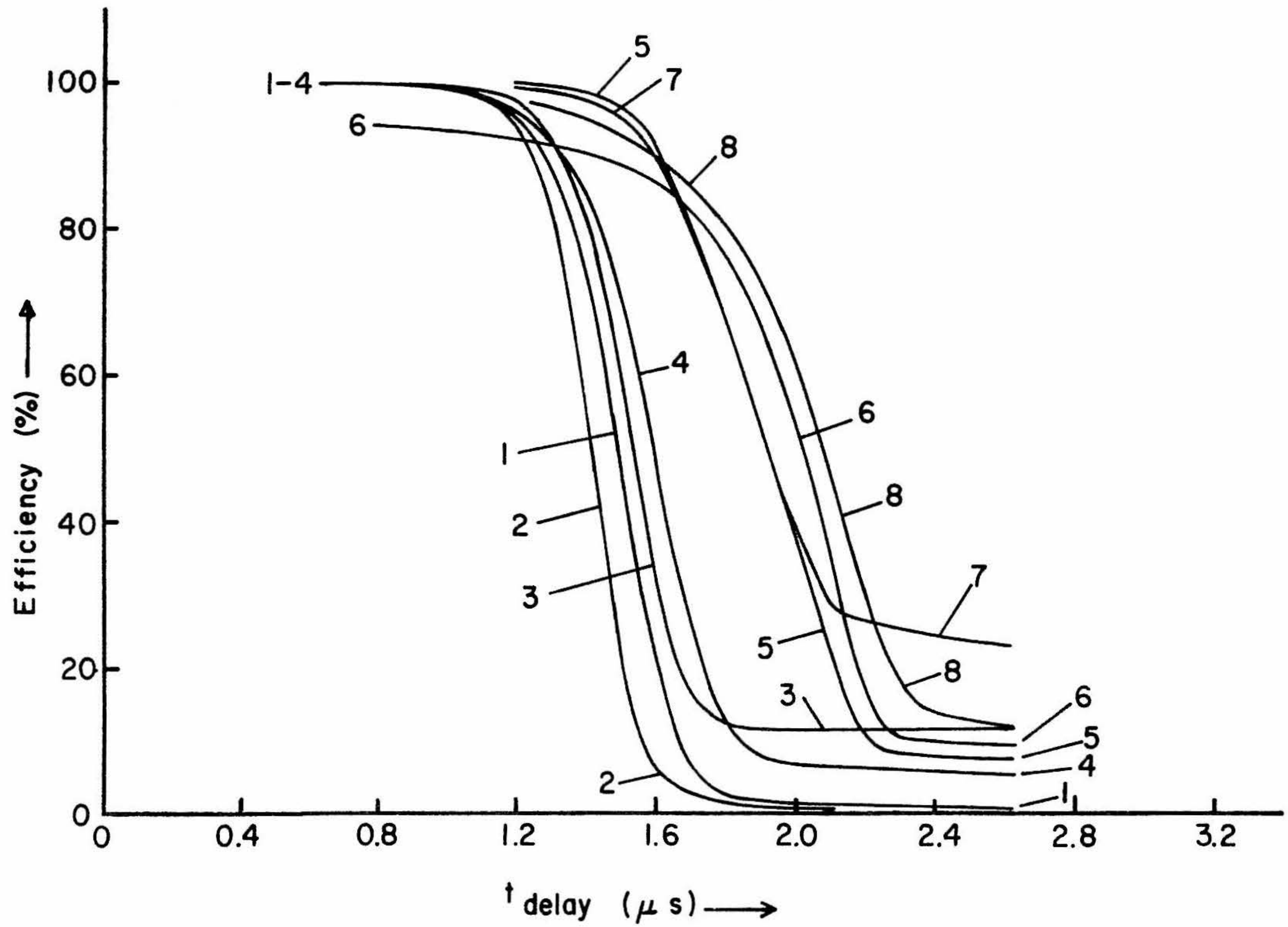

and tank-pure argon. The numbers labelling the different curves on each figure refer to the numbers assigned to the gaps in the two spark chambers. The gaps were numbered from 1 to 8 starting at the gap at the top of the top chamber and working down.

The data can be seen to have the following features. For small time delays (t_{delay}'s), the efficiency per gap was nearly 100%. The efficiency then decreased quite suddenly for time delays on the order of five microseconds for helium, eight microseconds for the AHE mixture, and 1.8 microseconds for argon. For longer time delays, the efficiency was not zero, but was either constant or a slowly decreasing function of t_{delay}, depending on the type of gas and the gap considered. These non-zero efficiency values, which existed well beyond where one might expect the efficiencies to reach zero on the basis of the slopes of the sudden fall-offs, will be referred to as the "tails" on the efficiency curves. These tails were on the order of ten to twenty percent for helium, zero to ten percent for argon, and intermediate for the AHE mixture.* Tails of comparable size have been observed by other investigators.[46]

Such features can be understood qualitatively as follows. When a charged particle passes through a gap, a "column" of electrons is formed which moves slowly out of the gap in response to a sweeping

---

*The variation in efficiency in the tails from gap to gap for a given pure gas might be a reflection of the different surface characteristics of the various aluminum plates in the chambers. Different surface conditions could change the probability that the de-excitation of a metastable state in the gas would result in photoionization of an atom at the surface of a plate. Such considerations may be important if the metastable theory to be discussed in this section is found to correctly describe the tails.

field. At a time t_{delay} after the passage of the particle, there is a high probability of getting a spark upon application of a pulsing field only if the number of electrons remaining in the gap at that time is at least N. This is undoubtedly the case for small t_{delay}'s, so the sparking efficiency is near 100% there. For long t_{delay}'s, this is not the case, so the efficiency is very small.

The situation at moderate time delays can be understood by first considering the hypothetical case in which the electrons liberated through ionization by a particle traversing a gap are not distributed in a random fashion across the gap but are distributed in a uniform fashion and are not subject to diffusion in their subsequent motions. There would then be a unique t_{delay} for each gas, dependent only on the drift velocity of electrons in that gas, at which the N^{th} electron remaining is just being swept out of the gap. At this t_{delay}, the sparking efficiency would drop discontinuously from 100% to 0%. In reality, no unique t_{delay} exists because statistical fluctuations and diffusion are present. The discontinuity is therefore rounded to what we have termed a "sudden fall-off."

At long t_{delay}'s, when the column of electrons has been swept completely out of the gap, the efficiency would be expected to be 0%. Because our data show that the efficiency is not 0%, there must be another source of free electrons --- a source which allows the probability of finding N or more electrons in the gap to be on the order of 5% to 20%. As we will show later, one possible source is the collisional de-excitation of metastable states in the gas with subsequent photoionization of atoms in the walls of the gap or in the gas itself. The metastable states would presumably be populated at the same time the column of electrons is formed during the passage of a charged particle.

To determine the parameter N, four theoretical models were fit to the measured data. A mathematical description of each model is given in appendix C.

The first model is believed to describe the basic physical processes governing the sudden fall-off in efficiency at moderate time delays. This model includes an assumption that the number of electrons which have been liberated through ionization by a particle traversing a spark-chamber gap, but which have not yet been swept out of the gap by a certain t_{delay}, can be described using Poisson statistics. The model is therefore labelled the "Poisson Theory."

In this model, there are three parameters which are assumed to vary: 1) N, the minimum number of electrons required in a gap to cause spark formation when the pulsing field is applied, 2) m, the average number of electrons produced in the gap by the passage of a cosmic-ray muon, and 3) v, the drift velocity of the electrons in the gap in response to the sweeping field. The motion of the electrons is assumed to be governed only by the effects of the sweeping field and diffusion. The efficiency per gap for a particular time delay is assumed to be the probability that N or more electrons are still remaining in the gap at that time.

The expression which describes the efficiency as a function of time delay in this model was fit to the measured data for each gap and each gas by the method of least chi squares. This was done using a computer program designed to handle expressions in which the parameters appear in a nonlinear fashion (c.f. program #3094 on the IBM SHARE library).

Specific results will be presented in connection with the next model to be discussed. In general, one finds that the Poisson Theory can adequately describe the efficiency data up to and partially through the sudden fall-offs, but it can't describe the processes responsible for the tails.

For this reason, the model called the "Poisson Theory + Metastables" was devised. In this model, the tails are attributed to the presence in each gap of additional free electrons which are liberated through the collisional de-excitation of metastable states in the gas, with subsequent photoionization of atoms in the walls of the gap (or in the gas itself in the case of mixtures). This model is described in detail in appendix section C.4.

The general features of the model are the following. The number of atoms in metastable states at $t=t_{delay}$ is represented by $H(t) = H_o \exp(-t/\tau)$.* The probability that the de-excitation of an atom in one of these states will result in the addition of one electron to those already in the gap at time t_{delay} is designated by R_o. The total number of electrons remaining in the gap at a particular time is still assumed to be described by Poisson

---

*For the low metastable densities to be considered, the metastable density is expected to decay exponentially with time (see references 47-49).

statistics, but the average number expected in the gap at that time now includes the effects of the metastable states.

In fitting the model to the data, two parameters in addition to N, m, and v were assumed to vary: 1) τ, the mean life of the metastable states in the environment in the gap, and 2) H_oR_o, the total average number of additional electrons furnished by the de-excitation of metastable states.

The results of fitting this model and the Poisson Theory to the measured data will now be presented. We shall consider only gaps #1 and #4 because the results for these gaps are typical of the results as a whole.

The measured data for these gaps are given in figures 18 through 23. The vertical errors shown are the standard deviations expected on the basis of binomial statistics. These errors are too conservative, for they do not include the systematic errors which we shall describe later. Nevertheless, these were the only errors considered in minimizing chi square for the fits.

The errors in t_{delay} shown for helium and the AHE mixture arose because of instabilities in the electronics which produced the time delays. These instabilities were removed before taking data for argon, and the errors expected there are negligible in comparison to the size of the data points.

The fits accompanying these data are the fits for the Poisson Theory + Metastables model using N=1 (solid curves) and

FIGURE 18: EFFICIENCY vs t_{delay} AND FITS FOR N=1

HELIUM GAP #1

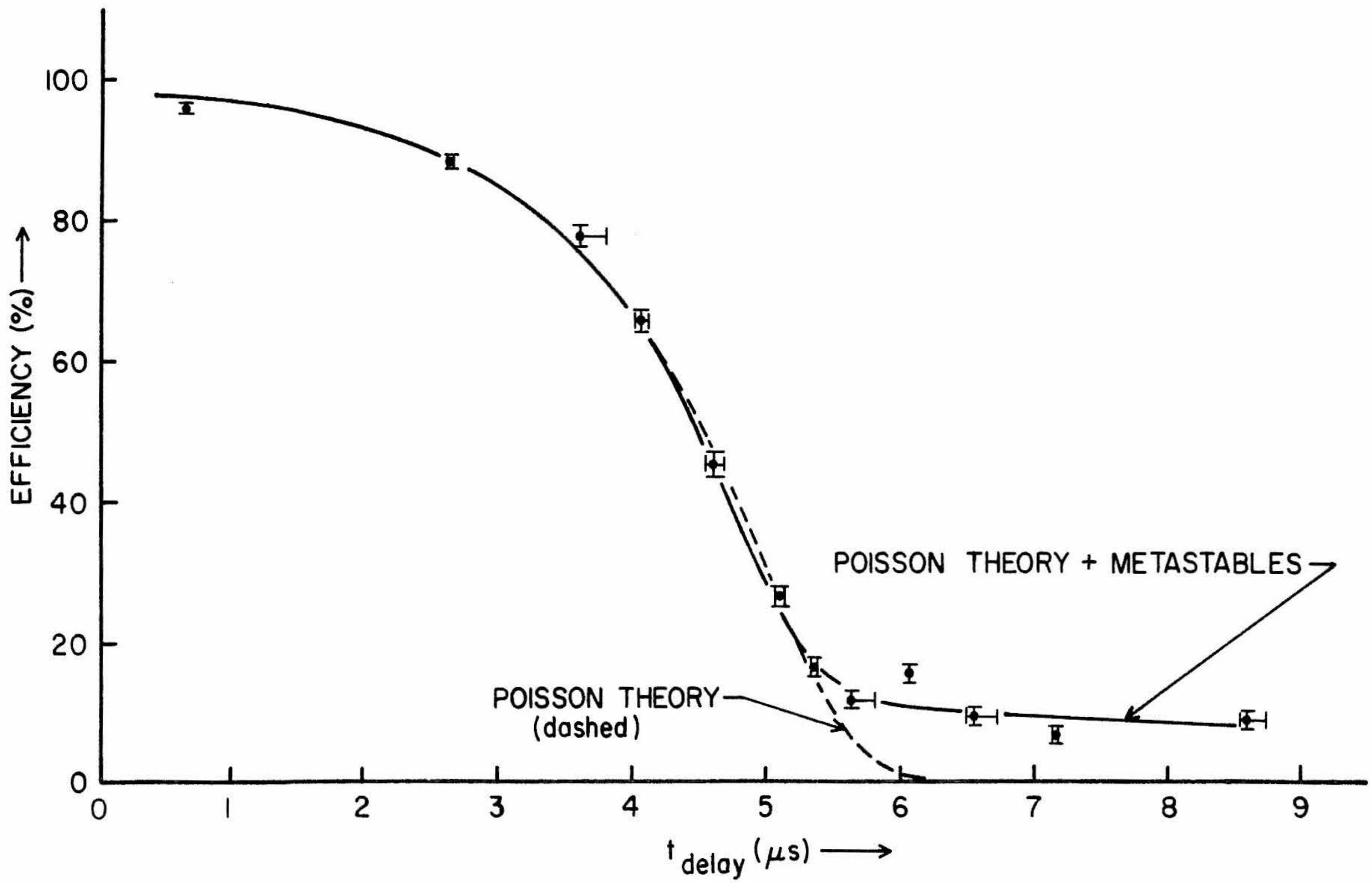

FIGURE 19: EFFICIENCY vs t_{delay} AND FITS FOR N=1

HELIUM GAP #4

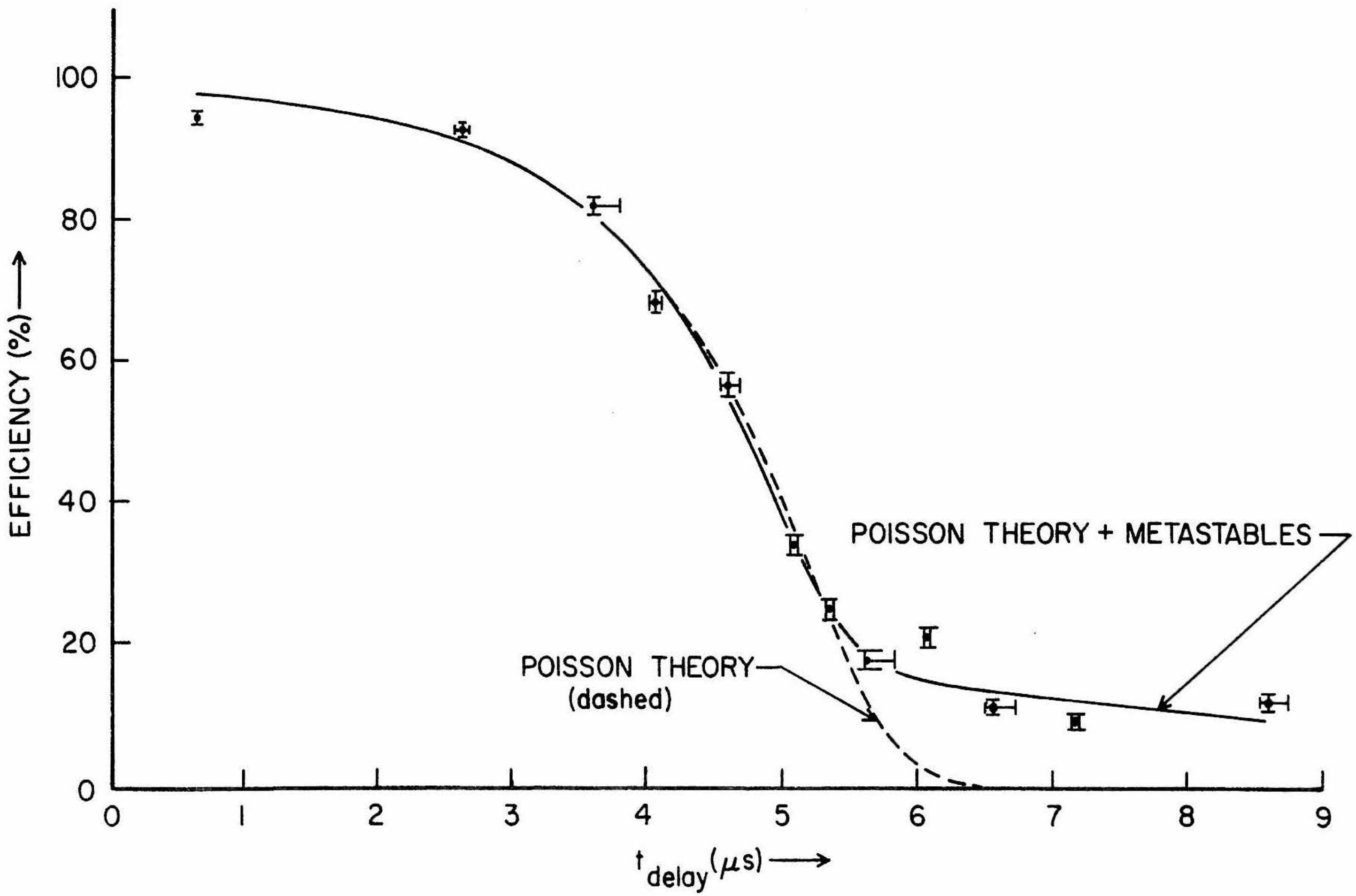

FIGURE 20: EFFICIENCY vs t_{delay} AND VARIOUS FITS: AHE GAP #1

PARAMETERS HELD CONSTANT DURING FITTING ARE INDICATED

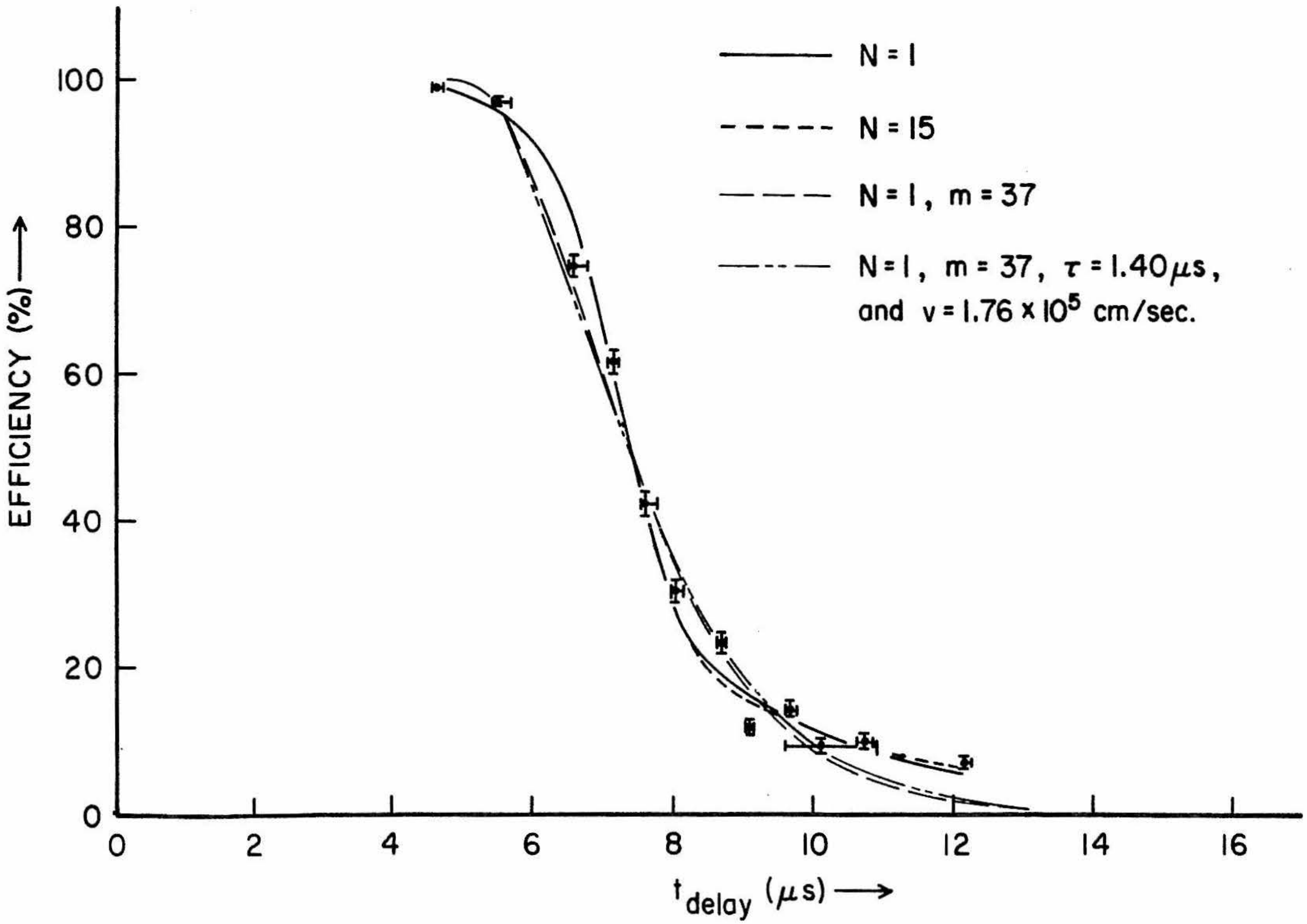

FIGURE 21: EFFICIENCY vs t_{delay} AND VARIOUS FITS: AHE GAP #4

PARAMETERS HELD CONSTANT DURING FITTING ARE INDICATED

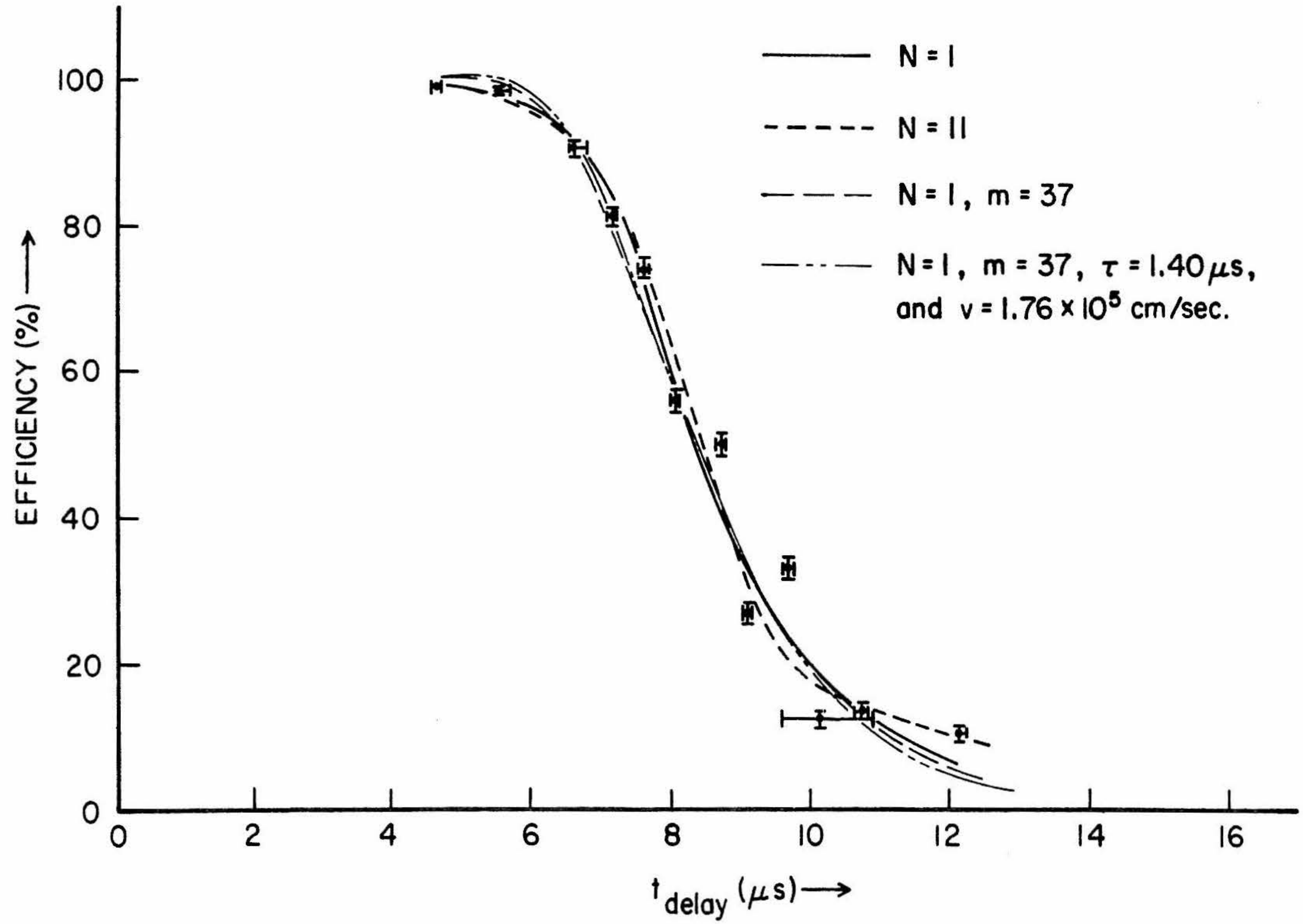

FIGURE 22: EFFICIENCY vs t_{delay} AND POISSON THEORY + METASTABLES FIT FOR N=1

ARGON GAP #1

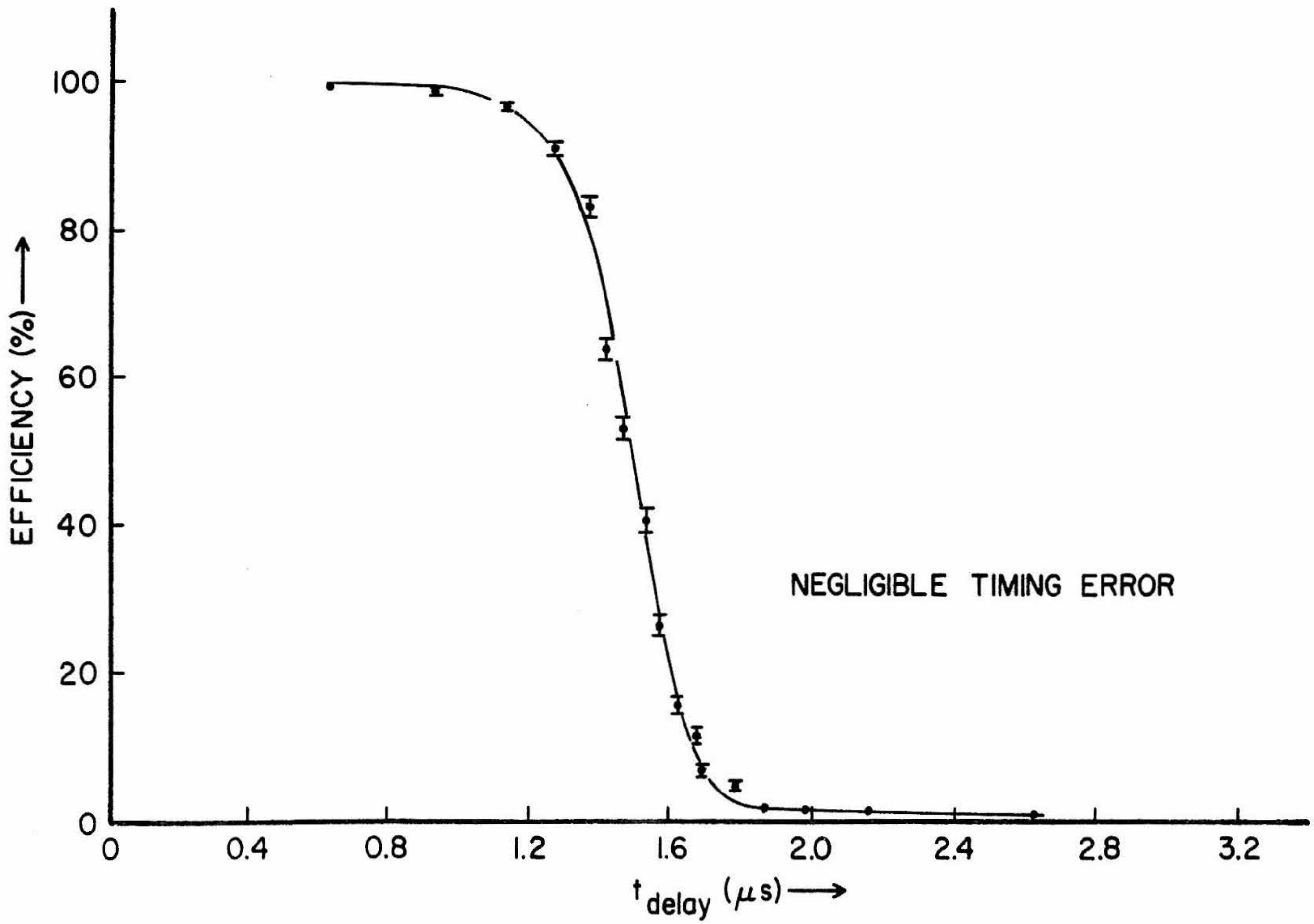

FIGURE 23: EFFICIENCY vs t_{delay} AND POISSON THEORY + METASTABLES FIT FOR N=1

ARGON GAP #4

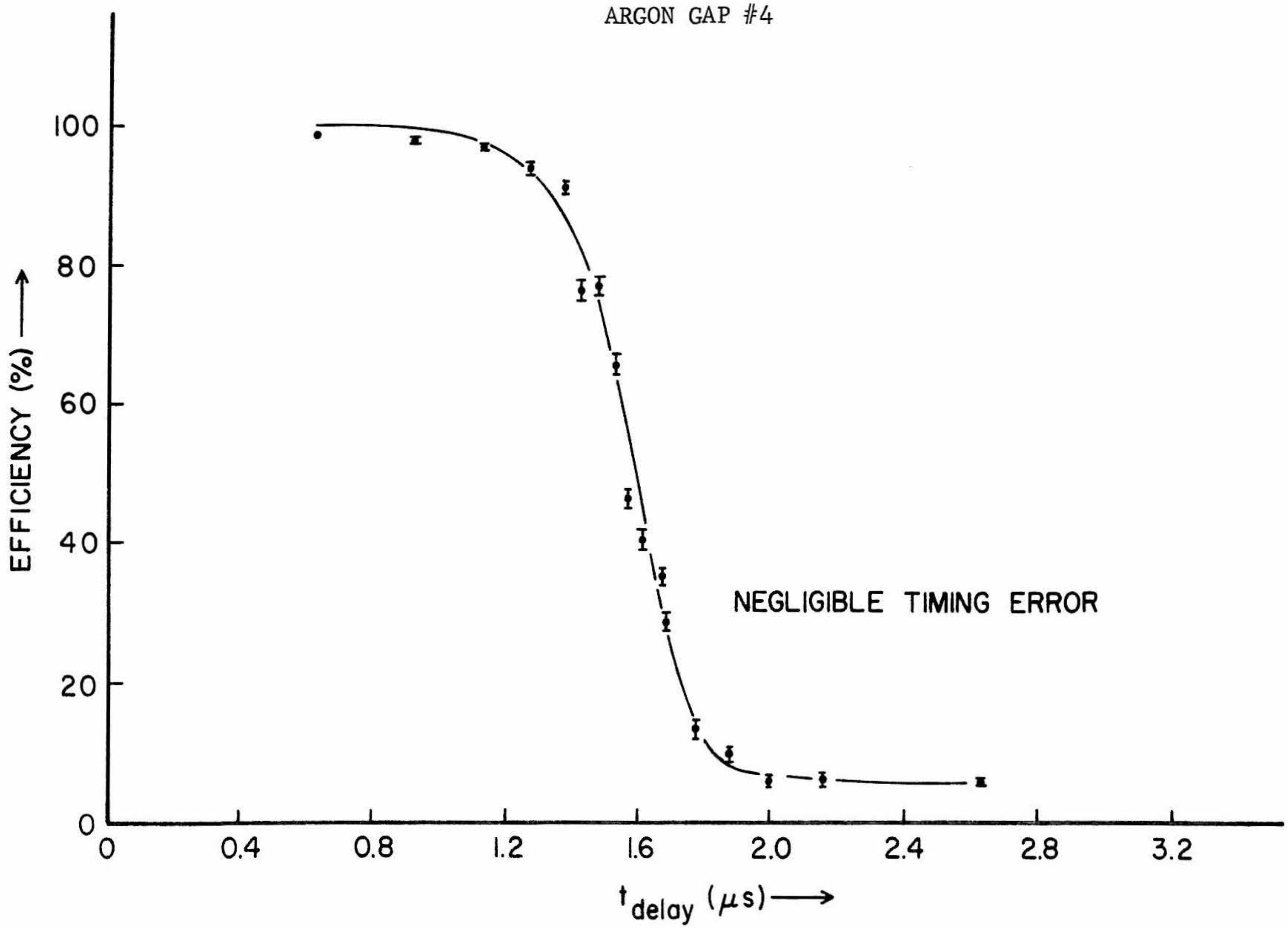

fits shown to illustrate certain points (dashed curves). In figures 18 and 19, the dashed curves give the fits for the Poisson Theory, the data points in the tails having been ignored (the fits look approximately the same even if the tails are included). In figures 20 and 21, the short-dashed curves illustrate fits for the metastable model with N held fixed at values which yield the smallest chi squares. Note how insensitive the results are to changes in N (figure 20). The curves drawn with long dashes in figures 20 and 21 illustrate fits in which N was held fixed at 1 and m was held fixed at 37, while other parameters were held fixed as shown (these fits will be discussed later).

The values of chi square obtained for the various fits are given in figures 24 and 25 as a function of N. As one can see, the value of N which minimizes chi square is most likely one for helium and argon, but is probably on the order of ten to fifteen for the mixture. The fitted values of the other parameters are given as a function of N in figures 26 through 31. In figures 26 through 29, the solid curves refer to the Poisson Theory + Metastables model, while the dashed curves refer to the Poisson Theory by itself (tails ignored).

The best values obtained for the parameters when N is fixed at one, all gaps considered, are summarized in table 5. The estimated 95%-confidence error figures given in this table are based on those computed using the binomial errors and the methods employed by IBM SHARE program #3094.

FIGURE 24: CHI-SQUARE OF FIT vs N

GAP #1

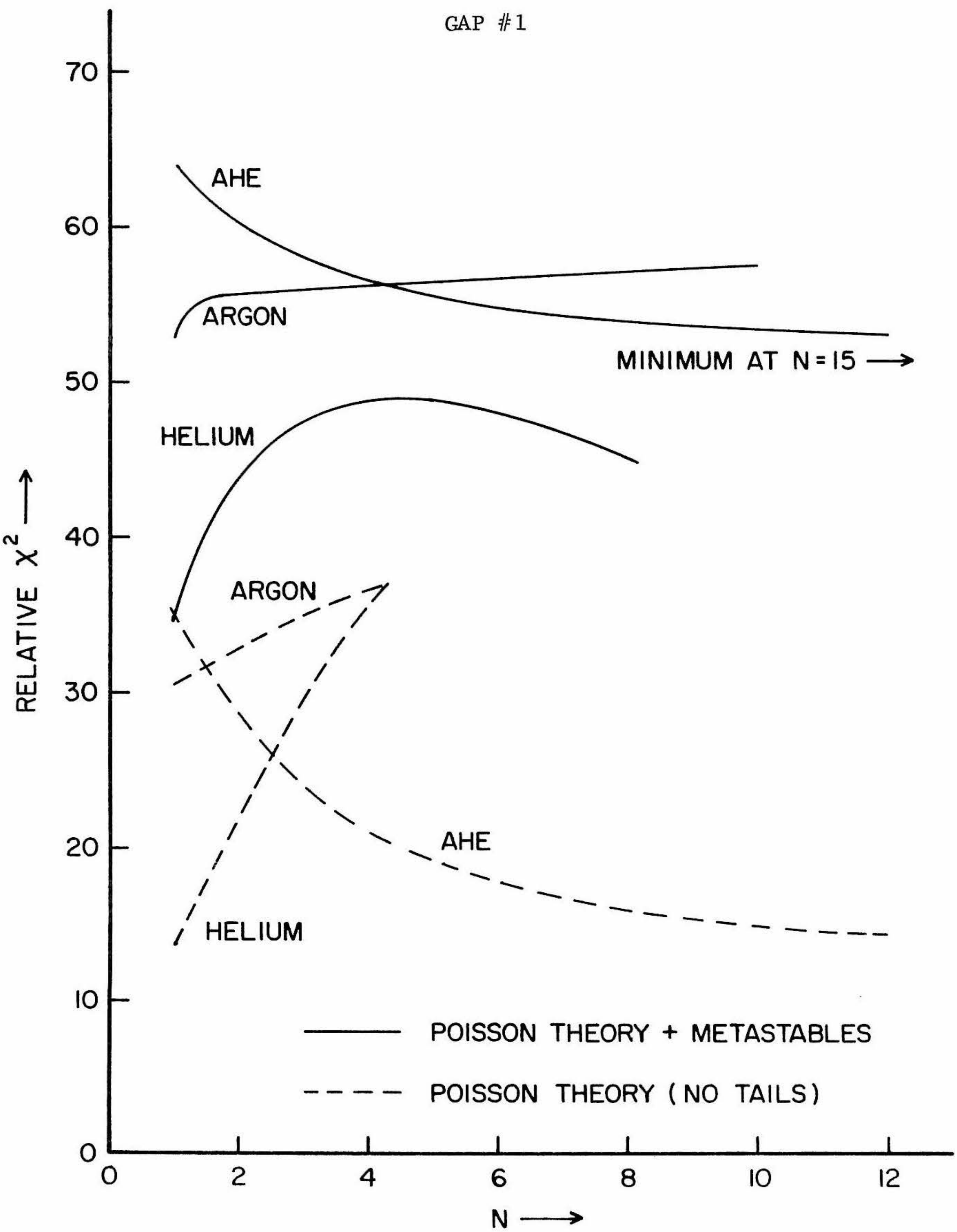

FIGURE 25: CHI-SQUARE OF FIT vs N

GAP #4

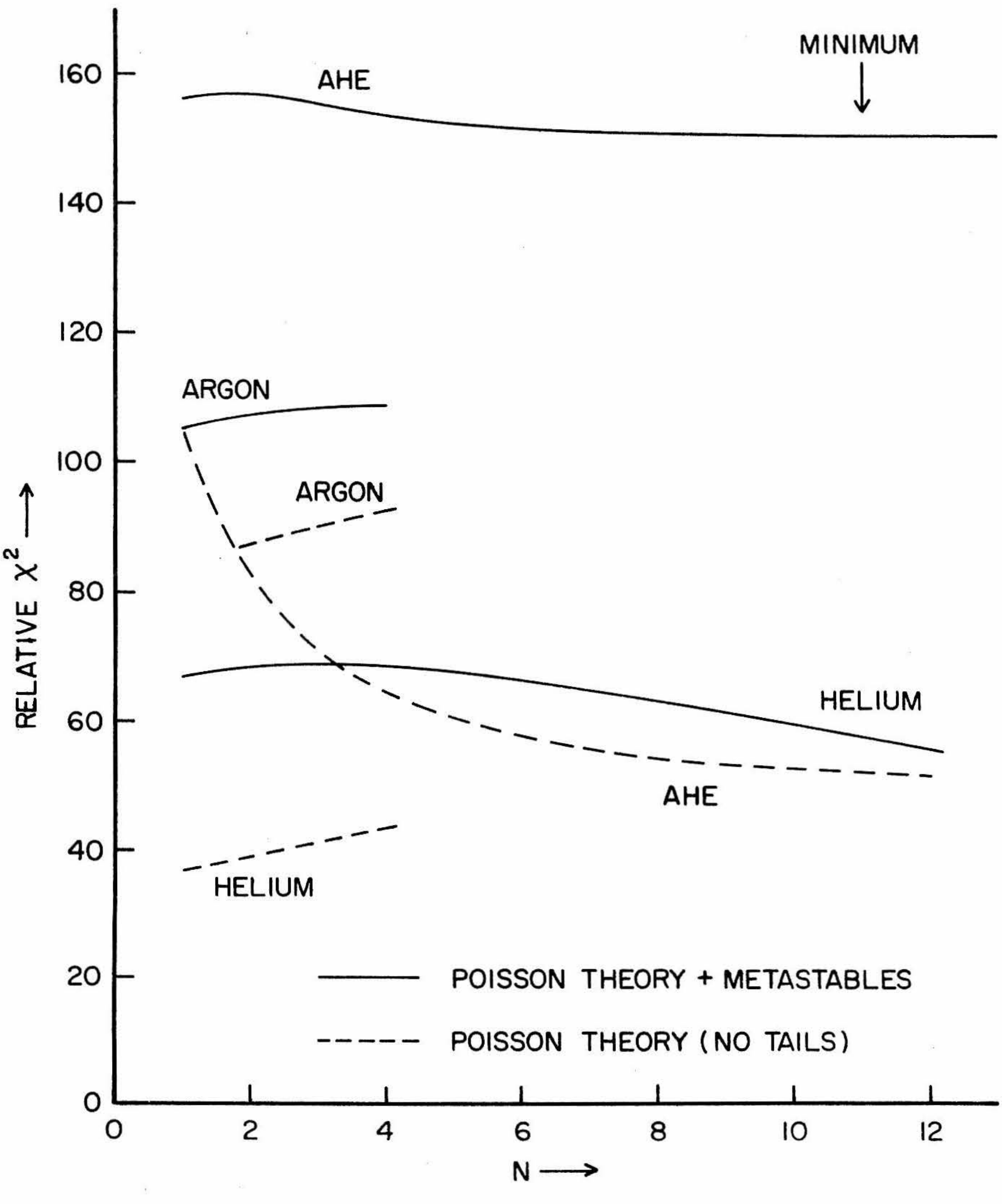

FIGURE 26: PRIMARY ION DENSITY "m" vs N

GAP #1

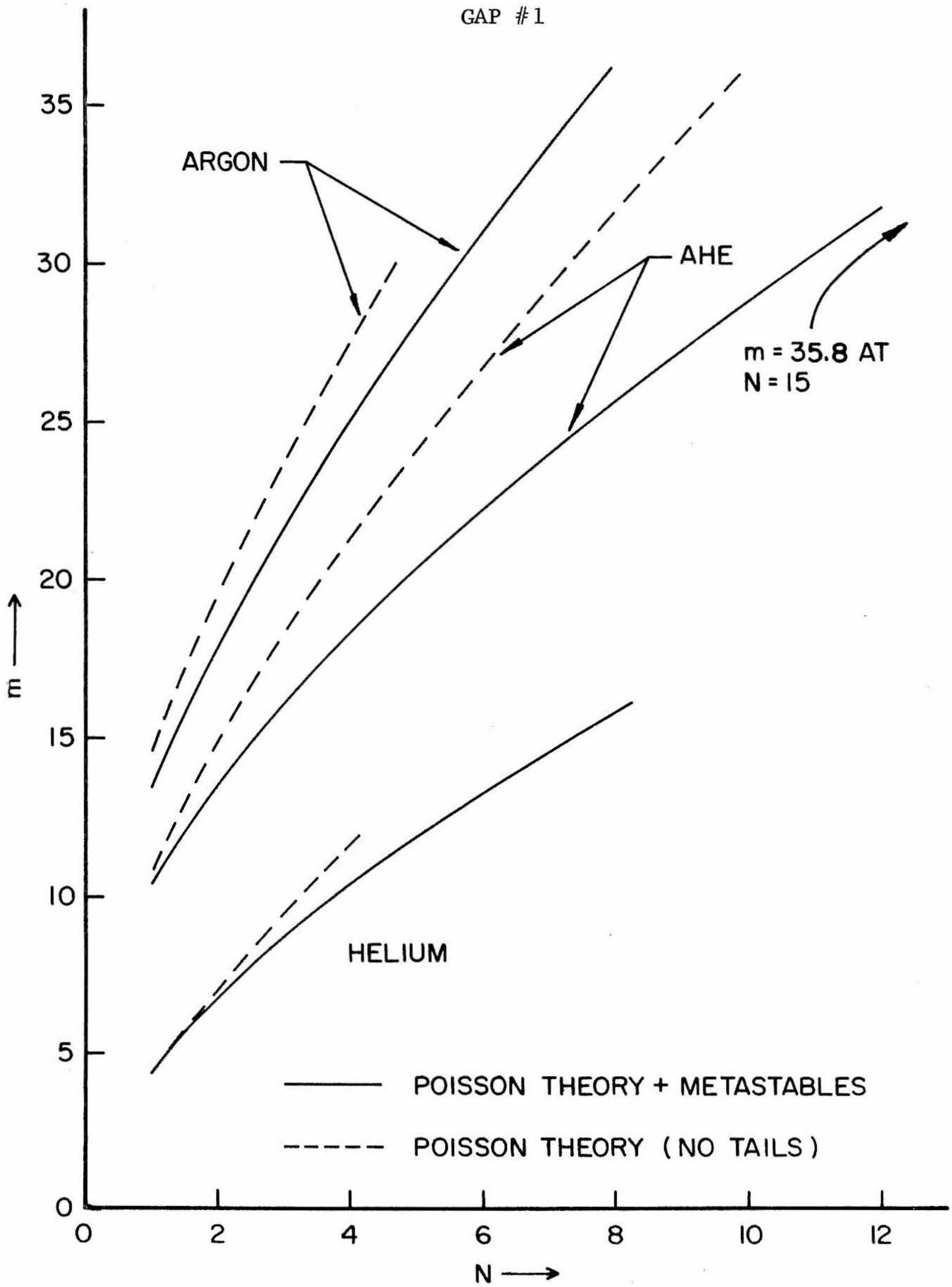

FIGURE 27: PRIMARY ION DENSITY "m" vs N

GAP #4

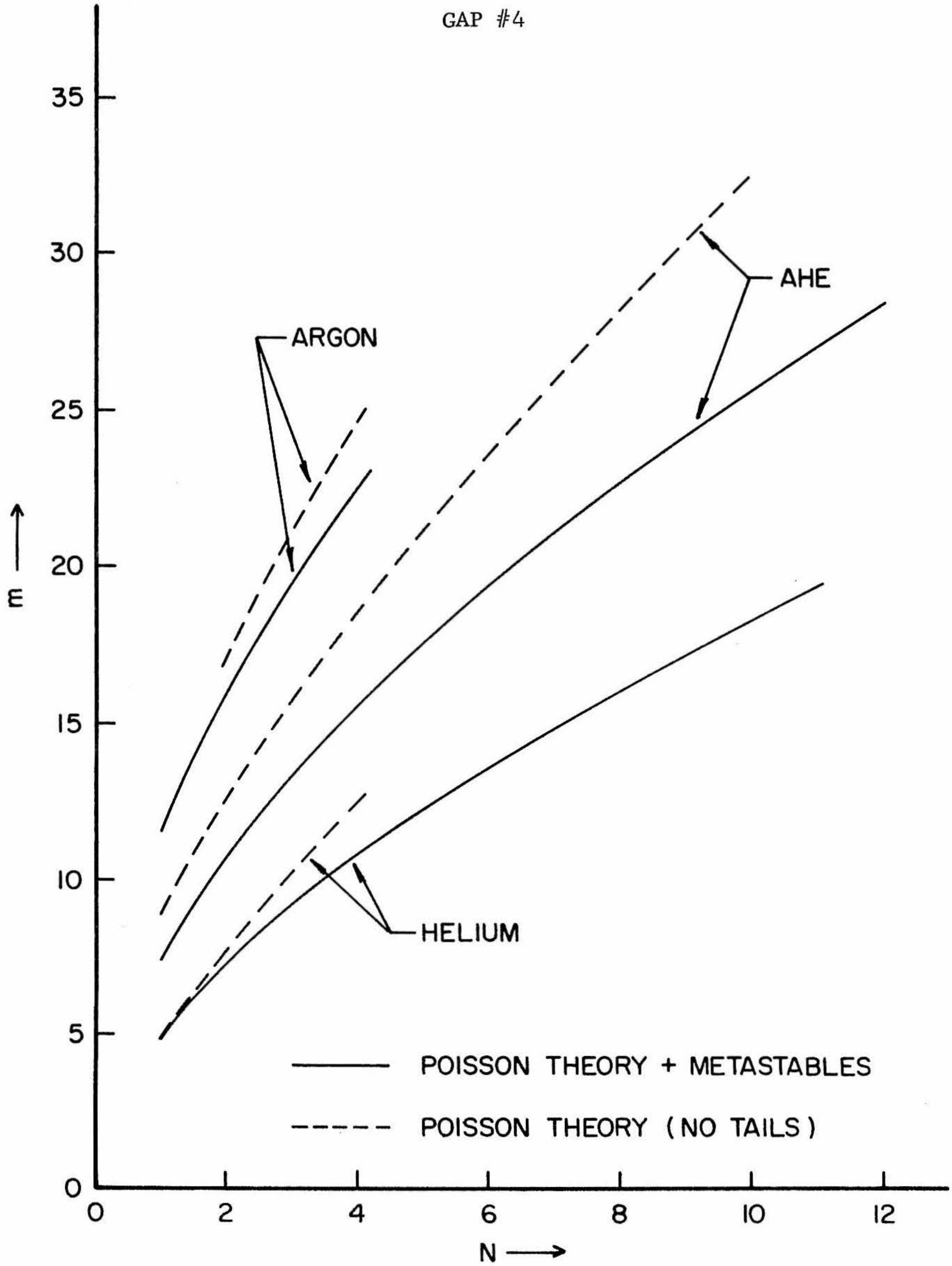

FIGURE 28: ELECTRON DRIFT VELOCITY vs N

GAP #1

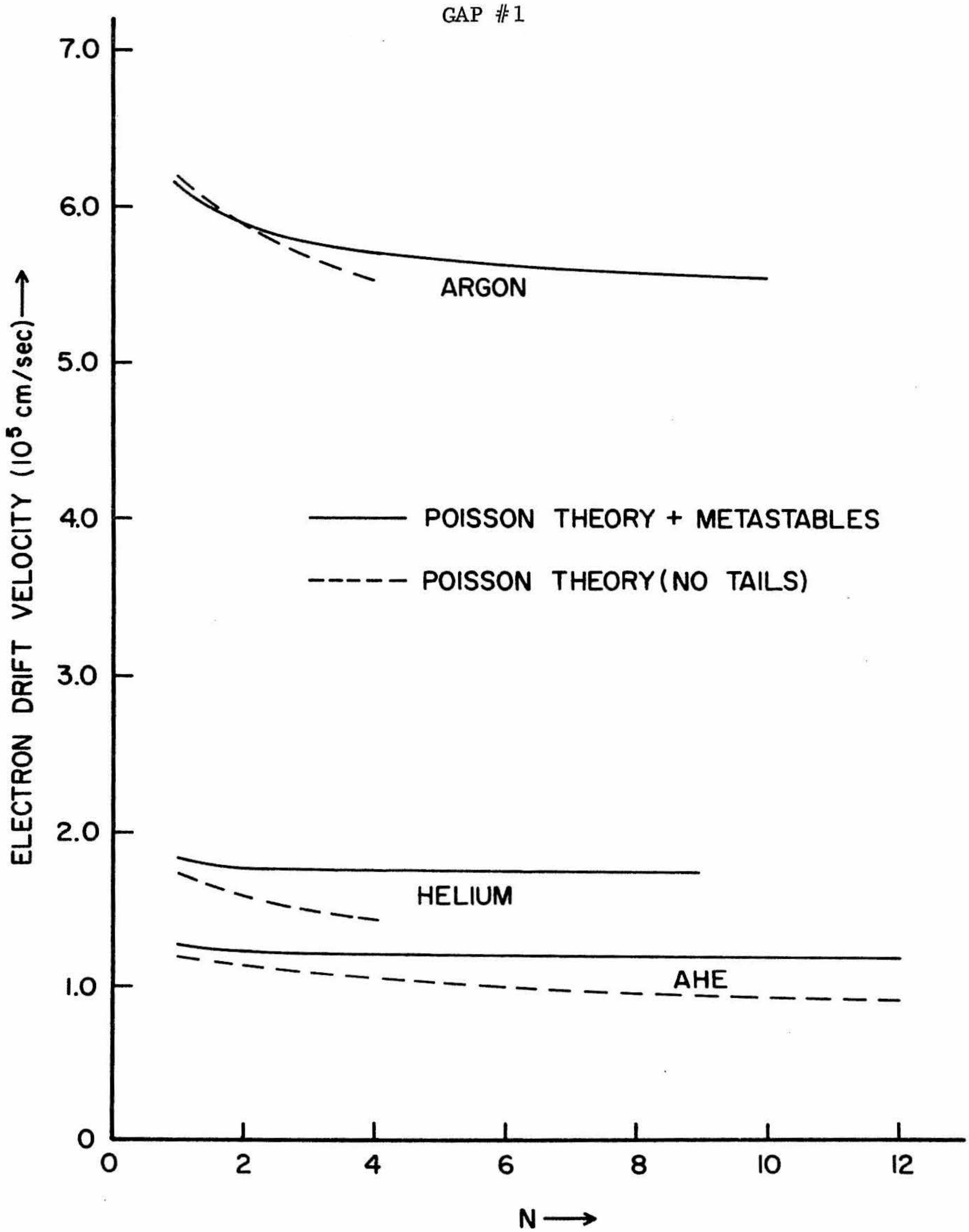

FIGURE 29: ELECTRON DRIFT VELOCITY vs N

GAP #4

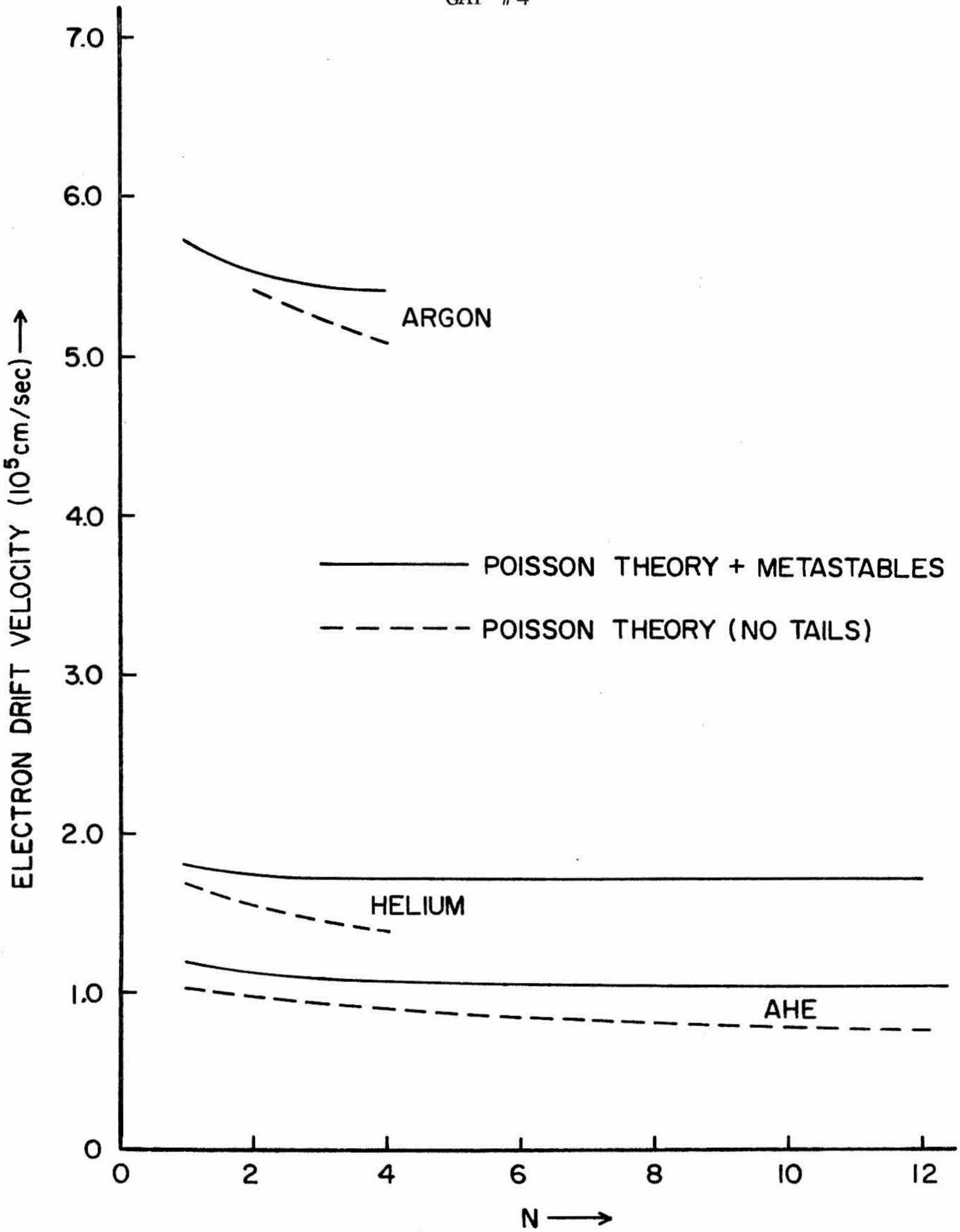

FIGURE 30: MEAN LIFETIME OF METASTABLE STATES vs N

GAPS #1 AND #4

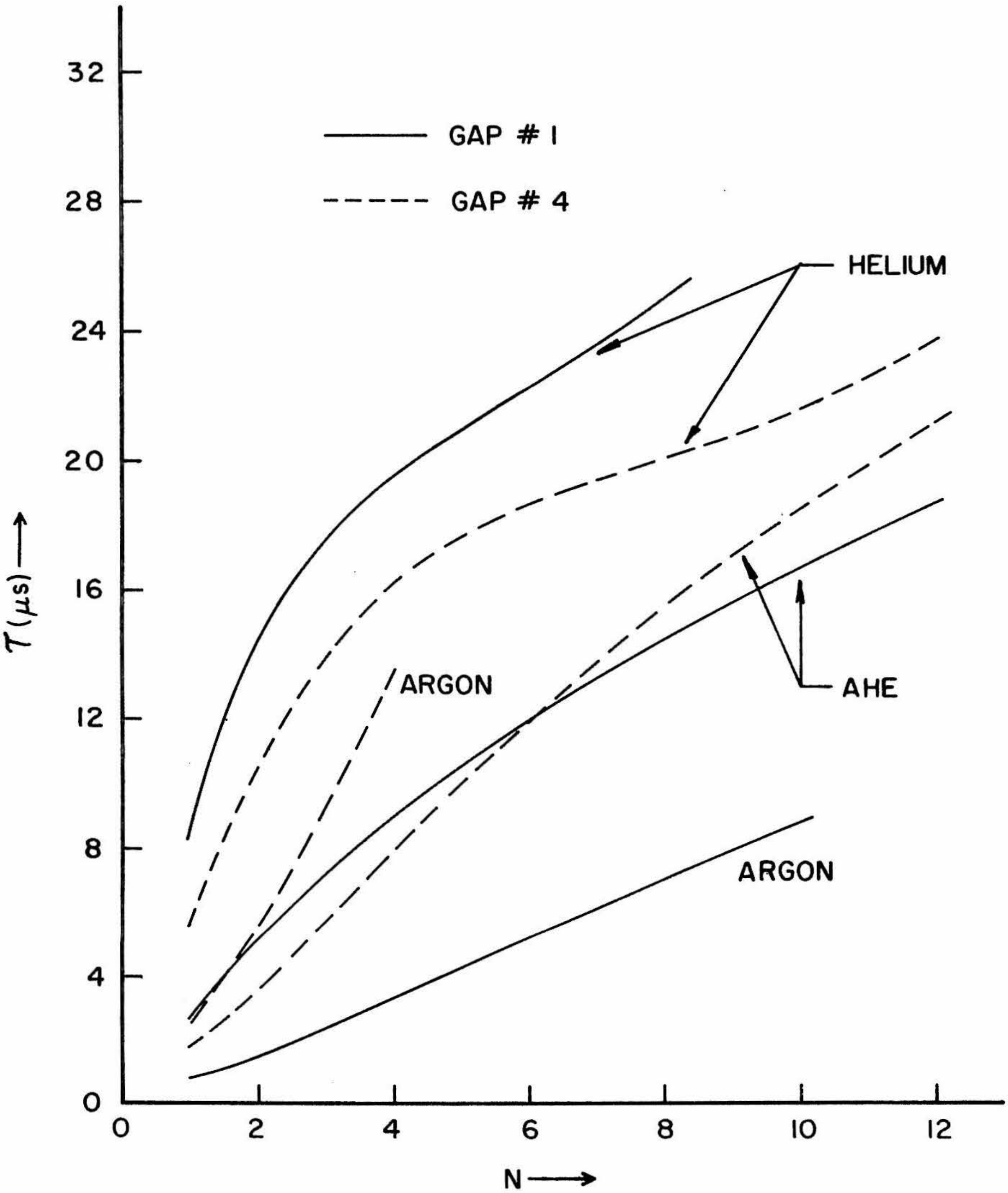

FIGURE 31: TOTAL NUMBER OF ELECTRONS PRODUCED

BY THE DE-EXCITATION OF METASTABLE STATES

GAPS #1 AND #4

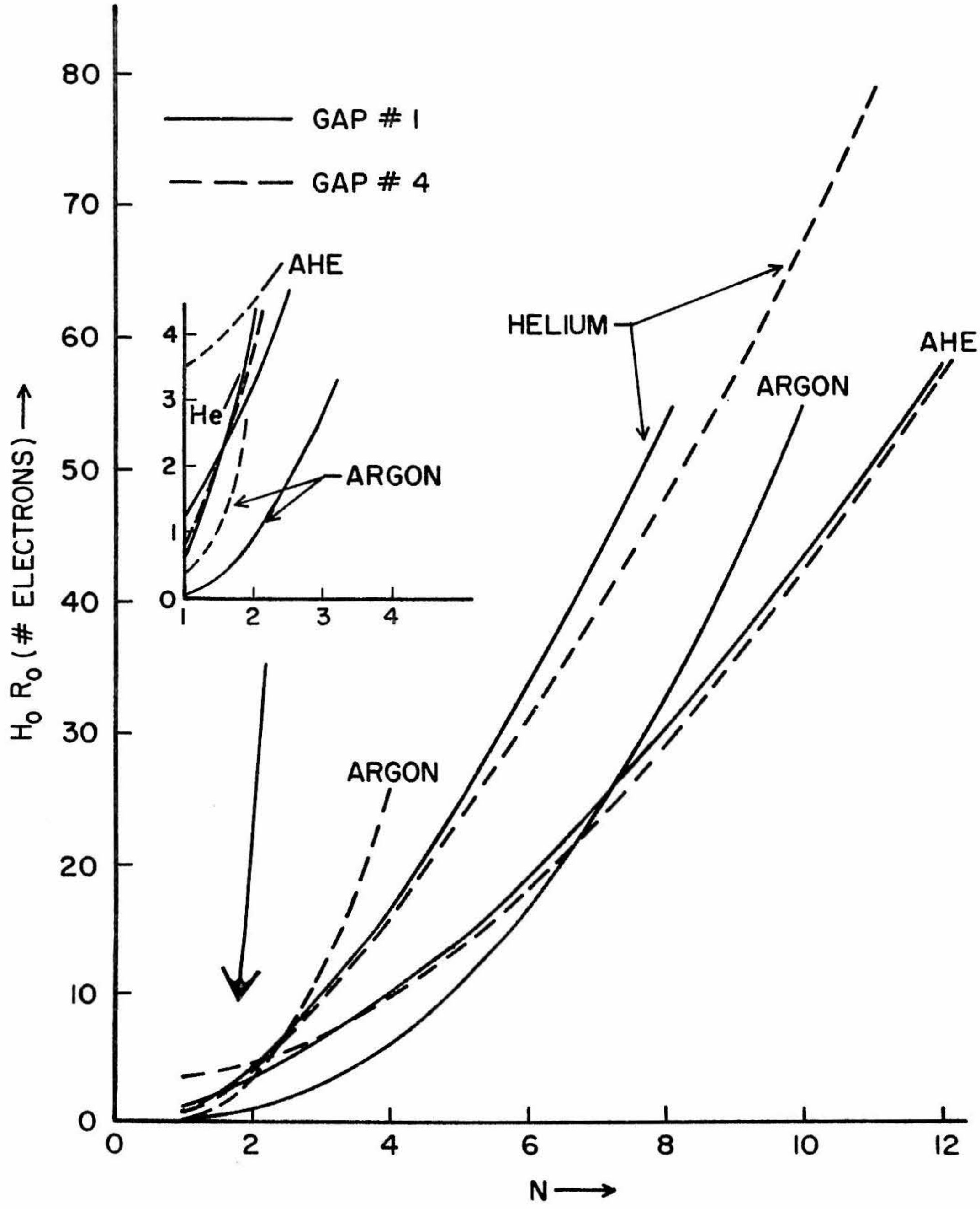

TABLE 5: SUMMARY OF THE VALUES OBTAINED FOR THE PARAMETERS WHEN CONSIDERING N=1 AND THE POISSON THEORY + METASTABLE FITS

Parameters Which Were Varied:

Gas	Parameter	Mean	Estimated 95% Confidence Region		
Helium	m	4.6	3.5	to	6.5
	v (10^5 cm/sec)	1.82	1.74	to	1.90
	τ (μs)	7.	1.	to	16.
	H_oR_o	0.75	0.40	to	1.20
AHE	m	11.	7.	to	19.
	v (10^5 cm/sec)	1.27	1.12	to	1.41
	τ (μs)	3.	1.	to	10.
	H_oR_o	1.2	0.4	to	4.0
Argon	m	14.	10.	to	20.
	v (10^5 cm/sec)	5.9	5.2	to	6.7
	τ (μs)	0.9	0.2	to	9.0
	H_oR_o	0.2	0.0	to	10.0

Parameters Held Constant:

G = 3/8 inch (gap spacing)
T = 24.0° C. (gas temperature)
V = 10.0 volts (sweeping voltage on each gap)
N = 1

Before discussing the results and their significance, it is worthwhile to consider the systematic errors and the sensitivity of the results to shifts in the data. One systematic error which was not included in the fits was an error of a few percent or less that arose in scanning the spark-chamber pictures and recording which gaps had not sparked. Another arose because the spacing for each gap was not measured, but was just assumed to be the design value of 3/8 inch.

To illustrate that the efficiency curves are quite sensitive to changes in gap spacing (but not to changes in sweep voltage or gas temperature), the effects of a one-millimeter change in spacing (or 20 degrees in temperature, or 0.5 volt in sweep voltage) is shown in figure 32 for a particular helium case. Note that a shift in spacing is equivalent to a shift in t_{delay}. For this reason, most of the variation in time of the 50% points on the curves shown in each of figures 15 through 17 is attributed to variations in spacing from gap to gap.* In fact, except for gap #7 in the case of helium, the order of reaching 50% efficient is consistent with the sequence 2, 1, 3, 4, 5, 7, 6, and then 8.

To illustrate that the "best" value obtained for N is extremely dependent on the accuracy of the data which are fit, one

---

*Some of the variation from gaps in one chamber (1-4) to gaps in the other chamber (5-8) might be a result of different chamber characteristics in regards to pulsing (e.g. the effective chamber capacitance, the way in which the high-voltage cables were attached, et cetera).

FIGURE 32: THE EFFECTS OF CHANGES IN THE PARAMETERS HELD CONSTANT IN FITTING THE POISSON THEORY TO THE EFFICIENCY DATA

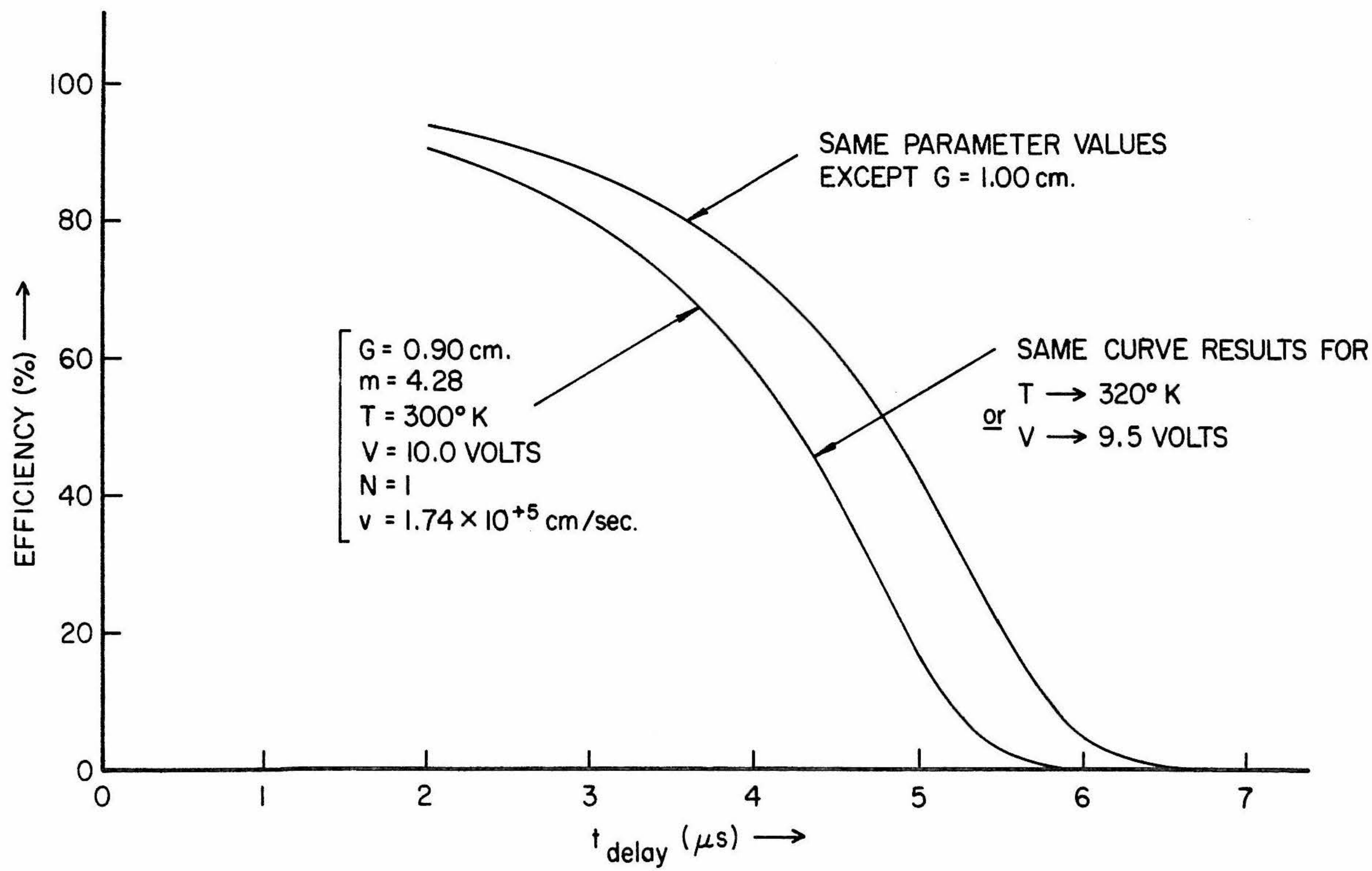

is again referred to figure 20. There one can see that the curves for N=1 and N=15 lie almost on top of each other. It is for this reason that chi square does not vary greatly as a function of N. For example, the variation in chi square from the value for N=1 to the minimum value is only 4% for the AHE mixture and gap #4 (c.f. figure 25). Clearly, a chi square is <u>not</u> a very sensitive indicator of the best value for N.

To gain further insight on the value for N, one can supplement the chi-square indication with the consistency of the values of m, v, τ, and H_oR_o with available experimental data.

For example, suppose we estimate what one might expect m to be for each gas, and compare each estimate with the values obtained from the fits. Using 27 eV/ion-pair for argon and 32 eV/ion-pair for helium,[41] and assuming that a minimum-ionizing muon loses 1.55 MeV/(g/cm^2) in argon and 2.00 MeV/(g/cm^2) in helium,[42] one can compute that such a muon should produce approximately 96 electron-ion pairs per centimeter in argon and 10 electron-ion pairs per centimeter in helium. The values expected for m are significantly less than these numbers, however, because these numbers include the effects from infrequent high-energy delta rays. Such delta rays are considered to be infrequent because a delta ray of energy E eV is expected to occur in a gas of atomic number Z only every 0.145 E/Z centimeters.[37] The production of energetic delta rays in a one-centimeter gap is therefore so improbable that their production can be ignored here.

In general, the ratio of a minimum-ionizing particle's energy loss through delta rays of energy larger than E_{min} and the particle's total average energy loss is $\frac{1}{2}\ln(9.2\text{MeV}/E_{min})$ / $\ln(9.2\text{MeV}/I)$, where I is the average ionization potential of the gas.(37)* For E_{min} near I, the ratio is one-half. Thus, one might expect to have $\frac{1}{2}(10) = 5$ ion pairs/cm in helium, approximately $\frac{1}{2}(0.75)(96) + \frac{1}{2}(0.25)(10) = 37$ ion pairs/cm in the AHE mixture, and $\frac{1}{2}(96) = 48$ ion pairs/cm in argon.†

According to all of the fits which we have made, the values of m which correspond to the relative minimums in chi square as a function of N are between 4 and 5 for helium (N=1), between 27 and 40 for the AHE mixture (N = 10 to 15), and between 11 and 18 for argon (N=1). These values are consistent with those expected except in the case of argon, where the value for N=1 is a factor of three smaller than expected.

Because there is no reason to suspect m to be significantly smaller than 48 for argon,** one may wonder whether the errors in

---

*The particle considered is tacitly assumed to be much heavier than the electron so that the maximum energy which can be lost in a collision with an electron is 9.2 MeV.

†Frost and Nielsen, using cloud-chamber techniques, have measured the number of ion pairs produced by fast electrons and have included delta rays up to 25 times the energy/ion-pair (i.e. up to about 800 eV).(40) Their results are 53 ± 3 ion pairs/cm in argon and 8.1 ± 0.5 ion pairs/cm in helium.

**At the electron densities considered here, electron-ion recombination and attachment are completely negligible for both argon and helium.

the data and any inadequacies in the theoretical models considered have combined in the case of argon to yield a relative minimum in chi square at N=1 when in fact it should have occurred near N=15 (c.f. figures 26 and 27). A possible explanation for N being larger than one for argon is that electron avalanches grow much more slowly in argon than in helium or neon (i.e. argon has a much smaller first Townsend ionization coefficient).[46] Even so, it is doubtful that N would be as large as 15 when the pulsing field is 30 kV/cm.

On the other hand, it is not improbable for N to be much larger than one for the AHE mixture, expecially if N is larger than one for argon. The reason for this is that the mixture contains ethanol, which is a quenching agent. Such a substance is an effective absorber of photons because its molecules absorb photons through dissociation rather than excitation. This feature is helpful in reducing spurious sparking in a spark chamber, but it also hinders the photoionization processes which are essential in the transformation of an electron avalanche into a streamer, and then into a spark (see appendix D). Nevertheless, the effect of a quenching agent on these transformations has not yet been studied in detail, so it may be that N would not be expected to be as large as 15 even with a great deal of ethanol present.

Which N is preferred can not be ascertained by comparing our values for the drift velocities (figures 28 and 29) with those which have been measured by other investigators because the drift velocity is such a slowly varying function of N. We can merely check to see whether our values are of comparable size.

According to Pack and Phelps,[50] the drift velocity for electrons in either helium or argon at E/p = 10 volts / 760 mm-Hg should be between 1.0×10^5 and 1.5×10^5 cm/sec. Our fits yield consistent values for helium (1.7×10^5 to 1.8×10^5), but much higher values for argon (5.4×10^5 to 6.2×10^5). Nevertheless, it is known that drift velocity measurements are very dependent on the amount of contaminants. In fact, the data measured for gases obtained from "tanks" are generally somewhat higher than the drift velocities measured for pure gases.[46] In 99.99%-pure argon, for example, it is not uncommon to measure drift velocities which are too large by a factor of five.[46] Moreover, it has been found that the use of alcohol lowers the drift velocity.[46] Our values are therefore believed to be entirely consistent with experimental data.

Experimental verification of our values for τ and $H_o R_o$ is more difficult. Measurements of τ for noble gases have been made at 300° Kelvin for pressures up to 100 mm-Hg.[47-49] If these data are extrapolated in various ways to a pressure of 760 mm-Hg, one finds that τ might be expected to be at least 0.2 microsecond for argon and somewhere between 6 and 10 microseconds for helium.

The values which we have obtained for N=1 are 0.2 to 1.2 microseconds for argon (one gap having 2.5 microseconds) and 5.6 to 8.4 microseconds for helium. These values are entirely consistent with the values one might expect. For N much larger than one, however, it is difficult to see how our values for these gases could be consistent with those indicated above (c.f. figure 30).

The τ expected for the AHE mixture is uncertain because measurements of the effects of helium and ethanol in argon are still lacking. We are therefore unable to verify that a value for N between 10 and 20 is preferred to a value for N near 1. Note that it is not impossible for τ to be much larger in the AHE mixture than in pure helium or pure argon (as would be the case for the values of N which minimize chi square). The presence of the ethanol, for example, may reduce the effective destruction frequency of the helium and argon metastable atoms by allowing collisions which might otherwise cause de-excitation to result in the formation of metastable molecules.[47-49,51] Such arguments, however, are purely speculative.

Quantitative confirmation of our H_oR_o values appears to be impossible at this time. Investigators have done quite a lot of work on the destruction of metastable states, but not a great deal of work on the cross sections for the formation of these states. The H_oR_o data may therefore not be used in our efforts to find indicators for the best values for N.

To see how sensitive the above results are to the particular assumptions made regarding what physical processes are responsible for the tails, another model was considered which was, in a sense, a crude approximation of the Poisson Theory + Metastables. The assumption was made, even though there does not seem to be any physical justification for doing so, that there is a constant probability that one electron will always be in the gap when it is pulsed.* The model which resulted is the modification of the Poisson Theory which is necessary to incorporate the effects of this assumption.

When this model was fit to the data, the results were approximately the same as those for the Poisson Theory + Metastables. The constant-probability parameter turned out to have the values which one would expect from the size of the tails seen in figures 15 through 17.

The last model considered was devised in an attempt to add to the Poisson Theory the effects of delta rays produced along the particle's path of ionization. The delta-ray contribution was expected to be small for the gases and gap spacing which we considered. Nevertheless, the model was included for the sake of completeness.

In the model considered (appendix C), the contribution from delta rays is a rather complicated function of E_{min}, the minimum energy which an electron must have if it is going to be called a delta ray. It is also a rather complicated function of I, the average ionization potential of the gas. The approximate dependence, as mentioned previously, is such that one expects the ratio of a minimum-ionizing particle's energy loss through delta rays of

---

*At room temperature, cold field emission from the aluminum plates is entirely negligible even at 30 kV/cm (see references 52-54).

energy larger than E_{min} and the particle's total average energy loss to be approximately $(1/2)\cdot\ln(9.2\text{MeV}/E_{min})$ / $\ln(9.2\text{MeV}/I)$.[37]

What we found when considering the possible production of one delta ray per gap width, and using E_{min} and I as input parameters, was that the contribution from delta rays makes m smaller by an amount which is consistent with what one might expect from the above considerations. For argon (I = 28 eV), for example, m comes out approximately 20% smaller for E_{min} = 200 eV than for E_{min} = 10 MeV. It is interesting to note, however, that the chi squares for the fits using E_{min} = 200 eV are at least three times as large as those for the fits using E_{min} = 10 MeV, and the contribution from delta rays with energies above 10 MeV is entirely negligible.

In summary, many fits have been made in an effort to determine N for the AHE mixture. The conclusions which we can draw are as follows.

In fitting various theoretical models to the data measured for the sparking efficiency per gap as a function of t_{delay}, we found that the Poisson Theory + Metastables model can give an adequate description of the data.* Nevertheless, the efficiency curves which

---

*One should not misconstrue this statement as indicating that the Poisson Theory + Metastables model is indeed the model which correctly describes the physical processes responsible for the tails. To establish this for certain, a great deal more investigation will be required.

one might compute using this model need not be very different for different values of N if other model parameters are allowed to vary. For this reason, and because our knowledge of appropriate values for the other parameters is rather limited, our data have errors which are large in comparison to those which would allow an accurate determination of N. It is for this reason that very little significance could be given to a chi square as an indicator of the best value for N.

To supplement the chi-square indications, consistency checks were made on whether the fitted values for the parameters m, v, τ, and H_oR_o agree with other experimental data. Because drift-velocity determinations are highly subject to contaminants and are quite insensitive to changes in N, while experimental determination of values of τ and H_oR_o for different gases is in a state of infancy, the only worthwhile consistency check was that for m. Unfortunately, the only discrepancies which arose were those in making this check, so the results of the test are as a whole somewhat uncertain.

In the case of tank-pure helium, both the chi-square indication and the consistency checks are in favor of N=1. We can therefore say with great reliability that N is certainly small and most likely one for pure helium.

In the case of tank-pure argon, the chi-square indication and all but one of the consistency checks are in favor of N=1. The consistency check which failed is that for m, the N=1 value for m being a factor of three smaller than the value expected. The best value for N is therefore uncertain.

Because so little is known about argon-helium-ethanol mixtures, only the chi-square indication and the m consistency check can be considered in the case of the AHE mixture. Both of these are in favor of N on the order of 15. This is demonstrated, for example, by the curves shown in figures 20 and 21. There is rather good agreement between all of the data and the fits made holding N fixed at a value corresponding to a minimum in chi square, these values for N lying between 10 and 15 and the fitted values for m lying between 25 and 40 (short-dashed curves). On the other hand, there is very poor agreement between the data in the tails and the fits made holding N=1 and m=37 even though the other three parameters were allowed to vary (long-dashed curves).

If N is really about 15 for the AHE mixture, then the chambers would not have been able to detect the small ionization levels expected for quarks. As previously stated, such a large value of N might be the result of using a 1.5% concentration of ethanol in the AHE mixture. A quenching agent such as this may hamper the photoionization processes which are essential to spark formation.

The indications that N should be about 15 for the AHE mixture should not be taken too seriously, however, because the fits made holding N=1 and m=37 are not that different from the fits made in which N comes out near 15. For example, we might expect N, m, v, and τ to be the same for both gaps #1 and #4. H_oR_o, on the other hand, may depend on the surface conditions of the plates forming the gaps. If we make fits holding all four of N, m, v, and τ constant, with N=1, m=37, and values for v and τ which correspond to the best overall fit to the data of both gaps (i.e. $v=1.76\times10^5$ cm/sec, $\tau=1.40$ μs), then we get the ——-—— curves indicated in figures 20 and 21. The disagreement between these curves and the data is clearly not very striking.

A curious fact which may shed some light on the proper choice for N in the mixture is that the m values corresponding to N=1 for argon (m=14) and the AHE mixture (m=11) are in approximately the same ratios with the helium value (m=5) as those expected (i.e. 14/5 is to 48/5 approximately as 11/5 is to 37/5 --- c.f. figures 26 and 27, and table 5). Because it seems unlikely that N is very large in argon, as it would have to be to obtain m=48, we favor the interpretation that the "pure" argon we used had m=14 for some unknown reason. The data for both argon and the AHE mixture would then be consistent with N=1.

In short, on the basis of this test, we can conclude nothing about the efficiency of the chambers with any high level of confidence. The reason for this is undoubtedly that the processes which contribute to spark formation in the environment considered and which complicate the basic statistical processes involved are not fully understood. The exact role played by metastable states, for example, is yet to be determined. Perhaps a test conducted in an entirely different fashion would have proved to be more fruitful.*

In conclusion, we are forced to estimate the efficiency of the chambers as used in this experiment on the basis of the tests with helium described at the first of this section. From the results of those tests, one would expect the spark-chamber system to be at least 99% efficient for the detection of minimum-ionizing particles with charges at least as small as ~ 1/3. We therefore assume that the spark chambers were 100% efficient for the entire range of energy lossses considered.

---

*Krider, Bowen, and Kalbach(55) "poisoned" their 90%-helium 10%-argon gas mixture with a small concentration of SF_6. Electrons liberated by the passage of a unit-charged particle were thereby lost as a function of time through attachment to the SF_6 molecules. For a delay corresponding to 1/9 minimum ionization, they detected "no appreciable loss in efficiency."

C. The Overall Efficiency

Besides the inefficiencies discussed in the previous two sections, there were a few which arose in recording and in analyzing the data. The combined efficiency of the analyzer for accepting events for pulse-height digitization and of the Tally papertape punch for recording the pulse-height data was determined to be 98.1% ± 0.3%. The efficiency associated with scanning the spark-chamber film to select all of the events having "single" tracks was estimated to be 98.4% ± 0.2% by comparing the results of the original scan with the results of the rescan of two-thirds of the film. The X^2 analysis had an estimated efficiency of 98.4% ± 0.3% as determined from the data for figure 5. Finally, because the track misalignment data were expected to have fluctuations based on the statistics of 206 measured cosmic-ray events, the efficiency associated with the spark-chamber track-misalignment analysis was estimated to be 99.5% ± 0.5%.

The product of the efficiency factors given above is 94.5% ± 0.7%. With the efficiency of the spark chambers assumed to be 100%, the overall efficiency of the system as a function of the square of the charge of any minimum-ionizing particle detected is the product of 94.5% ± 0.7% and the efficiency function shown in figure 14.

VI. THE EXPERIMENTAL RESULTS

A. A Summary

The experiment was run for 4,664 hours. During this period, 2.12×10^8 cosmic-ray particles passed through the array, and 93,000 events occurred which corresponded to energy losses between 0.03 and 0.7 minimum in each of the six counter trays. None of these 93,000 events had the necessary properties to satisfy the analysis requirements for an event produced by a particle with fractional charge.

The analysis criteria used to determine whether an event had resulted from the passage of a real particle were based on the response of the system to cosmic-ray particles. For an event to be acceptable as one made by a real particle, the misalignment of the tracks seen in the two spark chambers was required to be no worse than the worst misalignments measured for cosmic-ray events. In addition, a quantity X^2, whose smallness was an indication of the probability that the pulse heights in the six trays actually corresponded to the energy losses of a particle traversing the array, was required to be smaller than a certain limit. This limit was set so high in comparison to the values of X^2 found for cosmic-ray events that the analysis was rather insensitive to the exact details of the energy-loss distributions assumed for particles with fractional charges.

The analysis showed that no event which corresponded to energy losses between 0.04 and 0.7 minimum in each tray was representative of an event made by a real particle (c.f. table 4). Thus, in contrast to previous experiments which had used only scintillation counters, our experiment was not limited by background.

Although the spark chambers had proved to be useful in reducing the background, there had been some question whether spark chambers could function efficiently for the low levels of ionization expected from particles with small fractional charges. The ionization resulting from the passage of a fractionally charged particle was expected to be much smaller than that for any known particle because the number of ion pairs produced per centimeter in a gas by a particle is proportional to the square of the particle's charge. To determine whether our spark chambers had indeed been sensitive for the entire range of energy losses considered, several tests were conducted to determine the efficiency of the chambers as they had been used in this experiment.

In one test, the chambers were operated with pure helium rather than with the AHE mixture (76.0% argon, 22.5% helium, 1.5% ethanol). Because a particle produces fewer ion pairs per centimeter in helium than it does in the AHE mixture, the use of helium allows one to simulate a level of ionization with unit-charged particles which should correspond to the level obtained from the passage of a fractionally charged particle through the AHE mixture.

When using pure helium and triggering on unit-charged cosmic-ray particles, the efficiency of the spark-chamber system was determined to be slightly more than 99%. The chambers were then operated with 99.35% helium and 0.65% ethanol to determine the effect of a small concentration of ethanol, which is a "quenching" agent. In this case, the efficiency of the spark-chamber system was determined in the same way to be even higher than when using pure helium.

With the results of these tests in mind, one might expect the system to be at least 99% efficient when operated with the AHE mixture in search of any fractionally charged particle which produces no fewer ion pairs per centimeter than that produced by a unit charged particle in helium. Approximately 5 ion pairs are produced per centimeter for minimum ionization in pure helium while about 37 ion pairs are produced per centimeter for minimum ionization in the AHE mixture. One might therefore expect the chambers as operated in this experiment to have been at least 99% efficient for the detection of particles with fractional charges at least as small as $(5/37)^{1/2} \cong (0.37)$.

Another test was conducted in an effort to substantiate a theoretical prediction that only one electron is necessary (on the average) in a one-centimeter gap to cause spark formation in the noble gases considered when a 30-kV pulsing voltage is applied. This test revealed that indeed only one electron is required in tank-pure helium. For either tank-pure argon or the AHE mixture, however, the required number of electrons could unfortunately not be ascertained with any high level of confidence. This test was therefore not helpful in estimating the efficiency of the spark chambers as they were used in this experiment.

On the basis of the results of the tests conducted with helium, we assumed that the spark-chamber system had been 100% efficient for the track-selection criteria used. The overall efficiency of the system was therefore the product of the efficiencies of the recording equipment and the analysis procedures (94.5% ± 0.7%) and the efficiency of the counter system (figure 14). In particular, the overall efficiency of the system was 87.9% ± 0.7% for the detection of minimum-ionizing quarks of charge 1/3 and 42.5% ± 0.7% for the detection of minimum-ionizing quarks of charge 2/3.

B. Upper Limits For the Flux of Quarks in Cosmic Rays

Using the efficiency values quoted above, the experimental acceptance, and the length of time the experiment was conducted, we may express the results of this experiment in the form of upper limits for the flux of quarks in cosmic rays near sea level.

Because the probability of obtaining zero events is 10% when the average number of events expected is 2.3, according to Poisson statistics, we shall consider that the average number of events which one would observe in the length of time we searched is 2.3. In this way, we shall derive 90%-confidence flux limits.

First note that the product of the acceptance of the array and the length of time we searched is $(0.15\pm0.01\ m^2sr)(4{,}664\ hrs) = 700\pm47\ m^2sr\ hrs$. The 90%-confidence upper limits for the flux of minimum-ionizing quarks in cosmic rays near sea level are therefore the following:*

$$\left\{\begin{array}{ll} (1.04\pm0.07)\times10^{-10}\ cm^{-2}sr^{-1}sec^{-1} & \text{for quarks of charge } 1/3 \\ (2.03\pm0.16)\times10^{-10}\ cm^{-2}sr^{-1}sec^{-1} & \text{for quarks of charge } 2/3 \end{array}\right\}$$

These limits are, respectively, factors of at least 25 and 10 lower than those quoted for an Adair experiment.(18) When they are compared with the results of another experiment using spark

---

*A report on two-thirds of the data acquired in this experiment is presented in the Physical Review Letters.(56)

chambers,[22] our results represent an improvement of approximately a factor of 14 for charge 1/3 and a factor of 7 for charge 2/3. When compared to the results of an Argonne experiment which terminated at about the same time as this experiment,[21] our results represent an improvement of a factor of 4 and a factor of 8, respectively.

Although the results of many cosmic-ray experiments have been reported since our experiment terminated in the middle of 1967,[57-58] the lowest flux limits set to date are only a factor of two lower than ours. Garmire, Leong, and Sreekantan have reported a 95%-confidence limit of 0.66×10^{-10} $cm^{-2} sr^{-1} sec^{-1}$ for quarks of charge 1/3.[57] Ashton _et al_. have reported a 90%-confidence limit of 0.8×10^{-10} $cm^{-2} sr^{-1} sec^{-1}$ for quarks of charge 2/3.[57]

C. Significance of the Results

Two types of cosmic-ray experiments have been conducted in search of quarks. In one type, an array of detectors is used to search for a quark which is not preceded or followed by any integrally charged particles for a time interval which is at least as large as several microseconds. Any quark which is detected must thereby be completely "isolated" from all integrally charged particles both in space and time. Most cosmic-ray experiments, including ours, have been of this type.*

In the other type of cosmic-ray experiment, an array of detectors is used to search for quarks in cosmic-ray air showers by triggering on the arrival of a shower front. Such a front is composed of photon-produced integrally charged particles, and is expected to precede any quarks which might be present by a time interval much shorter than one microsecond. Any quark which is detected must therefore arrive at the site of the experiment in close association with a shower of integrally charged particles.

Because experiments using "shower-front" techniques may be less familiar, we shall describe two experiments of this type. In one experiment, Jones *et al*. made the assumption that quarks are quite massive and then conducted a search for massive hadrons which lag behind the fronts of cosmic-ray air showers.(58) They assumed,

---

*For our array, which had a cross-sectional area of 1/4 m^2, the isolation interval was set at ten microseconds because the spark chambers had a memory on the order of seven microseconds.

in particular, that strongly interacting particles of total energy E and mass M, if produced at a height Z above their experimental apparatus, would arrive at the apparatus delayed by a time interval T with respect to the arrival of the associated air shower of photons and extremely relativistic leptons. Because the speed of the strongly interacting particles depends only on E and M, the time interval T is a function only of Z, E, and M. They could therefore estimate M by measuring E and T, and by making some assumption to specify Z.

By measuring sets of E's and T's for showers arriving at an altitude of 10,600 feet, Jones et al. found one event which corresponded to a particle of mass 6.5 BeV/c^2 and a flux on the order of 10^{-10} $cm^{-2}sr^{-1}sec^{-1}$ (its charge was not determined). The particle's energy and range in a total absorption spectrometer were reported to be atypical of those measured for a nucleus. Nevertheless, there was an 8% chance that the event had been produced by a nucleon. For this reason, the event was not regarded as significant evidence for the existense of massive particles.

In a somewhat similar fashion, McCusker et al. have conducted a search for particles of charge 2/3 in the cores of cosmic-ray air showers.[58] Four 30-cm-diameter expansion-delayed Wilson cloud chambers, three of which were shielded by 15 cm of lead, were placed in an array of more than 64 plastic scintillation counters set at distances up to 55 meters from the chambers. Triggering was accomplished by the coincidence of pulses from three small Geiger-counter trays placed roughly two meters apart and over the chambers. After running for more than one year and detecting approximately 7×10^3 showers (7×10^4 tracks), McCusker et al. found five tracks having about half the number of droplets as tracks made by relativistic electrons.

To interpret McCusker's observations without the introduction of quarks, one may assume that the electrons whose tracks were chosen as the basis for droplet normalization had speeds which put them partially up on the 40% to 50% relativistic rise in energy loss above that for minimum ionization in the gas mixture considered. One may then estimate the probability that a "half-ionized" track might be the result of a statistical fluctuation in the energy loss of a minimum-ionizing integrally charged particle. This can be done using Poisson statistics based only on the droplets in the primary ionization (i.e. on about 1/3 of the total number of droplets[59]). One then finds that observation of only five tracks with "half ionization" is entirely consistent with the interpretation that the particles producing the tracks were minimum-ionizing unit-charged particles. Consequently, McCusker's five tracks do not in any way serve as conclusive evidence for the existence of quarks.

By not observing any quarks, we and other investigators have been able to set various upper limits for the flux of quarks in cosmic rays. To know how meaningful the flux limits set by any particular experiment are, one must know the efficiency of the method of detection which has been employed. An efficiency of this kind can be determined only through a knowledge of quark dynamics, for a knowledge of the manner in which quarks should be found presupposes a knowledge of how and where quarks are produced and how they interact. Unfortunately, a complete theory of quark dynamics is non-existent at the present time, so we do not know whether an "isolation" technique or a "shower-front" technique should be more feasible. We can speculate, however, and in this way make a few qualitative remarks.

If quarks exist only in the primary cosmic radiation and interact only very weakly, they might reach sea level unaccompanied by other particles. In such a case, the use of an "isolation" technique would be essential.

If quarks exist in the primary cosmic radiation and undergo strong interactions with the known hadrons, or if quarks are produced in the upper atmosphere by cosmic-ray particles (regardless of the strength of their subsequent interactions), they will usually be accompanied by an associated shower of integrally charged particles through at least part of their way down to sea level. If the energies involved are not too large, such a shower might be expected to "die out" before reaching an experimental site. This may indeed be the case for sea-level sites, because the largest yield of quarks produced by cosmic rays should occur near the production threshold (c.f. Chapter VII).* As a result, if quarks are not too massive, it may be much more effective to use an "isolation" technique for an experimental site near sea level.

Even if quarks are "accompanied" by a shower all the way to sea level, however, there is still a chance that an "isolation" technique may be more effective. It is possible, for example, that the average transverse momentum imparted to a quark during its production and through subsequent interactions is one or perhaps two orders of magnitude larger than the several hundred MeV/c measured for existing hadrons. A search based on a "shower-front" technique, which is concentrated near the cores of air showers, may then be ineffective. A search based on an "isolation" technique, on the other hand, is restricted to the outskirts of these showers, where the average particle density is smaller than the reciprocal of the cross-sectional area of the array used.

There are several reasons why such large transverse momenta might be expected. First, the average transverse momenta found for the known hadrons produced at accelerator energies is a slightly increasing function of the mass of the particle considered.[60] Second, all efforts to use Monte Carlo calculations to simulate central electron densities found in multiple-core shower events and lateral muon densities found in single-core shower events have

---

*The threshold for quark production in cosmic rays is approximately $(2m_q+M)^2/2M$, where m_q is the mass of a quark and M is the mass of a nucleon.

failed when the average transverse momenta considered are restricted to be less than 1 BeV/c.(63) However, when larger transverse momenta are allowed, the results of these calculations can be made to agree with observations.(63) Third, there is evidence for the occurrence of multi-cored showers of size greater than 10^6 particles and total energy greater than 10^{13} eV which seem to have associated transverse momenta which increase with the total shower energy involved and which are on the order of 5 BeV/c or larger.(63-64)

If it turns out that the large transverse momenta found in multi-cored showers are those attributed to quarks, then the best place to look for quarks is somewhere outside the cores of air showers. Just how far out one should look depends on the relative sizes of the longitudinal and transverse momenta involved. For large distances, an "isolation" technique would certainly be more effective.

In contrast, if the mass of a quark is larger than 100 BeV/c^2 so that quarks are produced only in "extensive air showers" (i.e. showers with energies above 10^{13} to 10^{14} eV and more than 10^5 to 10^6 particles), and if the average transverse momentum imparted to a quark is only of the order of several hundred MeV/c, then most quarks would probably be found within a distance on the order of meters from the shower axis.* The integrally-charged-particle density, on the other

---

*For specific data on the density of the known leptons and hadrons as a function of distance from the axis of showers produced by primaries of various energies, see references 60, 61, and 62.

hand, would not fall below one in an area equal to the cross-sectional area of our array until a distance on the order of 10's to 100's of meters from the shower axis. Thus, for large showers and relatively small transverse momenta, use of a "shower-front" technique would be essential.

These qualitative remarks are of course mere speculation because, as we mentioned earlier, our knowledge of quark dynamics is very limited. Any statements concerning the preferability of either a "shower-front" technique or an "isolation" technique must at the present time be regarded as pure conjecture.

Because quarks have not yet been discovered through the use of various methods of search (accelerator, terrestrial, cosmic-ray, solar, or galactic),[5-10,13-22,24-33,57-58,65] one might think that it is becoming increasingly more difficult to suspect that quarks do actually exist in nature but have somehow managed to escape detection. One must remember, however, that there is a tacit assumption underlying any interpretation of the present experimental evidence as evidence against the existence of quarks in nature. This assumption is that the cross section for quark production off nucleons and the cross section for quark-nucleon interactions have the same order of magnitude as the corresponding cross sections where observed hadrons are involved instead of quarks. We emphasize that this assumption may not be correct.

As we point out in the next chapter, it may be that the production cross section for quarks is significantly smaller than one might have expected on the basis of the strong interactions which occur between particles whose masses are less than 1 BeV/c^2. If a quark is assigned a Regge trajectory with unit slope, for example, the total cross section for the production of quarks in cosmic rays is extremely dependent on the size of the quark mass. In particular, we find the cross section to be approximately 10^{-36} cm^2 for a mass of 1.5 BeV/c^2 but as low as 10^{-72} cm^2 for masses as large as 3.0 BeV/c^2.* With such a dependence, the mass of a quark need be only as large as about 1.3 BeV/c^2 to explain why quarks have not yet been observed. The reason for this is that the flux of primaries with energies above the quark-production threshold is then so small that no cosmic-ray experiments conducted to date would have been expected to observe any quarks (see Chapter VII).

To search for quarks with masses larger than a few BeV/c^2, in case the quark trajectory does have unit slope, an experiment which is conducted for a time much longer than in the past is in order. This could be a cosmic-ray experiment which uses a larger-acceptance array and is conducted for a time on the order of years at mountain altitudes (or for a time on the order of weeks at balloon altitudes). It could also be an accelator experiment.

Besides the possibility that the cross section for quark production is very small, there is a chance that the quark-nucleon

---

*Note that, at present, the smallest estimate for the upper limit of the total cross section for the production of quarks in accelerators is of the order of 10^{-39} cm^2.(65)

interaction is much stronger than expected. In such a case, quarks produced in the upper atmosphere, if they are able to reach sea level at all, may not arrive with speeds sufficiently high to enable their energy losses by ionization to be less than that for a minimum-ionizing unit-charged particle. If this is so, a search conducted at higher altitudes would certainly be in order.

In the light of these remarks, one must say that it is still a matter of speculation whether quarks actually exist in nature or whether their existence is merely theoretical.

VII. LOWER LIMITS FOR THE MASS OF A QUARK

A. Introduction

As we mentioned in Chapter I, it is convenient in expressing certain symmetries of the strong interactions to think of mesons and baryons as being composed of quarks. Since these symmetries can be expressed without a knowledge of the mass of a quark, the quark mass remains unspecified in the theory and is therefore a matter of assumption.

One might expect the mass of a quark to be on the order of a couple hundred MeV/c^2 because mesons are assumed to be composed of a quark-antiquark pair and baryons are assumed to be composed of three quarks. It is unlikely that the quark mass is this small, however, because real hadrons with masses of a couple hundred MeV/c^2 have been observed in a very large number of experiments. Therefore, unless the cross section for quark production is for some reason many orders of magnitude smaller than cross sections associated with strong interactions, quarks with such small masses would also have been observed by now.* One is thereby led to suppose that, if quarks do

---

*It is possible that a quark inside a meson or a baryon sits in a potential well which is quite shallow relative to the zero-energy level but which has huge barriers that must be surmounted (or tunnelled through) before the quark can be freed. A quark need therefore not be very massive if a great deal of energy is required to produce it, for it may merely be bound within huge barriers. Nevertheless, in such a case, we shall speak as though its mass were larger. Consequently, when we refer to the "mass" of a quark, we shall mean its effective rest mass as a constituent of a meson or a baryon, not its rest mass as a free particle.

exist as real particles, the mass of a quark is considerably larger than several hundred MeV/c^2. Just how large the quark mass need be to explain the lack of observation is dependent on the models considered for their production.

In the past, several approaches have been used to obtain lower limits for the quark mass from various experimental results. The general method employed has been to make some assumption to specify the production cross section and then to choose a quark mass which is large enough to explain the observed yield.* DeLise and Bowen, for example, chose a flat cross section on the order of ten microbarns and obtained a limit between 7 and 9 BeV/c^2.[(66)] Adair and Price, in computing a momentum spectrum of quarks in the atmosphere, assumed that the quark production cross section has a particular behavior near threshold and is asymptotically one microbarn.[(67)] Approaches using cross sections based on statistical arguments, such as Hagedorn's thermodynamic arguments, have also been considered.[(68)]

The approach that we shall use here is one in which the quark-production cross section is estimated in what we think is a more justifiable manner. The model to be considered is one involving the multi-peripheral Regge hypothesis.[(69)]

In particular, we propose that if quarks are produced by cosmic rays, they are probably produced in pairs through the

---

*The yield of quarks is usually a decreasing function of quark mass because of kinematical considerations and/or because of the mass dependence assumed for the production cross section.

interactions of primary cosmic-ray protons or secondary pions with nitrogen or oxygen nuclei in the upper atmosphere. Of the many processes which could contribute to such production, we find it necessary to consider only those which contribute near the production threshold. Processes with higher thresholds have smaller yields because the primary cosmic-ray proton spectrum falls with increasing primary energy.

Cross sections for the lowest-threshold processes are computed using multi-peripheral Reggeized amplitudes (section B).[69] Model parameters are estimated by assuming that quark couplings are strong and of the order of proton couplings. Because the cross section for each process is extremely dependent on the intercept and therefore on the slope of the quark's Regge trajectory, two separate cases are considered: a quark trajectory of slope 1 $(\text{BeV}/c)^{-2}$, and a flat quark trajectory. The energy dependence assumed for the total production cross section is derived in section C.

Once produced, the quarks are assumed to lose energy through inelastic collisions with the nuclei which they encounter on their way down through the atmosphere. A detailed treatment of these interactions could not be precise because a complete theory of quark dynamics is still lacking. These interactions are therefore parameterized in terms of an attenuation length for the quarks. The flux of quarks at any depth in the atmosphere is then obtained through the use of a simple diffusion equation (section D).

The rate of quarks through our array is obtained from the expression for the flux at sea level and the experimental acceptance. By comparing this rate with the rate observed experimentally, we obtain an expression which gives a lower limit for the mass of a quark as a function of its attenuation length in the atmosphere. Taking this attenuation length to be on the order of the attenuation length for a proton, we find the following lower limits for the mass of a quark (section E): 1.3 ± 0.2 BeV/c^2 if quarks have a Regge trajectory with unit slope, just as the existing hadrons do; 6 ± 2 BeV/c^2 if quarks are "elementary" with a flat trajectory; and intermediate lower limits if the slope of the quark trajectory is somewhere between one and zero $(\text{BeV}/c)^{-2}$.

These results depend heavily on an assumption that the production amplitudes factor into two-body-like amplitudes each of which can be Reggeized and each of which fall when certain four-momentum transfers get large. A discussion of the dependence of the results on our choice of parameter values and on the particular assumptions which were made is given in section F. The significance of the results is discussed in section G.

B. Production Cross Section Near Threshold

We assume that if quarks are produced in cosmic rays, the most likely production mechanism is the breakup of a meson or a baryon into its constituent quarks. This breakup is expected to occur in particle interactions taking place near the top of the atmosphere. The incident particles would be primary cosmic-ray protons or secondary pions because they are the most abundant of the highly energetic strongly interacting particles (table 6). The target particles would be nitrogen or oxygen nucleons. For incident energies just above the production threshold, typical interactions might be those represented by the diagrams in figure 33. Note that a particle which is decomposed can be either an incident particle or an exchanged particle. The symbol POM represents the Pomeranchuk trajectory (diffraction).

For larger incident energies, more and more channels become available. It would be possible, for example, to have interactions like those in figure 33 with the addition of a number of final-state mesons, or even a baryon-antibaryon pair.

If we consider the production of one of the known hadrons, the cross section per channel generally decreases as more final-state particles are added (resonance formation being neglected). The number of contributing channels, however, usually increases faster than the cross section per channel decreases when all allowed exchanges, final-state particles, and permutations of the positions on the

TABLE 6: RELATIVE COSMIC-RAY ABUNDANCES FOR SOME STRONGLY INTERACTING PARTICLES[60]

Primary	Relative Abundance	Combined Differential Flux $N_p(0,E)$
H	70	$2.35(E \text{ in BeV})^{-2.67}$ nucleons $cm^{-2} sr^{-1} sec^{-1} BeV^{-1}$ (at the top of the atmosphere)
He	10	
$Z \geq 3$	1	

Secondary	Differential Flux Ratios at Depth x g/cm^2		
Charged Pions	$N_\pi(x,E)/N_p(x,E)$	$\approx$ 0.3	for all x
Kaons	$N_K(x,E)/N_\pi(x,E)$	$\sim$ 0.1	for all x

FIGURE 33: DECOMPOSITION OF MESONS AND BARYONS

REACTION	DIAGRAM
$\pi N \longrightarrow q\bar{q}N$	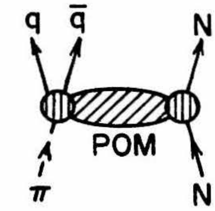
$pN \longrightarrow qqqN$	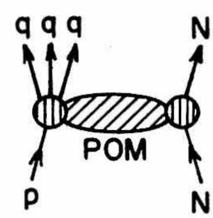
$pN \longrightarrow pNq\bar{q}$ $\pi N \longrightarrow \pi Nq\bar{q}$	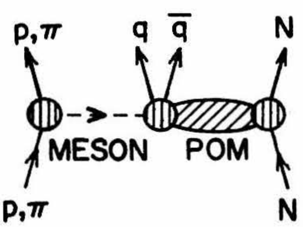
$\pi N \longrightarrow \overline{\text{BARYON}}\ N\ qqq$	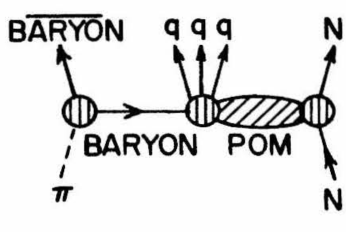

diagrams of all final-state particles are considered. As a result, the total cross section for the production of a certain particle in an interaction involving two given incident particles is generally an increasing function of incident energy up to energies well above threshold. This is true, for example, in the production of pions, kaons, or anti-protons in proton-nucleon collisions.[(70)] We shall therefore assume that it is true for quark production.

The general shape of the total cross section as a function of s for the production of quarks in cosmic rays is thus assumed to be quite similar to that illustrated in figure 34 for the case of anti-proton production in proton-proton interactions.* The Lorentz-invariant quantity s is the square of the energy available in the CM frame. The cross section does not rise indefinitely, of course, because the relatively flat total inelastic cross section serves as an upper bound.

To obtain the yield of quarks in cosmic rays, one must integrate the product of a production cross section of this sort and the incident flux. Because the flux of primary cosmic-ray protons and the flux of secondary pions both fall with increasing energy E approximately as $dN/dE \sim E^{-2.67}$ (table 6), the yield of quarks at small s is expected to be much larger than the yield at very large s. The exact behavior of the total production cross section at very large s is therefore of no real importance

---

*The curve in figure 34 is obtained by numerical integration of Sanford and Wang's empirical differential cross sections under the assumption that the total proton-proton cross section is proportional to the total proton-beryllium cross section (see reference 70).

FIGURE 34: THE EMPIRICAL TOTAL CROSS SECTION FOR ANTI-PROTON PRODUCTION IN PROTON-PROTON INTERACTIONS[70]

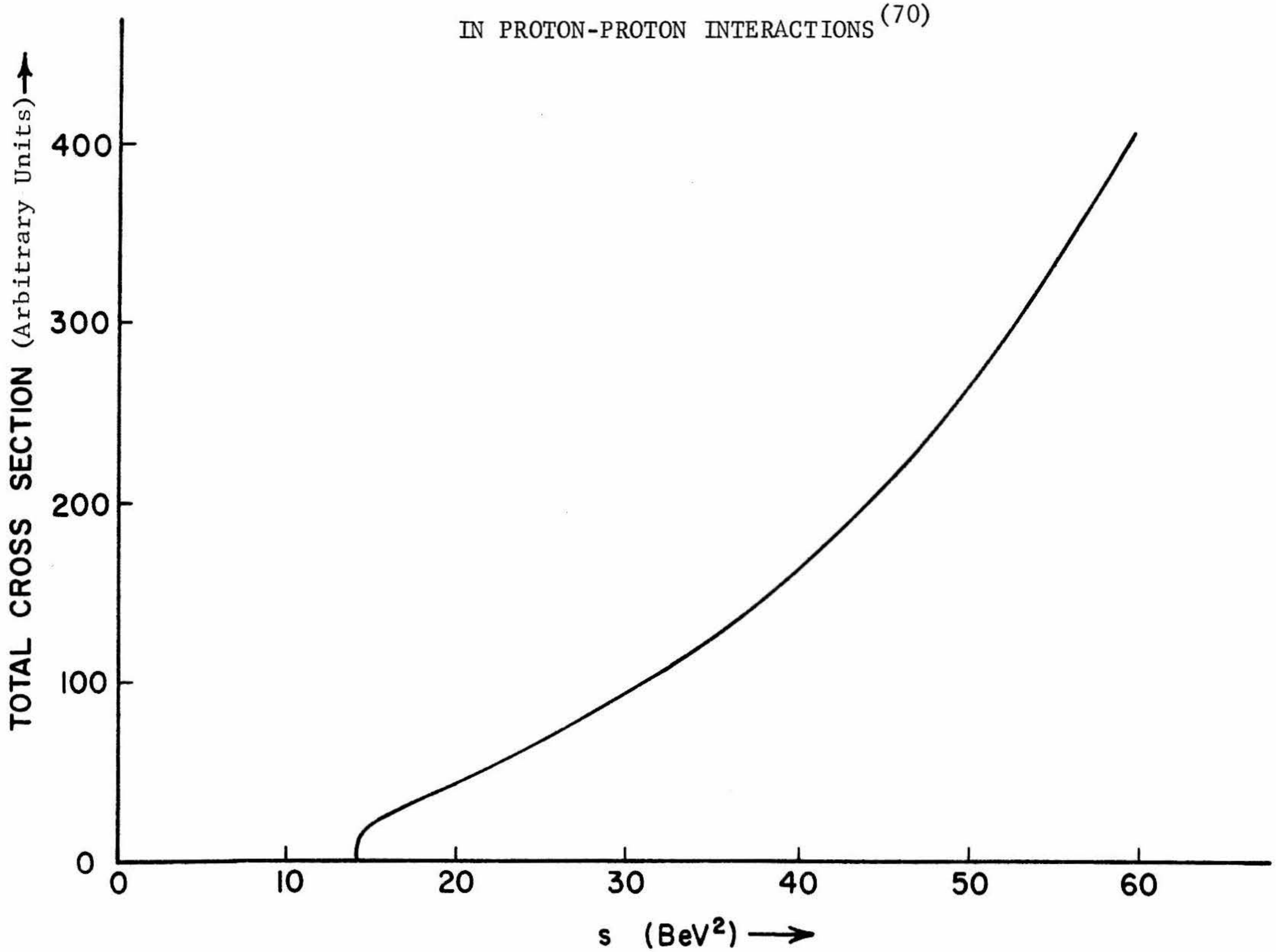

here. For this reason, we shall treat in detail only those processes which contribute near the production threshold and assume that the large-s dependence of the production cross section is merely of the same character as that observed in the production of the known hadrons (e.g. in the production of anti-protons).

To decide which diagrams have the highest yield near the production threshold, one must consider not only the relative cross section but also the type of incident particle and the size of the threshold for each diagram, for the latter affect the magnitude of the incident flux. In our model, the cross section for a process involving the decomposition of a baryon is expected to be at least two orders of magnitude smaller than the cross section for the corresponding process involving the breakup of a meson.* Because baryon decomposition produces three final-state quarks while meson decomposition produces only two, the ratio of threshold energies for these processes is approximately $(3/2)^2 = (9/4)$. The corresponding ratio of integrated incident fluxes is therefore approximately

---

*Baryon decomposition involves one more exchange, one more vertex, and one more final-state particle. From the latter half of reference 76, one can see that the extra exchange (which is a "di-quark" Reggeon) introduces a factor $1/(1-\alpha)$, where α is the intercept of the di-quark trajectory. This intercept may be as small as $-(2m_q)^2$, where m_q is the quark mass. The extra vertex introduces another diffractive factor of $1/2a_i = 1/5$ (see appendix section E.1 for the definition of a_i) and one more coupling-constant factor $(g/4\pi)^2$, which is of the order of 1/2. The extra final-state particle introduces a phase-space factor of 1/2. One might therefore expect baryon decomposition to be suppressed relative to meson decomposition by a factor on the order of $1/(80m_q^2)$.

$(4/9)^{1.67} \cong (1/4)$. For these reasons, we will consider only those processes involving the production of one quark and one anti-quark. Processes treating the decomposition of baryons will be ignored.

One may note that the threshold for quark production is approximately $(2m_q+M)^2/2M$, where m_q is the mass of a quark and M is the mass of a nucleon (c.f. figure 33). If we assume that m_q is of the order of a couple of BeV/c^2, the threshold is approximately 10 BeV. At these and higher energies, processes with direct-channel resonance formation are assumed to be negligible in comparison to processes with exchanges.* A process with a Pomeranchuk exchange is assumed to dominate a similar process without Pomeranchuk exchanges. Diagrams with multi-Pomeranchuk exchanges are ignored, however, because of the associated problems with unitarity violation[71-72] and because the few data which do exist seem to indicate that such processes are suppressed.[73] By assumption, vertices with more than three particles are always reduced to three-particle vertices by inserting appropriate exchanges.

The diagrams which we shall consider are therefore only those belonging to the four classes of diagrams shown in figure 35. The brush-like particle structure leaving each vertex shown symbolizes one or more particles. It is assumed that each vertex circle with

---

*Although this assumption is probably not 100% valid for small quark masses, especially near threshold, the effect of its failure on the mass limits which we shall obtain is not expected to be significant.

FIGURE 35: DIAGRAMS FOR QUARK PRODUCTION

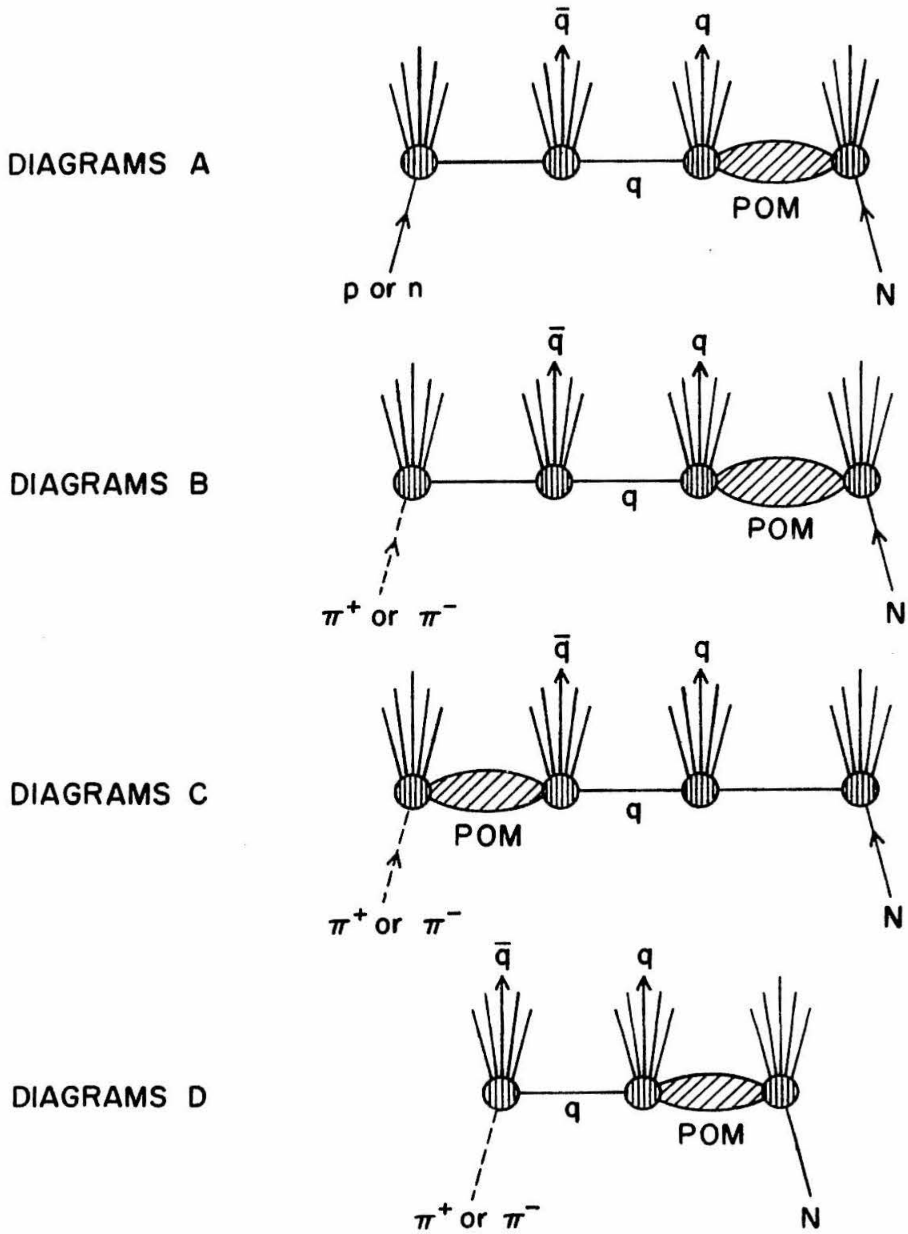

its "brush" is to be expanded by inserting exchanges until a given diagram to be considered contains only three-particle couplings. Note that quark production in all of the diagrams proceeds through the break-up of an incident meson (diagrams D) or an exchanged meson (diagrams A, B, and C).

All particle lines which are not labelled in figure 35 represent, for example, any member of the $J^P = 0^-$, 1^-, or 2^+ meson nonets, the $(1/2)^+$ baryon octet, or the $(1/2)^-$ antibaryon octet. The symbol q represents a quark, $\bar{q}$ represents an anti-quark, and POM refers to the Pomeranchuk exchange. Note that the q and $\bar{q}$ in each diagram can be interchanged.

The lowest-order diagrams are defined to be those having only one particle in each "brush." These diagrams are shown in a collective fashion in figure 36. Here M refers to any of the mesons considered, and B refers to any of the baryons considered. In computing the cross section for any one of these diagrams, all members of M and B are considered.

The next order diagram, as represented in figure 35, has one vertex with two final-state particles. This order corresponds to the addition of one final-state meson to the diagrams in figure 36. There are six such diagrams for class A and five for each of classes B, C, and D. The next order corresponds to the addition of two mesons or a baryon-antibaryon pair, with all possible permutations of the final-state particles considered. There are 24 such diagrams for class A, 20 for each of classes B and C, and 18 for class D.

FIGURE 36: LOWEST-ORDER DIAGRAMS FOR QUARK PRODUCTION

DIAGRAMS A

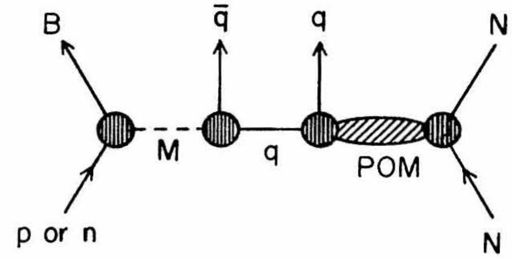

DIAGRAMS B

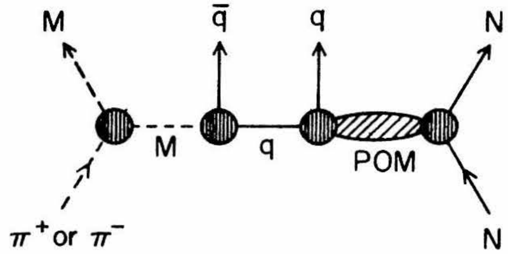

DIAGRAMS C

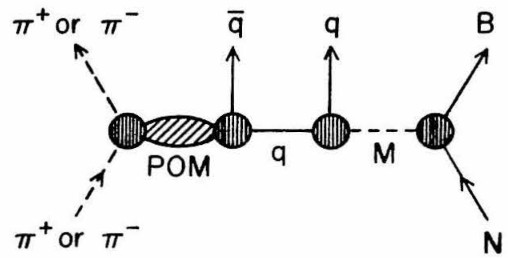

DIAGRAMS D

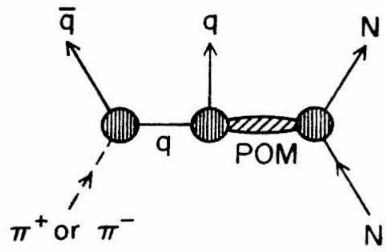

To obtain the total production cross section near threshold, we could compute cross sections for all diagrams of each of the first few orders. Lower limits for the quark mass could then be determined by assuming some reasonable form for the dependence of the total production cross section on s. If this were done, however, one would find that the mass limits obtained are dependent only on the order of magnitude of the production cross section near threshold and on the fact that the production cross section rises above threshold as a function of s. Just how the cross section rises, how it levels out at some asymptotic value (if it indeed does), and how large the asymptotic value is are all of no real importance.

For these reasons, we shall determine the total production cross section near threshold just to an accuracy of within a factor of two. The corresponding accuracy in the mass limits obtained will be better than 10%. The diagrams which we shall consider for this purpose are only those for the lowest-threshold processes (diagrams D, figure 36). These processes are a subclass of those involving the decomposition of secondary pions. The incident flux to be considered is approximately 3/10 of the cosmic-ray proton flux (table 6).

After computing the magnitude of the total production cross section near threshold in this manner, we shall consider two methods for obtaining its s dependence: one based on the total cross section for anti-proton production in proton-proton interactions and another employing techniques which are quite arbitrary (section C). The two ways in which the total production cross section will be assumed to rise are relatively extreme in comparison to a rise one might expect, the rise being somewhat too fast as a function of s in one case and too slow in the other. Because of the variety of possible cross sections which lie between these two extremes, we shall effectively obtain results as a function of the s dependence assumed for the total production cross section.

The calculational techniques which we shall use in computing cross sections for the lowest-threshold diagrams are patterned after the techniques which have been used for similar diagrams involving the known hadrons instead of quarks.[69,73] If the quarks and anti-quarks in the lowest-threshold diagrams are replaced respectively by nucleons and anti-nucleons, for example, the resulting diagrams are those which might be used to describe the reaction $\pi^- p \rightarrow \bar{p} n p$ at high energies. Although experimental data for this reaction are somewhat limited, a significant fraction of the events observed for an incident pion momentum of 8 BeV/c appear to be multi-peripheral events.[69,74] One might therefore expect the amplitudes for quark production to be multi-peripheral. Such a choice would be consistent with the multi-peripheral Regge hypothesis, which asserts that cross sections for most processes at high energies can be computed under the assumption that the amplitude for each process can be factored into two-body-like amplitudes each of which can be Reggeized, and that each such process is dominated by multi-peripheral events.[(69)*]

We therefore choose the amplitudes for the lowest-threshold diagrams for quark production to be multi-peripheral. The model considered is thereby a subclass of those in which an exponential damping in four-momentum transfer is assumed at each vertex.

For the reaction $\pi^- p \longrightarrow \bar{p}np$ with 8-BeV/c pions, the fraction of events which are multi-peripheral may be as low as ten to forty per cent.[(74)†] Although larger percentages are generally expected as incident energies increase, the yield of quarks is expected to be largest near the quark-production threshold. The possibility therefore exists that quark production may not be completely multi-peripheral, and that the cross sections which we shall compute may only be lower limits. In section F, we shall estimate the size of the factors by which the cross sections may be too small, and then discuss what effect such factors have on the final results.

One may note that there are just two diagrams of lowest-order of class D (figure 36) for a given incident charged pion, one diagram corresponding to each of the two final-state locations of the antiquark. Multi-peripheral amplitudes for these two diagrams are expected to interfere just above threshold, where four-momentum

---

*The consistency of this assumption with experimental data is still under investigation. The multi-peripheral Regge hypothesis has, however, been shown to be consistent in at least one case.[(73)]

†Of the events having the square of the invariant mass of each pair of final-state particles above 3 BeV^2, seventy-five per cent are multi-peripheral (reference 74, Andrews' thesis).

transfers are large. Further above threshold, however, smaller four-momentum transfers are possible (c.f. appendix section E.3). Although the yield of quarks is expected to be highest somewhere near the production threshold, as mentioned previously, we assume that most of the production occurs enough above threshold to enable all four-momentum transfers to be quite small. The major contributions from the two diagrams are then in different kinematic regions, so little interference is expected. In other words, for the accuracy desired here, we assume that all interference effects are negligible.*

To be consistent with the multi-peripheral Regge hypothesis, the amplitude for each diagram is assumed to factor in the kinematic regions considered into two-body-like amplitudes each of which can be Reggeized.[75] Each amplitude is therefore of the following form:[69]

$$\text{Amplitude} = f_1(t_1)\; g_2(t_1,w,t_2)\; f_3(t_2)\; \beta(t_1,t_2)\; S(t_1,t_2)$$

$$\cdot \frac{(s_{12}/s_o)^{\alpha_q(t_1)}}{\sin\{\pi\, \alpha_q(t_1)\}} \cdot \frac{(s_{23}/s_o)^{\alpha_{Pom}(t_2)}}{\sin\{\pi\, \alpha_{Pom}(t_2)\}}$$

---

*The failure of this assumption will be treated in section F in connection with the failure of the assumption that the production amplitudes are multi-peripheral.

The notation used here is the following: $f_1(t_1)$ is the coupling at the $\pi\bar{q}q$ vertex, $g_2(t_1,w,t_2)$ is the coupling at the central (qqPom) vertex, $f_3(t_2)$ is the coupling at the ppPom vertex, β contains the remaining residue factors, S contains the signature factors, $\alpha_q(t)$ is the Regge trajectory associated with a quark,* $\alpha_{Pom}(t)$ is the Pomeranchuk trajectory, t_i is the four-momentum transfer at the i^{th} left-most vertex,† s_{12} is the square of the invariant mass of the $\bar{q}q$ pair, s_{23} is the square of the invariant mass of the pair composed of the q or $\bar{q}$ at the central vertex and the final-state nucleon, s_o is a scaling factor on the order of 1 BeV^2, and w is a Toller variable[76] which is of no concern to us (see appendix E for the details).

To accommodate the multi-peripheral character, the vertex functions are assumed to contain the factors $e^{a_1t_1}$ and $e^{a_2t_2}$, where the a_i are constants.** For simplicity, all other factors depending on t_1 and t_2, except the $(s_{ij}/s_o)^{\alpha_k(t_i)}$, are assumed to vary so slowly in comparison to $\exp(a_1t_1+a_2t_2)$ that they are essentially constant. For example, kinematical singularities in the residues are ignored,

---

*Because a quark is a fermion, its α is chosen to be (J-1/2).

†We use a metric whereby $\vec{p}^2 = E^2-\bar{p}^2$ for four-momentum $\vec{p}$, energy E, and three-momentum $\bar{p}$; the t_i are therefore either near zero or negative.

**We assume that $f_i(t_i) = f_i\, e^{b_it_i}$, $g_2(t_1,w,t_2) = g_2\, e^{d_1t_1+d_2t_2}$ independent of w, and choose $a_i = b_i+d_i$. Note that f_1, g_2, and f_3 are equal to the respective vertex functions evaluated at $t_1 = t_2 = 0$.

and the quotient of the signature factors and the trigonometric factors is assumed to be a constant. The overall magnitude of the residue, signature, and trigonomitric factors is assumed to be one for the normalization chosen for the coupling constants. The amplitudes considered are therefore of the form

$$\text{Amplitude} = f_1\, g_2\, f_3 \quad e^{a_1 t_1}\; e^{a_2 t_2} \quad (s_{12}/s_o)^{\alpha_q(t_1)} \quad (s_{23}/s_o)^{\alpha_{Pom}(t_2)}$$

where f_1, g_2, and f_3 are the couplings at $t_1 = t_2 = 0$. With such an amplitude, the total cross section for a diagram of class D (figure 36) can be obtained using the formulas derived in appendix section E.1.

One may note that the crossed-channel cosines were chosen to be just s_{ij}/s_o. This was done for simplicity. The difficulties associated with a detailed treatment of threshold behavior are thereby ignored. Moreover, only two numerical integrations are then required to obtain a total cross section for either diagram as a function of s.

A discussion of the values assumed for the various parameters involved is given in appendix section E.2. There we show that plausible values are $\alpha_{Pom}(t)=1$, $(f_1/4\pi)^2=1$, $(g_2/4\pi)^2=(f_3/4\pi)^2=2/3$, $a_1 = 2.5$ $(BeV/c)^{-2}$, and $a_2 = 5.0$ $(BeV/c)^{-2}$. In choosing the coupling constants, we assumed that quark couplings, anti-quark couplings, and nucleon couplings are identical. Because quarks and anti-quarks are treated in the same manner, both of the lowest-threshold diagrams have the same cross section. The total production cross section near threshold is therefore just twice the total cross section for either diagram.

We shall find that the lower limit obtained for the mass of a quark is very insensitive to small changes in every parameter except $\alpha_q(t)$, the Regge trajectory assigned to a quark. As a matter of fact, the choice for $\alpha_q(t)$ is critical. We therefore consider two distinct cases: $\alpha_q(t) = -m_q^2 + t$, m_q being the mass of a quark, and $\alpha_q(t) = 0$. These two cases correspond to what are perhaps the two most likely choices for the slope of a quark's trajectory: a slope of 1 $(\mathrm{BeV}/c)^{-2}$, just as for all hadrons, or a slope of zero $(\mathrm{BeV}/c)^{-2}$, in case quarks are "elementary."

In either case, as we shall illustrate shortly, the total cross section for the two lowest-threshold diagrams rises above threshold and then levels out to what might be termed an asymptote. How fast the cross section levels out to this asymptote depends on the size of the quark mass, the rise from threshold to the asymptote being very sharp for quark masses near 1 BeV/c^2 but very slow for quark masses larger than several BeV/c^2.

Instead of dealing with a total production cross section whose threshold behavior is dependent on the quark mass considered, it is convenient to assume that the total production cross section $\sigma_q(m_q, s_o, s)$ rises abruptly from threshold to a value $\sigma_{threshold}(m_q, s_o)$, and then rises as a function of s according to

$$\sigma_q(m_q, s_o, s) \equiv \sigma_{threshold}(m_q, s_o) \cdot F(s)$$

The function F(s), which provides the s dependence, is assumed to be unity at threshold (examples are given in the next section). $\sigma_{threshold}(m_q,s_o)$ is defined to be the weighted average of $\sigma(m_q,s_o,s)$, the total cross section for the two lowest-threshold diagrams. The weighting function used in computing this average, W(s), is defined to be the product of F(s) and the primary cosmic-ray proton flux $N_p(s)$:

$$\sigma_{threshold}(m_q,s_o) \equiv \frac{\int_{threshold}^{\infty} ds \quad \sigma(m_q,s_o,s)\ W(s)}{\int_{threshold}^{\infty} ds \quad W(s)}$$

$$\equiv \frac{\int_{threshold}^{\infty} ds \quad \sigma(m_q,s_o,s)\ F(s)\ N_p(s)}{\int_{threshold}^{\infty} ds \quad F(s)\ N_p(s)}$$

The value of s at which $\sigma(m_q,s_o,s)$ reaches $\sigma_{threshold}(m_q,s_o)$ will be designated $s^{\#}$.

Such an approach enables one to obtain the quark yield, which is proportional to

$$\int_{\text{threshold}}^{\infty} ds \;\; \sigma(m_q, s_o, s) \; F(s) \; N_p(s) \quad =$$

$$\sigma_{\text{threshold}}(m_q, s_o) \quad \cdot \quad \int_{\text{threshold}}^{\infty} ds \;\; F(s) \; N_p(s),$$

by avoiding the indicated numerical integration of $\sigma(m_q, s_o, s)$, which is itself given only by numerical integration (c.f. appendix section E.1). One may instead fit some algebraic function to a representative list of values for $\sigma_{\text{threshold}}(m_q, s_o)$, and use this algebraic function in solving the equation which we shall consider to obtain a mass limit. The numerical calculations are thereby greatly simplified.

We first consider the case in which $\alpha_q(t) = -m_q^2 + t$. The range of quark masses which will be considered in this case is from 0.5 to 3.0 BeV/c^2. For these masses and $s_o = 1\ \text{BeV}^2$, the general shape of the total cross section for the lowest-threshold diagrams is that illustrated in figure 37. $\sigma(m_q, s_o, s)$ for a particular m_q is designated in this figure merely as $\sigma(s)$. Note that the rise from threshold is much faster for $m_q = 1\ \text{BeV/c}^2$ than for $m_q = 2\ \text{BeV/c}^2$.

The values of $s^{\#}$ in this case are of the order of several hundred BeV^2, larger $s^{\#}$ corresponding to larger m_q. The variation in each $\sigma(m_q, s_o, s)$ over the range of $s^{\#}$ involved is less than about 10%. We are therefore entirely justified for the accuracy desired

FIGURE 37: TOTAL CROSS SECTIONS $\sigma(m_q, s_o, s)$ FOR $\alpha_q(t) = -m_q^2 + t$ AND $s_o = 1$ BeV^2, NORMALIZED TO UNITY AT $s^{\#} = 500$ BeV^2

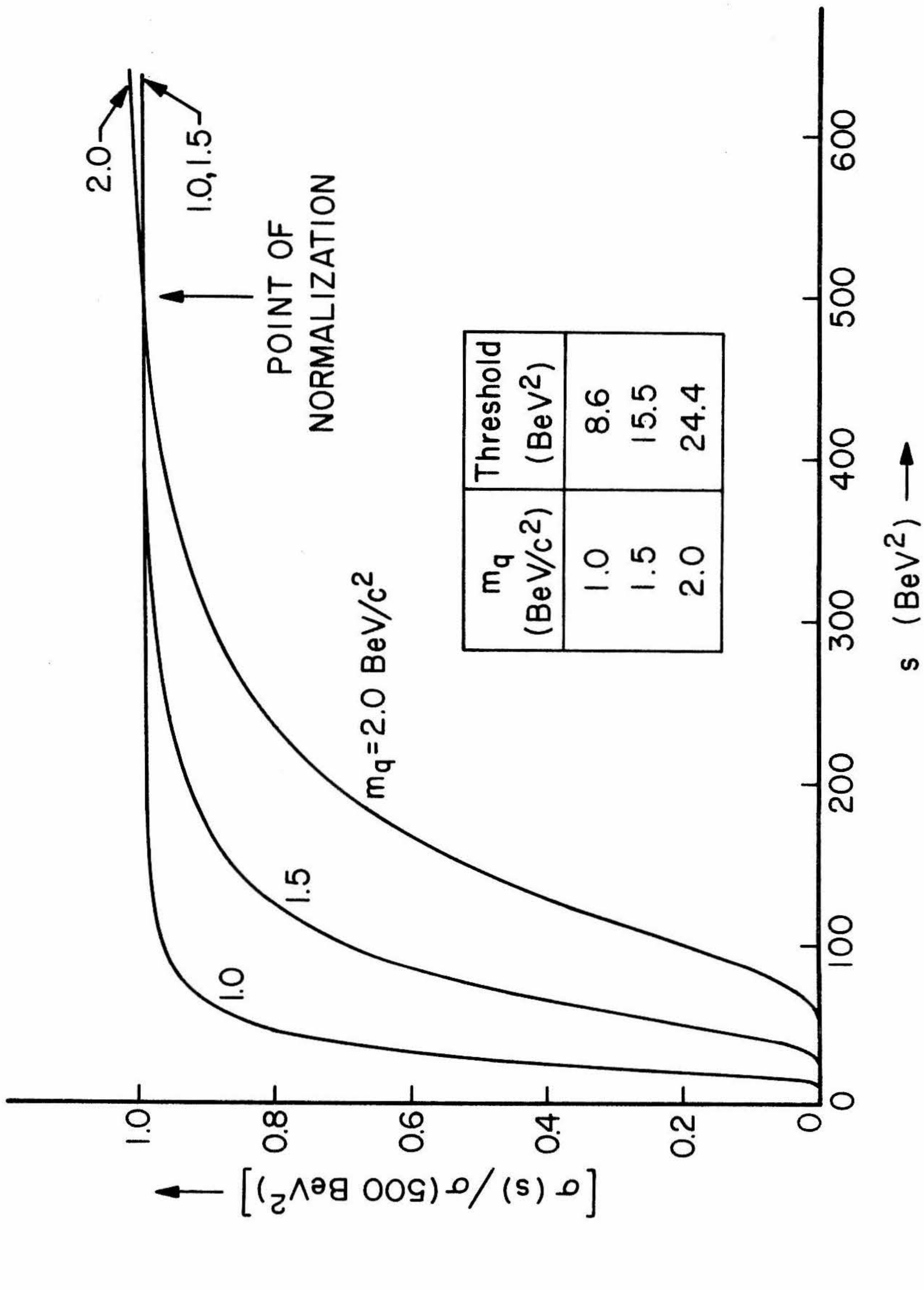

to assume (for convenience) that all $\sigma(m_q, s_o, s)$ to be considered in this case have the same $s^{\#}$. This common $s^{\#}$ is chosen to be the representative value $s^{\#} = 500 \text{ BeV}^2$.

Using this $s^{\#}$, one finds that the magnitude of $\sigma_{\text{threshold}}(m_q, s_o)$ is highly dependent on the value of m_q and quite dependent on the value of s_o. This dependence is illustrated in table 7. Note that $\sigma_{\text{threshold}}(m_q, s_o)$ falls off extremely fast as a function of m_q for $s_o = 1 \text{ BeV}^2$. This behavior is a direct reflection of the assumption that the intercept for a quark's Regge trajectory is $\alpha_q(0) = -m_q^2$.*

In order to have some idea of the algebraic dependence of $\sigma_{\text{threshold}}(m_q, s_o)$ on m_q and s_o, we have fit several arbitrary functions of m_q and s_o to an extensive list of cross sections computed at $s = 500 \text{ BeV}^2$. The approximate dependence found is the following:†

$$\sigma_{\text{threshold}}(m_q, s_o) \sim s_o^{(2 m_q^2 - 2)} \exp(-7.0\ m_q^{2.4}) \Big/ (1 + m_q^2)$$

---

*Had we chosen the intercept to be the constant $\alpha_q(0) = -1$, for example, $\sigma_{\text{threshold}}(m_q, s_o)$ for $s_o = 1 \text{ BeV}^2$ would have fallen by slightly less than eight orders of magnitude from $m_q = 1 \text{ BeV/c}^2$ to $m_q = 3 \text{ BeV/c}^2$, rather than by forty-one orders of magnitude as shown in table 7.

†A function which reproduces an extensive list of values for $\sigma_{\text{threshold}}(m_q, s_o)$ to an accuracy of within 1.5% for values of s_o between 1 and 5 BeV^2 and for values of m_q between 0.5 and 3.0 BeV/c^2 is the following: $\sigma_{\text{threshold}}(m_q, s_o) = (1+m_q^2)^{-1}\ s_o^A\ m_q^B \exp(C) / D$ millibarns, where $A = (-2.282 + 2.305\ m_q^{1.969})$, $B = (-.8399 + .0003\ s_o^{3.154})$, $C = (4.252 - 6.980\ m_q^{2.424} + 3.055\ s_o^{.2578})$, and $D = (3683. + 18.25\ s_o^{.0047} - 457.3\ m_q^{1.735}\ s_o^{.0440})$.

TABLE 7: VALUES OF $\sigma_{\text{threshold}}(m_q, s_o)$ IN MILLIBARNS

FOR THE CASE $\alpha_q(t) = -m_q^2 + t$

s_o (BeV^2) ↓ \ m_q (BeV/c^2) →	0.5	1.0	1.5	2.0	3.0
1	$1.62\text{x}10^{-1}$	$2.11\text{x}10^{-4}$	$9.47\text{x}10^{-10}$	$4.13\text{x}10^{-18}$	$3.41\text{x}10^{-45}$
2	$9.20\text{x}10^{-2}$	$3.96\text{x}10^{-4}$	$1.24\text{x}10^{-8}$	$8.22\text{x}10^{-16}$	$1.60\text{x}10^{-39}$
3	$6.87\text{x}10^{-2}$	$5.98\text{x}10^{-4}$	$5.92\text{x}10^{-8}$	$1.94\text{x}10^{-14}$	$3.64\text{x}10^{-36}$
4	$5.72\text{x}10^{-2}$	$8.21\text{x}10^{-4}$	$1.84\text{x}10^{-7}$	$1.90\text{x}10^{-13}$	$9.23\text{x}10^{-34}$
5	$5.04\text{x}10^{-2}$	$1.07\text{x}10^{-3}$	$4.53\text{x}10^{-7}$	$1.14\text{x}10^{-12}$	$6.97\text{x}10^{-32}$

Parameters: (c.f. appendix section E.2)

$m_\pi = 0.1396$ BeV/c^2, $m_p = 0.9383$ BeV/c^2

$\alpha_q(t) = -m_q^2 + t$, $\alpha_{Pom}(t) = 1.0$

$s = s^{\#} = 500$ BeV^2, $a_q = 2.5$ (BeV/c)$^{-2}$, $a_{Pom} = 5.0$ (BeV/c)$^{-2}$

$(f_{\pi qq}/4\pi)^2 = 1.0$, $(g_{qqPom}/4\pi)^2 = (f_{ppPom}/4\pi)^2 = 2/3$

If a polynomial in m_q is considered in the argument of the exponential instead of the "condensed" form m_q^n, the approximate exponential dependence is $\exp(12.8\ m_q - 13.0\ m_q^2 - 0.547\ m_q^3)$.

Note that a factor $s_o^{(2m_q^2-2)}$ is expected because the amplitudes contain $(1/s_o)^{\alpha_q(t_1) + \alpha_{Pom}(t_2)}$ with $\alpha_q(0) = -m_q^2$ and $\alpha_{Pom}(0) = 1$. A factor $(1+m_q^2)^{-1}$ is also expected because the differential cross section $d\sigma/dt_1dt_2$ contains the factor $(\alpha_{Pom}(t_2) - \alpha_q(t_1))^{-1}$, as one can see from equation (11) of Bali, Chew, and Pignotti's paper.[76]

We now consider the case of a flat quark trajectory, $\alpha_q(t) = 0$. In this case, the amplitudes contain a factor of unity at $t_1 = 0$ instead of $(s_{12}/s_o)^{-m_q^2}$, so the total quark-production cross section for a given m_q and s_o is generally much larger. For this reason, we shall find that the mass limits determined for this case are somewhat larger than those determined for the case in which $\alpha_q(t) = -m_q^2 + t$. The range of masses to be considered here is from about 2 BeV/c^2 to about 8 BeV/c^2. An adequate representation of $s^{\#}$ over this mass range is given by $s^{\#} = 1200 + 800(m_q-3)$ BeV^2 independent of s_o.

Because larger quark masses will be considered, the total cross section for the two lowest-threshold diagrams rises to what might be termed an asymptote much more slowly than before. This is illustrated in figure 38, where we represent $\sigma(m_q,s_o,s)$ merely as $\sigma(s)$. Note that $\sigma(m_q,s_o,s)$ reaches $s^{\#}$ long before "levelling out," especially for the larger m_q. The results obtained for this case

FIGURE 38: TOTAL CROSS SECTIONS $\sigma(m_q, s_o, s)$ FOR $\alpha_q(t) = 0$ AND ANY s_o, NORMALIZED TO UNITY AT $s^{\#} = 1200 + 800(m_q - 3)$ BeV^2

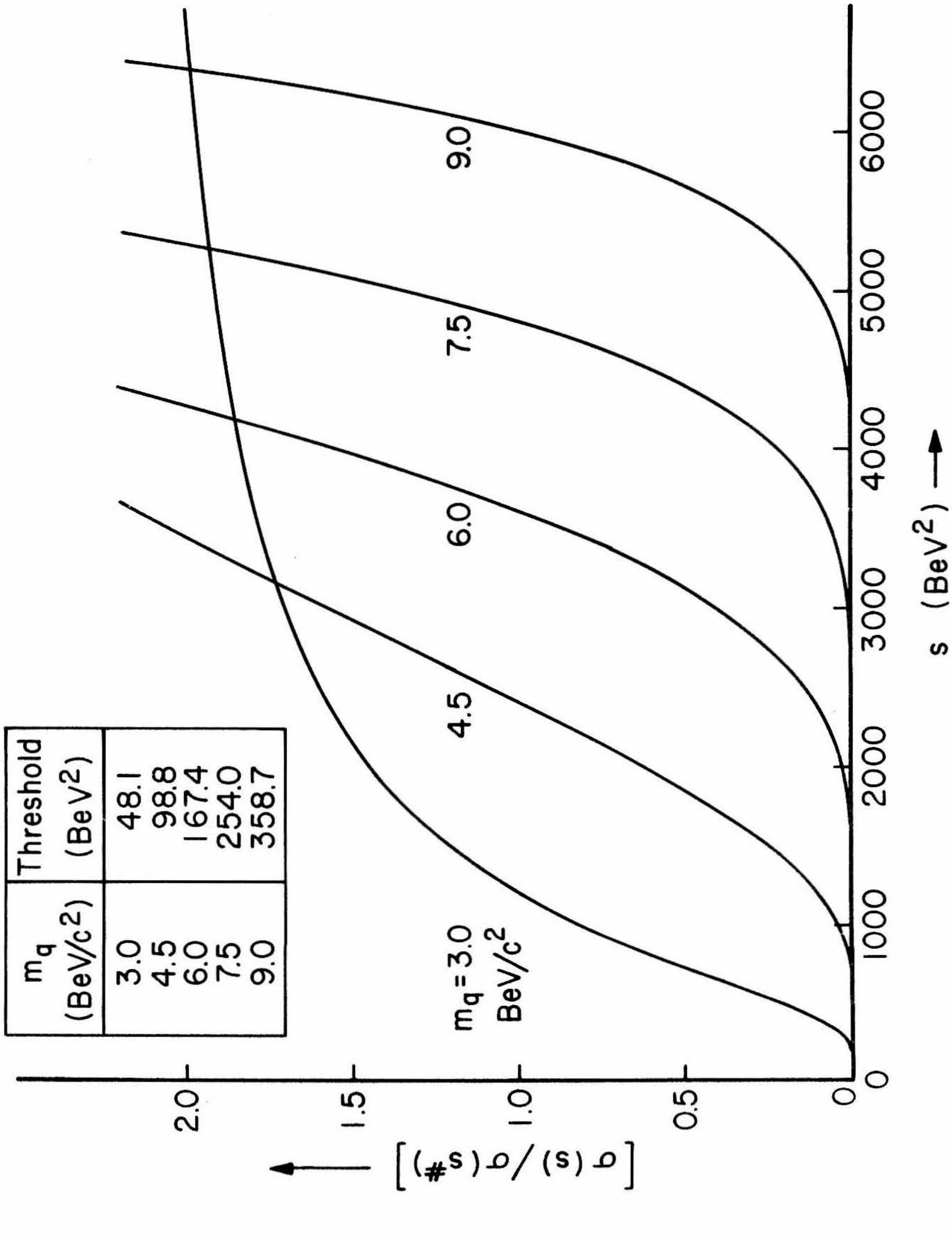

will obviously be more dependent on the assumption that the Reggeized amplitudes considered do give a sufficient representation of the behavior of $\sigma(m_q, s_o, s)$ as it rises above threshold.

As one can see from table 8, the dependence of $\sigma_{threshold}(m_q, s_o)$ on m_q and s_o is not as dramatic in this case (c.f. table 7). In order to have some idea of the algebraic dependence involved, we have fit several arbitrary functions to a more extensive list of numerical data. The approximate dependence found is the following:*

$$\sigma_{threshold}(m_q, s_o) \sim \exp(-0.86\ m_q^{1.4}) \ / \ s_o^2$$

A form which is slightly better is

$$\sigma_{threshold}(m_q, s_o) \sim \exp(-0.58\ m_q - 0.065\ m_q^2 - 0.0061\ m_q^3) \ / \ s_o^2$$

The s_o dependence shown is exact, for the only s_o dependence in the amplitude is that in $(s_{23}/s_o)^{\alpha_{Pom}(t_2)} = (s_{23}/s_o)$.

Before leaving this section, we would like to point out that it is common practice to set s_o equal to 1 BeV^2 when treating processes in which the particles have masses less than one BeV/c^2.

---

*A function which reproduces the m_q dependence of $\sigma_{threshold}(m_q, s_o)$ to an accuracy of within 1% for values of m_q between 2 and 10 BeV/c^2 is the following: $\sigma_{threshold}(m_q, s_o) = s_o^{-2} \exp(A) \ / \ B$ millibarns, where $A = (-6.079 - 0.5759\ m_q - 0.06529\ m_q^2 - 0.006070\ m_q^3 - 7.271\text{x}10^{-5}\ m_q^4)$ and $B = (0.1951 - 0.2273\ m_q + 0.1312\ m_q^2 - 0.02076\ m_q^3 + 0.001664\ m_q^4)$.

TABLE 8: VALUES OF $\sigma_{threshold}(m_q, s_o)$ IN MILLIBARNS

FOR THE CASE $\alpha_q(t) = 0$

m_q (BeV/c^2)	$\sigma_{threshold}(m_q, s_o)$ for $s_o = 1$ BeV^2
2.0	4.21×10^{-3}
2.5	1.75×10^{-3}
3.0	7.11×10^{-4}
3.5	2.86×10^{-4}
4.0	1.11×10^{-4}
4.5	4.13×10^{-5}
5.0	1.44×10^{-5}
5.5	4.64×10^{-6}
6.0	1.38×10^{-6}
6.5	3.72×10^{-7}
7.0	9.10×10^{-8}
7.5	2.00×10^{-8}
8.0	3.93×10^{-9}
8.5	6.86×10^{-10}
9.0	1.06×10^{-10}
9.5	1.43×10^{-11}
10.0	1.70×10^{-12}

Exact s_o Dependence: $\sigma_{threshold}(m_q, s_o) \sim 1/s_o^2$

Parameters: (c.f. appendix section E.2)

$m_\pi = 0.1396$ BeV/c^2, $m_p = 0.9383$ BeV/c^2,

$a_q = 2.5$ (BeV/c)$^{-2}$, $a_{Pom} = 5.0$ (BeV/c)$^{-2}$,

$s = s^{\#} = 1200 + 800(m_q - 3)$ BeV^2, $\alpha_q(t) = 0$, $\alpha_{Pom}(t) = 1.0$

$(f_{\pi qq}/4\pi)^2 = 1.0$, $(g_{qqPom}/4\pi)^2 = (f_{ppPom}/4\pi)^2 = 2/3$

We emphasize, however, that no one knows how s_o should vary as a function of the masses of the particles considered. In particular, we do not know whether s_o depends on the size of m_q or whether s_o is dependent merely on the choice of residues.* Therefore, in each of the two cases considered, we shall obtain a lower limit for the quark mass as a function of s_o.

---

*Note that considering different values of s_o is equivalent to considering residues which differ by factors of the form $c^{\alpha_q(t_1)+\alpha_{Pom}(t_2)}$ for different values of the constant c.

C. Production Cross Section As A Function of s

With a procedure at hand to provide values of $\sigma_{threshold}(m_q, s_o)$, the next step was to choose a function F(s) in such a way as to provide a suitable s dependence for the production cross section. Because we have assumed that quark couplings are of the same order as proton couplings, it seems natural to choose a dependence based on the experimentally observed total cross section for anti-proton production. Rather than treat anti-proton production in pion-proton interactions, for which there is relatively little data, we chose to consider the production reaction $pp \rightarrow \bar{p}$+anything. Experimental data are available for this reaction from measurements of anti-proton yields off nuclear targets in accelerators.[70]

In choosing an F(s) for quark production, we first fit the antiproton-production data (figure 34) using a cubic in s (ignoring the sharp rise just above threshold):

$$\sigma_{\bar{p}}(s) \propto \left[(2.709\text{x}10^{-3})s^3 - (1.567\text{x}10^{-1})s^2 + (7.757)s - (69.38)\right]$$

Letting T be the threshold energy and z be the energy above threshold,* $s = (T+z)^2$, we transformed the fit to

$$\sigma'_{\bar{p}}(z) \propto \Big[(2.709\text{x}10^{-3})z^6 + (6.637\text{x}10^{-2})z^5 + (5.208\text{x}10^{-1})z^4 + (1.130)z^3 + (3.381)z^2 + (39.13)z + (28.96)\Big]$$

---

*In each case, the frame considered is the center-of-mass frame of the two incident particles.

This was then scaled so that, at z=0, the cross section would be $\sigma_{threshold}(m_q, s_o)$, the cross section provided by the numerical calculations of section B. The result was the following:

$$\sigma'_q(m_q, s_o, z)_{Cubic} = \Big[(9.354\text{x}10^{-5}) z^6 + (2.292\text{x}10^{-3}) z^5 + (1.799\text{x}10^{-2}) z^4 + (3.901\text{x}10^{-2}) z^3 + (0.1167) z^2 + (1.3513) z + 1\Big] \cdot \sigma_{threshold}(m_q, s_o)$$

Because this cross section might rise as a function of z somewhat faster than the quark production cross section,* we also considered an arbitrary "linear" form (involving $s^{1/2}$) which would probably make the corresponding $\sigma'_q(m_q, s_o, z)$ rise much too slowly. Treatment of these two cases will effectively allow us to treat all cases in between. The arbitrary linear form was chosen to be (6.378z + 1):

$$\sigma'_q(m_q, s_o, z)_{Linear} = \Big[(6.378) z + 1\Big] \cdot \sigma_{threshold}(m_q, s_o)$$

The energy dependence of each $\sigma'_q(m_q, s_o, z)$ is illustrated in figure 39.

Each $\sigma'_q(m_q, s_o, z)$ was then transformed to a $\sigma_q(m_q, s_o, s)$ using $T = (2m_q + M)$ and $z = (s^{1/2} - T)$, T being the energy at threshold in

---

*For example, one might expect the quark production cross section to be better represented by a function $R(s/s_q)$ where s_q is the value of s corresponding to the quark-production threshold in πN interactions, s_p is the similar threshold for anti-proton production in pp interactions, and $R(s/s_p)$ is the cross section in figure 34 re-scaled in terms of s_p. The quark-production cross section would then rise just as fast in units of s_q as does the cross section for anti-proton production in units of s_p. Such a rise, when expressed in terms of z, is slower than that represented by $\sigma'_q(m_q, s_o, z)_{Cubic}$.

FIGURE 39: DEPENDENCE OF THE PRODUCTION CROSS SECTION ON THE ENERGY ABOVE THRESHOLD IN THE CM FRAME

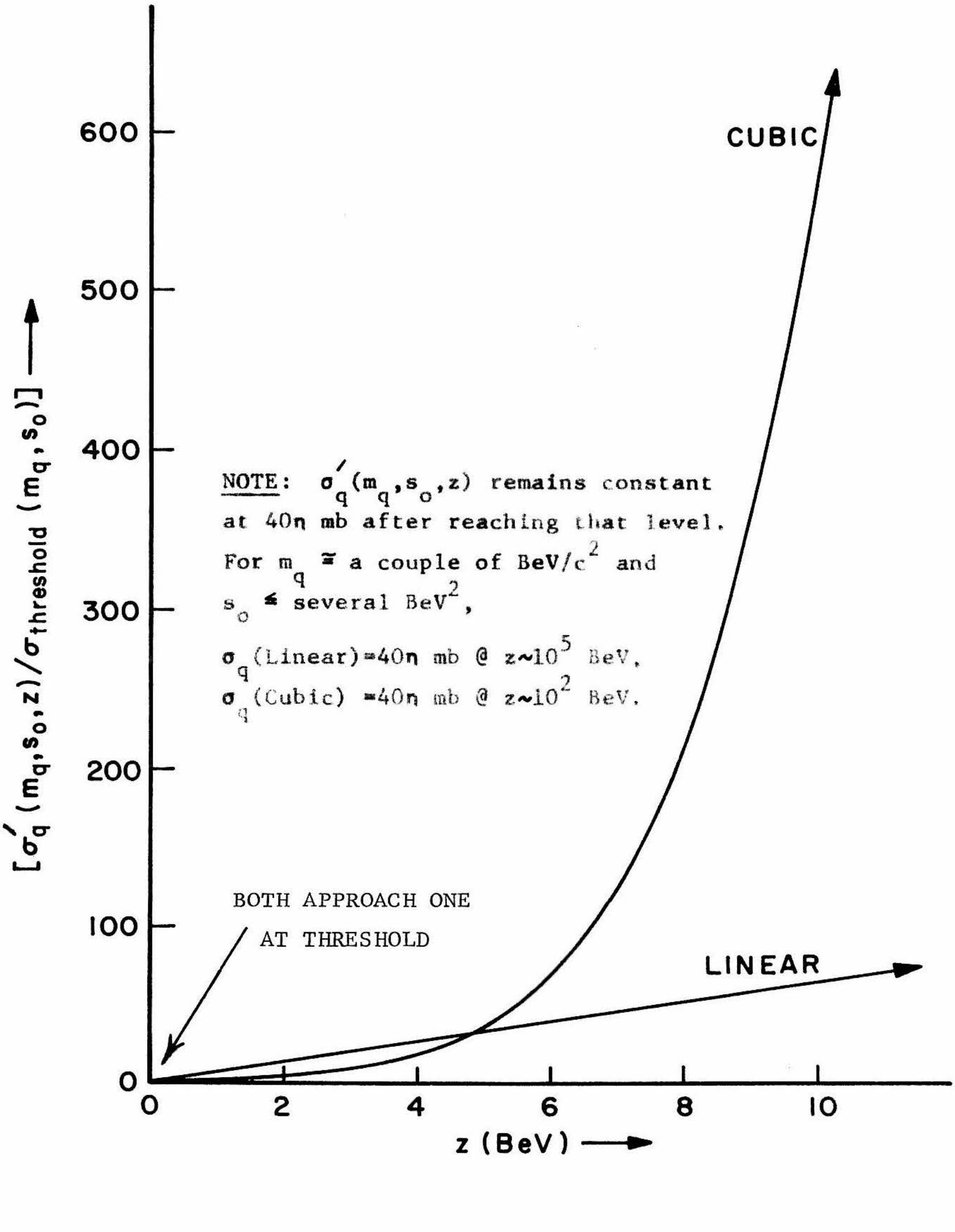

the CM frame and M being the mass of a nucleon (all masses will be expressed in BeV/c^2). With this transformation, the functions inside the square brackets above are the functions F(s) referred to in section B.

It is assumed that the production cross section rises according to $\sigma_q(m_q, s_o, s)$ until $\sigma_q(m_q, s_o, s)$ reaches a certain fraction (designated by η) of 40 millibarns. Thereafter, the cross section is assumed to be a constant 40η millibarns. In this way, we can obtain results as a function of η and thereby check to see if our results are indeed very insensitive to the size of the production cross section at very large s.

D. Quark Production and Loss in the Atmosphere

So far, we have been discussing quark production with nucleon targets. In the atmosphere, however, the targets are actually nitrogen or oxygen nuclei. The production cross section must therefore be multiplied by factors which take this into account (e.g. a nuclear form factor). The particular factors which are necessary depend on whether the production is coherent or incoherent.

Because the mechanism of quark production considered is based on exponential dampings in four-momentum transfer, production can be assumed to be limited to near-forward angles. One might therefore expect the production to be coherent.

This is not the case, however, because the energies involved are not quite large enough to allow the production to reach the small four-momentum transfers required for coherence. To see this, consider the vertex at the far right in the diagram shown in figure 40. The notation is similar to that used in appendix E: t and t', which are negative, are four-momentum transfers; $\vec{p}_i$ is the four-momentum for particle i; $s=(\vec{p}_a+\vec{p}_b)^2$ and $s'=(\vec{p}_x+\vec{p}_{bb'})^2$ are each the square of the sum of the energies of the two particles indicated by the subscripts, in their center-of-mass frame.

One can show that the minimum four-momentum transfer to the nucleus is on the order of*

$$(-t)_{min} \sim \left[(m_x{}^2-t')\ A\ M\ /\ s'\right]^2 > \left[m_x{}^2\ A\ M\ /\ s\right]^2$$

---

*See appendix section E.3.

FIGURE 40: PRODUCTION OFF A NUCLEUS

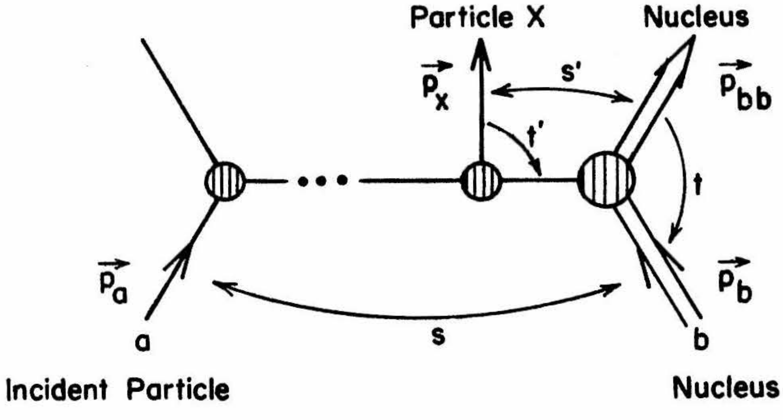

where m_x is the mass of particle X, A is the atomic weight of the nucleus, and M is the mass of a nucleon (0.94 BeV/c^2). For cases in which A is 14, $s \cong (2m_q+M)^2$, and particle X is a quark, we see that $(-t)_{min}$ near the production threshold is at least as large as $(14/4)^2 \cong 12\ (BeV/c)^2$.

Coherent production is not expected, however, unless $(-t)_{min}$ is less than about 0.04 BeV^2.[(77)] For this reason, we assume that the production is completely incoherent, with a nuclear form factor of one.

The cross section for production off nuclei of atomic weight A might then be expected to be equal to the cross section for production off an isolated nucleon multiplied by A.* There is a chance, however, that an incident pion (or nucleon) will interact in the nuclear matter before it can reach a particular target nucleon and in this way be effectively unable to interact with this nucleon. There is also the chance (however slight) that a quark, once formed, may interact in such a way before leaving the nucleus that it is effectively lost as a component of the flux of relativistic quarks.

Such effects can be included by using an effective atomic weight A_{eff} instead of A. We originally thought that a dependence of the sort $A_{eff} \sim A^{1/3}$ would be adequate, so results are obtained using $A_{eff} = 1.6\ A^{1/3}$.[(77)] A more realistic dependence, however, is $A_{eff} \sim A^{2/3}$.[(77)] The mass limits which we shall obtain are therefore too small, but only by about 10%.

---

*No distinction is made here between neutrons and protons as target nucleons.

With these considerations in mind, we assumed that the production of quarks and their subsequent interactions in the atmosphere could be adequately described by the diffusion equation derived in appendix F. There we show that the flux of quarks at depth x grams per square centimeter in the atmosphere is given by

$$\text{Flux} = \frac{N_o\, A_{eff}\, \Lambda_p}{A\,(1-\Lambda_p/\Lambda_q)} \left[e^{-x/\Lambda_q} - e^{-x/\Lambda_p} \right] W(m_q, s_o) \quad \text{quarks/cm}^2\text{/sr/sec}$$

while the rate of quarks traversing our array can be estimated to be

$$\text{Rate} = \frac{(2.94\text{x}10^{28})}{(1-120/\Lambda_q)} \left[e^{-1033/\Lambda_q} - e^{-1033/120} \right] W(m_q, s_o) \ \text{quarks/sec}$$

where N_o is Avogadro's number, Λ_q and Λ_p are respectively the attenuation lengths (in grams per square centimeter) for quarks and nucleons (e.g. protons) in the atmosphere, and W is the integrated product of incident cosmic-ray flux and total quark production cross section. Note that Λ_p has been assumed to be 120 g/cm^2 in the expression for the rate. W is a function of m_q and s_o, and is given by

$$W(m_q, s_o) = \sum_{\substack{\text{Diagrams}\\ j}} K(j) \cdot \int_{\substack{\text{Threshold}\\ j}}^{\infty} ds\, \frac{N_p(0, E_j)}{2M}\, \sigma_j(m_q, s_o, s)$$

where $\sigma_j(m_q,s_o,s)$ is the cross section for the production of quarks via diagram j, M is the mass of a nucleon, $s=(\vec{p}_i+\vec{p}_N)^2$ for incident-particle four-momentum $\vec{p}_i$ and target-nucleon four-momentum $\vec{p}_N$, and the incident flux ratio K(j) is 0.3 for incident pions and 1.0 for incident nucleons. The energies (in natural units, $\hbar=c=1$) are $E_j=(s-M^2-m^2)/2M$ for incident pions and $E_j=(s-2M^2)/2M$ for incident nucleons, where m is the mass of a pion. Note that $dE_j/ds=1/2M$, which is the factor of 1/2M appearing in the integrand above. The primary cosmic-ray nucleon flux is taken to be $N_p(0,E) = 2.35\ E^{-2.67}$ nucleons $cm^{-2}ster^{-1}sec^{-1}BeV^{-1}$.[(60)*] All mass-energies are expressed in BeV.

When treating collective diagrams for πN interactions having a total cross section $\sigma_q(m_q,s_o,s)$, as we do, W becomes

$$W(m_q,s_o) = (0.3)(2.35)(2M)^{1.67}\int_{(2m_q+M)^2}^{\infty} ds \frac{\sigma_q(m_q,s_o,s)}{(s-M^2-m^2)^{2.67}}$$

Note that the production threshold is of order m_q^2, while $\sigma_q(m_q,s_o,s)$ for $s_o \cong 1\ BeV^2$ is of order $m_q^{-2}\exp(-7\ m_q^{2.4})$ for $\alpha_q(t) = -m_q^2 + t$ and of order $\exp(-0.9\ m_q^{1.4})$ for $\alpha_q(t) = 0$. The rate of quarks traversing our array is thus approximately proportional

---

*This includes nucleons in nuclei having $Z \geqslant 2$. However, for simplicity and because of their small abundances (table 6), these nucleons were treated as if they were free.

either to $m_q^{-16/3} \exp(-7\ m_q^{2.4})$ or to $m_q^{-10/3} \exp(-0.9\ m_q^{1.4})$, depending on the choice for $\alpha_q(t)$.

In passing, we would like to point out that it would have been to our advantage to have run an experiment at a higher altitude. In fact, as we show in appendix F, the maximum quark flux for Λ_q on the order of 120 g/cm^2 occurs at an altitude of approximately 50,000 feet. The gain in quark flux which could have been expected by conducting an experiment at this altitude rather than at sea level is approximately a factor of 230. At 6,000 feet, the gain would have been a factor of four.

E. Lower Limits for the Mass of a Quark

To obtain a lower limit for m_q, the expression given in section D for the rate of quarks through the array can be equated to the upper limit for the rate as determined by this experiment. The experimental upper limit for the rate, based on 90% confidence, is merely the ratio of 2.3* and the effective length of time we spent searching for quarks: $(2.3/1.48 \times 10^7)$ quarks/second for charge 1/3, $(2.3/0.714 \times 10^7)$ quarks/second for charge 2/3.

By equating the expression for the rate to these upper limits and solving the resulting transcendental equation for m_q, one obtains a lower limit for the mass of a quark in terms of Λ_q, η, and s_o. This has been done, and the results are shown in figures 41 to 45 for the case $\alpha_q(t) = -m_q^2 + t$, and in figures 46 to 50 for the case $\alpha_q(t) = 0$. Note that both the cubic and the linear forms for $\sigma_q(m_q, s_o, s)$ have been considered. A lower limit for m_q can be obtained from these figures as soon as one decides what the values for the parameters ought to be.

Because a quark is assumed to interact strongly, the best guess for the quark's attenuation length in the atmosphere is just $\Lambda_q = \Lambda_p = 120$ g/cm^2. The best form for the s dependence of $\sigma_q(m_q, s_o, s)$ is most likely somewhere between the cubic and the linear forms, and probably quite close to the cubic. Because the results are so

---

*If the average number of quarks expected is 2.3, then the probability of finding no quarks is 10% according to Poisson statistics.

FIGURE 41: $(m_q)_{min}$ VS Λ_q FOR η=1.0 AND s_o=1.0

$\alpha_q(t) = -m_q^2 + t$

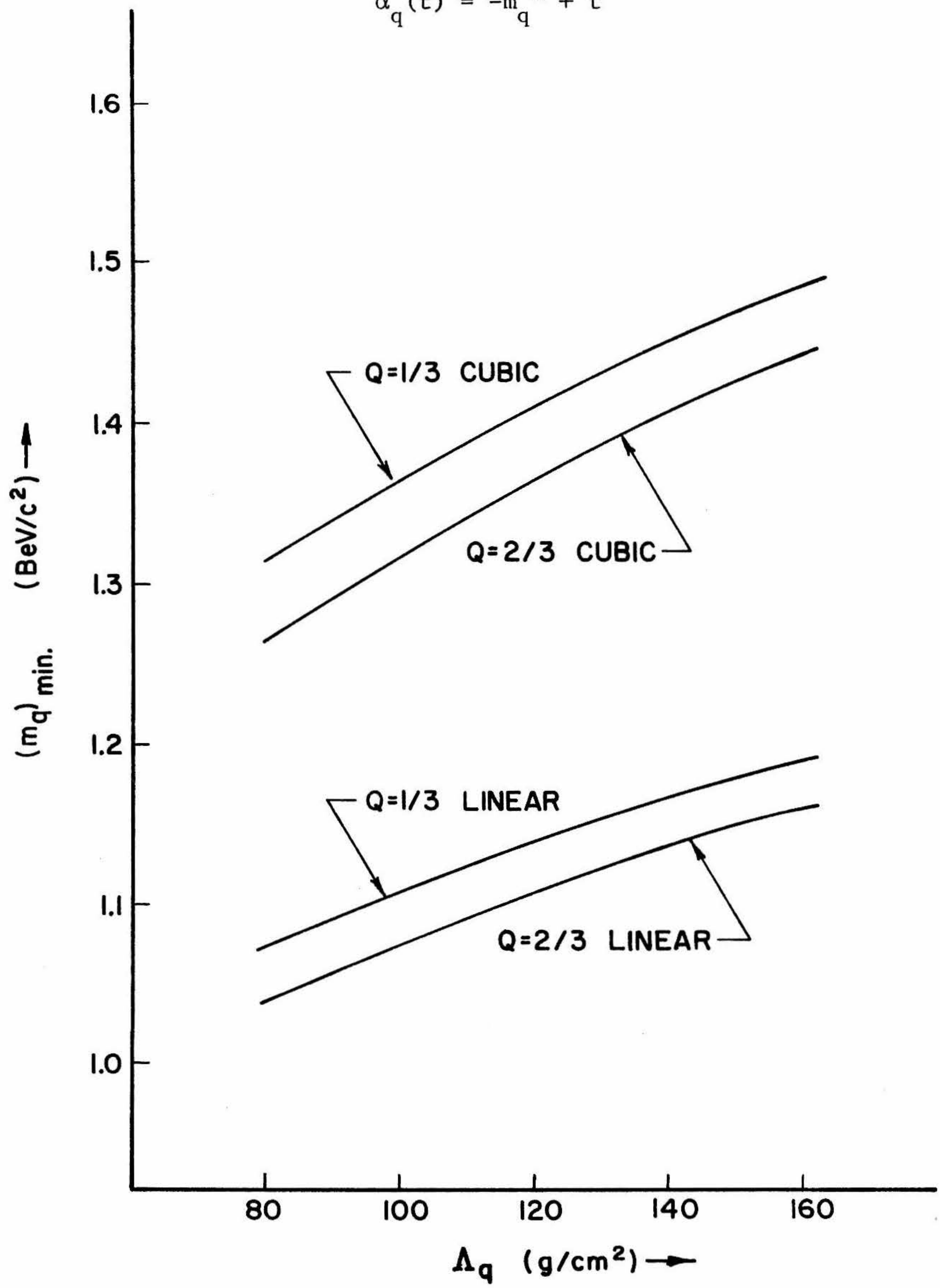

FIGURE 42: $(m_q)_{min}$ VS Λ_q FOR η=1.0 AND s_o=5.0

$\alpha_q(t) = -m_q^2 + t$

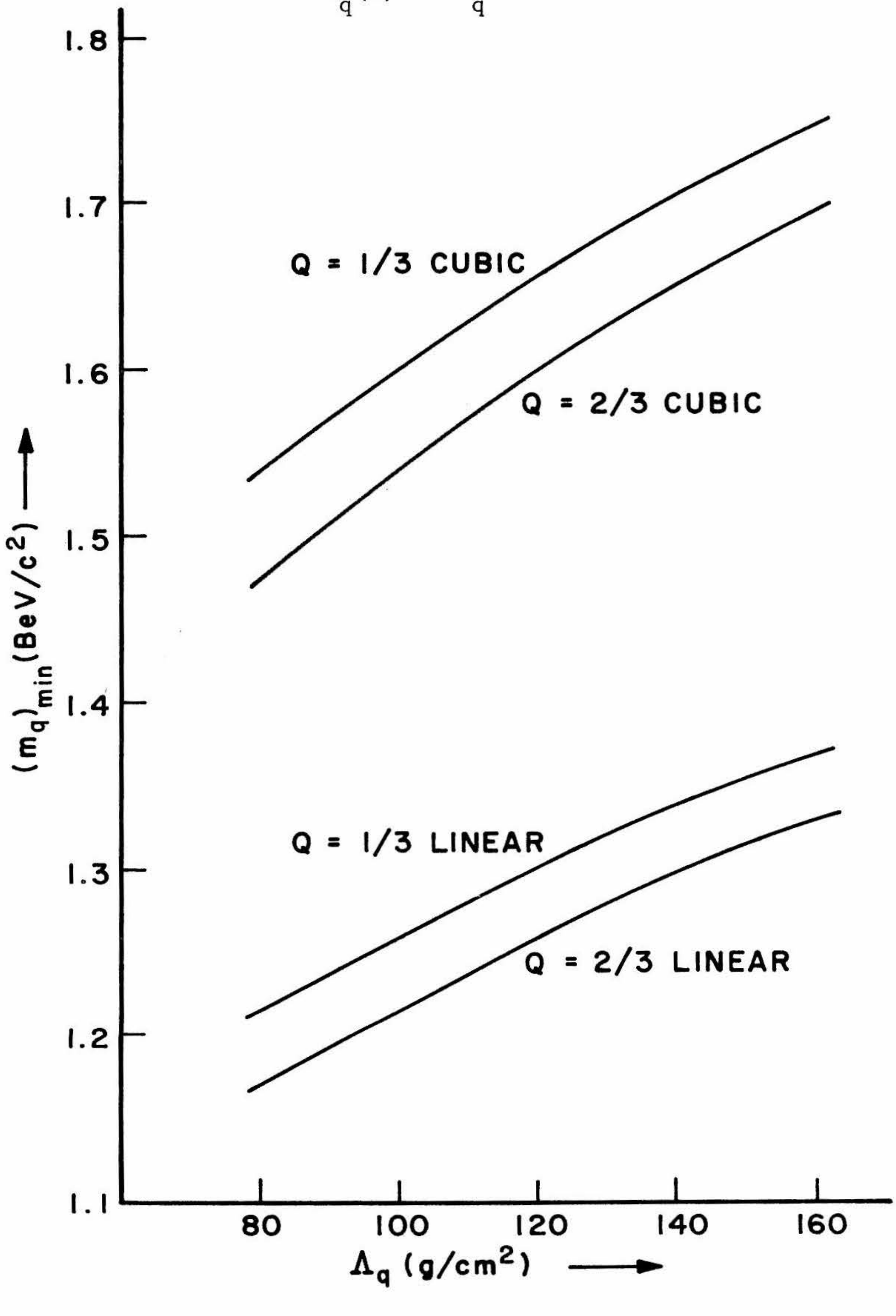

FIGURE 43: $(m_q)_{min}$ VS η FOR Λ_q=120 AND s_o=1.0

$\alpha_q(t) = -m_q^{\ 2} + t$

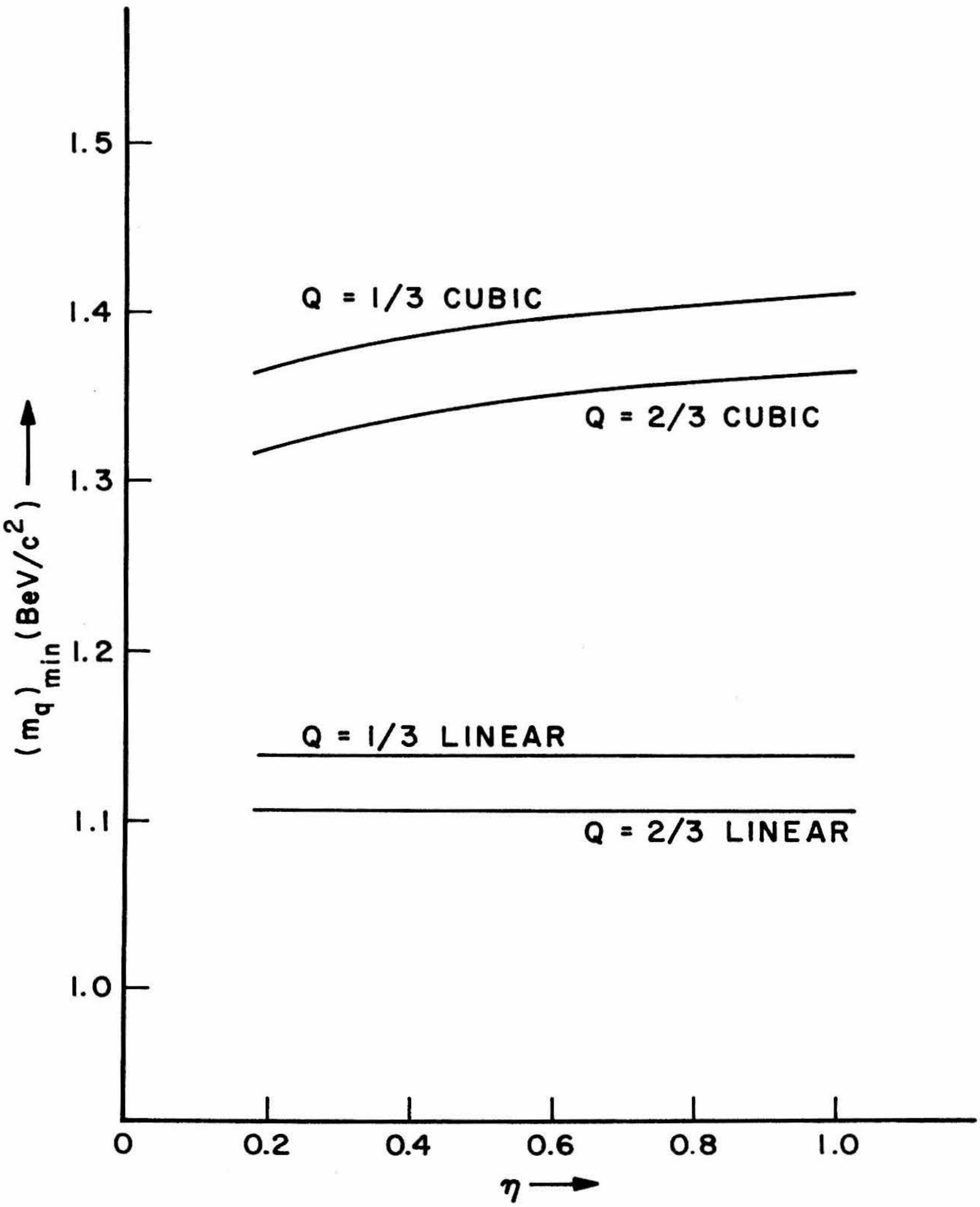

FIGURE 44: $(m_q)_{min}$ VS η FOR Λ_q=120 AND s_o=5.0

$\alpha_q(t) = -m_q^2 + t$

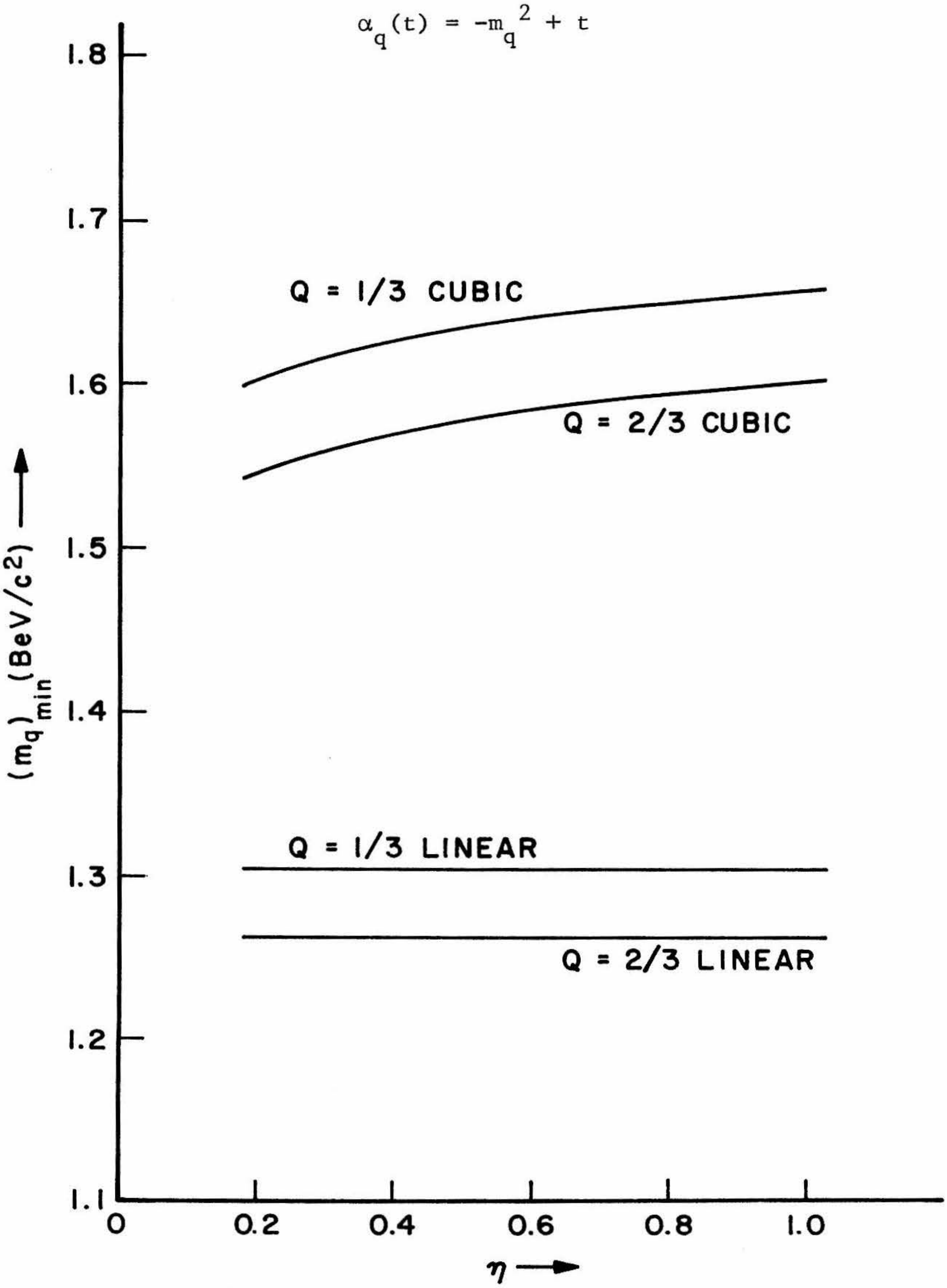

FIGURE 45: $(m_q)_{min}$ VS s_o FOR Λ_q=120 AND η=1.0

$\alpha_q(t) = -m_q^2 + t$

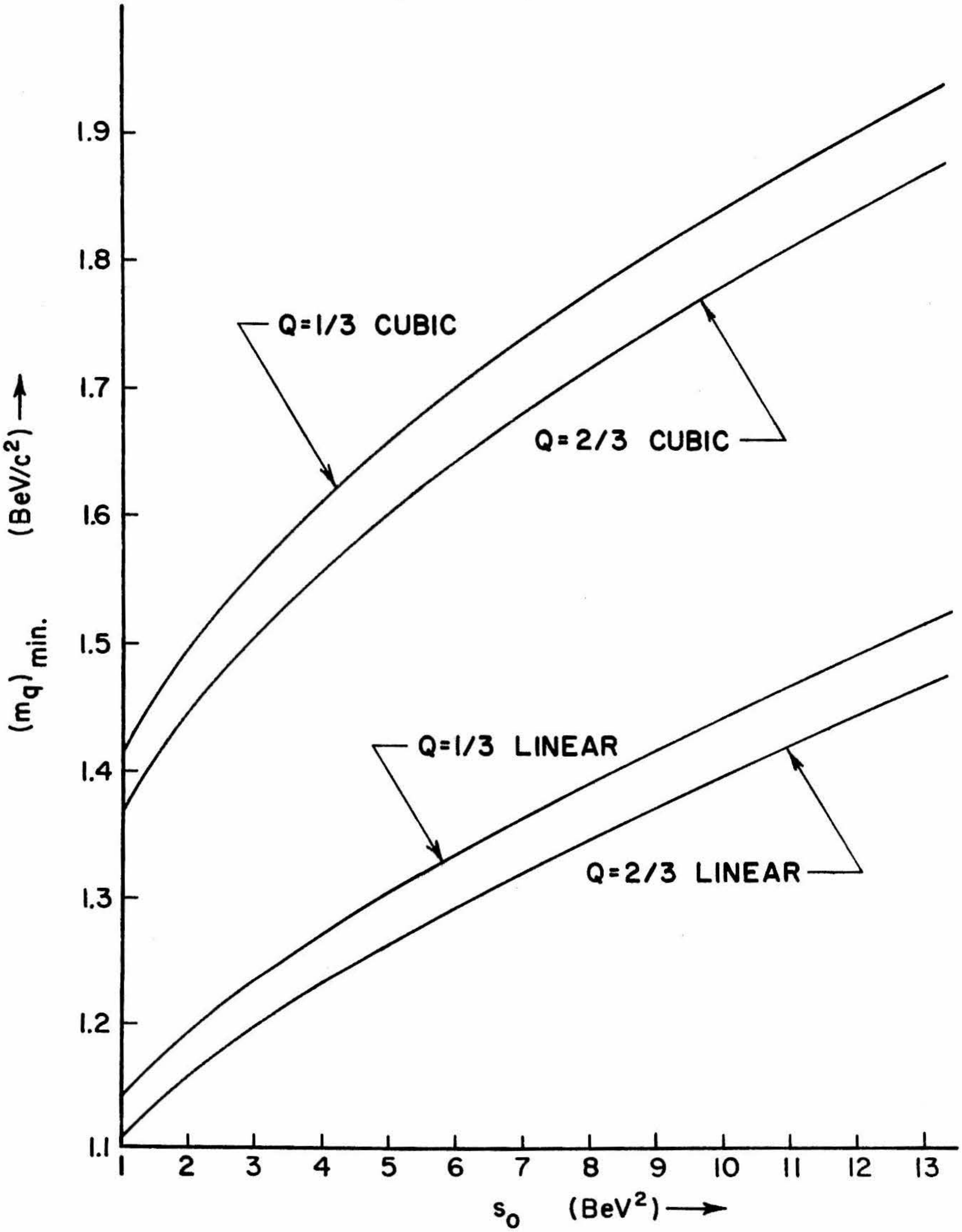

FIGURE 46: $(m_q)_{min}$ VS Λ_q FOR η=1.0 AND s_o=1.0

$\alpha_q(t) = 0$

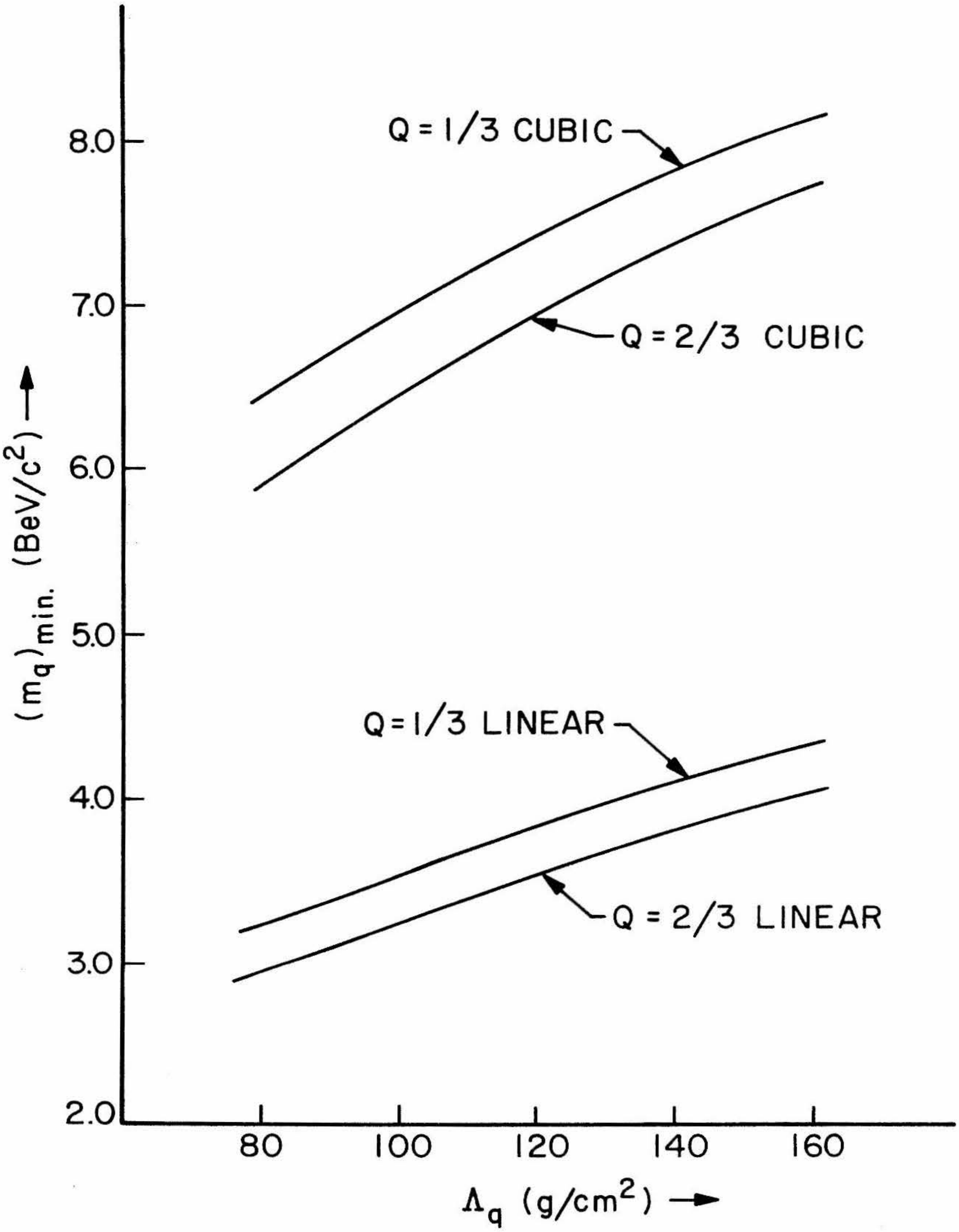

FIGURE 47: $(m_q)_{min}$ VS Λ_q FOR η=1.0 AND s_o=5.0

$\alpha_q(t) = 0$

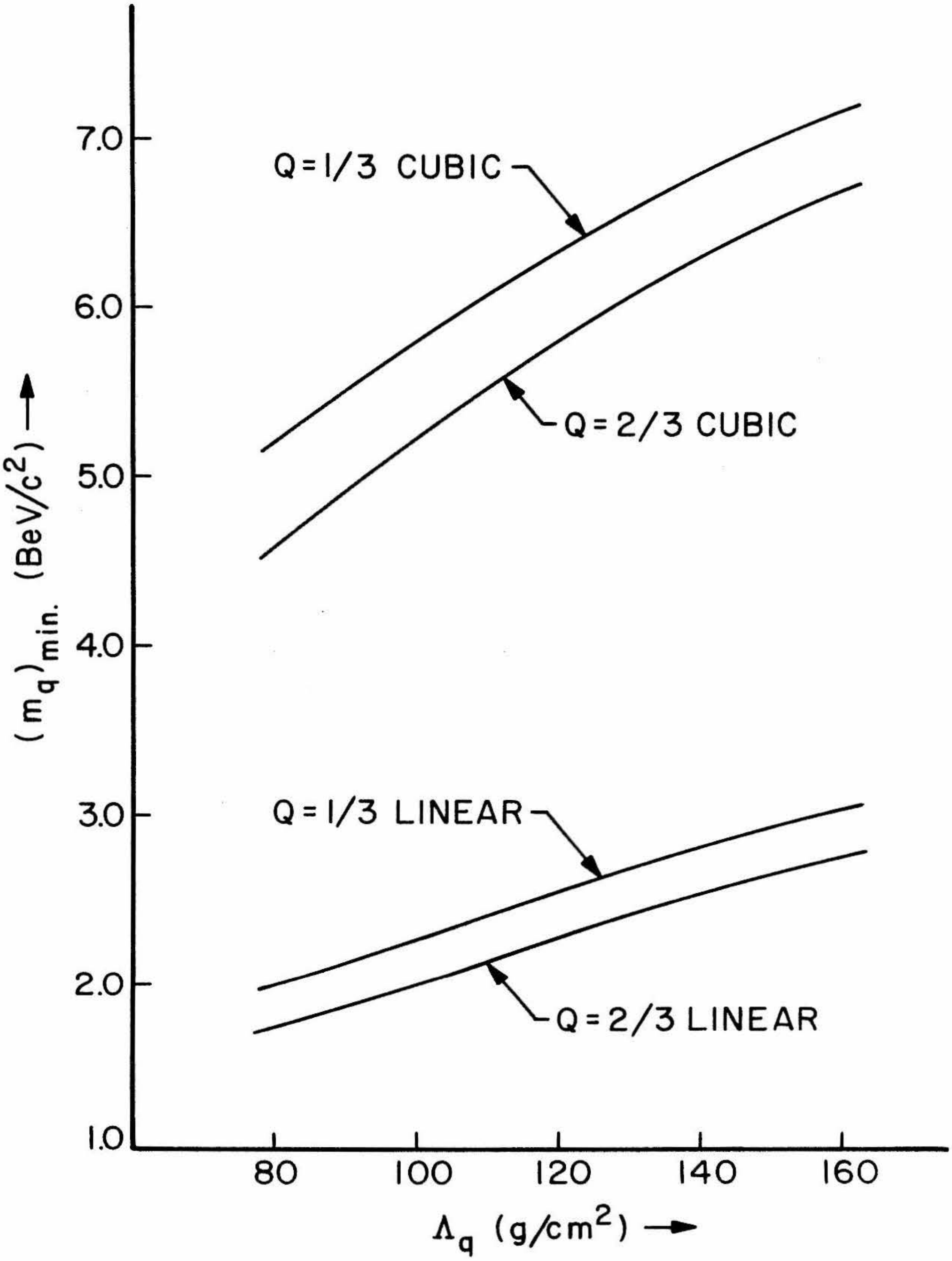

FIGURE 48: $(m_q)_{min}$ VS η FOR Λ_q=120 AND s_o=1.0

$\alpha_q(t) = 0$

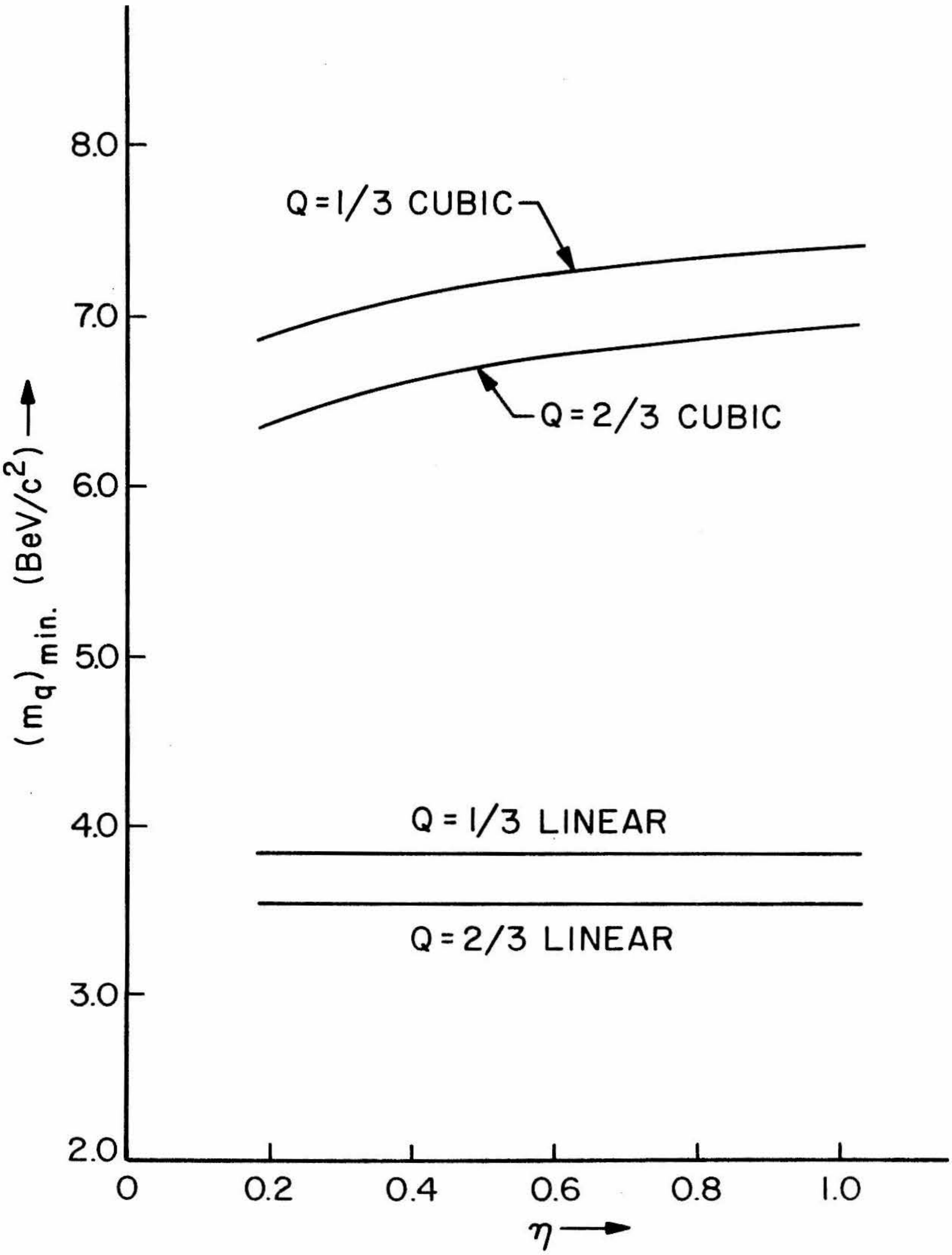

FIGURE 49: $(m_q)_{min}$ VS η FOR Λ_q=120 AND s_o=5.0

$\alpha_q(t) = 0$

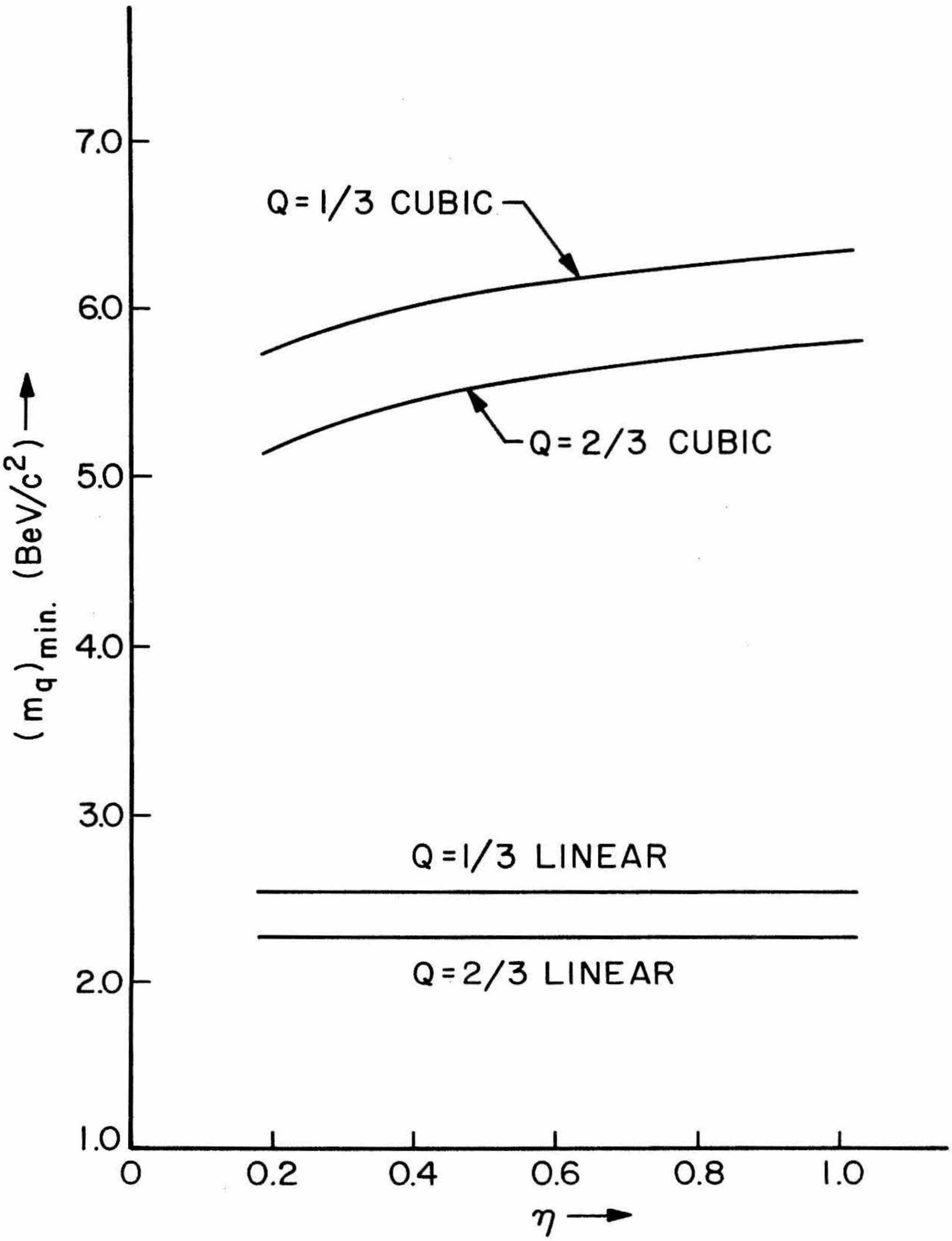

FIGURE 50: $(m_q)_{min}$ VS s_o FOR Λ_q=120 AND η=1.0

$\alpha_q(t) = 0$

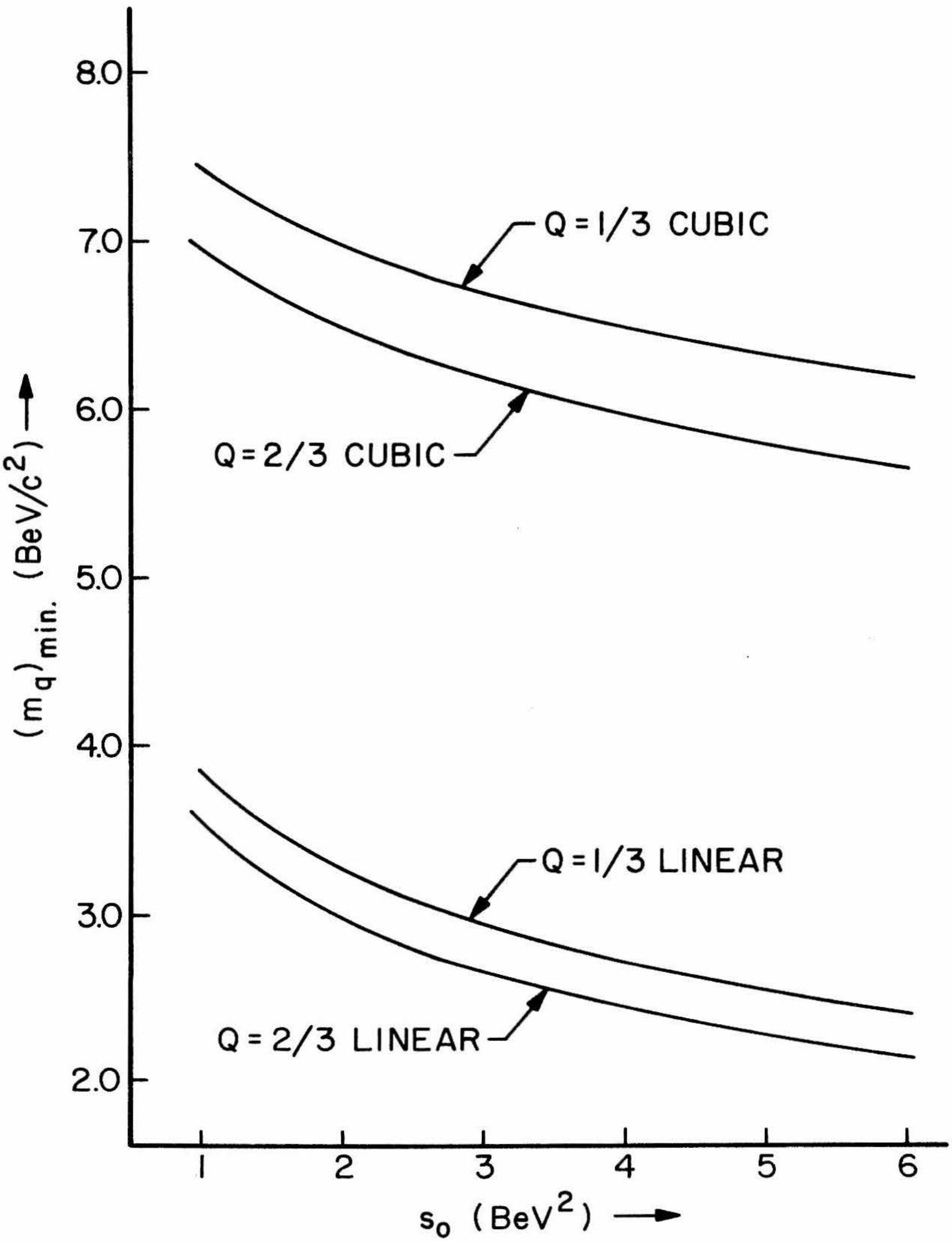

insensitive to the value given to η, as expected, the choice for η is really of no consequence. To be specific, we shall assume a value of one, which corresponds to an asymptotic production cross section of forty millibarns.

As we have mentioned previously, it is common practice when treating interactions between particles whose masses are less than one BeV/c^2 to assume that s_o is 1 BeV^2. In our case, because we consider multi-peripheral Reggeized amplitudes, a particular choice of values for s_o, for the four-momentum transfer damping coefficients a_i, and for the various coupling constants corresponds to a particular choice of residue functions. Because there is no experimental or theoretical evidence to indicate that another choice for s_o would be better, we shall assume that the best value for s_o for our choice of residues is the usual value of 1 BeV^2.

With Λ_q = 120 $\mathrm{g/cm}^2$, η= 1.0, and s_o = 1 BeV^2, the lower limits for m_q can be seen to be the following: 1.3 ± 0.2 BeV/c^2 for the case $\alpha_q(t) = -m_q^2 + t$, and 6 ± 2 BeV/c^2 for the case $\alpha_q(t) = 0$. The total production cross sections which correspond to these mass limits can be determined from the data given in tables 7 and 8. In the case $\alpha_q(t) = -m_q^2 + t$ (table 7), the total production cross section near threshold is extremely dependent on the size of m_q, being about 10^{-36} cm^2 for m_q = 1.5 BeV/c^2 and 10^{-72} cm^2 for m_q = 3.0 BeV/c^2. In the case $\alpha_q(t) = 0$ (table 8), the dependence on m_q is less dramatic, the total production cross section near threshold dropping from about 10^{-32} cm^2 at $m_q = 5.0$ BeV/c^2 to about 10^{-37} cm^2 at $m_q = 9.0$ BeV/c^2. In either case, the value of the total production cross section at very large s is of no importance.

F. Dependence of the Results on the Parameter Values and the Assumptions

Because the rate of quarks through our array depends on m_q in a way which varies from approximately $m_q^{-16/3} \exp(-7.0\ m_q^{2.4})$ to approximately $m_q^{-10/3} \exp(-0.9\ m_q^{1.4})$, depending on the Regge trajectory one might assign to a quark, the mass limits obtained are relatively insensitive to small changes in any of the parameters considered. All but two of the assumptions which were made are also not critical.

One assumption which is essential is the dynamical assumption that the production amplitudes are exponentially damped in certain four-momentum transfers. The only other assumption which is essential is the assumption that the production amplitudes factor into two-body-like amplitudes each of which can be Reggeized. Because the amplitudes are both multi-peripheral and Reggeized, the production cross section is highly dependent on the intercept of the quark's Regge trajectory.

The dependence of the results on the choice of s dependence for the production cross section and on the choice of values for the parameters Λ_q, η, and s_o is illustrated in figures 41 through 50. The dependence on those parameters which appear as factors in the expression for the quark rate can be inferred from the difference between the curves for charges 1/3 and 2/3 in these figures. This difference is indicative of the shift in the quark mass limits which would accompany a change in the production cross section of a factor of two (i.e. 93%/45%).

For parameters appearing squared in the expression for the rate, such as the coupling constant at any vertex and constant signature factors, the maximum dependence is approximately as the 3/8 power of any fractional change for the case $\alpha_q(t) = -m_q^2 + t$, and approximately as the 3/5 power of any fractional change for the case $\alpha_q(t) = 0$. For parameters appearing linearly, such as the pion-to-nucleon cosmic-ray flux ratio $K(j) = 0.3$, the effective atomic weight of a nitrogen or oxygen nucleus A_{eff}, and the normalization constant (2.35) for the primary cosmic-ray nucleon flux, the maximum sensitivity is approximately as the fifth root of any fractional change for the case $\alpha_q(t) = -m_q^2 + t$, and approximately as the cube root of any fractional change for the case $\alpha_q(t) = 0$.

The results are rather insensitive to small changes in the slope of the Pomeranchuk trajectory, but are somewhat dependent on its intercept. The results are of course critically dependent on the intercept of the quark trajectory, as one can see from tables 7 and 8, and figures 41 through 50. The dependence on the slope of the quark trajectory (with intercept fixed)* varies from a slight dependence for trajectories near $\alpha_q(t) = -m_q^2 + t$ to quite a dependence for trajectories near $\alpha_q(t) = 0$. Small changes in the four-momentum transfer damping coefficient a_{Pom} associated with the Pomeranchuk trajectory are of little consequence. Changes in the coefficient a_q associated with the quark trajectory have a somewhat

*Such variation is of course unphysical because the trajectory must go through zero at $t = + m_q^2$.

greater consequence. For purposes of illustration, one is referred to table 9, where we give the sensitivity of $\sigma_{\text{threshold}}(m_q, s_o)$ to changes in the trajectory parameters and the four-momentum transfer damping coefficients for two cases: $\alpha_q(t) = -m_q^2 + t$ with $m_q = 1.5$ BeV/c^2, and $\alpha_q(t) = 0$ with $m_q = 6.0$ BeV/c^2.

In short, the maximum error in the production cross section resulting from inaccuracies in the parameters chosen for the Regge trajectories and from inaccuracies in the four-momentum transfer damping coefficients is expected to be not much larger than a factor of two. The corresponding variations in the quark mass limits are those indicated by the differences between the curves for charges 1/3 and 2/3 in figures 41 to 50.

To verify that the use of s_{ij}/s_o for the crossed-channel cosines in the Reggeized amplitudes is not really essential, one may consider the use of $(\nu_{ij}/s_o') = (s_{ij}-u_{ij})/(2s_o')$ with s_{ij} and u_{ij} being extensions of the usual two-body kinematic scalers s and u. With such a form, one obtains production cross sections and corresponding quark mass limits which are the same as those obtained here for s_o if we set $s_o = s_o' + \Delta(s_o')$. For the case $\alpha_q(t) = -m_q^2 + t$, $\Delta(s_o')$ is less than $+0.5$ BeV^2 for $s_o' = 1$ BeV^2 and approximately $+2$ BeV^2 for $s_o' = 5$ BeV^2. For the case $\alpha_q(t) = 0$, $\Delta(s_o')$ is approximately $+0.2$ BeV^2 independent of s_o'.

As we have already mentioned, the results are quite dependent on the dynamical assumptions that the production amplitudes

TABLE 9: SENSITIVITY OF $\sigma_{threshold}(m_q, s_o)$ TO CHANGES IN a_i AND TRAJECTORY PARAMETERS

CHANGES MADE / PARAMETERS CHANGED					EFFECT ON $\sigma_{threshold}(m_q, s_o)$			
$\Delta a_q/a_q$	$\Delta a_{Pom}/a_{Pom}$	$\Delta\alpha_{Pom}(0)/\alpha_{Pom}(0)$	$\Delta\alpha'_{Pom}/\alpha'_{Pom}$	$\Delta\alpha_q'/\alpha_q'$	$m_q=1.5$ BeV/c^2		$m_q=6.0$ BeV/c^2	
$(BeV/c)^{-2}$	$(BeV/c)^{-2}$		$(BeV/c)^{-2}$	$(BeV/c)^{-2}$	$s_o=1$	$s_o=5$	$s_o=1$	$s_o=5$
+0.5/2.5					-1.7	-2.1	-3.9	-3.9
-0.5/2.5					+1.8	+2.3	+4.5	+4.5
	+0.5/5.0				-8.2%	-8.3%	-23%	-23%
	-0.5/5.0				+10.0%	+10.0%	+32%	+32%
		-0.1/1.0			-2.4	-1.8	-2.6	-1.9
			+0.1/0.0		-7.3%	-5.3%	-22%	-15%
				-0.1/1.0	+38%	+17%		
				+0.1/0.0			-6.7	-4.4

Explanations:
1) A plus sign indicates an increase; a minus sign indicates a decrease.
2) Effects on $\sigma_{threshold}(m_q, s_o)$ are given as factors unless otherwise indicated.
3) Changes in trajectory slopes are made holding intercepts fixed.

factor into two-body-like amplitudes which involve exponential dampings in certain four-momentum transfers. Note that this dependence is quite natural, because factorization and dampings in four-momentum transfers seem to be well-founded concepts for high-energy interactions. Nevertheless, it is the use of multi-peripheral amplitudes which partially explains why the production cross sections and the mass limits that we report are so low.

If quark production is not dominated by multi-peripheral events, our mass limits are somewhat low. The factor by which the mass limits should be increased is approximately the n^{th} root of the reciprocal of the fraction of the number of events which are multi-peripheral, where n is 5 for the case $\alpha_q(t) = -m_q^2 + t$ and 3 for the case $\alpha_q(t) = 0$.

For example, suppose the quark mass is as low as 1.5 BeV/c^2. Quarks could then be produced at incident energies as small as approximately 8 BeV. Using anti-baryon production as a basis, we might estimate that the fraction of the number of events which are multi-peripheral at these energies may be on the order of 10%. The total production cross section would then be a factor of ten larger than we have reported, yet the quark mass limit would be only 60% larger.

In any case, the fraction of the number of events which are multi-peripheral can be determined only through assumption. We shall therefore assume that the fraction is large enough so that our results are essentially correct.

G. Discussion of the Results

As one can see from the end of section D and appendix F, the monatomically decreasing cosmic-ray flux makes the rate of quarks through an array depend only on the 10/3 root of the production cross section. This is fortunate in one sense because a mass limit obtained for a quark on the basis of a cosmic-ray experiment is therefore not very sensitive to the particular assumptions which are made. On the other hand, the inherent insensitivity makes it very difficult to determine whether one method of obtaining the production cross section is more plausible than another, because the mass limits obtained are nearly always in the range from a couple of BeV/c^2 to tens of BeV/c^2.

In our case, as in all others, many assumptions have been made. Our assumptions, however, rather than appearing completely arbitrary, are all tied to a model which seems to be important in the treatment of high-energy interactions. We therefore feel that our methods are better than those previously reported.[(66-68)]

By using multi-peripheral Reggeized amplitudes, we find the total cross section for quark production to be significantly smaller than the cross sections assumed by other investigators. As a result, we find that the mass of a quark need not be anywhere near as large as ten BeV/c^2 to explain why quarks have not yet been observed. Just how small the quark mass might be is critically dependent on how low the intercept of the quark's Regge trajectory is assumed to be. If this intercept is as low as $-m_q^2$, which corresponds to a trajectory of slope 1 $(\mathrm{BeV}/c)^{-2}$, just as for the known hadrons, the quark mass need not be any larger than 1.3 ± 0.2 BeV/c^2. For quark masses larger than this, the production cross section becomes extremely small, being about 10^{-72} cm^2 for $m_q = 3.0$ BeV/c^2. A consequence is that, if no other production mechanism becomes important, experiments conducted in search of heavy quarks will most likely be limited by time if not by background.

APPENDIX A: ELECTRONIC DETAILS

The blocks of electronics shown in figure 2 are described in detail in the following sections. The trigger inhibitor is described in section 1. Descriptions of B-Logic and G-Logic are given in sections 2 and 3 respectively. The manner in which Q-TR was used to trigger the spark chambers and the recording equipment is described in section 4.

1. The Trigger Inhibitor

The trigger inhibitor served two purposes: 1) it served as a clock to measure the time during which the system had been operative, and 2) it forced the system to treat at most one event at any time.

If no pulses between 0.03 and 0.7 minimum occurred in time coincidence in the six counter trays, a negative square gate pulse one second long was generated by the trigger inhibitor every 1.019 seconds. The time in seconds during which the experiment had been sensitive for the detection of fractionally charged particles was measured by a scaler which counted the number of these gate pulses generated during the quark runs.

If a trigger occurred during a certain gate pulse, that pulse was immediately terminated and the generation of another pulse was inhibited until the camera system had indicated that the necessary pictures had been taken. The electronics could not recognize any other event during this recording period* because the lack of a gate pulse made the main coincidence-anticoincidence circuit dead.

2. B-Logic

The electronic details of the B-Logic block are presented in figure 51. For convenience, each circuit is shown as a box enclosing code symbols which indicate the type of circuit used. The explanation of this circuit code is given in table 10 along with the descriptive symbols which these circuits have been given by the California Institute of Technology Synchrotron staff.†

B-Logic was used to generate the signal B-TR and to operate the light system. The B-counter electronic inputs were added, after passing through 25-nanosecond passive integrators, to form S1 and S2. These pulses were multiplexed so that they could be sent to the analyzer, to the lower-bias discriminators, and to the upper-bias discriminators.

---

*This three-second pause was more than enough time for the spark-chamber pulsing system to re-charge.

†E.g., see Alvin V. Tollestrup, California Institute of Technology Synchrotron Laboratory CTSL INTERNAL REPORT NO. 31.

FIGURE 51: B-LOGIC

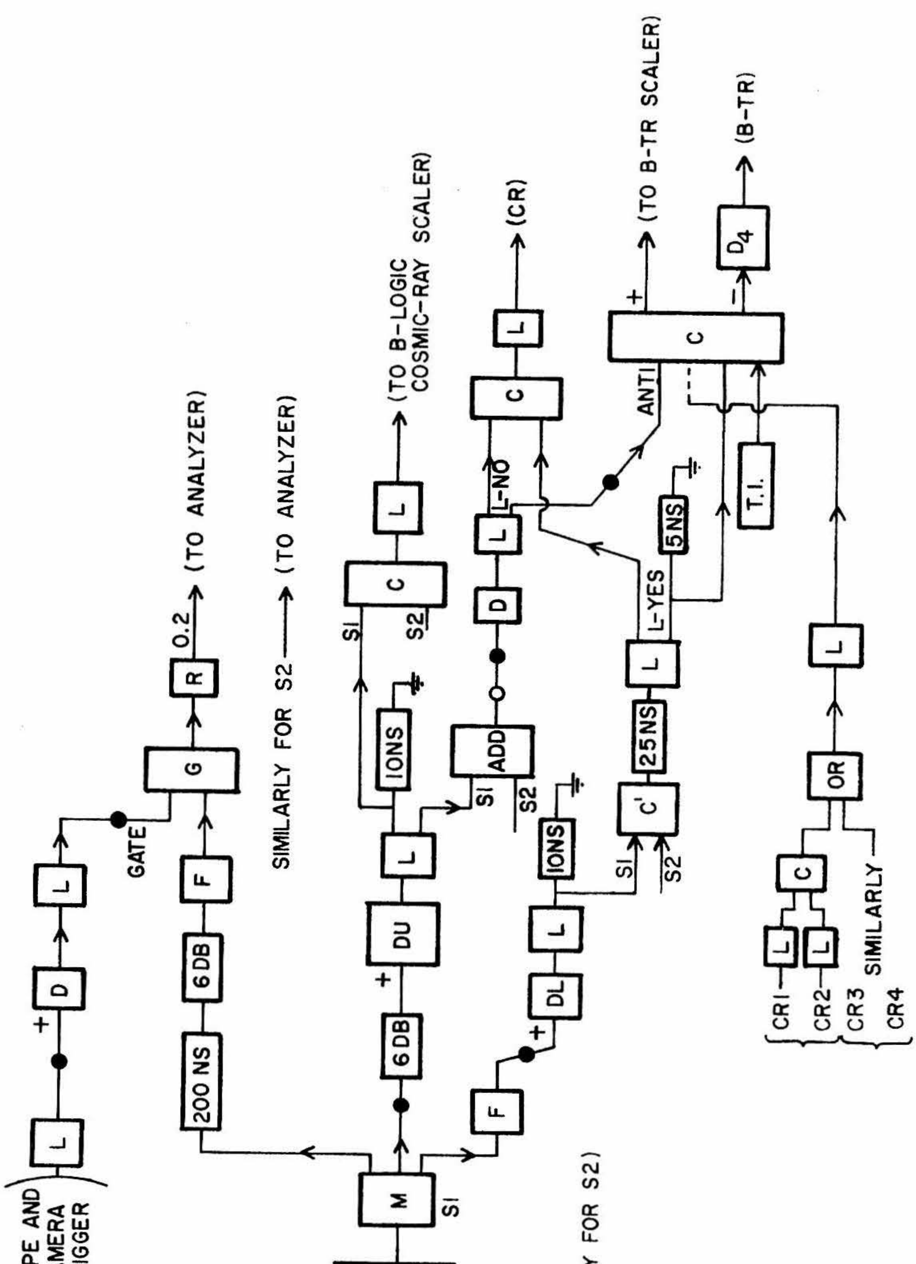

TABLE 10: ELECTRONIC-CIRCUIT NOMENCLATURE

Circuit Code	Circuit Description	Synchrotron Circuit
A	Amplifier	TA-11
AC	Anti-Coincidence Circuit	GM-1
ADD	Adder	TM-3 or TS-3
C	Coincidence-Anticoincidence	TC5-B
C'	Coincidence Circuit	TC-5
C^*	Coincidence Circuit	SDTM (10μs gate)
D	Discriminator	TVD-3
D''	Discriminator	TVD-3B
DL	Discriminator for lower bias	TVD-3
DL'	Discriminator for lower bias	½ TVD-4 (87NS reset, 38NS clipping cable)
DU	Discriminator for upper bias	TVD-3
DU'	Discriminator for upper bias	½ TVD-4 (87NS reset, 2.5NS clipping cable)
D_1	Discriminator	½ TVD-4 (2.5NS+.005μf reset, 7.5NS clipping cable)
D_2	Discriminator	½ TVD-4 (87NS reset, 44NS clipping cable)
D_3	Discriminator	½ TVD-4 (44NS reset, 44NS clipping cable)
D_4	Discriminator	½ TVD-4 (12NS reset, 7.5NS clipping cable)
F	Fast Amplifier	½ TA-11B
FA	Fast Amplifier	½ SA2-F
G	Fast Linear Gate	TG-3

TABLE 10: (Continued)

Circuit Code	Circuit Description	Synchrotron Circuit
GD	Gated Discriminator	TVD-3
GOR	Gated "OR" Circuit	GM-1
L	Limiter	L1-B
M	Multiplexer	TM-4
OR	"Either-or" Circuit	GM-1
PS	Delay-Line Pulse Shaper	½ DLPS-2
PS'	Capacitive Pulse Shaper	(not in common use)
R	Passive Resistive Divider	(none)
SA	Slow Amplifier	SA-1B
T	Adder	(not in common use)
T.I.	Trigger Inhibitor	(not in common use)

Additional Symbols	Circuit Element
O	25 nanosecond passive integrator
●	1 nanosecond inverting transformer
X	1 nanosecond non-inverting transformer
+	Positive output
−	Negative output
E.F.	Negative emitter-follower output

(NS = nanosecond)

Multiplexed portions of the S1 and S2 signals were sent to gating networks and then to the analyzer to be recorded. The pulses were first delayed by 200-nanosecond delay cables and attenuated by 6 db passive attenuators. They were then amplified and sent to fast linear gates which were gated by that part of the multiplexed trigger pulse Q-TR called the scope and camera trigger.

The gating networks were used for the S pulses and not for the G pulses because the B phototube outputs were more subject to statistical variations than the G-counter phototube outputs.* The gates allowed the S1 and S2 pulses to pass through a 0.2 resistive divider to the analog inputs of the analyzer only if they arrived within 40 nanoseconds of the time corresponding to the occurrence of the ionization in the counters which caused Q-TR to be generated.†

Other portions of the multiplexed S1 and S2 signals were used to indicate that a cosmic-ray particle had traversed the B counters (i.e., that S1 and S2 had energy losses above 0.7 minimum). These signals were used to run a B-Logic cosmic-ray scaler and to generate the signal L-NO. The S1 and S2 pulses were sent to the upper-bias discriminators and then to limiters which shaped and multiplexed the discriminator outputs. The signal L-NO was generated by adding the limited S1 pulse to the limited S2 pulse, integrating

---

*The B phototubes had only 40 photocathode electrons for minimum ionization while the G phototubes had 600.

†That is, the coincidence between the gate signal and the S1 or S2 signal allowed a relative timing shift of about ±40 nanoseconds.

the result with a passive 25-nanosecond integrator, inverting, and sending the result to a discriminator whose output was shaped by another limiter. The B-Logic cosmic-ray scaler was operated by clipping the limited S1 and S2 pulses with ten-nanosecond shorted cables and requiring a coincidence between the two clipped pulses. This scaler thus counted events with a coincident energy loss of more than 0.7 minimum in both S1 and S2.

The third multiplexed portions of the S1 and S2 pulses were used to generate the signal L-YES. This signal indicated whether an event had occurred which corresponded to energy losses of more than 0.03 minimum in time coincidence in both S1 and S2.

To generate L-YES, the multiplexed S1 and S2 pulses were sent to the lower-bias discriminators by way of fast amplifiers, and then to limiters. The two limited pulses were clipped by ten-nanosecond shorted cables and then checked for coincidence. If they were in coincidence, the signal L-YES was generated.

The signals L-YES and L-NO were used to generate the signal B-TR, to operate the B-TR scaler, and to generate the signal CR. The signal to operate the B-TR scaler and to form B-TR after discrimination was generated by the coincidence of the gate pulse from the trigger inhibitor, the coincidence of L-YES clipped by a shorted five-nanosecond cable, and the anticoincidence of L-NO. When extra counters (labelled CR counters) were placed in the array to require near-vertical cosmic-ray particles, their limited coincident phototube responses were required at the above coincidence-anticoincidence circuit in place of L-NO and the clipped L-YES signal. The coincidence of L-YES and L-NO generated the signal CR, which served as the basis for the detection of cosmic-ray particles for the light system.

3. G-Logic

The electronic details for the G-Logic block are presented in a similar fashion in figure 52. The pulse entering the electronic input for each G counter was first sent to a three-way resistive-divider network. One of the divided signals, representing 42.5% of the output from each counter, was termed a "scope multiplexed output" because it went to the oscilloscope circuitry. Another divided signal representing 42.5% of the output from each counter passed through a 3 db passive attenuator to become a "G-Logic input." The remaining 15% of the divided signal was sent directly to the analog inputs of the analyzer.

The oscilloscope circuitry was set up so that the pulse from each G counter was displayed twice, once with one vertical gain and again 100 nanoseconds later with four times the vertical gain. All of the scope multiplexed outputs for the even-numbered G counters were delayed by forty nanoseconds. The scope signals were added in pairs (G1+G2, G3+G4, G5+G6, G7+G8). The sums were amplified, delayed by 200 nanoseconds, and sent to a divider-delay circuit which split each sum into two parts. The two parts for the G1+G2 and G5+G6 sums

FIGURE 52: G-LOGIC

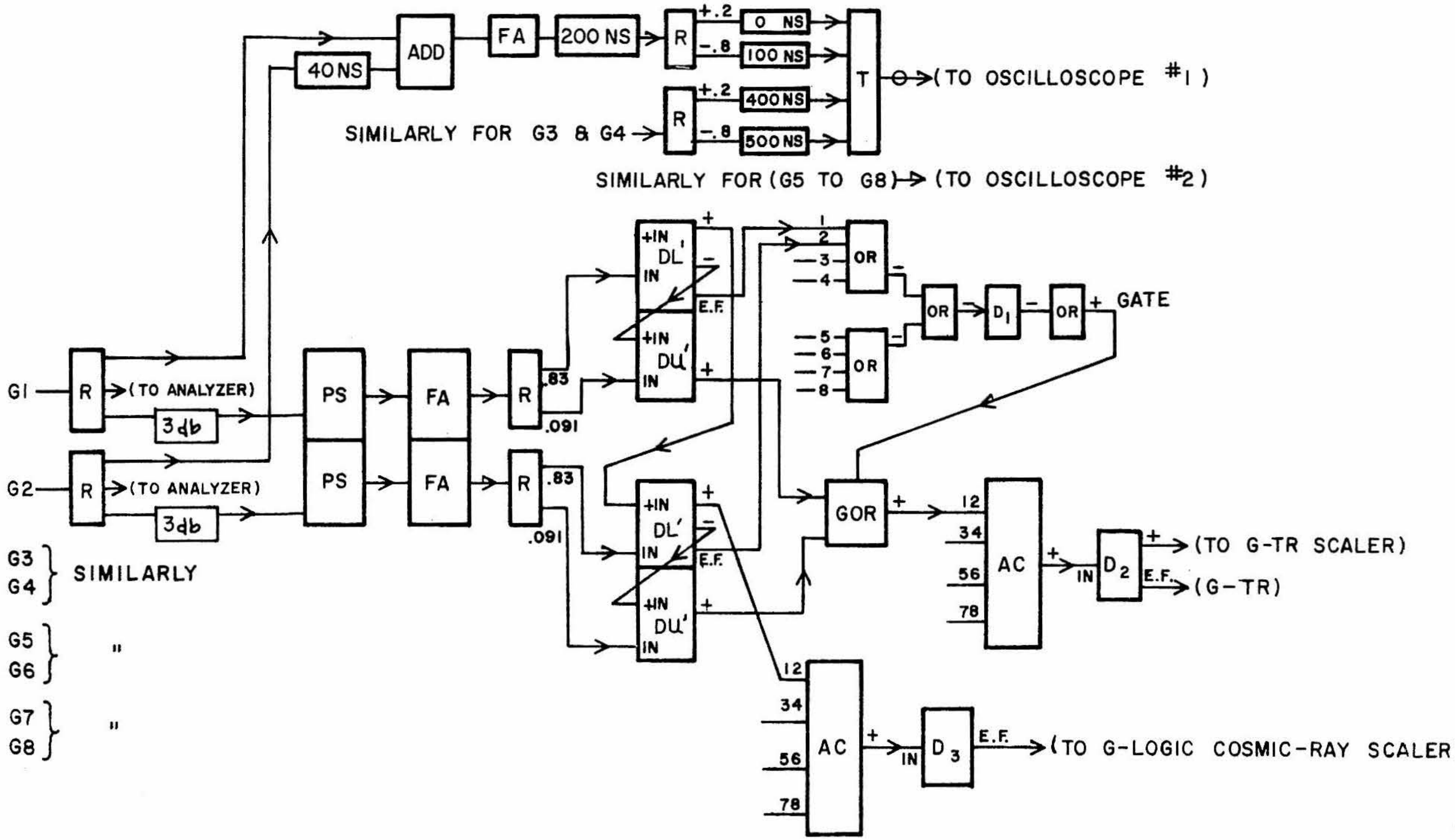

were +0.2 times the sum delayed by zero nanoseconds and -0.8 times the sum delayed by 100 nanoseconds. The two parts for the G3+G4 and G7+G8 sums were +0.2 times the sum delayed by 400 nanoseconds and -0.8 times the sum delayed by 500 nanoseconds. The parts for G1 through G4 were then added and sent to oscilloscope #1 through a passive 25-nanosecond integrator. The parts for G5 through G8 were treated in the same manner, but were sent to oscilloscope #2.

The G-Logic inputs were used to generate the signal G-TR. Each G-Logic input was shaped by a linear pulse-shaping circuit, amplified, and sent to a resistive divider. This divider sent 0.83 of its input to the lower-bias discriminators and 0.091 of its input to the upper-bias discriminators. The signals from the discriminators were used in pairs to operate two anti-coincidence circuits, which operated two scalers and generated the signal G-TR.

To generate G-TR, the negative output of the lower-bias discriminator was added to the positive output of the upper-bias discriminator of each counter, and the sums were sent in pairs (G1&G2, G3&G4, G5&G6, G7&G8) to an "either-or" circuit. This circuit operated on negative inputs and was gated by a pulse generated from the occurrence of (G1.or.G2.or.G3.or.G4.) <u>OR</u> (G5.or.G6.or.G7.or.G8.) from the emitter-follower outputs of the eight G lower-bias discriminators. The coincidence of the outputs from the four "either-or" circuits produced a pulse which, after passing through a discriminator, served as G-TR and operated the G-TR scaler.

The positive outputs of the lower-bias discriminators were added in pairs (G1+G2, G3+G4, G5+G6, G7+G8) and sent to a coincidence circuit. The discriminated output of this four-fold coincidence operated the G-Logic cosmic-ray scaler.

4. Triggering the System with Q-TR

A diagram illustrating how the generated trigger Q-TR was used to trigger the equipment is given in figure 53. After discrimination, pulse-shaping by limiters, and in some cases amplification, as shown, Q-TR served as the oscilloscope trigger, the camera-system trigger, the spark-chamber trigger, and the analyzer trigger. It was also used to operate the Q-TR scaler and to terminate the trigger-inhibitor gate and hence to start the dead time during which the data for that event were recorded.

Q-TR was also used in conjunction with the signal CR to operate the light system and its scalers. Signal CR generated a ten-microsecond pulse whose coincidence with Q-TR operated the "early-particle" light and its scaler.

The coincidence of a special gate pulse and the signal CR operated the "late-particle" light and its scaler. This special gate pulse was a long pulse generated by Q-TR. The gate was either terminated by the spark-chamber current-probe reset pulse when the chambers had been pulsed or it was continued for a period exceeding forty microseconds.

FIGURE 53: DISTRIBUTION OF Q-TR

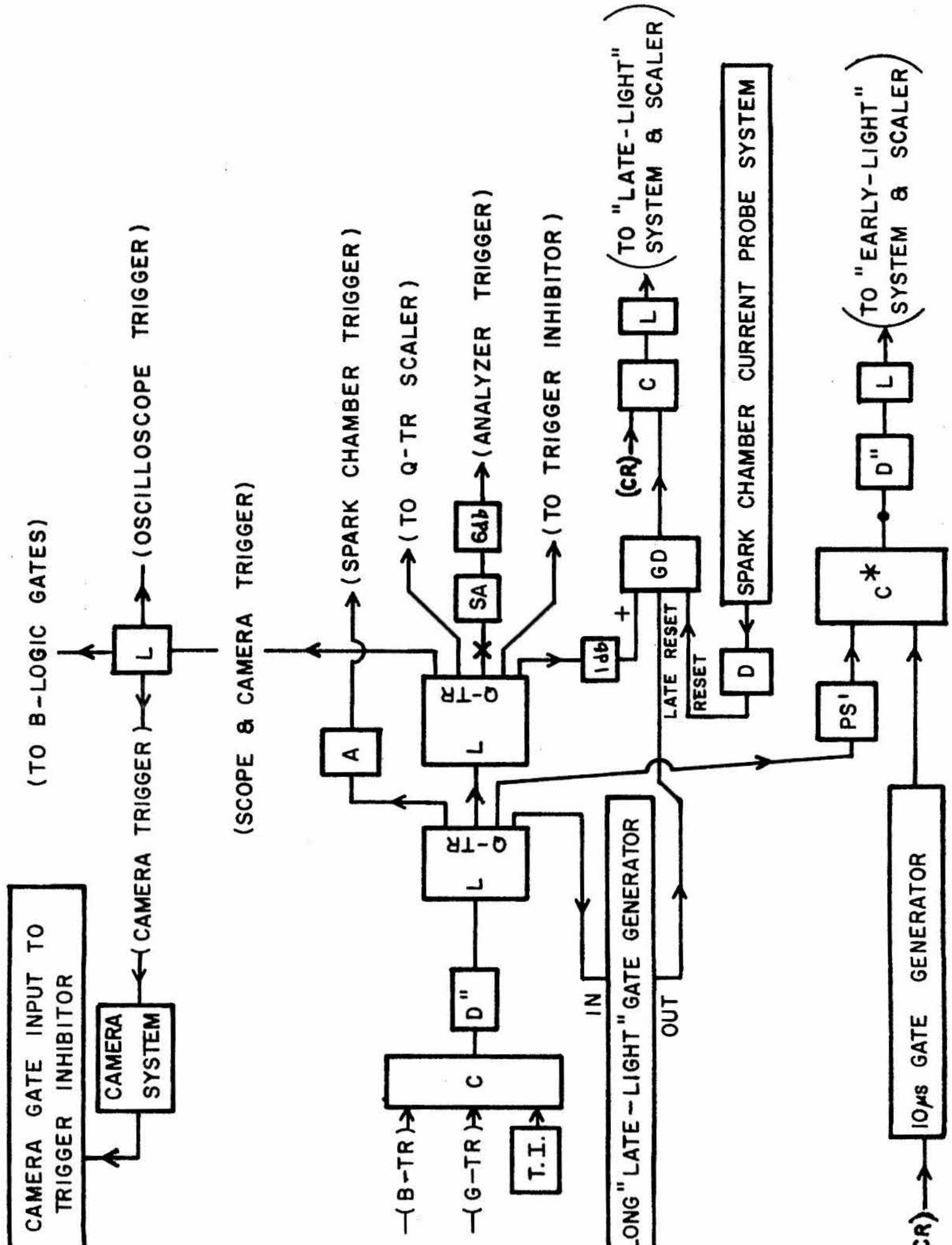

APPENDIX B: THE TECHNIQUES USED TO COMPUTE MPPH AND X^2

As described in section IV.D, a MPPH and a X^2 were computed for each combination of six normalized pulse heights between 0.04 and 0.7 minimum. The MPPH was computed to determine the most probable energy loss of the particle tentatively assumed to have traversed the array. The X^2 was computed to determine whether the six pulse heights for that combination actually corresponded to the energy losses of a particle traversing the array.

The formulas used in MPPH and X^2 calculations were derived using a maximum-likelihood method based on Gaussian distributions. However, because the experimentally observed pulse-height distributions were not Gaussian, the formulas derived were not used in a straight-forward manner. They were used, instead, in an iterative computational procedure which allowed the asymmetry of the pulse-height distributions to be introduced. The techniques utilized were chosen for their simplicity so that relatively little computer expense would be incurred. These techniques are described in detail in the following sections.

1. MPPH Techniques

To derive the mathematical expression used to compute the MPPH for a given combination, one first assumes that the six normalized pulse heights for that combination, x_i, $i=1,\ldots,6$, constitute a random sample of six independent Gaussian pulse-height distributions. The distributions are assumed to have the same mean μ, but may have different standard deviations σ_i. With these assumptions, the likelihood of obtaining that particular set of pulse heights is given by the function

$$L = \prod_{i=1}^{6} \left\{ \frac{1}{\sqrt{2\pi}\,\sigma_i} \exp\left[- \frac{(x_i-\mu)^2}{2\sigma_i^2} \right] \right\} \tag{B-1}$$

To obtain an expression which will provide the "best" estimate for μ, based on the given sample of six pulse heights, one can maximize this "likelihood function" relative to the parameter μ. The maximization can be accomplished by setting the partial derivative with respect to μ of the logarithm of L

$$\ln(L) = -3\cdot\ln(2\pi) - \sum_{i=1}^{6} \ln(\sigma_i) - \tfrac{1}{2}\cdot\sum_{i=1}^{6} \left[\frac{x_i-\mu}{\sigma_i}\right]^2 \tag{B-2}$$

equal to zero. When this is done, and one solves for μ, the result is the following expression for the weighted mean pulse height:

$$\mu = \frac{\sum_{i=1}^{6} \left(\frac{x_i}{\sigma_i^2} \right)}{\sum_{i=1}^{6} \left(\frac{1}{\sigma_i^2} \right)} \tag{B-3}$$

Note that this would be merely the average pulse height if all of the σ_i were identical.

The asymmetry of the experimentally observed pulse-height distributions was then introduced by using equation (B-3) in a special iterative computational procedure. The assumption was made that the distribution which would result from the passage of particles with a particular fractional charge and a given speed through the counter corresponding to the i^{th} pulse height would be composed of two Gaussian-like parts. The "left" part on the lower-energy-loss side of the peak, was assumed to be one-half of a Gaussian distribution having a standard deviation σ_{L_i}. The "right" part, on the higher-energy-loss side of the peak, was assumed to be one-half of a Gaussian distribution having the larger standard deviation σ_{R_i}.* The desired asymmetry was then introduced into the Gaussian-oriented maximum-likelihood method in the following way: either σ_{L_i}, σ_{R_i}, or their average, according to a prescription to be described shortly, was substituted for the σ_i in equation (B-3).

In order to determine what values should be used for the σ_{L_i} and σ_{R_i} for a particular set of six pulse heights, a model had to be adopted to indicate how the widths of the two Gaussian components of each pulse-height distribution were going to be assumed to change as a function of the most probable energy loss. Except for the contribution from electron statistics in the

*Although the left part of the distribution for cosmic rays (figure 3) does have a Gaussian shape, the right part does not because of the long tail at large pulse heights. The Gaussian approximations are close enough, however, so that no significant error in the MPPH was introduced by using the above assumptions (see figure 13 in section IV.H).

photomultiplier tube, the Gaussian components of each distribution were expected to scale as if distributions with smaller peak energy losses were equivalent to distributions of appropriately attenuated cosmic-ray pulse heights. For this reason, the assumption was made that pulse-height distributions corresponding to the passage of fractionally charged particles through the array could be formed by suitably scaling the experimentally observed cosmic-ray distributions in accordance with electron statistics in the corresponding photomultiplier tubes.*

For example, to form the distributions corresponding to the passage of particles whose most probable energy loss was $\frac{1}{2}$ minimum, one would proceed as follows. First, the contribution from electron statistics would be removed from the distributions resulting from the passage of cosmic-ray muons through the counters in the array. Second, the resulting distribtuions would be scaled so that their most probable pulse heights were all at $\frac{1}{2}$ minimum. Third, the scaled distributions would be broadened in accordance with the electron statistics appropriate for the counters considered and for $\frac{1}{2}$ minimum.

---

*A tacit assumption here is that the distribution of speeds for fractionally charged particles is the same as that for cosmic-ray muons; that is, when scaling the widths in this manner, all particles were assumed to be minimum ionizing.

In this fashion, pulse-height distributions were formed whose most probable energy losses covered the entire range between 0.04 and 0.7 minimum. The squares of the standard deviations of the "left" and "right" parts of each distribution were computed, and then plotted as a function of most probable pulse height (Y). The data were consistent with the following quadratic relationship:

$$(\sigma_{k_i})^2 = (A_{k_i}) \cdot Y + (B_{k_i}) \cdot Y^2 \qquad \text{(B-4)}^*$$

Here, k is either L ("left") or R ("right"). The coefficients A_{k_i} and B_{k_i} for the i^{th} counter were determined to be the following (for Y and σ in normalized channels):

	A_L	B_L	A_R	B_R
S1 & S2	2.37	0.0120	3.15	0.132
G1 through G8	0.24	0.0034	0.00	0.092

*Such a quadratic relationship is expected in the limit where Symon-Landau statistics (references 37-39) become Gaussian for the following reasons. If the electron statistics associated with an average of N electrons produced at the photocathode are incorporated into a Gaussian energy-loss distribution with standard deviation σ_S and mean μ_S to form a pulse-height distribution which is approximated by a Gaussian distribution with standard deviation σ and mean μ, then

$$(\sigma / \mu)^2 = (\sigma_S/\mu_S)^2 + (c/N)$$

where c is a constant which depends on the efficiencies for the production of electrons at the various electrodes in the phototube. Furthermore, μ is proportional to N. With $Y=\mu$, equation (B-4) results. The "parts" of the pulse-height distributions considered in the analysis above are sufficiently Gaussian so that a similar relationship applies.

With these coefficients at hand, the appropriate σ_{L_i} and σ_{R_i} for a given distribution could be computed as soon as its peak Y had been determined.* The cosmic-ray data considered in determining the above coefficients are those from the L-V-CR runs.

The computation of a MPPH given the six normalized pulse heights for a particular combination was performed according to the following iterative procedure. First the σ_{L_i} and the σ_{R_i} were computed using equation (B-4) with Y equal successively to each of the six pulse heights x_i. The average of σ_{L_i} and σ_{R_i} was then used for the σ_i in equation (B-3) to compute a very approximate estimate for a weighted mean pulse height. The σ_{L_i} and σ_{R_i} were recomputed using this mean for the Y in equation (B-4), and their average was used for the σ_i in equation (B-3) to compute a second and more accurate estimate for the weighted mean.

---

*That part of a pulse-height distribution not due to electron statistics is expected to scale according to the reciprocal of the cosine of the angle of the tracks in the spark chambers in addition to the square of the particle's charge (see section IV.H). One might therefore think that a more accurate procedure for obtaining the standard deviations appropriate for a particular combination of pulse heights would be to incorporate the cosine of the angle of inclination of the spark-chamber tracks for that event at this point. One should note, however, that the same reciprocal cosine factor would be involved for each of the six pulse heights, and a common factor in the σ_i in equation (B-3) is irrelevant.

Because the MPPH and not a weighted mean pulse height was desired,* the procedure was altered at this point and the asymmetry of the pulse-height distributions was introduced. The σ_{L_i} and σ_{R_i} were recomputed using the second-step μ for the Y in equation (B-4), as above. The μ in equation (B-3), however, was now computed using

1) $\sigma_i = \sigma_{L_i}$ if x_i was smaller than the μ computed in the previous step, or

2) $\sigma_i = \sigma_{R_i}$ if x_i was larger than the previous μ.

This new procedure was repeated four times. The result was that the computed μ shifted from a weighted mean to the most probable position of the peaks of the pulse-height distributions expected to be involved on the basis of the sample of six pulse heights given. The MPPH for that combination was thus set equal to the final value computed for μ.

The convergence of the computed μ's in shifting from the weighted mean pulse height to the MPPH was oscillatory in nature. After the second step, the value computed for μ would overshoot (undershoot) the convergence limit, then undershoot (overshoot), et cetera, with the final value usually within 0.1 of a normalized channel from the convergence limit. This oscillatory convergence is illustrated by the sequences of μ's shown in table 11 as they were computed for a combination with a very large X^2 and for a

*For a Gaussian pulse-height distribution, which is symmetrical about its peak, the weighted mean pulse height would also be the MPPH.

TABLE 11: THE CONVERGENCE OF μ'S TOWARD A MPPH

Characteristic	Event #1	Event #2
Pulse Heights	65.5	88.0
	35.5	78.8
	6.5	72.8
	26.5	109.3
	129.5	129.1
	8.2	108.0
MPPH	19.2	80.2
X^2	430.5	8.2
Sequence of μ's:		
Step: 1	8.86	93.13
2	43.21	101.22
3	18.74	80.3972
4	19.34	80.2286
5	19.13	80.2340
6	19.20	80.2338
7	19.17	80.2338

combination with a small value of X^2. As indicated in the table, the amplitudes of the oscillations obtained for different combinations seemed to be larger at corresponding steps for combinations having larger values of X^2.

2. X^2 Techniques

After the MPPH had been obtained for a given combination, the corresponding X^2 was computed using

$$X^2 = \sum_{i=1}^{6} \left[\frac{x_i - \text{MPPH}}{\sigma_i} \right]^2 \qquad \text{(B-5)}$$

where the σ_i were chosen so that

1) σ_i = the last σ_{L_i} computed in the MPPH computation, if x_i was smaller than the MPPH, or

2) σ_i = the last σ_{R_i} computed in the MPPH computation, if x_i was larger than the MPPH.

If the x_i had been independent random variables having Gaussian distributions, the right side of equation (B-5) would have been a value assumed by a random variable having a chi-square distribution with 6-1=5 degrees of freedom.* The experimental pulse-height distributions, however, were asymmetrical (see figure 3). Therefore, X^2 did not have the usual chi-square distribution;

*See reference 36, pages 194-195.

the probability measure associated with X^2 had to be determined through calibration. The calibration procedure which was used is described near the end of section IV.D.

APPENDIX C: THEORETICAL MODELS FOR THE SPARK-CHAMBER EFFICIENCY FITS

1. Introduction

In this appendix, we describe the mathematical models used in fitting the spark-chamber efficiency data discussed in section V.B. To apply these models, the chambers considered must be operated with a sweeping field and must be pulsed at a time t_{delay} after they have been traversed by a charged particle. The sparking efficiency of each gap must then be measured as a function of t_{delay}.

Four mathematical models are considered. The first is believed to describe the basic physical processes governing the sudden fall off in efficiency at moderate t_{delay}'s. This model includes an assumption that the number of electrons which were liberated through ionization by a particle traversing a spark-chamber gap, but which have not yet been swept out of the gap by a certain t_{delay}, can be described using Poisson statistics. The model is therefore labelled the "Poisson Theory."

The second model was devised in an attempt to add to the Poisson Theory the effects of delta rays produced along the particle's path of ionization.* The delta-ray contribution was expected to be small for the gases which we considered because a minimum-ionizing muon is expected to produce a delta ray in these gases in a distance which is, on the average, much larger than the gap width (3/8").

*The definition of a delta ray is given at the beginning of section 3.

Nevertheless, this model was included for the sake of completeness.

Although the Poisson Theory can adequately describe the efficiency data up to and partially through the sudden fall-off in efficiency, it can not describe the processes responsible for the small efficiencies which exist for larger t_{delay}'s. That is, the Poisson Theory alone can not describe the "tails" on the efficiency curves.

The third model was developed in an attempt to remedy this situation. In this model, the tails are attributed to the presence in the gap of additional free electrons, which are liberated through the collisional de-excitation of metastable states in the gas, with subsequent photo-ionization of either a gas atom or an atom in the aluminum walls of the gap.

The fourth model is, in a sense, a crude approximation of the third model, and was considered to see how sensitive the results were to the particular assumptions made regarding what physical processes were responsible for the "tails." The assumption was made, even though there does not seem to be any physical justification for doing so, that there is a constant probability that one electron will always be in the gap when it is pulsed.* The fourth model is the modification of the Poisson Theory which is necessary to incorporate the effects of this assumption.

*At 30 kilovolts/centimeter, cold field emission from the aluminum plates is still expected to be entirely negligible (see reference 52-54).

2. Poisson Theory*

Consider a plane-parallel gap of width G centimeters having an applied sweeping voltage V. Let the gap contain a gas in which free electrons have a drift velocity v and diffusivity (diffusion coefficient) D. When a charged particle traverses the gap, we assume that the electron-ion pairs produced will be distributed in a random fashion along the path of the particle with a mean number m per unit length.

Because delta rays† occur so infrequently in the gases which we shall consider, in comparison to the 3/8-inch gap spacing which we use, we shall ignore any secondary production of electron-ion pairs for the time being.** We assume, however, that m will turn out to be approximately half of what one might otherwise expect because about half of a minimum-ionizing particle's energy loss by ionization is expected to be in the form of delta rays.

---

*Most of the Poisson Theory was first developed by Dr. Joe H. Mullins at the California Institute of Technology.

†A delta ray is defined in section 3.

**Symon (reference 37) gives an expression for the probability that in going distance x a particle with a given energy will suffer one energy-loss collision and lose an amount of energy E' which is large compared with atomic ionization potentials. If one uses his expression, considers an ideal gas (of atomic number Z) at 300°K and atmospheric pressure, and considers all energy losses above E' electron-volts, one finds that a cosmic-ray muon should produce a delta ray in a distance, on the average, of approximately E'/6.9Z centimeters (where E' is expected to be at least 200 eV). See section 3.

Let a charged particle traverse the gap perpendicularly to the plates at time $t = 0$. Under the action of the sweeping field, the "column" of electrons formed along the particle's path begins to be swept out of the gap at the constant speed v. As they drift, the electrons also diffuse (diffusion coefficient D). At time t, the gap is pulsed. We assume that a spark will occur if the gap contains N or more electrons, regardless of their orientation or how far they can be accelerated by the pulsing field.*

We assume that the number of electrons in the portion of the column still inside the gap at time t can be described using Poisson statistics. That is, let w(t) be the average number of electrons remaining in the gap at time t. The probability that N electrons will still be in the gap at time t is then

$$C(t,N) = w(t)^N e^{-w(t)} / N! \qquad \text{(C-1)}$$

The sparking efficiency of the gap is therefore

$$\text{Efficiency}_N(t) = 1 - \sum_{i=0}^{N-1} C(t,i) \qquad \text{(C-2)}$$

---

*One might expect the efficiency to depend on whether the pulsing field is in the same direction or is opposite to the sweeping field. Nevertheless, such considerations are ignored here (we used a pulsing field opposite to the sweeping field).

We adopt the coordinate system shown in figure 54. We imagine the column of electrons to be stationary (except for diffusion) and the plates to be moving with speed v. Coordinate $x = -G + vt$ is the negative of the distance between the position of plate A at time $t = 0$ and the position of plate B (which is intercepting the electrons).

By considering element dx'' in the column, and ignoring lateral diffusion, one can show that

$$w(t) = m \int_{-G-x}^{-x} dx'' \int_{-x''}^{G-x''} dx' \int_{-\infty}^{+\infty} dy' \int_{-\infty}^{+\infty} dz' \frac{e^{-r^2/4Dt}}{(4\pi Dt)^{3/2}} \qquad \text{(C-3)}$$

$$= m \int_{-G-x}^{-x} dx'' \int_{-x''}^{G-x''} dx' \frac{e^{-x'^2/4Dt}}{(4\pi Dt)^{\frac{1}{2}}} \qquad \text{(C-4)}$$

where $r^2 = x'^2 + y'^2 + z'^2$.

Now let $d = d(t) = (4Dt)^{\frac{1}{2}}$, and approximate $d \ll vt$,* so that $(G-x'')$ and $(G + x)$ are both much larger than d; or, more exactly, make the approximation that

*For the gases we consider, v is approximately 10^5 cm/sec., D is approximately 260 cm^2/sec., so d(t) is smaller (larger) than one millimeter for times under (over) ten microseconds. The above assumption is therefore excellent for times over ½ microsecond: e.g. $erf(vt/d)$ is about 10^{-5} for $t = 1$ microsecond.

FIGURE 54: COORDINATE SYSTEM CONSIDERED FOR THE MOTION OF AN ELECTRON COLUMN

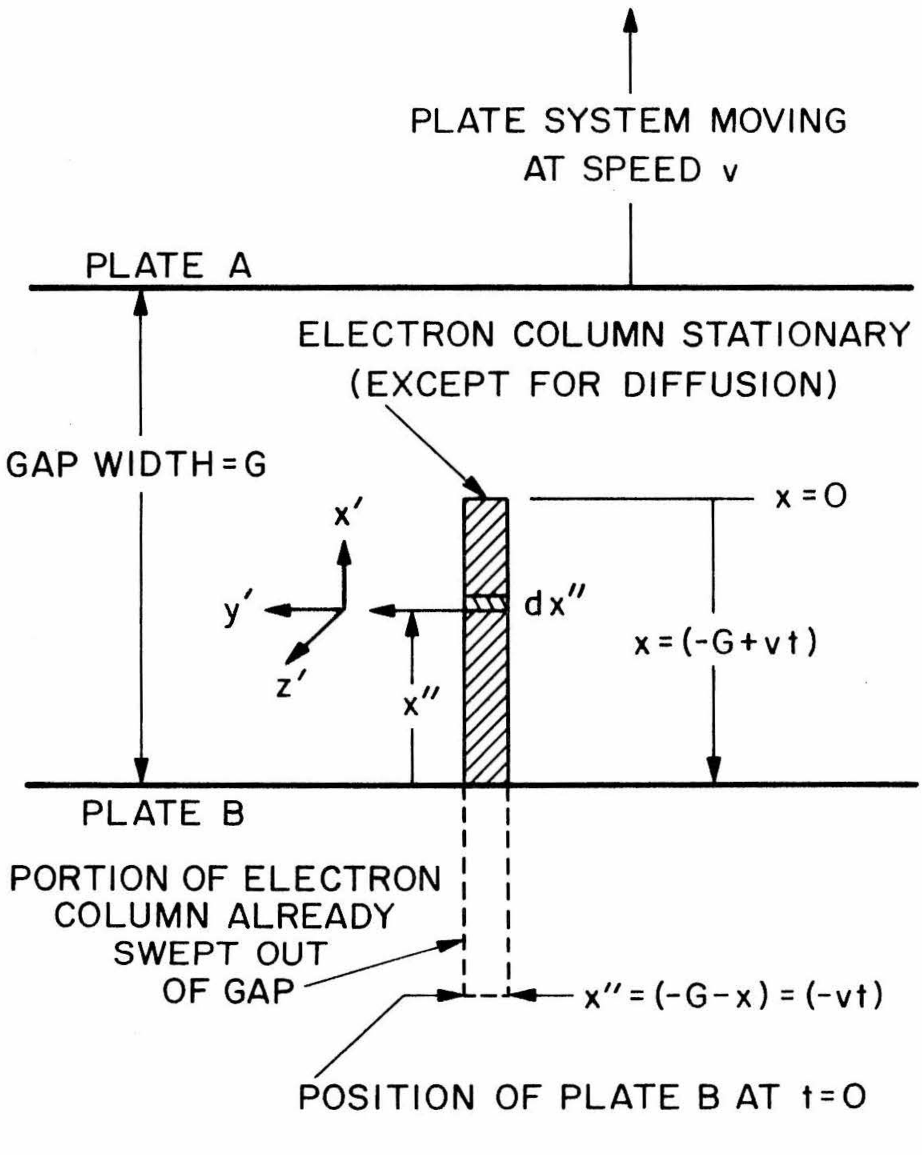

$$\int_{x/d}^{(x+G)/d} dz\ \tfrac{1}{2}\left[\mathrm{erfc}(z)-\mathrm{erfc}(z+G/d)\right] \cong \int_{x/d}^{+\infty} dz\ \tfrac{1}{2}\ \mathrm{erfc}(z) \qquad (C-5)$$

Then, with $u = -x''/d$ and $q = x'/d$, we find that

$$w(t) \cong m\,\frac{d}{\sqrt{\pi}} \int_{x/d}^{+\infty} du \int_{u}^{+\infty} dq\ e^{-q^2} \qquad (C-6)$$

$$= \tfrac{1}{2}\ m\ d \int_{x/d}^{+\infty} du \left[1-\mathrm{erf}(u)\right] \qquad (C-7)$$

$$= m\ d(t)\ \phi(t) \qquad (C-8)$$

where

$$\phi(t) = \int_{x/d}^{+\infty} du\ \tfrac{1}{2}\ \mathrm{erfc}(u) \qquad (C-9)$$

To relate D to the other parameters, we now assume that 1) the electrons in the column are in thermal equilibrium with the gas molecules (Maxwellian distribution), and that 2) v is much smaller than the thermal velocity expected for the electrons. These assumptions should be well satisfied: for example, v is on the order of 10^5 cm/sec while the thermal velocity is about 10^7 cm/sec.

Under these circumstances, for constant mobility $v/(V/G)$,

$$D = (kT/e)\cdot\text{mobility} = (kT/e)\cdot(vG/V) \qquad \text{(C-10)}$$

Thus,

$$d(t) = 2\cdot(kTvG/Ve)^{\frac{1}{2}}\, t^{\frac{1}{2}} \qquad \text{(C-11)}$$

The efficiency of the gap at time t is therefore given by equations (C-1) and (C-2) using equations (C-8), (C-9), and (C-11).

$$\text{Efficiency}_N(t) = \left\{ 1 - \sum_{i=0}^{N-1} \frac{(m\cdot d(t)\cdot\phi(t))^i}{(i)!}\, e^{-[m\cdot d(t)\cdot\phi(t)]} \right\} \qquad \text{(C-12)}$$

3. Poisson Theory + Delta Rays

For this discussion, a delta ray is defined to be an electron liberated by ionization in an energy-loss interaction in which a particle loses an energy between E_{min} and E_{max}. E_{min} is an energy much larger than the average ionization potential of the gas atoms considered (200 to 10,000 eV).[37] E_{max} is the maximum energy which the particle can transfer to an electron. For a cosmic-ray muon, with $(v/c)^2 \cong 0.9$, E_{max} is approximately 9.2 MeV.[38] Energy losses smaller than E_{min} will be said to be part of the particle's continuous energy-loss spectrum, as opposed to the discrete spectrum which delta rays afford.[37]

The assumptions made for the Poisson Theory will also be made here. That is, erfc(vt/d) is assumed to be small enough so that the integral limits (G-x") and (G+x) are essentially infinite. The electrons liberated by ionization along the path of a particle are assumed to be in thermal equilibrium. Their drift velocity is assumed to be much smaller than their thermal velocity so that Einstein's relation can be used: D=kTvG/Ve. Lateral diffusion in the electron column is ignored. We assume that a spark will occur in a gap when it is pulsed if it contains N or more electrons. In short, the Poisson Theory is assumed to apply except for its neglect of delta rays.

In addition to these assumptions, we also assume the following. We assume that a delta ray loses energy only through ionization of the gas (e.g., radiation processed are ignored).

For delta-ray energies much less than $E_{max} = 9.2$ MeV, this approximation should be good to much better than 15%.[38]

The electrons liberated through ionization of the gas atoms by a delta ray as it stops are assumed to lie close enough to the primary particle's continuous-ionization column, as far as spark formation is concerned, to be essentially a part of this column. A 9.2-MeV electron, however, can have a path length of about 5 g/cm^2 (i.e. a few tens of meters in argon, a few hundreds of meters in helium).[42] One therefore does not expect the ionization from the most energetic delta rays to lie physically within the column even if straggling is considered. Nevertheless, these delta rays occur rather infrequently, so no serious errors are expected to be introduced.

We assume that the number of electron-ion pairs formed per unit energy loss of a delta ray is independent of the energies of the delta ray and the particle which produced the delta ray.[37-38] We also assume that the cross section for the production of delta rays is correctly given by the Bethe formula. Delta rays yielding fewer than N electrons, where N is the number required to cause spark formation, will be ignored. Furthermore, we assume that a primary particle can not produce more than one delta ray between x and x+dx.

We now turn to the mathematical details. The notation adopted is given in table 12. The coordinate system used to treat

TABLE 12: NOTATION FOR POISSON THEORY + DELTA RAYS

Symbols	Explanation
A	atomic weight for the gas in the gap
β	ratio of the speed of a delta ray to the speed of light
c	speed of light
D	diffusion coefficient for the electrons in the gas
E	energy lost by a particle in going from x to x+dx
E_{min}	minimum energy which a particle is assumed to lose in one "collision" ($E_{min} >> I$)
E_{max}	maximum energy which a particle can lose in a "collison" with an electron
e	electronic charge
G	gap spacing
I	average ionization potential for the gas in the gap
k	Boltzmann constant
m	rest mass of an electron
N	number of electrons required (on the average) in a gap with spacing G to cause spark formation when a given pulsing field is applied
N_o	Avogadro's number
n	total number of electron-ion pairs formed by a delta ray before it stops
r_o	classical electron radius
V	applied sweeping voltage
v	drift velocity of electrons in the gas considered, for sweeping field V/G
Z	atomic number for the gas in the gap

TABLE 12: (Continued)

Probability Function		Explanation
$X(E)dEdx$	=	the probability that in going dx a particle will suffer one collision in which it loses an energy between E and E+dE
$Q(n)dx$	=	the probability that in going dx a particle will suffer one collision in which it produces one delta-ray which produces n electron-ion pairs before it stops
$R(t,x')$	=	the probability that an electron will diffuse so that it lies between x' and x'+dx' at time t when it was at x'=0 at t=0
$P_i(N)$	=	the probability that in going a distance G a particle will suffer one collision in which it produces one and only one delta-ray and this yields i electrons before stopping of which N diffuse so as to remain in the same gap G under the influence of a sweeping field V/G
$P(t,N)$	=	the probability that at time t after the passage of a particle through a gap G having sweeping field V/G there remain exactly N electrons in the gap due to the ionizations from delta rays
$P_M(t,N)$	=	P(t,N) when exactly M delta rays were produced in the gap
$C(t,N)$	=	the probability that at time t after the passage of a particle through a gap G having sweeping field V/G there remain exactly N electrons in the gap due to the primary particle's continuous ionization (see equations C-1 and C-8)
$E(t,N)$	=	the probability that at time t after the passage of a particle through a gap G having sweeping field V/G there remain exactly N electrons in the gap due to all contributing processes

the continuous-ionization column is that given in figure 54 (i.e. the same coordinate system as used in the Poisson Theory).

For mesons or protons with kinetic energies between 1 MeV and 1 BeV, Symon gives the following collision spectrum:[37]

$$X(E)\,dEdx = \begin{cases} 0 & \text{for } E > E_{max} \\ \dfrac{F}{\beta^2}\,\dfrac{dEdx}{E^2}\,(1-\beta^2 E/E_{max}) & \text{for } E_{min} < E < E_{max} \end{cases} \tag{C-13}$$

where $F = 2mc^2\pi r_o^2 N_o Z/A\cdot$(gas density). For an ideal gas at temperature T (degrees Kelvin) and pressure P (atmospheres), $F = (6.24)Z(300/T)(P)$ eV/cm.

For a delta ray of energy $E = nI$, assuming that n is much larger than one, the continuous collision spectrum above can be transformed to the discrete spectrum

$$Q(n) = \begin{cases} 0 & \text{for } n > (E_{max}/I) \\ \dfrac{F}{n^2\beta^2 I}\,(1-\beta^2 nI/E_{max}) & \text{for } (E_{min}/I) < n < (E_{max}/I) \end{cases} \tag{C-14}$$

Diffusion is treated just as in the Poisson Theory. That is,

$$R(t,x')\,dx' = \frac{1}{d\sqrt{\pi}}\exp(-x'^2/d^2)\,dx' \tag{C-15}$$

where

$$d = (4Dt)^{\frac{1}{2}} \tag{C-16}$$

$$D = (kTvG/Ve) \tag{C-17}$$

$$\int_{-\infty}^{+\infty} dx' \; R(t,x') = 1 \tag{C-18}$$

Using the coordinate system of figure 54, one can see that the probability of finding an electron in the gap at time t when it was produced between x'' and x''+dx'' at time t=0 is

$$S = \int_{-x''}^{G-x''} dx' \; R(t,x') \tag{C-19}$$

If i electrons had been produced between x'' and x''+dx'', the probability of finding exactly N electrons in the gap at time t is

$$B(i,N) = \frac{i!}{N!\,(i-N)!} S^N (1-S)^{i-N} \qquad N \leqslant i \tag{C-20}$$

The probability distribution is binomial because the motion of each electron is assumed independent, and each electron is either in the gap or not.

The probability of producing exactly one delta ray in the gap and between x'' and x''+dx'' (and nowhere else), and this delta ray yields exactly i electrons through ionization is

$$W_i dx'' = T_1 \cdot T_2 \cdot Q(i)\, dx'' \tag{C-21}$$

where $Q(i)dx''$ is the probability of getting one delta ray in dx'' which yields i electrons, T_1 is the probability of not getting any delta rays elsewhere in the gap which yield i electrons, and T_2 is the probability of not getting any delta rays anywhere in the gap which yield $j \neq i$ electrons. Because we have assumed that each dx either has one delta ray or none, we get

$$T_1 = \prod_{\substack{\text{All } dx_j \text{ in} \\ G \text{ except } dx''}} (1 - Q(i)\, dx_j) \tag{C-22}$$

$$= \lim_{q \to \infty} (1 - Q(i) \cdot G/q)^q \Big/ (1 - Q(i)\, dx'') \tag{C-23}$$

$$= \exp(-G \cdot Q(i)) \Big/ (1 - Q(i)\, dx'') \tag{C-24}$$

$$\cong \left[\exp(-G \cdot Q(i))\right] (1 + Q(i)\, dx'') \tag{C-25}$$

$$\Gamma_2 = \prod_{\substack{k \neq i \\ k=N_{min}}}^{N_{max}} \exp(-G \cdot Q(k)) \tag{C-26}$$

$$= \exp\left\{ - G \cdot \sum_{\substack{k \neq i \\ k=N_{min}}}^{N_{max}} Q(k) \right\} \tag{C-27}$$

where N_{min} and N_{max} are defined to be the nearest integers to E_{min}/I and E_{max}/I, respectively. Thus

$$W_i dx'' \cong Q(i)\, dx'' \cdot (1+Q(i)\, dx'') \cdot \exp(-G \cdot y) \tag{C-28}$$

$$\cong Q(i)\, dx'' \cdot \exp(-G \cdot y) \tag{C-29}$$

where

$$y = \sum_{k=N_{min}}^{N_{max}} Q(k) = \int_{E_{min}}^{E_{max}} dE\ X(E) \tag{C-30}$$

Thus we note that, to order dx'', $W_i dx''$ is the product of the probability of getting one delta ray in dx'' which yields i electrons and the probability of getting no delta rays anywhere in the gap.

Combining equations (C-20) and (C-29), we see that the probability of getting exactly one delta ray in the gap G and between x" and x"+dx" (and nowhere else), and this delta ray yields i electrons of which exactly N diffuse so as to remain in the gap at time t is $W_i B(i,N)\,dx''$. This is integrated over x" to get

$$P_i(N) = W_i \int_{-G-x}^{-x} dx''\, B(i,N) \qquad \text{(C-31)}$$

and summed over i to get

$$P_1(t,N) = \sum_{\substack{i = \text{larger of} \\ N \text{ and } N_{min}}}^{N_{max}} W_i \int_{-G-x}^{-x} dx''\, B(i,N) \qquad \text{(C-32)}$$

We now assume erfc(vt/d) is close enough to zero so that (G-x") and (G+x) are essentially infinite. Using the same techniques as we did to get equation (C-7), we find that

$$\int_{-\infty}^{-x} dx''\, B(i,N) = \frac{d \cdot i!}{N!\,(i-N)!} \int_{x/d}^{+\infty} dz\, \left(\tfrac{1}{2}\mathrm{erfc}(z)\right)^N \left(1-\tfrac{1}{2}\mathrm{erfc}(z)\right)^{i-N} \qquad \text{(C-33)}$$

Combining equations (C-29), (C-30), (C-32) and (C-33), we get

$$P_1(t,N) = d \cdot P_o \cdot \sum_{\substack{i = \text{larger of} \\ N \text{ and } N_{min}}}^{N_{max}} r_{Ni} \cdot \phi_{Ni}(x/d) \qquad \text{(C-34)}$$

where

$$r_{Ni} = \frac{i!}{N!\,(i-N)!}\, Q(i) \qquad \text{(C-35)}$$

$$\phi_{Ni}(Z) = \int_Z^{+\infty} du\, \left(\tfrac{1}{2}\mathrm{erfc}(u)\right)^N \left(1-\tfrac{1}{2}\mathrm{erfc}(u)\right)^{i-N} \qquad \text{(C-36)}$$

P_o is the probability of getting no delta rays in the gap:

$$P_o = \exp\left[- G \cdot \int_{E_{min}}^{E_{max}} dE\, X(E) \right] \qquad \text{(C-37)}$$

Moreover,

$$P_2(t,N) = \sum_{j=0}^{N} P_1(t,j)\; P_1(t,N-j) \tag{C-38}$$

$$P_3(t,N) = \sum_{i,j=0}^{N} P_1(t,i)\; P_1(t,j)\; P_1(t,N-i-j) \tag{C-39}$$

et cetera. The probability of having N electrons in the gap at time t due to all delta-ray ionizations is

$$P(t,N) = \sum_{i=1}^{\infty} P_i(t,N) \tag{C-40}$$

If the collision spectrum is integrated from E_{min} to E_{max}, and one considers a cosmic-ray muon, one finds that the probability of getting a delta ray per centimeter is approximately $6.9Z/E_{min}$. One expects E_{min} to be larger than about 200 eV (and perhaps as large as 10^4 eV),[37] so the probability of having a delta ray produced in a one-centimeter gap is no larger than approximately 60% for pure argon and 7% in pure helium. In practice, we may therefore approximate $P(t,N)$ as merely $P_1(t,N)$.

Because the continuous and delta-ray ionizations are assumed to be independent, the total probability of having N electrons in the gap at time t is

$$E(t,N) \quad = \quad P_o \cdot C(t,N) + \sum_{j=0}^{N} C(t,j) \cdot P(t,N-j) \qquad \text{(C-41)}$$

where C(t,N) is given by equations (C-1), (C-8), (C-9), and (C-11). The sparking efficiency for the gap is thus

$$\text{Efficiency}_N(t) \quad = \quad 1 - \sum_{j=0}^{N-1} E(t,j) \qquad \text{(C-42)}$$

$$= \quad 1 - P_o \sum_{j=0}^{N-1} C(t,j) \; - \; \sum_{j=0}^{N-1} \sum_{i=0}^{j} C(t,i) \cdot P(t,j-i) \qquad \text{(C-43)}$$

$$= \quad 1 - P_o \sum_{j=0}^{N-1} C(t,j) \; - \; \sum_{i=0}^{N-1} \left\{ C(t,i) \cdot \sum_{j=0}^{N-1-i} P(t,j) \right\} \qquad \text{(C-44)}$$

4. Poisson Theory + Metastables

We now ignore delta rays, and consider another modification of the Poisson Theory. The notation used here is the same as that used in section 2.

We assume that at t=0, when a charged particle traverses the gap, there are H_o atoms in the gas which are left in metastable states.* The number of these states is assumed to decrease exponentially with time (e.g. because of de-excitation through thermal collisions).[47-49] The number of atoms in metastable states at time t will be represented by

$$H(t) = H_o e^{-t/\tau} \tag{C-45}$$

We further assume that an electron can be liberated somewhere in the gap as a result of the de-excitation of an atom in a metastable state, and that the probability for this happening is R_o. The collisional de-excitation of metastable states thus acts as a source of free electrons. These electrons, which are in addition to those produced by the primary particle, are assumed to be randomly distributed along the original path of ionization in the gap.† The electrons liberated in this fashion during a very small increment in time will be assumed to form a "column" of electrons which behaves

*Argon and helium, to be sure, do have metastable states (see references 47-49).

†Just as in the delta-ray case, the electrons liberated are assumed to lie close enough to the continuous-ionization column so that spark formation will still occur, for all practical purposes, along the ionization path of the incident particle.

under the action of the sweeping field V/G (and diffusion) just as the column of continuous ionization treated for the Poisson Theory.

For example, the number of electrons so created between t' and t'+dt', on the average, is

$$-R_o \cdot dH(t') \quad = \quad + \; (R_o H_o/\tau) \; e^{-t'/\tau} \; dt' \qquad \text{(C-46)}$$

These electrons act as a diffusing column swept towards one plate just as in the Poisson Theory, except the time scale is now (t-t'). That is, the number of these electrons remaining in the gap at time t is

$$- \; R_o \; dH(t') \; d(t-t') \; \phi(t-t') \qquad \text{(C-47)}$$

where d(t) is given by equation (C-11) and $\phi(t)$ is given by equation (C-9).

For simplicity, we approximate the combined influence of all such columns (i.e. for all t') by integrating the above expression for all t' up to t. The efficiency of the gap is then given by equations (C-1) and (C-2)

$$\text{Efficiency}_N(t) \quad = \left\{ 1 \; - \; \sum_{i=0}^{N-1} w(t)^i \; e^{-w(t)} \; / \; i! \right\} \qquad \text{(C-48)}$$

with

$$w(t) = \left\{ m\ d(t)\ \emptyset(t) + (R_o H_o/\tau) \int_0^t dt'\ e^{-t'/\tau}\ d(t-t')\ \emptyset(t-t') \right\} \quad \text{(C-49)}$$

5. Poisson Theory + Constant Probability

The last model considers the simple modification of the Poisson Theory which is required if there exists a constant probability J_o that one electron will always be present in the gap when it is pulsed.

In this case, the probability of getting N electrons in the gap at time t is

$$L(t,N) = \left[J_o \cdot C(t,N-1) + (1-J_o) \cdot C(t,N) \right] \tag{C-50}$$

where C(t,N) is given by equations (C-1), (C-8), (C-9), and (C-11). The gap efficiency is therefore

$$\text{Efficiency}_N(t) = \left\{ 1 - \sum_{j=0}^{N-1} L(t,j) \right\} \tag{C-51}$$

APPENDIX D:
THE MECHANISM OF SPARK BREAKDOWN IN PLANE-PARALLEL GAPS

No longer is the mechanism of spark breakdown in plane-parallel gaps believed to be the modified Townsend mechanism, the streamer mechanism, or a combination of the Townsend mechanism for pd $\lesssim$ 200 mm-Hg-cm and the streamer mechanism for larger pd.(78)* According to the view most widely accepted today, spark breakdown may begin with a multiple-avalanche or a single-avalanche mechanism, but it ultimately requires the formation of streamers.(79-86)

Which avalanche mechanism initiates the breakdown is not determined by the value of pd, but is determined by the percentage overvoltage (% o.v.) on the gap.(79)† For small % o.v.'s, a spark can be produced only after the formation of a low-order discharge, as in the Townsend theory, during which many 100's or perhaps 1,000's of avalanches must traverse the gap before streamers are able to form. With sufficiently large % o.v.'s, sparks develop (through streamers) directly from single avalanches, as in the streamer theory. For any % o.v., however, the formation of a narrow luminous spark is always preceded by the formation of streamers.(79-86)

---

*p is the gap pressure (mm Hg) and d is the gap width (cm).

†The overvoltage ($V-V_s$) is the voltage applied in excess of the sparking threshold V_s. The percentage overvoltage is then % o.v. = 100% $(V-V_s)/V_s$.

The streamer stage in the breakdown process is believed to be started by the onset of photoionization in the gas. This occurs when an electron avalanche has developed the necessary charge densities in its head to produce a sufficient number of photons through electron-ion recombination. The required charge densities are perhaps as large as 7×10^{11} cm^{-3}.[78-79] According to Raether,[78] the required densities correspond to a few times 10^8 electrons in the avalanche.[87]

The first electron avalanche, which develops from an initial ion pair formed in the gap by external means, is unable to reach the critical size if the % o.v. is too low. In this case, subsequent avalanches are required which develop from electrons produced near the cathode by Townsend secondary processes[78] (usually photoelectric emission at the cathode by photons produced in the preceding avalanche).[88-89] The accumulated positive space charge left behind by enough of these avalanches can sufficiently enhance the applied field to enable a following avalanche to reach critical size. The average number of avalanches required before one is able to transform into a streamer is apparently a function only of the type of gas used in the gap and the % o.v.; the parameter pd is important only in the determination of the sparking threshold V_s (see reference 78: Paschen's Law).[79]

At V_s and for small % o.v.'s, when 100's to 1,000's of avalanches must cross the gap, the breakdown begins with a diffuse low-order Townsend (e.g., glow) discharge[80-81,83,86,90-91] and the spark formative time* may be ten's of microseconds or longer.[79,92-93]≠ Such is the case for about a 2% overvoltage in air[94] and about a 100% overvoltage in argon.[95] The sequence of events in any one of these multiple-avalanche stages can be quite complicated; ionizing potential waves may sweep back and forth across the gap to establish the glow stage.[96] Spark development nears completion, however, only when an avalanche with a sufficient charge density is able to transform into a streamer by initiating the necessary photoionization in the gas.[79-86]

If the % o.v. is increased enough, only one avalanche is required because the adequate charge density is developed in the head of this first avalanche as it reaches the anode. In such a case, a cathode-directed streamer is formed[97] and the formative time reduces to the order of magnitude of the transit time of the electrons across the gap.[79,92-93,98] Further increase in the % o.v. causes the formation of mid-gap streamers[97] and allows formative times to be as low as 10 to 100 nanoseconds.[98]**

---

*The formative time is the time needed for the spark to form after a source of initial ion pairs has been provided at the cathode.

≠This discussion of course assumes that the gap voltage V is always applied for a time longer than the formative time.

**Such is usually the case for spark formation in spark-chamber gaps, where the % o.v. must be large enough to cause spark formation before the end of the (e.g. 100-nanosecond) applied voltage pulse.

The above description is of course a somewhat simplified picture of spark breakdown. For example, there are complications because of attachment processes (e.g. in air[99]) and because of the effects of resonance radiation and metastable states (e.g. for argon-neon mixtures).[51,89,95,98,100-101] Moreover, recent image-intensifier and streak-photographic studies have illustrated that the development of a spark can involve a very complex sequence of processes subject to large statistical fluctuations.[86,91,102] Other studies have shown that the post-streamer stages of spark development are not well understood.[86,103-106] Furthermore, that the transition from multiple-avalanche to single-avalanche breakdown depends only on the type of gas used and on the % o.v. has not yet been proved conclusively. More experimental and theoretical work is therefore needed before the understanding of spark breakdown will be complete.

APPENDIX E: CROSS SECTION FORMULAS, PARAMETER VALUES, AND $(-t)_{min}$

In this appendix, we outline the derivation of the formulas used in computing cross sections for the lowest-threshold diagrams involved in quark production (Chapter VII, section B, figure 36, diagrams D). We also list the values which were assumed for the various parameters and coupling constants. We then derive an expression for the minimum four-momentum transfer which is possible in a two-body process at a given $s = (\text{CM energy})^2$. This expression is helpful in estimating the minimum four-momentum transfer to a target nucleus in the interactions considered (Chapter VII, section D).

1. Cross Section Formulas

The differential cross section for the process $a+b \rightarrow 1+2+3$ (figure 55) can be expressed in terms of many different sets of variables. One set, however, is particularly useful in obtaining the total cross section. When this set is used, only two of the integrations over phase space must be done numerically. All of the other integrations can be performed analytically if the form of the amplitude is at least as simple as the one which we shall consider.

FIGURE 55: DIAGRAM FOR 3-BODY PRODUCTION SHOWING RELEVANT SCALERS

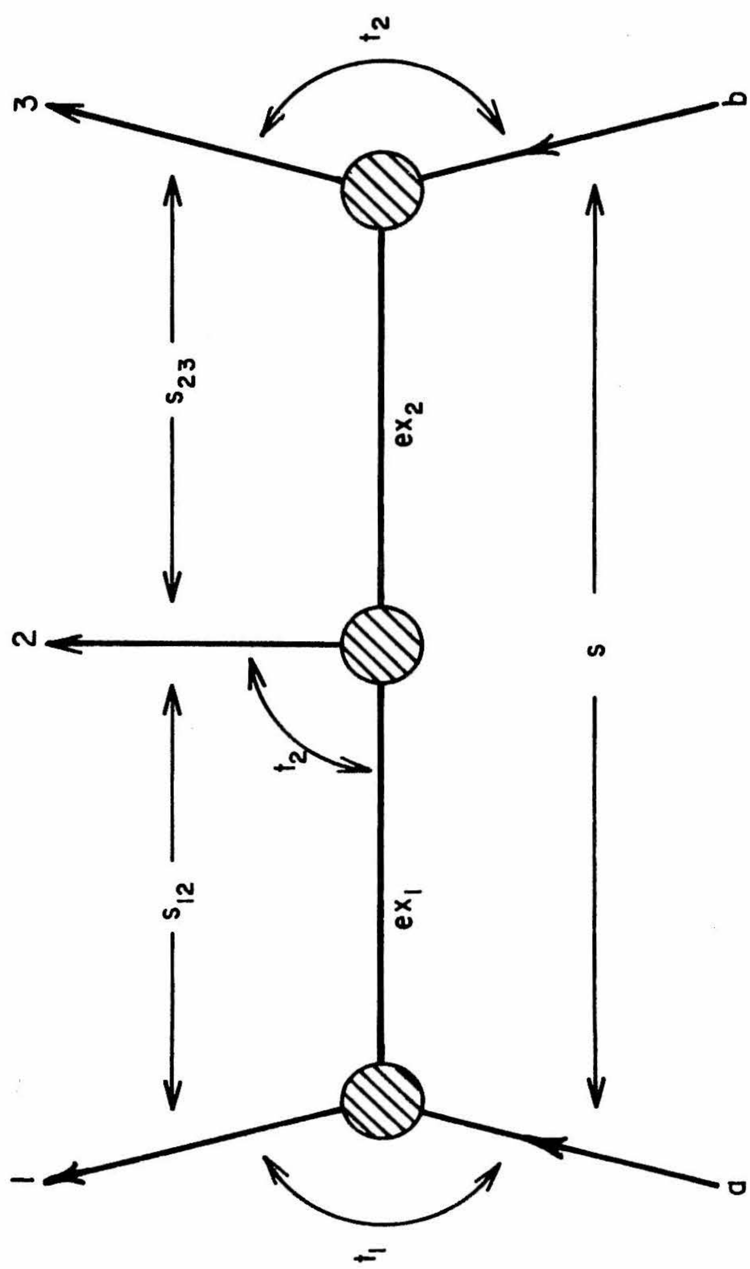

We use the following notation:

$\vec{p}_k$ = $(E_k, \bar{p}_k)$ = four-momentum of particle k; (p_k = $|\bar{p}_k|$)

m_k = mass of particle k

s_{ij} = $(\vec{p}_i+\vec{p}_j)^2$, the square of the invariant mass of pair ij

s = $(\vec{p}_a+\vec{p}_b)^2$

t_k = $(\vec{p}_1+\vec{p}_2+\ldots+\vec{p}_k-\vec{p}_a)^2$, a four-momentum transfer

$\rho_{invariant}$ = density of states in phase space (a Lorentz scaler)

M_F = Feynman amplitude

a_i = a four-momentum transfer damping coefficient

w = a Toller variable[76]

$f_1(t_1)$, $g_2(t_1,w,t_2)$, $f_3(t_2)$ = couplings at the vertices indicated by the subscripts on f and g

f_1, g_2, f_3 = coupling constants at $t_1=t_2=0$

$\lambda(r,u,v)$ = $r^2+u^2+v^2-2ru-2rv-2uv$

$\beta(t_1,t_2)$ = residue factors (other than those given as couplings)

$S(t_1,t_2)$ = signature factors

$\alpha_i(t_i)$ = Regge trajectory for the i^{th} Reggeon

s_o = a scaling factor for s_{ij}

x = the cosine of the angle between $\bar{p}_1$ and $\bar{p}_a$ in the CM frame of particles a and b

y = the negative of the cosine of the angle between $\bar{p}_3$ and $\bar{p}_b$ in the CM frame of particles a and b

z = the cosine of the angle between $\bar{p}_1$ and $\bar{p}_3$ in the CM frame of particles a and b

$\emptyset(q)$ = 1 for $q \geq 0$, 0 for $q < 0$.

We use natural units ($\hbar=c=1$).

In a frame in which the three-momenta of particles a and b are parallel, the differential cross section is

$$d\sigma = \frac{\rho_{\text{invariant}} \cdot \left| M_F \right|^2}{2\,(\,\lambda(s, m_a{}^2, m_b{}^2)\,)^{\frac{1}{2}}} \tag{E-1}$$

where

$$\rho_{\text{invariant}} = \frac{1}{(2\pi)^5}\ \delta^4(\vec{p}_a+\vec{p}_b-\vec{p}_1-\vec{p}_2-\vec{p}_3)\ \frac{d^3\bar{p}_1}{2E_1}\,\frac{d^3\bar{p}_2}{2E_2}\,\frac{d^3\bar{p}_3}{2E_3} \tag{E-2}$$

and

$$d^3\bar{p}_i = p_i\ E_i\ dE_i\ d(\cos\theta_i)\ d\phi_i \tag{E-3}$$

Integrating over $\bar{p}_2$, one finds that

$$\rho_{\text{invariant}} = \frac{1}{8(2\pi)^5 E_2}\ \delta(E_a+E_b-E_1-E_2-E_3)\ p_1 p_3 dE_1\ dE_3\ d(\cos\theta_1)\ d\phi_1\ d(\cos\theta_3)\ d\phi_3 \tag{E-4}$$

In the center-of-mass frame of particles a and b, in a coordinate system with the z-axis along $\bar{p}_a$ with $\phi_1=0$,

$$\delta(E_a+E_b-E_1-E_2-E_3)$$

$$= \delta\left[s^{\frac{1}{2}}-E_1-E_3-\sqrt{m_2^{\,2}+p_1^{\,2}+p_3^{\,2}+2p_1p_3(\cos\theta_1\cos\theta_3+\sin\theta_1\sin\theta_3\cos\phi_3)}\right] \tag{E-5}$$

Noting that the argument of the delta function has two roots as a function of ϕ_3 for ϕ_3 between 0 and 2π, one can integrate over ϕ_3 to obtain

$$\rho_{\text{invariant}} =$$

$$\frac{1}{4(2\pi)^5}\;\frac{dE_1\;dE_3\;d(\cos\theta_1)\;d\phi_1\;d(\cos\theta_3)}{|\sin\theta_1\;\sin\theta_3\;\sin\phi_3|}\;\phi(\,1-|\sin\phi_3|\,) \tag{E-6}$$

Integrating over the azimuthal freedom of $\bar{p}_1$, and using the following relations

$$E_1 = (s+m_1^{\,2}-s_{23})\;/\;(2s^{\frac{1}{2}})$$

$$E_3 = (s+m_3^{\,2}-s_{12})\;/\;(2s^{\frac{1}{2}}) \tag{E-7}$$

one obtains

$$d\sigma(s) = \frac{1}{2(4\pi)^4}\;\frac{|M_F|^2}{s\;(\;\lambda(s,m_a^{\,2},m_b^{\,2})\;)^{\frac{1}{2}}}\;\frac{ds_{12}\;ds_{23}\;dx\;dy\;\phi(W)}{W^{\frac{1}{2}}} \tag{E-8}$$

where

$$W = 1-x^2-y^2-z^2+2xyz \tag{E-9}$$

and x, y, and z are the cosines defined in the paragraph on notation.

We shall consider a multi-peripheral amplitude which can be factored into two-body-like amplitudes each of which can be Reggeized:[(69)]

$$M_F = f_1(t_1)\ g_2(t_1,w,t_2)\ f_3(t_2)\ \beta(t_1,t_2)\ S(t_1,t_2)$$

$$\cdot\ \frac{(s_{12}/s_o)^{\alpha_1(t_1)}}{\sin\left[\pi\,\alpha_1(t_1)\right]}\ \cdot\ \frac{(s_{23}/s_o)^{\alpha_2(t_2)}}{\sin\left[\pi\,\alpha_2(t_2)\right]} \tag{E-10}$$

We have chosen the crossed-channel cosines to be just s_{ij}/s_o for simplicity. This choice avoids the difficulties associated with the introduction of daughter trajectories,[(107)] and allows a total cross section to be obtained after just two rather than four numerical integrations. The signature factors are

$$S(t_1,t_2) = (1\pm e^{-i\pi\alpha_1(t_1)})/2 \cdot (1\pm e^{-i\pi\alpha_2(t_2)})/2 \tag{E-11}$$

where the plus signs are for positive signature and the minus signs are for negative signature. All trajectories are assumed to be linear:

$$\alpha_i(t_i) = \alpha_i + \alpha_i'\ t_i \tag{E-12}$$

To accommodate the multi-peripheral character, the vertex couplings are assumed to be

$$\left.\begin{aligned} f_1(t_1) &= f_1\, e^{b_1 t_1} \\ g_2(t_1,w,t_2) &= g_2\, e^{d_1 t_1 + d_2 t_2} \\ f_3(t_2) &= f_3\, e^{b_2 t_2} \end{aligned}\right\} \qquad \text{(E-13)}$$

Note that we have assumed $g_2(t_1,w,t_2)$ to be independent of w.* We now choose

$$a_i = b_i + d_i \qquad \text{(E-14)}$$

The vertex couplings thus contribute the factors $e^{a_1 t_1}$ and $e^{a_2 t_2}$. For simplicity, all other factors depending on t_1 and t_2, except the $(s_{ij}/s_o)^{\alpha_i(t_i)}$, are assumed to vary so slowly in comparison to $\exp(a_1 t_1 + a_2 t_2)$ that they are essentially constant. For example, kinematic singularities in the residues are ignored, and the quotient of the signature factors and the trigonometric factors is assumed to

---

*This has been found to be true for at least one case.(73) Moreover, Chung-I Tan and Jiunn-Ming Wang, in a Princeton preprint (Caltech 69-607) "The w-dependence of Internal Regge Coupling," prove that any Reggeon-Reggeon-particle coupling $g(t_1,w,t_2)$ is independent of w when either or both of t_1 and t_2 vanish. The above assumption is therefore consistent with the use of multi-peripheral amplitudes.

be constant. For the normalization chosen for the coupling constants, we assume that the overall magnitude of the residue, signature, and trigonometric factors is unity.

The amplitude considered is therefore of the form

$$M_F = f_1 \, g_2 \, f_3 \; e^{a_1 t_1} \, e^{a_2 t_2} \; (s_{12}/s_o)^{\alpha_1(t_1)} \; (s_{23}/s_o)^{\alpha_2(t_2)} \tag{E-15}$$

Note that f_1, g_2, and f_3 are the couplings at $t_1 = t_2 = 0$ (f_1 and f_3 are dimensionless, g_2 has the dimensions of $1/s^{1/2}$). With the above amplitude, the differential cross section becomes

$$d\sigma(s) = \tag{E-16}$$

$$\left\{ \frac{2(2\pi)^2 \, (f_1/4\pi)^2 (g_2/4\pi)^2 (f_3/4\pi)^2}{s \, \left(\lambda(s, m_a^2, m_b^2) \right)^{\frac{1}{2}}} \, (s_{12}/s_o)^{2\alpha_1} \, (s_{23}/s_o)^{2\alpha_2} \cdot I \, ds_{12} \, ds_{23} \right\}$$

where

$$I = \int_{-1}^{+1} dy \int_{-1}^{+1} dx \, \exp\left[2\,\Omega_1 t_1 + 2\,\Omega_2 t_2 \right] \cdot \frac{\phi(W)}{W^{\frac{1}{2}}} \qquad \text{(E-17)}$$

$$\Omega_i = a_i + \alpha_i' \ln(s_{i,i+1} / s_o) \qquad \text{(E-18)}$$

We now use equations (E-7) and the following

$$\begin{aligned} p_1 &= \left(\lambda(s, m_1^2, s_{23}) \right)^{\frac{1}{2}} / (2s^{\frac{1}{2}}) \\ p_3 &= \left(\lambda(s, m_3^2, s_{12}) \right)^{\frac{1}{2}} / (2s^{\frac{1}{2}}) \\ E_a &= (s+m_a^2-m_b^2) / (2s^{\frac{1}{2}}) \\ E_b &= (s+m_b^2-m_a^2) / (2s^{\frac{1}{2}}) \\ p_a &= p_b = \left(\lambda(s, m_a^2, m_b^2) \right)^{\frac{1}{2}} / (2s^{\frac{1}{2}}) \end{aligned} \qquad \text{(E-19)}$$

$$\begin{aligned} t_1 &= (\vec{p}_1-\vec{p}_a)^2 = m_1^2+m_a^2-2(E_1E_a-p_1p_ax) \\ t_2 &= (\vec{p}_3-\vec{p}_b)^2 = m_3^2+m_b^2-2(E_3E_b+p_3p_by) \end{aligned} \qquad \text{(E-20)}$$

and define

$$\begin{aligned} \Delta_1 &= 4\,\Omega_1\, p_1 p_a \\ \Delta_2 &= 4\,\Omega_2\, p_3 p_b \end{aligned} \qquad \text{(E-21)}$$

Then

$$I = \exp\left[2\,\Omega_1 (m_1{}^2+m_a{}^2-2E_1E_a)+2\,\Omega_2 (m_3{}^2+m_b{}^2-2E_3E_b)\right] \cdot J \qquad \text{(E-22)}$$

where

$$J = \int_{-1}^{+1} dy \int_{-1}^{+1} dx\; e^{\Delta_1 x - \Delta_2 y} \left[\frac{\phi(W)}{(W)^{\frac{1}{2}}}\right] \qquad \text{(E-23)}$$

Noting that the theta function restricts x to values between $yz \pm (y^2z^2-y^2-z^2+1)^{\frac{1}{2}}$, one can change the variable of integration

$$x = (1-z^2)^{\frac{1}{2}} \cdot (1-y^2)^{\frac{1}{2}} \cdot \cos u + yz \qquad \text{(E-24)}$$

and obtain

$$J = \tfrac{1}{2} \int_{-1}^{+1} dy\; e^{\Delta_1 yz - \Delta_2 y} \int_{0}^{2\pi} du\; e^{\Delta_1 \cdot (1-z^2)^{\frac{1}{2}} \cdot (1-y^2)^{\frac{1}{2}} \cdot \cos u} \qquad \text{(E-25)}$$

The integrations in (E-25) may be performed very easily if one defines the vectors

$$\overline{\Delta} = [\ \Delta_1 \cdot (1-z^2)^{\frac{1}{2}},\ 0\ ,\ \Delta_1 z - \Delta_2\ ] \qquad \text{(E-26)}$$

$$\hat{r} = [\ \sin\zeta \cdot \cos u,\ \sin\zeta \cdot \sin u,\ \cos\zeta\ ] \qquad \text{(E-27)}$$

as if using spherical coordinates. J is then an integral over the solid-angle increment (dy du), where y = cos ζ , so in the coordinate system where $\overline{\Delta}$ is parallel to the z-axis,

$$J = \tfrac{1}{2}(2\pi) \int_{-1}^{+1} d(\cos\theta)\, e^{\Delta \cdot \cos\theta} \tag{E-28}$$

$$= 2\pi \left[\sinh\Delta \;/\; \Delta \right] \tag{E-29}$$

where Δ is the length of $\overline{\Delta}$.

$$\Delta = (\Delta_1^2 + \Delta_2^2 - 2 \cdot \Delta_1 \cdot \Delta_2 \cdot z)^{\frac{1}{2}} \tag{E-30}$$

Collecting the results and doing some algebra, we obtain a form for the differential cross section in which all but two of the integrations have been performed analytically:*

$$d\sigma(s) = \frac{2(2\pi)^3(\hbar c)^2}{\lambda(s, m_a^2, m_b^2)} \left[\frac{f_1}{4\pi}\right]^2 \cdot \left[\frac{g_2}{4\pi}\right]^2 \cdot \left[\frac{f_3}{4\pi}\right]^2 \cdot \left[\frac{s_{12}}{s_o}\right]^{2\alpha_1} \cdot \left[\frac{s_{23}}{s_o}\right]^{2\alpha_2}$$

$$\cdot \left[\frac{\sinh\Delta}{Q_o}\right] e^{H_1+H_2} \cdot ds_{12}\, ds_{23} \tag{E-31}$$

---

*This result is consistent with a similar result obtained by Chan, Kajantie, and Ranft (reference 108).

where

$$Q_o = \Big[\Omega_1^{\,2} \cdot \lambda(s, m_1^{\,2}, s_{23}) + \Omega_2^{\,2} \cdot \lambda(s, m_3^{\,2}, s_{12}) \tag{E-32}$$

$$+ 2\,\Omega_1\,\Omega_2\,\{ s(s - m_3^{\,2} - m_1^{\,2} + 2m_2^{\,2} - s_{12} - s_{23}) - (s_{12} - m_3^{\,2})(s_{23} - m_1^{\,2}) \} \Big]^{\frac{1}{2}}$$

$$\Delta = Q_o\ (\lambda(s, m_a^{\,2}, m_b^{\,2}))^{\frac{1}{2}} / s \tag{E-33}$$

$$H_1 = \Omega_1\ \{ s_{23} - s + m_1^{\,2} + m_a^{\,2} + m_b^{\,2} + (s_{23} - m_1^{\,2})(m_a^{\,2} - m_b^{\,2})/s \} \tag{E-34}$$

$$H_2 = \Omega_2\ \{ s_{12} - s + m_3^{\,2} + m_a^{\,2} + m_b^{\,2} + (s_{12} - m_3^{\,2})(m_b^{\,2} - m_a^{\,2})/s \} \tag{E-35}$$

$$(\hbar c)^2 = 0.390 \text{ mb-BeV}^2 \tag{E-36}$$

The limits of integration for s_{12} can be found by keeping z physical, or more simply, from

$$s_{12} = \left[m_1^{\,2} + m_2^{\,2} + 2E_1E_2 \pm 2p_1p_2 \right] \tag{E-37}$$

where the E's and p's are expressed in the frame in which $\bar{p}_2 + \bar{p}_3 = 0$:

$$E_1 = (s - s_{23} - m_1^{\,2}) \;/\; (2 s_{23}^{\,\frac{1}{2}})$$

$$E_2 = (s_{23} + m_2^{\,2} - m_3^{\,2}) \;/\; (2 s_{23}^{\,\frac{1}{2}})$$

$$\text{(E-38)}$$

$$p_1 = (\,\lambda(s, s_{23}, m_1^{\,2})\,)^{\frac{1}{2}} \;/\; (2 s_{23}^{\,\frac{1}{2}})$$

$$p_2 = (\,\lambda(s_{23}, m_2^{\,2}, m_3^{\,2})\,)^{\frac{1}{2}} \;/\; (2 s_{23}^{\,\frac{1}{2}})$$

The limits of integration for s_{23} are then $(m_2+m_3)^2$ and $(s+m_1^{\,2}-2m_1 s^{\frac{1}{2}})$.

2. Parameter Values

The parameters whose values will be discussed here are the coupling constants, the Pomeranchuk trajectory and the four-momentum transfer damping coefficients a_i. Where possible, these parameters were chosen to be the same as those involved in two-body interactions. All character of the central vertex in figure 55 as being different from that of an external vertex was thereby essentially ignored. We tacitly assumed, for example, that $b_i = d_i = a/2$ in equation (E-14). Quark couplings were arbitrarily assumed to be of the same order as nucleon couplings. The four-momentum transfer damping coefficient corresponding to the quark trajectory was arbitrarily assumed to be of the same order as the coefficients corresponding to the trajectories of the known hadrons.

We first consider the coupling of two external nucleons to the Pomeranchuk trajectory. This coupling was chosen to be consistent with an asymptotic value of approximately 8.4 millibarns for high-energy proton-proton elastic scattering:[109]

$$(f_{NNPom}/4\pi)^2 = 2/3 \tag{E-39}$$

Because the nature of a coupling involving a quark is not yet known, the quark couplings which we shall consider can be determined only through assumption. What assumption should be made most likely depends on whether quarks are really fundamental constituents of mesons and baryons, or just heavy particles.

Consider the $\pi q\bar{q}$ coupling, for example. One could take the view that a π is sometimes a $\pi\rho$, less frequently a $p\bar{p}$, even less frequently an $N^*\overline{N^*}$, ... , and sometimes a $q\bar{q}$. The $\pi q\bar{q}$ coupling might then be an extrapolation of pion-baryon-antibaryon couplings, a quark being considered merely as a heavy particle.

Alternately, one might believe that the pion is actually a bound state of a quark and an antiquark. It is then plausible that the $\pi q\bar{q}$ coupling is larger than the $\pi p\bar{p}$ coupling, for $\pi \rightarrow q\bar{q}$ requires that the $q\bar{q}$ binding be overcome while $\pi \rightarrow p\bar{p}$ also requires the formation of two $q\bar{q}$ pairs (the proton being composed of 3 quarks).

To avoid a discussion of which of the above views is more plausible, quark couplings were assumed to be strong and of the same order as nucleon couplings. For example, the coupling of an external quark to the Pomeranchuk trajectory and an exchanged quark was chosen to be the same as that given in equation (E-39):

$$(g_{qqPom}/4\pi)^2 = 2/3 \tag{E-40}$$

Because a π^- is considered as being composed of one "antiproton-like" quark $\overline{P}_o$ and one "neutron-like" quark N_o, while a π^+ is considered as being composed of one $\overline{N}_o$ and one P_o (table 1), we shall assume that the coupling of a charged pion to an external quark and an exchanged quark is of the same order as the well-known antiproton-pion-neutron coupling:

$$(f_{\bar{p}\pi^- n})^2 / 4\pi = 14.45 \tag{E-41}$$

We choose simply

$$(f_{\pi qq}/4\pi)^2 = 1 \qquad \text{(E-42)}$$

The true nature of the Pomeranchuk trajectory is not yet understood. Experimental data are consistent with its intercept being within a couple hundredths of unity and its slope being less than 0.3 $(\mathrm{BeV}/c)^{-2}$. We choose the commonly used form

$$\alpha_{Pom}(t) = 1 \qquad \text{(E-43)}$$

The parameters a_i appearing in the factors $e^{2a_i t_i}$ in the differential cross sections were chosen to be consistent with present experimental data for two-body interactions. For example, letting $d\sigma/dt \sim e^{bt}$, one finds that b is between 8 and 11 for high-energy elastic pp, $\pi^- p$, $\bar{p}p$, and $K^- p$ interactions.[110] We therefore choose $2a_{Pom}$ to be simply 10:

$$a_{Pom} = 5.0\ (\mathrm{BeV}/c)^{-2} \qquad \text{(E-44)}$$

For pion or nucleon exchanges, however, b is generally found to be between about 4 and about 6. For example, in np charge exchange, b is approximately 4.6 (for $|t| > 0.03\ (\mathrm{BeV}/c)^{-2}$),[111] while in backward $\pi^- p$ charge exchange, b is approximately 4.4.[112] We therefore choose twice the coefficient associated with the quark trajectory to be of this order:

$$a_q = 2.5\ (\mathrm{BeV}/c)^{-2} \qquad \text{(E-45)}$$

3. Minimum Four-Momentum Transfer For A 2-Body Process

Using the notation of section E.1 (with $t_1=t$), we now derive an expression which gives the minimum four-momentum transfer, $(-t)_{min}$, which is allowed kinematically in a 2-body interaction (figure 56) at a given value of s.

By definition,

$$\begin{aligned} t &= (\vec{p}_1-\vec{p}_a)^2 \\ &= m_1^2 + m_a^2 - 2(E_1E_a - \bar{p}_1\bar{p}_a\text{Cos}\theta_{1a}) \end{aligned} \tag{E-46}$$

where θ_{1a} is the angle between $\bar{p}_1$ and $\bar{p}_a$. $(-t)_{min}$ is obtained from this merely by setting $\text{Cos}\theta_{1a}=1$.

Because t is a Lorentz scaler, it can be evaluated in any coordinate frame. We choose the CM frame of particles a and b (which is also the CM frame of particles 1 and 2). Then, using equations (E-19) and their counterparts obtained by replacing $a \rightarrow 1$ and $b \rightarrow 2$, we see that

$$\begin{aligned} (-t)_{min} = \Big[&-m_1^2-m_a^2+(s+m_1^2-m_2^2)(s+m_a^2-m_b^2)/2s \\ &- \sqrt{\lambda(s,m_1^2,m_2^2)\cdot\lambda(s,m_a^2,m_b^2)}/2s \Big] \end{aligned} \tag{E-47}$$

By expanding the square-root factor in decreasing powers of s and collecting terms, we find after some algebra that

FIGURE 56: DIAGRAM FOR 2-BODY PRODUCTION SHOWING RELEVANT SCALERS

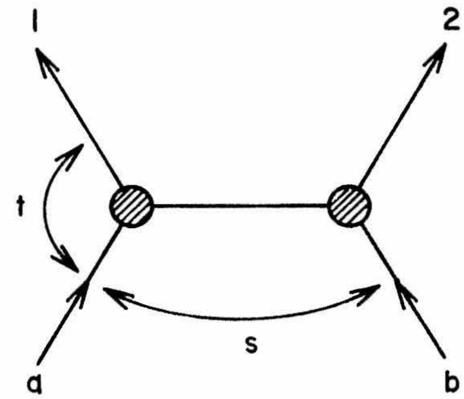

$$(-t)_{min} = \left[\frac{(m_a{}^2-m_1{}^2)(m_b{}^2-m_2{}^2)}{s}\right] + \left[\frac{(m_a{}^2m_b{}^2-m_1{}^2m_2{}^2)(m_a{}^2+m_b{}^2-m_1{}^2-m_2{}^2)}{s^2}\right] + 0\left[\frac{1}{s^3}\right] \tag{E-48}$$

Note that if $m_b=m_2=m$,

$$(-t)_{min} = \left[\frac{(m_1{}^2-m_a{}^2)\ m}{s}\right]^2 + 0\left[\frac{1}{s^3}\right] \tag{E-49}$$

APPENDIX F: THE DIFFUSION EQUATION FOR QUARKS AND ITS SOLUTION

To derive the diffusion equation for the propagation of quarks through the atmosphere, the following assumptions were made:

1) Each production process considered yields one quark (or one antiquark) in the forward direction.

2) Quarks do not decay; that is, they are "long-lived."

3) Quark production by secondary nucleons can be neglected. Secondary nucleons include those produced by either primary or secondary cosmic rays or by quarks.*

4) A quark loses energy only through inelastic collisions with the nuclei which it encounters (energy losses by ionization are ignored).

5) "Screening" among nuclei can be neglected for total cross section considerations in the atmosphere.

6) Fermi motions in nuclei can be ignored.

Furthermore, all fluctuations in particle intensities were ignored. For the sake of simplicity, incident particles were assumed to be inclined to the vertical by angles small enough so that the atmosphere could be considered planar, and so primary cosmic-ray intensities could be considered isotropic.

We shall use the following notation:

A = the atomic weight of nitrogen or oxygen.

A_{eff} = the effective number of nucleons in a nitrogen or oxygen nucleus, nuclear "absorption" considered.

M = the mass of a nucleon.

---

*If this assumption is wrong, the final mass limit is only slightly too low.

m_j = the mass of the incident particle (pion or nucleon) in diagram j.

N_o = Avogadro's number.

s = $(\vec{p}_i+\vec{p}_N)^2$ for incident-particle four-momentum $\vec{p}_i$ and target-nucleon four-momentum $\vec{p}_N$.

x = the depth in the atmosphere, measured in g/cm^2 from the top.

z = the depth in the atmosphere along a direction making an angle theta to the vertical ($z = x/\cos\theta$). z is also measured in g/cm^2 from the top of the atmosphere.

$\sigma_j(s)$ = the total quark production cross section off nucleons for diagram j.

$Q_j(z)$ = the number of quarks/cm^2/sr/sec, at depth z, the quarks having been produced in the interaction represented by diagram j.

$N_p(z,E)$ = the number of primary cosmic-ray nucleons of energy E at depth z per cm^2sr sec BeV (secondary nucleons being ignored).

Λ_i = the attenuation length for the i^{th} particle, in g/cm^2 (i=p for nucleons, i=q for quarks)---for example, $dN_p(z,E) = -N_p(z,E)\, dz/\Lambda_p$.

$K(j)$ = the ratio of the flux of the incident particles of energy E at z for diagram j to $N_p(z,E)$.

A diffusion equation can then be written:

$$dQ_j(z) \;=\; d\{\text{Quark Production}\} - d[\text{Quark Loss}] \;=$$

$$\left\{\int_{\text{threshold}_j}^{\infty} ds \begin{pmatrix}\text{incident}\\ \text{flux}\end{pmatrix}\cdot\begin{pmatrix}\#\text{target}\\ \text{nuclei}\end{pmatrix}\cdot\begin{pmatrix}\text{nuclear}\\ \text{cross section}\end{pmatrix}\right\} - d\begin{bmatrix}\text{quark}\\ \text{loss}\end{bmatrix} \tag{F-1}$$

The number of target nuclei which an incident particle passes in going dz is $N_0 dz/A$. The total quark production cross section off nuclei for incident particles of type j is $A_{eff}\,\sigma_j(s)$ (complete incoherence).

The quark loss could be expressed in a particular model for quark-nucleon collisions (e.g., the model of Adair and Price). However, we chose to lump all collisional considerations into one parameter: an energy-independent attenuation length.* Consequently, the quark loss term above is just $Q_j(z)\cdot dz/\Lambda_q$.

According to the data collected by Yash Pal (table 6), the charged pion flux at z is approximately 3/10 of the nucleon flux, independent of energy and z. With charge independence, the neutral pion flux might then be expected to be 0.15 of the nucleon flux. However, the neutral pion flux can be assumed to be negligible because π^0's decay into photons in 2×10^{-16} second. The incident particle flux can therefore by represented as $K(j)\cdot N_p(z,E)\cdot dE/ds$ where $K(j)=1$ for incident nucleons, $K(j)=0.3$ for incident pions, $N_p(z,E) = N_p(0,E)\exp(-z/\Lambda_p)$, and $dE/ds=1/(2M)$ for nucleons at rest.

Inserting these results, we see that the diffusion equation is

---

*It can be shown that the use of an energy-independent attenuation length Λ is equivalent to using an energy-independent entity n giving the fraction of energy retained in a collision and an interation length L for a differential cosmic-ray spectrum $dN/dE \sim E^{-m}$, where $\Lambda = L/(1-n^{m-1})$.

$$dQ_j(z) =$$

$$\left\{ \int_{\text{threshold}_j}^{\infty} ds \;\; K(j)\cdot N_p(0,E_j) \frac{e^{-\left[z/\Lambda_p\right]}}{2M} \left(\frac{dz\ N_o}{A}\right)\left(A_{eff}\ \sigma_j(s)\right) \right\} - \left[Q_j(z) \frac{dz}{\Lambda_q}\right] \tag{F-2}$$

Its solution is

$$Q_j(z) = \frac{K(j)\ Y(j)\ N_o\ A_{eff}\ \Lambda_p}{A\ (1-\ \Lambda_p/\ \Lambda_q)} \left[e^{-z/\Lambda_q} - e^{-z/\Lambda_p}\right] \tag{F-3}$$

where

$$Y(j) \equiv \int_{\text{threshold}_j}^{\infty} ds \left[\frac{N_p(0,E_j)}{2M}\right] \sigma_j(s) \;, \quad E_j = \left[\frac{s-M^2-m_j^{\ 2}}{2M}\right] \tag{F-4}$$

Suppose we now consider a particle incident upon our array in the solid angle increment $d\Omega$ at Ω and at the point (u,v) on the top of the array. Let $Acc(\Omega,u,v)$ be the probability that the particle can traverse the array rectilinearly and leave through the bottom. The rate of quarks traversing an experimental array described by such an "acceptance function" and located at sea level (x=1033) is then

Rate (quarks/second) =

$$\sum_{\substack{\text{diagrams}\\ j}} \left\{ \iiint_{\text{array}} du\ dv\ d\Omega\ \ Q_j(1033\ \cos\theta)\cdot \mathrm{Acc}(\Omega,u,v) \right\} \tag{F-5}$$

For simplicity, we make the approximation that the

Rate (quarks/second) $\cong$

$$\sum_{\substack{\text{diagrams}\\ j}} \left(Q_j(1033) \cdot \iiint_{\text{array}} du\ dv\ d\Omega\ \ \mathrm{Acc}(\Omega,u,v) \right) \tag{F-6}$$

The acceptance integral for our array is $1.5\times10^3\ \mathrm{cm^2 sr}$, so

Rate (quarks/second) $\cong$

$$\frac{(1.5\times10^3)\ N_o\ A_{eff}\ \Lambda_p}{A\ (1-\Lambda_p/\Lambda_q)} \left[e^{-\frac{1033}{\Lambda_q}} - e^{-\frac{1033}{\Lambda_p}} \right] \cdot \sum_{\text{Diagrams } j} K(j)\ Y(j) \tag{F-7}$$

We use the values

$$\left\{ \begin{aligned} N_o &= 6.02\times10^{23} \\ \Lambda_p &= 120\ \mathrm{g/cm^2} \\ A_{eff}/A &= \underset{\text{nitrogen}}{80\%(3.86)/14} + \underset{\text{oxygen}}{20\%(4.03)/16} = 0.271^{*} \end{aligned} \right. \tag{F-8}$$

---

*We use $A_{eff} = 1.6\ A^{1/3}$ here because we originally thought that a dependence of the sort $A_{eff} \sim A^{1/3}$ would be adequate. A more realistic dependence, however, is $A_{eff} \sim A^{2/3}$. See reference 77, and section VII.D.

so that the

Rate (quarks/second) $\cong$

$$\frac{(2.94\times10^{28})}{\left(1-\frac{120}{\Lambda_q}\right)}\left[e^{-1033/\Lambda_q} - 1.826\times10^{-4}\right]\cdot\sum_{\text{Diagrams } j} K(j)\ Y(j) \tag{F-9}$$

Note that the

$$\lim_{\Lambda_q\to 120}\left\langle \text{Rate (quarks/second)}\right\rangle \cong \left[(2.94\times10^{28})\cdot(1.572\times10^{-3})\cdot\sum_{\substack{\text{Diagrams}\\ j}} K(j)\ Y(j)\right] \tag{F-10}$$

Equations (F-9) and (F-10), together with (F-4), are the equations used to obtain the mass limits presented in section E of Chapter VII.

We now turn to a discussion of the advantages of running an experiment of this type at a higher altitude. If the expression for the quark flux (equation F-3) is maximized as a function of depth x for $\theta=0^{\circ}$ (z=x) and $\Lambda_p = 120$ g/cm^2, one finds that the depth at which the flux is a maximum is a function of Λ_q (figure 57). In particular, for Λ_q on the order of 120 g/cm^2, the optimum depth is approximately 120 g/cm^2. This corresponds to an altitude in the neighborhood of 50,000 feet. The gain in flux at this altitude is a factor of about 234, as one can see from equation (F-3). It is therefore much more productive (but perhaps much more difficult) to run a cosmic-ray experiment at balloon altitudes.

FIGURE 57: DEPTH x AT WHICH QUARK FLUX IS MAXIMUM

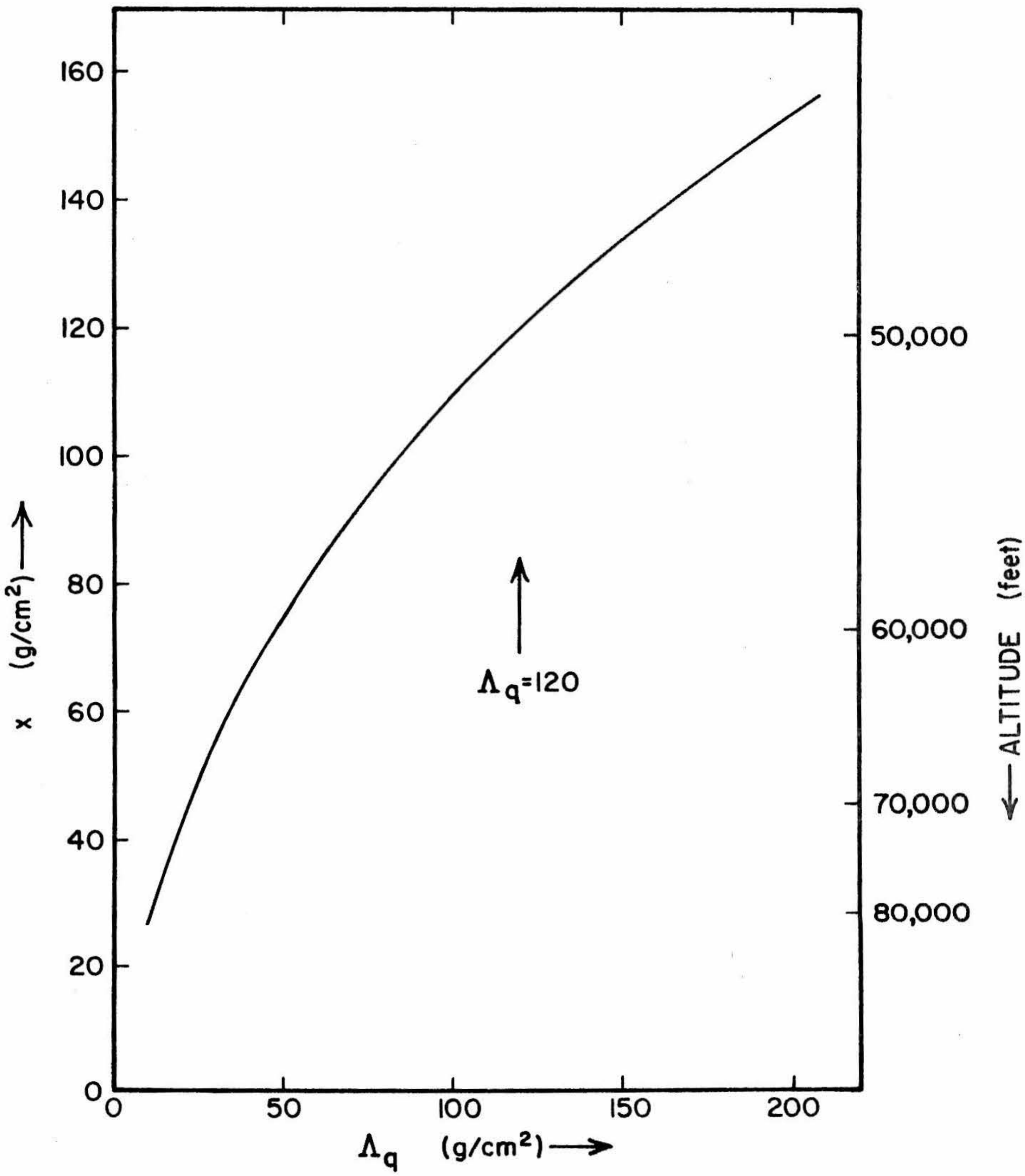

The gain in flux expected at mountain altitudes, although not as striking, is still significant. For example, with $\Lambda_q = 120\ g/cm^2$, the ratio of the flux of quarks at depth x to that at sea level is $(x/120\ e^{-x/120})\ /\ (1033/120\ e^{-1033/120})$. The gain in flux is therefore a factor of 4.0 for an altitude of 6,000 feet ($x \cong 841$).

REFERENCES

1. M. Gell-Mann, "A Schematic Model of Baryons and Mesons," Physics Letters, 8 (1 February 1964), 214-215.

2. G. Zweig, CERN Report No. 8419/Th. 412 (February 1964).

3. For a more detailed discussion of the quark model, see e.g. G. Zweig, "Fractionally Charged Particles and SU(6)," Lectures given at the International School of Physics "Ettore Majorana," Erice, Sicily (August 1964); and B. T. Feld, "The Quark Model of the Elementary Particles," CERN Report 67-21 (24 August 1967).

4. J. J. de Swart, "Search for Quarks," Physical Review Letters, 18 (10 April 1967), 618-619.

5. D. R. O. Morrison, "Experimental Limit on the Production by 24 GeV Protons of Long-Lived Particles with Fractional Electric Charge," Physics Letters, 9 (1 April 1964), 199-200.

6. H. H. Bingham, et al., "An Unsuccessful Search for Fractionally Charged Particles With Mass $\leq$ 2.2 GeV," Physics Letters, 9 (1 April 1964), 201-203.

7. V. Hagopian, et al., "Further Search for Fractionally Charged Particles," Physical Review Letters, 13 (24 August 1964), 280-281.

8. W. Blum, et al., "Search for Fractionally Charged Particles Produced by 27.5-GeV/c Protons," Physical Review Letters, 13 (14 September 1964), 353a-355a.

9. L. B. Leipuner, et al., "Particles With a Charge of 1/3 e," Physical Review Letters, 12 (13 April 1964), 423-425.

10. D. E. Dorfan, et al., "Search for Massive Particle," Physical Review Letters, 14 (14 June 1965), 999-1003.

11. E.g., J. D. Jackson, Classical Electrodynamics (N. Y.: John Wiley & Sons, Inc., 1963), sections 13.3 and 13.4.

12. L. I. Schiff, "Quarks and Magnetic Poles," Physical Review Letters, 17 (26 September 1966), 714-716; and A. Peres, "Singular String of Magnetic Monopoles," Physical Review Letters, 18 (9 January 1967), 50-51.

13. A. W. Sunyar, A. Z. Schwarzschild, and P. I. Connors, "Search for Charge 1/3 e Particles in Cosmic Rays," Physical Review, 136 (23 November 1964), B1157-B1159.

14. T. Bowen, et al., "Mountain-Altitude Quest for Fractionally Charged Particles," Physical Review Letters, 13 (14 December 1964), 728-731.

15. D. A. DeLise and T. Bowen, "Cosmic-Ray Search for Fractionally Charged Particles," Physical Review, 140 (25 October 1965), B458-B462.

16. T. Massam, Th. Muller, and A. Zichichi, "An Upper Limit to the Existence of Charges (2/3)e in the Cosmic Radiation at 500 m Above Sea Level," Nuovo Cimento, 40A (21 November 1965), 589-596.

17. J. C. Barton and C. T. Stockel, "The Non-appearance of Charge 2/3 Quarks at Great Depths Underground," Physics Letters, 21 (15 May 1966), 360.

18. H. Kasha, L. B. Leipuner, and R. K. Adair, "Search for Fractionally Charged Particles Produced by Cosmic Rays," Physical Review, 150 (28 October 1966), 1140-1147.

19. J. C. Barton, "An Investigation of Cosmic Rays Underground Using a Scintillator Stack: IV. An Upper Limit for the Rate of Relativistic Particles of Charge Two-Thirds," Proceedings of the Physical Society, 90 (January 1967), 87-90.

20. H. Kasha, et al., "Search for Charge-2/3 Quarks Produced by Cosmic Rays," Physical Review, 154 (25 February 1967), 1263-1264.

21. R. C. Lamb, et al., "Search for Quarks in Cosmic Rays," Physical Review Letters, 17 (14 November 1966), 1068-1070.

22. A. Buhler-Broglin, et al., "Search for Charges (1/3)e and (2/3)e in the Cosmic Radiation," Nuovo Cimento, 45A (21 September 1966), 520-526.

23. E.g., James D. Bjorken and Sidney D. Drell, Relativistic Quantum Mechanics (San Francisco: McGraw-Hill Book Co., 1964), pp. 127-131.

24. W. A. Chupka, J. P. Schiffer, and C. M. Stevens, "Experimental Search for Stable, Fractionally Charged Particles," Physical Review Letters, 17 (4 July 1966), 60-65.

25. C. Becchi, G. Gallinaro, and G. Morpurgo, "Measurement of Small Charges in Macroscopic Amounts of Matter: Discussion of a Proposed Experiment and Description of Some Preliminary Observations," Nuovo Cimento, 39 (1 September 1965), 409-412.

26. V. B. Braginskii, "One Method of Searching for Quarks," JETP Letters, 3 (15 January 1966), 43-45.

27. G. Gallinaro and G. Morpurgo, "Preliminary Results in the Search for Fractionally Charged Particles By the Magnetic Levitation Electrometer," Physics Letters, 23 (5 December 1966), 609-613.

28. V. B. Braginskii, et al., "Experiments in Search of Fractional Charges," Soviet Physics JETP, 25 (July 1967), 17-24.

29. V. I. Man'ko and M. A. Markov, "On the Possible Existence of a Quark State of Matter in Stars," Soviet Physics JETP, 24 (June 1967), 1143-1145.

30. O. Sinanoglu, B. Skutnik, and R. Tousey, "Search for Quarks in the Far Ultraviolet Solar Spectrum," Physical Review Letters, 17 (3 October 1966), 785-788.

31. W. R. Bennett, Jr., "Detection of Quarks in the Ultraviolet Solar Spectrum," Physical Review Letters, 17 (5 December 1966), 1196-1198.

32. T. K. Kuo and C. S. Shen, "Possibility of Detecting Quarks Through Astronomical Observations," Astrophysical Journal, 147 (January 1967), 356-359.

33. G. G. Fazio and B. Zuckerman, "On the Possibility of Searching for Quarks by Radio-Astronomical Techniques," Astrophysical Journal, 147 (March 1967), 1196-1199.

34. W. Heitler, The Quantum Theory of Radiation (Oxford: Clarendon Press, 1954), p. 368.

35. D. E. Groom and J. H. Marshall, "A 25-Input Pulse-Height Recording System," Review of Scientific Instruments, 33 (November 1962), 1249-1255.

36. J. E. Freund, Mathematical Statistics (Englewood Cliffs, N. J.: Prentice-Hall, Inc., 1962), pp. 223-225.

37. Keith R. Symon, "Fluctuations in Energy Lost by High Energy Charged Particles in Passing Through Matter," Harvard University Ph.D. Thesis (1948), especially pp. 140-141, 174.

38. B. Rossi, High Energy Particles (Englewood Cliffs, N. J.: Prentice-Hall, Inc., 1952), pp. 29-35.

39. L. Landau, "On the Energy Loss of Fast Particles by Ionization," Journal of Physics (USSR), 8 (1944), 201-205.

40. R. H. Frost and C. E. Nielsen, "The Specific Probable Ionization of Electrons Observed with a Wilson Cloud Chamber," Physical Review, 91 (15 August 1953), 864-870.

41. W. E. Stephens and T. Hurlimann, "Alpha Particles and Alpha Radioactivity," Handbook of Physics, edited by E. U. Condon and Hugh Odishaw (San Francisco: McGraw-Hill Book Co., 1967), p. 9-107.

42. "High-Energy Particle Data, Volume II: Range-Energy and dE/dx Plots of Charged Particles in Matter," UCRL Report #2426 (1966 Rev.).

43. W. A. Wenzel, "Spark Chambers," Annual Review of Nuclear Science, 14 (1964), 208.

44. R. C. Fletcher, "Impulse Breakdown in the 10^{-9}-Sec. Range of Air at Atmospheric Pressure," Physical Review, 76 (15 November 1949), 1504.

45. R. Kluckow, "On the Measurement of the Time-Dependent Increase in Current at Static Breakdown," Zeitschrift für Physik, 148 (1957), 564-581.

46. James W. Cronin, "Spark Chambers," Bubble and Spark Chambers: Principles and Use, Volume I (N. Y.: Academic Press Inc., 1967), pp. 315-405.

47. A. V. Phelps and J. P. Molnar, "Lifetimes of Metastable States of Noble Gases," Physical Review, 89 (15 March 1953), 1202-1208.

48. A. V. Phelps, "Absorption Studies of Helium Metastable Atoms and Molecules," Physical Review, 99 (15 August 1955), 1307-1313.

49. A. H. Futch and F. A. Grant, "Mean Life of the $^3P_2$ Metastable Argon Level," Physical Review, 104 (15 October 1956), 356-361.

50. J. L. Pack and A. V. Phelps, "Drift Velocities of Slow Electrons in Helium, Neon, Argon, Hydrogen, and Nitrogen," Physical Review, 121 (1 February 1961), 798-806.

51. A. V. Phelps, "Role of Molecular Ions, Metastable Molecules, and Resonance Radiation in the Breakdown of Rare Gases," Physical Review, 117 (1 February 1960), 619-632.

52. E. L. Murphy and R. H. Good, Jr., "Thermionic Emission, Field Emission, and the Transition Region," Physical Review, 102 (15 June 1956), 1464-1473.

53. R. H. Fowler and L. Nordheim, "Electron Emission in Intense Electric Fields," Proceedings of the Royal Society of London, 119 (1928), 179.

54. F. Llewellyn Jones and D. J. Nicholas, "Mechanism of Field Induced Emission from Cold electrodes in Gases," Proceedings of the Fifth International Conference on Ionization Phenomena in Gases, Volume II (Amsterdam: North-Holland Publishing Co., 1962), 1179-1187.

55. E. P. Krider, T. Bowen, and R. M. Kalbach, "A Search for Charge e/3 and 2e/3 Quarks in the Cosmic Radiation Near Sea Level," University of Arizona preprint (8 August 1969), submitted to the Physical Review.

56. R. Gomez, H. Kobrak, A. Moline, J. Mullins, C. Orth, J. Van Putten, and G. Zweig, "Search For Fractionally Charged Particles in Cosmic Rays Near Sea Level," Physical Review Letters, 18 (5 June 1967), 1022-1024.

57. COSMIC RADIATION (Q=1/3,2/3; "Isolation" Techniques):
A. V. Khrimyan, et al., "Search for Quarks with Unit and Fractional Charges in Cosmic Rays at 3200 Meters Above Sea Level," Bulletin of the Academy of Sciences of the USSR (Akademia Nauk SSSR, Bulletin), 30 (October 1966), 1719-1722;
H. Kasha, R. C. Larsen, L. B. Leipuner, and R. K. Adair, "Search for Particles with Charge 2/3e in Cosmic Rays," Canadian Journal of Physics (Tenth International Conference on Cosmic Rays, Calgary, 1967), 46 (15 May 1968), S730-S733;
Y. Hanayama, et al., "Search for Quarks in Cosmic Rays at Sea Level," loc. cit., S734-S736;
A. Buhler-Broglin, et al., "A Study of the Fractional Charge Content of the Cosmic Radiation," Nuovo Cimento, 51A (1 October 1967), 837-845;
G. Garmire, C. Leong, and B. V. Sreekantan, "Search for Quarks in Cosmic Rays at Sea Level," Physical Review, 166 (25 February 1968), 1280-1282;
F. Ashton, et al., "A Search for Relativistic Quarks in the Cosmic Radiation," Journal of Physics A, Proceedings of the Physical Society, 1 (September 1968), 569-577;

57. (Continued)

H. Kasha and R. J. Stefanski, "Search for Heavy Triplets in Cosmic Rays," Physical Review, 172 (25 August 1968), 1297-1303;
P. Franzini and S. Shulman, "Search for Massive Particles in the Cosmic Radiation at Sea Level," Physical Review Letters, 21 (30 September 1968), 1013-1015;
Y. Fukushima, et al., "Search for Quarks," Physical Review, 178 (25 February 1969), 2058-2060;
F. Ashton, H. J. Edwards, and G. N. Kelly, "Search for Heavy Mass Particles in the Sea Level Cosmic Radiation," Physics Letters, 29B (12 May 1969), 249-251; and
E. P. Krider, T. Bowen, and R. M. Kalbach, "A Search for Charge e/3 and 2e/3 Quarks in the Cosmic Radiation Near Sea Level," University of Arizona preprint (8 August 1969), submitted to the Physical Review.

58. COSMIC RADIATION (Q=1/3,2/3; "Shower-Front" Techniques):
L. W. Jones, et al., "Search for Massive Particles in Cosmic Rays," Physical Review, 164 (25 December 1967), 1584-1594;
C. B. A. McCusker and I. Cairns, "Evidence of Quarks in Air-Shower Cores," Physical Review Letters, 23 (22 September 1969), 658-659; and
C. B. A. McCusker, et al., a preprint (submitted to the Physical Review).
Also see: G. Damgaard, et al., "A New Method for Investigating the Production of Heavy Particles in the Cosmic Radiation," Physics Letters, 17 (1 July 1965), 152-154;
J. Bjørnboe, et al., "Search for Long-Lived Heavy Particles in Cosmic-Ray Events at Energies Above Several Thousand GeV," Nuovo Cimento, 53B (11 February 1968), 241-263; and
M. Dardo, P. Penengo, and K. Sitte, "Evidence for Strongly Interacting Heavy Shower Particles at 70 m w.e. Underground," Nuovo Cimento, 58A (1 November 1968), 59-86

59. Private communication, Professor Eugene W. Cowan, California Institute of Technology.

60. Yash Pal, "Cosmic Rays and Their Interactions," Handbook of Physics, Second Edition, edited by E. U. Condon and Hugh Odishaw (San Francisco: McGraw-Hill Book Company, 1967), 9-272 to 9-328.

61. E.g., K. Greisen, "Air Shower Density Spectrum," Progress in Cosmic Ray Physics (Amsterdam: North-Holland Publishing Co., 1956), Volume III, page 60; and Proceedings of the Tenth International Conference on Cosmic Rays, Calgary, June 1967, Canadian Journal of Physics, 46 (1968), S19, S99, S108, S123, and S136.

62. William Galbraith, Extensive Air Showers (N.Y.: Academic Press Inc., 1958).

63. C. B. A. McCusker, L. S. Peak, and M. H. Rathgeber, "Nuclear Interactions and Cosmic Radiation at Energies around 10^6 GeV," Physical Review, 177 (25 January 1969), 1902-1920.

64. M. Oda and Y. Tanaka, Journal of the Physical Society of Japan, Volume 17, Supplement A III (1962), 282;
S. Miyake, et al., Proceedings of the Tenth International Conference on Cosmic Rays, Calgary, June 1967, Canadian Journal of Physics, 46 (1968), S25; and
Japanese and Brazilian Emulsion Chamber Group, op. cit., S660.

65. ACCELERATOR:
E. H. Bellamy, et al., "Search for Fractionally Charged Particles," Physical Review, 166 (25 February 1968), 1391-1394;
Yu. M. Antipov, et al., "Search for the Particles with Fractional Charges (Quarks) at IHEP 70 GeV Accelerator," Physics Letters, 29B (12 May 1969), 245-248;
J. V. Allaby, et al., CERN preprint (to be published in Nuovo Cimento); and
Yu. A. Antipov, et al., "Further Search for Quarks at 70 GeV Proton Synchrotron of IHEP. Serpukhov, 1969," Institute of High Energy Physics preprint (Caltech 69-1131).

COSMIC RADIATION (Q=4/3):
A. Buhler-Broglin, et al., "Hunting Charges $\pm(4/3)e$ in the Cosmic Radiation," Nuovo Cimento, 49A (1 May 1967), 209-212;
A. Buhler-Broglin, et al., "A Study of the Fractional Charge Content of the Cosmic Radiation," Nuovo Cimento, 51A (1 October 1967), 837-845; and
H. Kasha, R. C. Larsen, L. B. Leipuner, and R. K. Adair, "Search for Particles with Fractional Charge $\geqslant (4/3)e$ in Cosmic Rays," Physical Review Letters, 20 (29 January 1968), 217-219.

GALAXY:
F. Pacini and E. E. Salpeter, "Quark Production in the Galaxy and Some Implications for Their Search," Nuovo Cimento, 51B (11 September 1967), 221-225; also see
G. Gallinaro and G. Morpurgo, Nuovo Cimento, 51A (21 October 1967), 1163-1164.

SOLAR:
R. A. Leacock, W. I. Beavers, and C. T. Daub, "A Search for Fractionally Charged Particles in the Solar Photosphere," Astrophysical Journal, 151 (March 1968), 1179-1186.

65. (Continued)

TERRESTRIAL:

V. I. Man'ko, "Experimental Searches for Fractionally Charged Quarks in Matter," Soviet Physics Uspekhi, 10 (Sept.-Oct. 1967), 262-264;

D. M. Rank, A Search for Stable Fractionally Charged Particles, University of Michigan thesis, 1967, 84 pp.;

D. M. Rank, "Search for Stable Fractionally Charged Particles," Physical Review, 176 (25 December 1968), 1635-1643;

G. Gallinaro and G. Morpurgo, "Preliminary Results in the Search for Fractionally Charged Particles by the Magnetic Levitation Electrometer," Proceedings of the Second International Conference on High-Energy Physics and Nuclear Structure, Rehovoth, 1967 (Amsterdam: North-Holland Publishing Co., 1967), 391;

G. Gallinaro and G. Morpurgo, Nuovo Cimento, 51A (21 October 1967), 1163-1164; and

V. B. Braginskii, et al., "An Upper Bound on the Number of Quarks Contained in Some Solids," Soviet Physics JETP, 27 (July 1968), 51-53.

LEPTONIC:

G. Bathow, et al., "Search for Leptonic Quarks in the Mass Range 100 to 900 MeV," Physics Letters, 25B (7 August 1967), 163-165;

J. Foss, et al., "A Search for Leptonic Quarks," loc. cit., 166-168;

L. Briatore, et al., "An Underground Search for Leptonic Quarks in the Cosmic Radiation," Nuovo Cimento, 57A (21 October 1968), 850-862; and references given therein.

REVIEWS:

E. L. Feinberg, "The Problem of Quarks in Cosmic Rays," Soviet Physics Uspekhi, 10 (Sept.-Oct. 1967), 256-261;

L. Lederman, "Hunting of the Quark," Comments on Nuclear and Particle Physics, 1 (Sept.-Oct. 1967), 155-159;

T. Massam, "The Quark Hunters' Progress," CERN Report 68-24 (8 July 1968);

J. G. Taylor, "Hunting the Quark," Science Journal, 4 (December 1968), 61-66;

G. Morpurgo, "The Quark Model," Proceedings of the 14th International Conference on High-Energy Physics (CERN, 1968), pp. 225-247; and

L. W. Jones, "Status of the Experimental Search for Physical Quarks," Paper presented at the International Conference on Symmetries and Quark Models, Wayne State University, June, 1969.

66. D. A. DeLise and T. Bowen, "Cosmic-Ray Search for Fractionally Charged Particles," Physical Review, 140 (5 October 1965), B461-B462.

67. R. K. Adair and N. J. Price, "Probable Momentum Spectra in the Atmosphere of Long-Lived Heavy Triplets Produced by Primary Cosmic Rays," Physical Review, 142 (February 1966), 844-851.

68. R. Hagedorn, Supplemento al Nuovo Cimento, 3 (1965), 147; and R. Hagedorn and J. Ranft, op. cit., 6 (1968), 169 and 311. Also see: I. N. Sisakyan, E. L. Feinberg, and D. S. Chernavskii, "Generation of Heavy Particle Pairs," Soviet Physics JETP, 25 (August 1967), 356-364; and E. L. Feinberg, "The Problem of Quarks in Cosmic Rays," Soviet Physics Uspekhi, 10 (Sept.-Oct. 1967), 256-261.

69. E.g., D. Amati, A. Stanghellini, and S. Fubini, "Theory of High-Energy Scattering and Multiple Production," Nuovo Cimento, 26 (December 1962), 896-954;
S. Frautshi, "Strong Damping of Large Momentum Transfers, and its Consequences for High-Energy Inelastic Processes," Nuovo Cimento, 28 (April 1963), 409-422;
K. A. Ter-Martirosyan, "The Asymptotic Values of the Amplitudes of Inelastic Processes," Soviet Physics JETP, 17 (July 1963), 233-241;
K. A. Ter-Martirosyan, "Asymptotic Behavior of Essentially Inelastic Collisions," Nuclear Physics, 68 (1964), 591-608;
Chan Hong-MO, K. Kajantie, and G. Ranft, "A Regge Model for High-Energy Collisions Producing Three Final Particles," Nuovo Cimento, 49 (1967), 157-182;
F. Zachariasen and G. Zweig, "Bounded-Momentum Transfer Restrictions on High-Energy Interactions," Physical Review, 160 (August 1967), 1322-1325; and
F. Zachariasen and G. Zweig, "High-Energy Interactions and a Multi-Regge-Pole Hypothesis," Physical Review, 160 (August 1967), 1326-1329.

70. J. R. Sanford and C. L. Wang, "Empirical Formulas for Particle Production in P-Be Collision between 10 and 35 BeV/c," Brookhaven National Laboratory AGS Internal Reports JRS/CLW-1 and JRS/CLW-2 (1 May 1967).

71. J. Finkelstein and K. Kajantie, "On Total Cross-Sections in the Multi-Regge Model," Topical Conference on High-Energy Collisions of Hadrons (Geneva, 15-18 January 1968), Volume II, 110-113; and
J. Finkelstein and K. Kajantie, "Total Cross-Section for n-Particle Production in a Multi-Regge Model," Nuovo Cimento, 56 (1968), 659.

72. J. Finkelstein and K. Kajantie, "Multiple Pomeranchuk Exchange Violates Unitarity," Physics Letters, 26B (February 1968), 305-307.

73. R. Lipes, G. Zweig, and W. Robertson, "Experimental Consistency of Multi-Reggeism in a High-Energy Reaction," Physical Review Letters, 22 (3 March 1969), 433-437; and
Richard G. Lipes, Ph.D. Thesis, California Institute of Technology (1969).

74. J. W. Andrews, et al., "Observation of the Reaction $\pi^- p \rightarrow p\bar{p}n$ at 8 GeV/c," Physical Review, 163 (25 November 1967), 1502-1509; and
J. W. Andrews, Ph.D. Thesis, University of Notre Dame (1968).

75. See reference 69: e.g., F. Zachariasen and G. Zweig, "High-Energy Interactions and a Multi-Regge-Pole Hypothesis," Physical Review, 160 (August 1967), 1326-1329.

76. M. Toller, "Three-Dimensional Lorentz Group and Harmonic Analysis of the Scattering Amplitude," Nuovo Cimento, 37 (1965), 631-657; and
N. F. Bali, G. F. Chew, and A. Pignotti, "Multiple-Production Theory Via Toller Variables," Physical Review Letters, 19 (4 September 1967), 614-618.

77. J. J. Veillet, "Coherent Production of Multipion Final States in π^- interactions with nuclei," Topical Conference on High-Energy Collisions of Hadrons (Geneva, 15-18 January 1968), I, 537; and
G. Bellettini, et al., "Proton-Nuclei Cross Sections at 20 GeV," Nuclear Physics, 79 (1966), 609-624.

78. For a general review of the subject, consult:
M. J. Druyvesteyn and F. M. Penning, "The Mechanism of Electrical Discharges in Gases of Low Pressure," Reviews of Modern Physics, 12 (1940), 87-174;
L. B. Loeb, Fundamental Processes of Electrical Discharge in Gases (N.Y.: John Wiley & Sons, Inc., 1939);
J. M. Meek and J. D. Craggs, Electrical Breakdown of Gases (Oxford: Clarendon Press, 1953);
I. S. Marshak, "Electric Breakdown of Gases at Pressures Close to Atmospheric Pressure," Soviet Physics Uspekhi, 3 (1961), 624-651; and
H. Raether, Electron Avalanches and Breakdown in Gases (Washington: Butterworths, 1964).

79. L. H. Fisher and B. Bederson, "Formative Time Lags of Spark Breakdown in Air in Uniform Fields at Low Overvoltages," Physical Review, 81 (1951), 109-114.

80. L. B. Loeb, "Streamer Breakdown and Sparking Thresholds," Physical Review, 81 (1951), 287.

81. L. B. Loeb, "Some Aspects of Breakdown Streamers," Physical Review, 94 (1954), 227-232.

82. J. M. Meek, "The Mechanism of Growth of Spark Discharges," Report of the International Symposium on Electrical Discharges in Gases (The Hague: Martinus Nijhoff, 1955), 275.

83. R. F. Saxe, "Uniform-Field Breakdown in Air," British Journal of Applied Physics, 7 (1956), 336-340.

84. See reference 78: Marshak, 624-651; Raether, 142.

85. L. B. Loeb, "High Voltage and High Pressure Discharges," Comptes Rendus de la VI^{e} Conference Internationale sur les Phenomenes d'Ionisation dans les Gaz (Paris, 1963), Volume II, 239-242.

86. A. A. Doran, "The Development of a Townsend Discharge in N_2 up to Breakdown Investigated by Image Converter, Intensifier and Photomultiplier Techniques," Zeitschrift für Physik, 208 (1968), 427-440.

87. J. M. Meek and J. D. Craggs, op. cit. reference 78, 252-271.

88. See reference 78: Marshak, 643-645; Raether, 114-124.

89. D. E. Golden and L. H. Fisher, "Anomalies in Ionization Coefficients and in Uniform Field Breakdown in Argon for Low Values of E/p," Physical Review, 123 (1961), 1085.

90. See reference 78: Loeb, 435; Marshak, 645; Raether, 142.

91. A. A. Doran and J. Meyer, "Photographic and oscillographic investigations of spark discharges in hydrogen," British Journal of Applied Physics, 18 (1967), 793-799.

92. See reference 78: Loeb, section 15; Meek and Craggs, 274-282; Marshak, 626, 639.

93. G. A. Kachickas and L. H. Fisher, "Formative Time Lags of Uniform Field Breakdown in N_2," Physical Review, 88 (1952), 878-883.

94. See reference 93 and J. Dutton, S. C. Hayden, and F. Llewellyn Jones, "Formative Time Lags in the Electrical Breakdown of Gases," British Journal of Applied Physics, 4 (1953), 170-175.

95. G. A. Kachickas and L. H. Fisher, "Formative Time Lags of Uniform Field Breakdown in Argon," Physical Review, 91 (1953), 775-779.

96. See reference 86; reference 78, Marshak; L. B. Loeb, "Significance of Formative Time Lags in Gaseous Breakdown," Physical Review, 113 (1959), 9; and W. P. Winn, "Ionizing Space-Charge Waves in Gases," Journal of Applied Physics, 38 (1967), 783-790.

97. See Raether, reference 78: 5, 124-128; L. B. Loeb and J. M. Meek, The Mechanism of the Electric Spark (Stanford: Stanford University Press, 1941), 40-41, 60; Reference 102; K. H. Wagner, Proceedings of the Seventh International Conference on Phenomena in Ionized Gases, Belgrade, 1965, Volume I, 571-576; and K. H. Wagner, Zeitschrift für Physik, 204 (1967), 177-197.

98. P. Felsenthal and J. M. Proud, "Nanosecond-Pulse Breakdown in Gases," Physical Review, 139 (1965), A1796-A1804.

99. See reference 78: Raether, 144-148.

100. M. Menes, "Buildup of a Discharge in Argon," Physical Review, 116 (1959), 481-486.

101. W. R. L. Thomas, "The Role of resonance radiation in electrical breakdown in Neon and Argon," Proceedings of the Seventh International Conference on Phenomena in Ionized Gases, Belgrade, 1965, Volume I, 566-568.

102. K. H. Wagner, "Vorstadium des Funkens, untersucht mit dem Bildverstarker," Zeitschrift für Physik, 204 (1967), 177-197.

103. T. Oshige, "Positive Streamer Spark Breakdown at Low Pressures in Air," Journal of Applied Physics, 38 (1967), 2528-2534.

104. J. Meyer, "Spectroscopic investigation of channel initiation in hydrogen sparks," British Journal of Applied Physics, 18 (1967), 801-806.

105. J. Koppitz, "Die radiale und axiale Entwicklung des Leuchtens im Funkenkanal, untersucht mit einer Wischkamera," Zeitschrift für Naturforschung, 22A (1967), 1089-1097.

106. P. N. Dashuk, "Investigations of Mechanism of Creeping Discharge and Conditions of its Conversion to Spark Stage," Proceedings of the Seventh International Conference on Phenomena in Ionized Gases, Belgrade, 1965, Volume I, 616-620.

107. See Lorella Jones and H. K. Shepard, "Analyticity and the Daughter Structure of Conspiring Regge Pole Families," Physical Review, 175 (November 1968), 2117-2140; and references contained therein.

108. Chan Hong-Mo, K. Kajantie, and G. Ranft, "A Regge Model for High-Energy Collisions Producing Three Final Particles," Nuovo Cimento, 49 (1967), 157-182. See equation (37).

109. G. Alexander, O. Benary, and U. Maor, "Data Compilation of Proton-Proton Interactions Between 1 and 32 GeV/c," Nuclear Physics, B5 (1968), 1-28.

110. E.g., see K. J. Foley, et al., "Elastic Scattering of Protons, Antiprotons, Negative Pions, and Negative Kaons At High Energies," Physical Review Letters, 15 (5 July 1965), 45-50; and reference 109.

111. E.g., Nina Byers, "High-Energy np Charge-Exchange Scattering and One-Pion Exchange," Physical Review, 156 (25 April 1967), 1703-1707; and
G. Manning, et al., "Elastic n-p Charge-Exchange Scattering at 8 GeV/c," Nuovo Cimento, 41A (1966), 167-188.

112. E.g., see the fits and references in V. Barger and D. Cline, "Backward πN Charge-Exchange Scattering and Pole Extrapolations of Baryon Regge-Exchange Amplitudes," Physical Review Letters, 19 (25 December 1967), 1504-1507.